THE EARTHQUAKE RESPONSE OF BRIDGE PILE FOUNDATIONS TO LIQUEFACTION INDUCED LATERAL SPREAD DISPLACEMENT DEMANDS

by

Sharid Khan Amiri

A Dissertation Presented to the
FACULTY OF THE GRADUATE SCHOOL
UNIVERSITY OF SOUTHERN CALIFORNIA
In Partial Fulfillment of the
Requirements for the Degree
DOCTOR OF PHILOSOPHY
(CIVIL ENGINEERING)

December 2008

DEDICATION

To my beloved parents who never stopped believing in me, for all their incredible support throughout the years and to all the people who refuse to give up their dreams for advancement of science for the benefit of humankind.

ACKNOWLEDGMENTS

The author wishes first to express his utmost gratitude to his advisor, Dr.Geoffrey Martin, for his mentorship, friendship, guidance and support. His invaluable knowledge and professional attitude made the long journey possible, the quest of knowledge exciting and a dream become reality. The author is also grateful for the helpful suggestions of his dissertation committee members. The support and suggestions of my professional colleagues in Caltrans throughout the research are also greatly appreciated. Finally, I want to thank my beloved wife for all her sacrifice and support.

TABLE OF CONTENTS

LIST OF TABLES

LIST OF FIGURES

ABSTRACT

The earthquake response of various types of pile foundations supporting a variety of bridge structures to liquefaction induced lateral spread displacement demands is analyzed using the concepts of pile ductility and pile pinning. The soil/pile model uses the stress-strain response of reinforced concrete and steel, incorporating both the axial and lateral loads for structural elements, and p-y curves to represent interface elements to assess the pile response during earthquake induced lateral spread displacement demands.

The analysis approach is incorporated in an improved design methodology using concepts documented in the FHWA "Recommended LRFD Guidelines for the Seismic Design of Highway Bridges (2003)".

Case studies of earthquake events, during which lateral spread displacement has caused damage to the bridge pile foundations are revisited to examine the response of these piles using the methodology developed in the research.

Design examples of several bridges supported by various types of pile foundations are also presented and the pile response in terms of plastic hinge development, pile ductility ratio and pile curvature response are studied. It is shown using the methodology developed in this research that given the subsurface conditions, the liquefaction and lateral spread potential and the structural details of the piles at a given bridge site, one can reasonably assess how close the pile is to acceptable ductility levels in plastic hinge zones. The method also provides a robust

approach to screen for the acceptability of existing bridge pile foundations subject to lateral spread during present day design earthquakes.

CHAPTER 1: INTRODUCTION

1.1. Background

Bridge pile foundations for ordinary bridges have often been designed in the past for axial and lateral load due to static loading. With an emphasis on designing bridge structures that would "perform" adequately in California during a maximum credible design earthquake, major research was conducted after the bridge failures during the 1989 Loma Prieta and 1994 Northridge earthquakes, to focus on performance based bridge design. Ductility based design for the superstructure and substructure components of bridges began in the mid-1990's. However, bridge pile foundations were capacity protected and were designed based on a force/capacity approach.

During the same time period, designers began focusing their attention on impact of "problematic" soils (i.e. liquefiable and soft soil) on the design of the bridge pile foundations. Bridge pile foundations in liquefiable soil were designed to remain elastic and not undergo any yielding and pile/liquefiable soils were modeled to achieve one objective and that is the deflection allowed at the top of the pile. This is in effect a constraint made by the bridge structure designer to accomplish his goal which is the allowable deflection of the bridge structure.

During the same period, inertia loading by the structure only was included into design of the bridge pile foundations and the phenomenon of lateral spreading and its impact on the design of the bridge pile foundations was not included since the

researchers did not have a clear understanding of the mechanics of the problem and there was no specific design approach to tackle the phenomenon.

In the last 10 years, major steps towards an understanding the behavior of the bridge pile foundations in laterally spreading soil have been accomplished. The emphasis has been in modeling the soil behavior in liquefiable soil and study the loading behavior of the laterally spreading soil on the piles. However, no major quantitative study had been performed into ductile behavior of the bridge piles in laterally spreading soil, which is the focal point of this study.

The lack of design guidance and quantitative information related to bridge pile foundation design in seismic zones and specifically in California has led designers to design piles elastically. In addition, the design approach has been to insure the piles do not form plastic hinges, simply because designers and owners do not want pile damage since it is not directly observable.

However, ductile behavior of bridge pile foundations in laterally spreading soil is acceptable for the following reasons:

1. Piles behaving inelastically would make the entire foundation system more flexible, which in turn could lead to an increase in earthquake energy dissipation and a potential reduction in the adverse impact of the earthquake on the bridge structure.

2. Analyses of pile inelastic behavior would allow the engineer to control the amount of plastic deformation of the pile structure to avoid significant pile damage.
3. The ductile analyses of piles provides the engineer with information required to design the transverse reinforcement.
4. A ductile displacement based design approach for bridge pile foundations is a better indicator of pile damage than a force based approach.
5. Ductile design of piles in laterally spreading soil provides a unified approach in seismic design that is rational and leads to an improved representation of the system response to earthquakes.

The objective of this research is to fundamentally study the ductile behavior of bridge piles and their response in laterally spreading soil and to improve the design methodology of pile foundations. It is important to note here that the impact of the seismic loading due to kinematic displacement demands and not inertia loading from bridge structures is studied. The role of inertia on the pile response is a separate phenomenon and is not considered in this study. To provide a framework for selecting and incorporating a meaningful and quantifiable performance criteria for bridge pile foundations from both a geotechnical and structural point of view, one needs to study the pile ductile response and related pile/soil interaction during lateral spread. The starting point for the research was the design guidelines documented in a National Cooperative Highway Research Program (NCHRP) Report (2003) which provided an initial framework for a ductile design approach.

1.2. Organization of the Dissertation

This dissertation has been organized in one volume comprised of 9 chapters in the following manner:

Chapter 2 presents case histories for past earthquakes that include the Great Alaskan (USA, 1964), the Edgecumbe (New Zealand, 1987), the Kobe (Japan, 1995), the Luzon (Philippines, 1990) and the Niigata (Japan, 1964) earthquakes, where pile damage due to lateral spreading of soil was observed. For each earthquake event, the physical nature of the event, description of the selected bridge structures that were damaged, the pile foundation types, the subsurface soil condition underlying the bridge foundation and the type of the damage are discussed.

Chapter 3 presents the evaluation of liquefaction induced lateral spread based on existing practice comprised of three segments: 1) Liquefaction Potential Assessment, 2) Residual Strength of Liquefied Soil and 3) Newmark Sliding Block Analysis. Prior to analyzing the impact of lateral spread on the bridge foundation, one needs to assess the potential for liquefaction, followed by determination of the stability of the body of soil once liquefaction occurs, which in turn requires an evaluation of the residual strength of the liquefied soil. Once it is determined that the body of soil is not stable during the earthquake and lateral spread would occur, then a Newmark Analysis is performed to assess the lateral free field displacement of the soil mass. (i.e. embankment and associated bridge abutment and bridge bents).

Chapter 4 presents the past major research done on the subject of the impact of lateral spreading on piles and offers an overview of modeling concepts used to evaluate the problem.

These concepts can be divided into two major categories: 1) Analytical models and 2) Centrifuge laboratory testing models. These two categories and the basis for their development and usage are presented. The analytical model used in this research to assess the earthquake pile response to lateral spread displacement demands is explained in detail by including the governing equations and the fundamentals covering these equations. Various work done by past researchers relevant to this current research and the main objectives and results yielded in past research are also presented.

Chapter 5 presents a discussion of the recently developed NCHRP 12-49 (2003) design approach and a re-evaluation of two bridge structure foundation design from a geotechnical and structural point of view. The pinning effect of the pile/soil system and plastic hinging of the piles for these bridges are discussed and the framework for the improved design methodology (presented in Chapter 7) is laid out. Finally a presentation of the NCHRP 12-49 pile ductility assumptions is also included to lay foundation for methods for improvement in analytical determination of pile plastic hinge development and its role in assessing pile response to kinematic loading due to lateral spread displacement demand.

As further background, Chapter 6 presents the current Caltrans approach on designing ordinary reinforced concrete bridge structure components for a maximum credible earthquake event as presented in Caltrans Seismic Design Criteria (2006). An overview of seismic performance criteria and seismic design philosophy in the Caltrans approach is also presented, which currently does not include allowance for ductile pile response. Additional discussion on two main aspects of the earthquake response of piles due to lateral loading is offered by first reviewing the current Caltrans design approach on geotechnical aspects of laterally spreading soil loading on piles and secondly going over an actual bridge pile design focused on the structural aspects of earthquake pile response. In summary, Chapter 6 provides a clear presentation of how piles for ordinary reinforced concrete bridges are designed due to lateral loading during a design credible earthquake, based on the current Caltrans State of Practice.

Chapter 7 presents the development of an improved design methodology incorporating ductile pile response. The approach is illustrated by revisiting two actual case histories for pile damage and their response during a major earthquake. These bridges are the Landing Road Bridge in New Zealand and the Uozakihama bridge in Japan. Both bridge piles were subject to laterally spreading soil due to liquefaction during earthquakes. Using the analytical methodology developed during this research, the pile structural details (i.e. type of reinforcement diameter, length, stress strain behavior of the pile material, etc…) provided, the piles were studied and

the pile ductility both on demand and capacity side and the plastic hinging in terms of distance and length were studied. A presentation for the response of these piles during these earthquakes incorporating the elements above is given.

Chapter 8 describes an extensive parametric study of the improved methodology as applicable to Bridge Pile Foundation response subject to lateral spreading during earthquakes. Various types of pile foundations typically used by Caltrans are studied using the improved design methodology. A sensitivity analysis is also conducted to study the impact of liquefiable sliding layer, both in terms of its location along the pile (i.e. shallow layer or deep layer) and its thickness on the response of the pile to lateral spreading.

Chapter 9 offers a discussion of the research results and the conclusions that can be drawn from them. Recommendations for a design approach for pile design in laterally spreading soil are summarized which offer improvements to both the NCHRP 12-49 guidelines and current Caltrans design approaches. Finally, recommendations for future studies and research are discussed.

CHAPTER 2: LIQUEFACTION INDUCED LATERAL SPREAD CASE HISTORIES

Although the effects of liquefaction have been long understood, it was more thoroughly brought to the attention of engineers in the 1964 Niigata, Japan and Alaska earthquakes. Extensive damage to bridge structure pile foundations due to liquefaction induced lateral spread occurred during these earthquakes and earthquakes of 1987 Edgecumbe, New Zealand, 1990 Luzon, Philippines and 1995 Kobe, Japan.

The following represents a general description of the above cited earthquakes and related damage to bridge structures with a focus on observed damage to the pile foundations caused by liquefaction induced lateral spread.

2.1. The Great Alaskan Earthquake

The March 27, 1964 "Good Friday" or Great Alaska earthquake (Figure 2-1) had a moment magnitude of 9.2 and was one of the most powerful earthquakes in the 20th century. The epicenter of this northern American continent was located in the Chugach Mountains near the northern end of Prince William Sound about 80 miles east-southeast of Anchorage. In terms of human loss, one hundred and fourteen people lost their lives and private property damage was estimated at 311 million dollars (1964 value).

The Alaska Earthquake caused very strong ground shaking and triggered numerous ground failure and landslides. Several towns, their ports and coastline facilities were damaged due to liquefaction of shoreline deposits and submarine landslides.

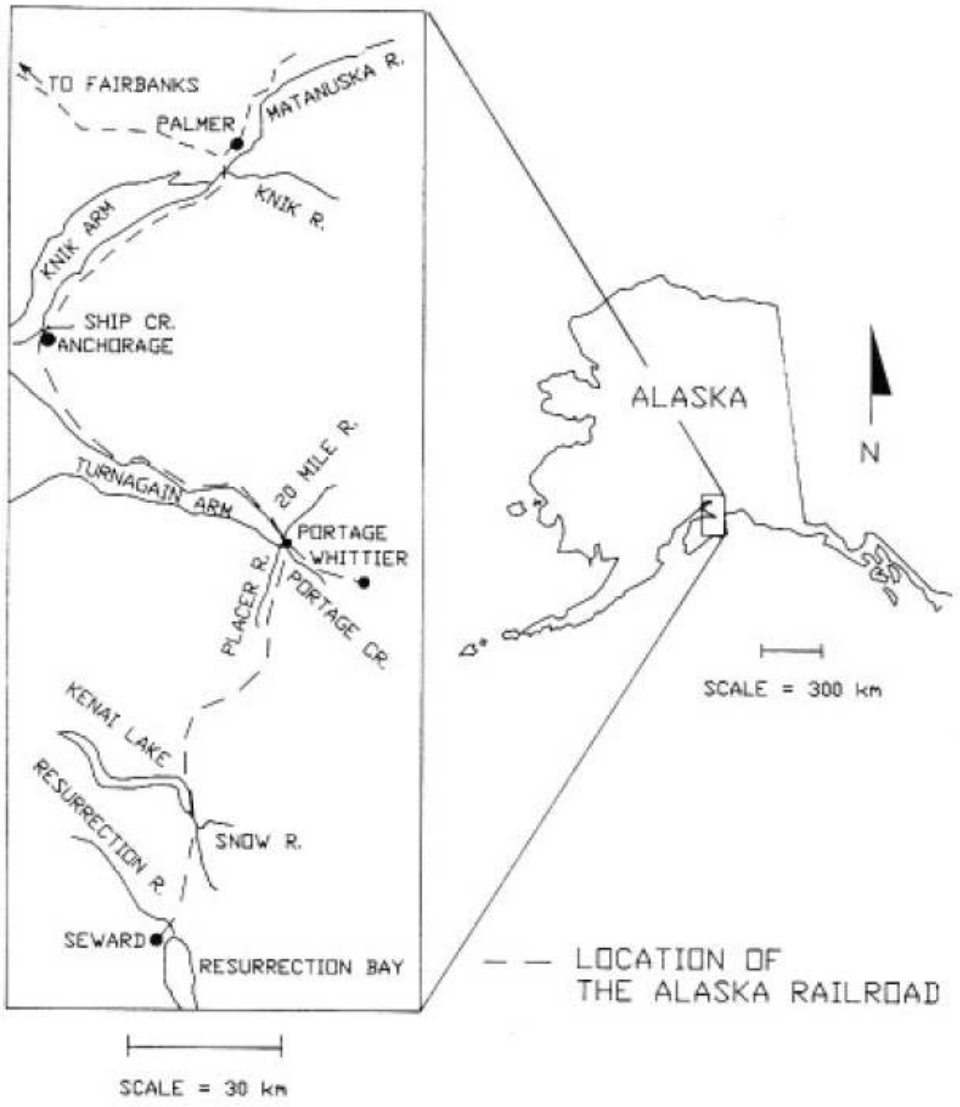

Figure 2-1: Great Alaska Earthquake Location Map (Hamada, 1992)

Liquefaction induced lateral spreads led to destruction of many railroad and highway bridge structures. Ninety two highway bridges were severely damaged or destroyed and another forty nine highway bridges were subject to moderate to light damage. The approximate total number of railroad bridges that were moderately to severely damaged was seventy five. (Hamada, 1992)

There is extensive tectonic activity ongoing along the Alaska's southern margin. The moment magnitude of 9.2 assigned to the earthquake qualifies it as the second largest earthquake of the 20th century (the largest was Chile Earthquake) and the largest in North America. Fault rupture during the earthquake generated a complex series of shocks in the Gulf of Alaska. The epicenter of the initial shock was located in the Chugach Mountains along the Unakwik Inlet and Prince William Sound. The depth to the hypocenter was not well defined, but has been estimated to be between 20 and 50 km.

The Alaskan earthquake generated a long duration of ground shaking throughout south central Alaska. There were no strong motion recording devices in Alaska at the time of the earthquake, so personal observations and timings of vibrations from mechanical automatic recording devices were used to estimate the duration of perceptible ground motion. In addition, empirical relationships based on earthquake magnitude and epicentral distance were utilized to estimate the duration of strong ground motion.

Reports from observers and empirical relationships suggest that strong ground motion lasted from 1 to 2 minutes in the region of significant liquefaction and bridge damage. Empirical magnitude-distance relationships predict that the maximum horizontal ground acceleration was approximately 0.4g, occurring at the Snow and Resurrection Rivers.

Liquefaction at these sites primarily occurred in recent fluvial silt, sand and gravel. Numerous railroad and highway bridges were severely compressed due to lateral spread of he floodplain and river banks. Bridge abutments and piers moved as much as 3m toward river channels and 2.5 to 3.0 m downstream at Portage and the Snow River. (Hamada, 1992)

As cited above, many highway and railroad bridges were damaged or collapsed. Unlike the railroad bridges, where lateral ground movement was measured, in the case of damaged highway bridges no measurement of horizontal soil movement was performed. Since pile, pier and abutment connections to the bridge superstructure appeared to have been easily broken at most bridges, it was concluded that the displacement of the piles, piers and abutments closely reflected the movement of the foundation material. In addition, the field investigators noted that most displaced piles and piers showed little rotation and appear to have been carried passively by the mobilized soil.

One of the major areas of damage was the southern end of the Turnagain Arm, which is a glacially carved trough where braided rivers meet the ocean. Highway bridge damage along the southern end of Turnagain Arm was some of the most severe in south-central Alaska. All of the 15 highway bridges in the area were severely damaged or destroyed. Many highway bridges partially or completely collapsed. Given the steepness of the valley, the bedrock lies at a considerable depth below the unconsolidated sediment that fills the valley. The depth of the sediment exceeds 200 meters and the groundwater elevation was within 0.6 m below the ground surface, near Portage during the time of the earthquake.

The railroad bridge (Mile Post 64.7) crossing the Twenty-Mile River was a 7 span 127.7 m long steel-truss structure supported by concrete piers and was damaged (Figure 2-2). The piers and abutments were each founded on 11 to 14 steel piles composed of three railroad rails welded together at the crown. Piers 5 and 6 experienced 18 and 8 inches of lateral movement respectively.

Figure 2-2: Damage to Twenty Mile River Bridge (Anchorage Museum of Arts and History, 1964)

The subsurface soil stratigraphy corresponding to the liquefied sites, where liquefaction induced lateral spread occurred and caused severe damage to the bridges consisted generally of sand and gravel to gravelly silty sand, silty clay, silty sand and sandy silt. The following (Figure 2-3) represents select borings performed at the above mentioned railroad bridge.

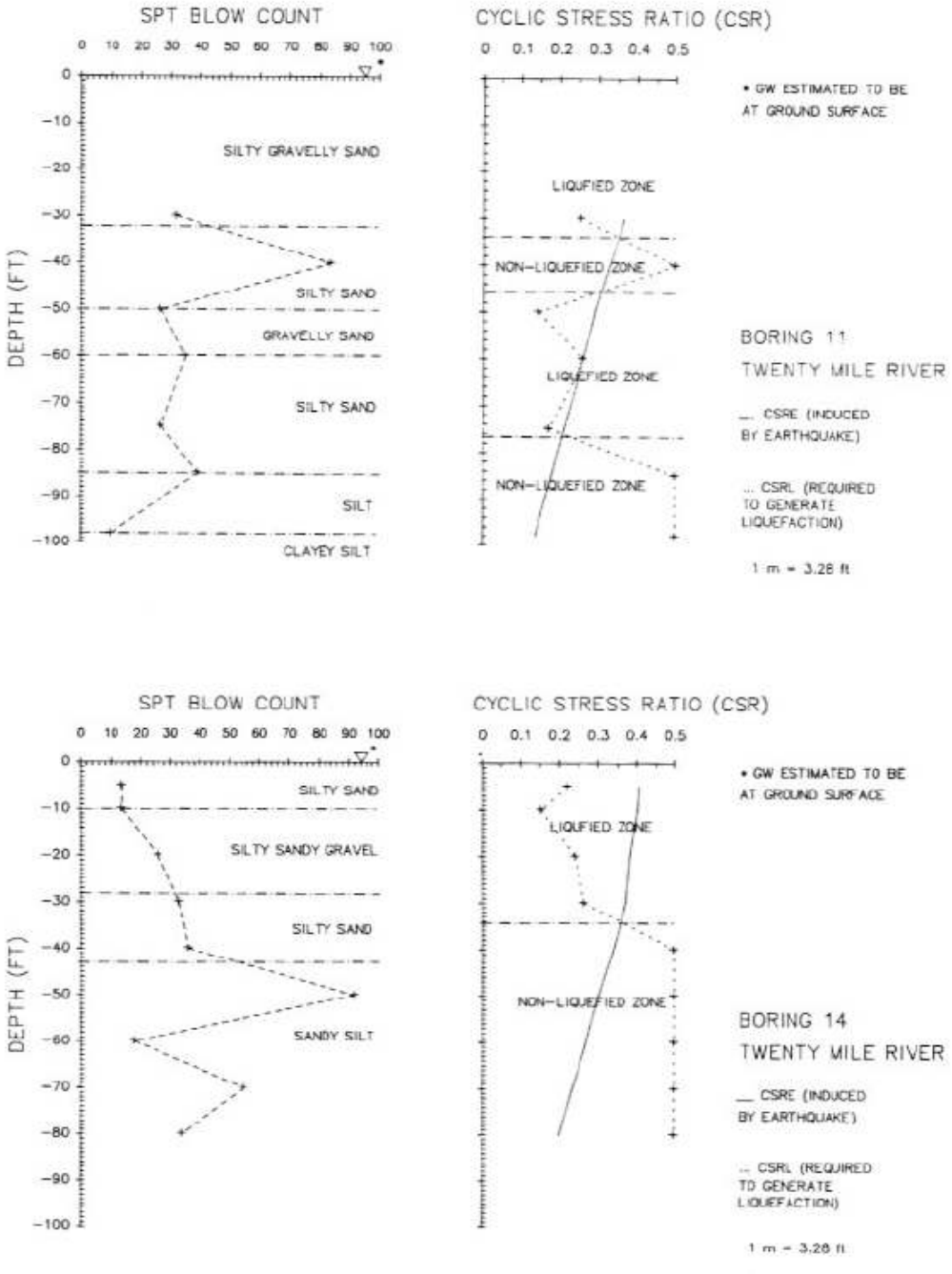

Figure 2-3: Log of Test Boring For Twenty Mile River Bridge (Hamada, 1992)

This steel-girder highway bridge (figure 2-4) collapsed when the steel piling upon which it rested snapped during the earthquake. The piling consisted of used railroad tracks. The bridge rested on thick water- saturated alluvium.

Figure 2-4: Steel-Girder Highway Bridge Collapse (USGS1)

The rails in this approach to a railroad bridge near the head of Turnagain Arm were torn from their ties and buckled laterally by streamward movement of the riverbanks during the earthquake (figure 2-5). The bridge was also compressed and developed a hump from vertical buckling.

Figure 2-5: Railroad Approach Damage Due to River Bank Movement (USGS2)

The concrete abutments of this steel girder highway bridge (figure 2-6) were carried channel ward by the underlying sediments, but the steel girders resisted the compressive movement. As a result, the upper part of this abutment, which was held more or less in place by the girders, was torn loose from the lower part, which was below the girders and moved channel ward.

Figure 2-6: Railroad Approach Damage Due to River Bank Movement (USGS3)

Collapsed no. 4 span and horizontal fracture in no. 4 pier of the Million Dollar Bridge on the Copper River Highway (figure 2-7)

Figure 2-7: Span Collapse, Million Dollar Bridge, Copper River Highway (USGS4)

The following Figure 2-8 shows another photo of Million Dollar Bridge consisting of the temporary bridging of the partial collapse of the Million Dollar bridge into the Copper River in Alaska following the 1964 Good Friday earthquake.

Figure 2-8: Temporary Bridging of Million Dollar Bridge, Copper River Highway (Molnia, B.)

The following (Figure 2-9) shows damage to railroad and highway bridge areas on Twenty mile River.

Figure 2-9: Damage to Railroad and Highway Bridge areas on Twenty Mile River (USGS5)

The 1964 Alaskan earthquake demonstrated that bridge structures built in liquefiable soils and subject to lateral spread could suffer severely from liquefaction induced lateral spread. Soil liquefaction and landslides lead to first zoning and land use regulations related to seismic hazards. (NEES 2004)

2.2. The Edgecumbe Earthquake

Just after 1.42 pm. on March 2nd 1987, an earthquake measuring moment magnitude 6.3 hit New Zealand's Bay of Plenty, centered on the town of Edgecumbe. (1987 Edgecumbe earthquake, 2008). Because the earthquake was very shallow, approximately 8 km from the earth's surface, it was felt over a large area. The earthquake was the most damaging New Zealand has experienced in recent decades,

with approximately 50% of the houses in Edgecumbe being damaged by the quake. Whakatane and Kawerau were among the other towns worst hit.

The epicenter of the quake was approximately 2.24 km south-south-east of the town of Matata, or 15 km north-north-west of Edgecumbe.(NZDSIR, Staff , 1987) The intense ground shaking caused by the earthquake led to a large number of ground surface failures, including sand boils, ridge-top shatters and debris avalanches on steeper slopes (Franks, C.A.M., 1988).

The Earth's crust and upper mantle are made up of several large, thin, quite rigid plates (tectonic plates) that move. Fault lines develop where the plates meet and are likely sources of earthquakes. Figure 2-10 shows active fault lines along the length of New Zealand, where the Pacific and Australian plates meet. East of the North Island, the Pacific Plate is dipping below the Australian Plate. This movement is causing the land to compress, squeeze upwards and move sideways. This map shows the direction and relative speed of the Pacific and Australian Plates in millimeters per year.

Figure 2-10: Relative Speed of Pacific and Australian Plates (Environment Waikato Regional Council, 2008)

Only one indirect casualty occurred: one person died at the time as a result of a heart attack. Property damage totaled 400 million dollars (1987 value). A crack seven kilometers long opened in the Rangitaiki Plains near Edgecumbe as a result of the earthquake. It is now known as the Edgecumbe Fault (Figure 2-11). At one point, the land close to the fault dropped 2 m.

Figure 2-11: Edgecumbe Fault (The Encyclopedia of New Zealand)

The following Figures 2-12 and 2-13 show the location map of the earthquake, where Whakatane is located in New Zealand and the location of Edgecumbe with respect to the Whakatane region.

Figure 2-12: Location of Whakatane within New Zealand (Expediamaps.com, Microsoft 1998)

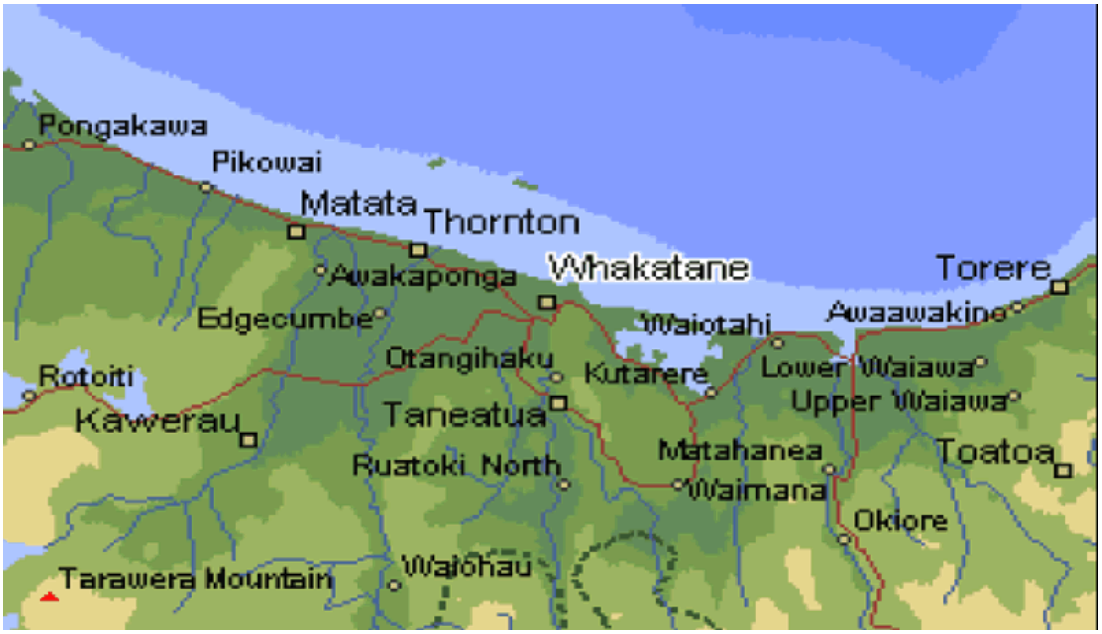

Figure 2-13: Edgecumbe Regional Map (Expediamaps.com, Microsoft 1998)

Liquefaction induced lateral spread occurred during the Edgecumbe earthquake and at least 6 bridges, ranging in size from a single span to the 240 m long Landing Road Bridge, suffered damage accordingly. Its evidence was discussed for the case study performed for the Landing Road Bridge. (Berrill et.al. 1997)

2.2.1. Landing Road Bridge

This structure (Keenan, 1996) consisted of a 13 span highway bridge, across the Whakatane River at the town of Whakatane on the east coast of the North Island of New Zealand. The Bridge was constructed in 1962 and it comprised of simply supported spans 18.3 m long, carrying a two lane concrete deck and two footpaths. The superstructure consists of 5 percent post-tensioned concrete I-beams, bearing on 16 mm rubber pads. The spans are interlinked with bolts through diaphragms over the piers and through the abutment backwalls. The beams are tied down using holding bolts at all piers and abutments, forming a quite stiff monolithic structure. The substructure comprises concrete slab piers running the full width of the superstructure and supported by eight 406 mm square raked prestressed concrete piles. The abutments are also supported by 406 mm square raked piles, 5 piles on the river side and 3 on the approach side. The abutment backwall is tight packed and bolted to the beam diaphragm. There are no approach slabs. Five river piers were additionally underpinned with two 1.1 m diameter concrete cylinders each, around 1985 after one pier had been undermined by flooding.

The bridge crosses the river and liquefaction occurred through a strip of land about 300 m wide on the internal, left, bank of the bend. About 1.5 m of lateral movement was observed towards the river channel.

The subsurface soil conditions consisted of a soil crust consisting of clay, underlayed by liquefiable (Figure 2-14) sand overlaying non liquefiable sand. According to Keenan, the strength of the pile/pier system showed that the superstructure was much stiffer and stronger than the substructure, making it a redundant component in the structural system for longitudinal loads.

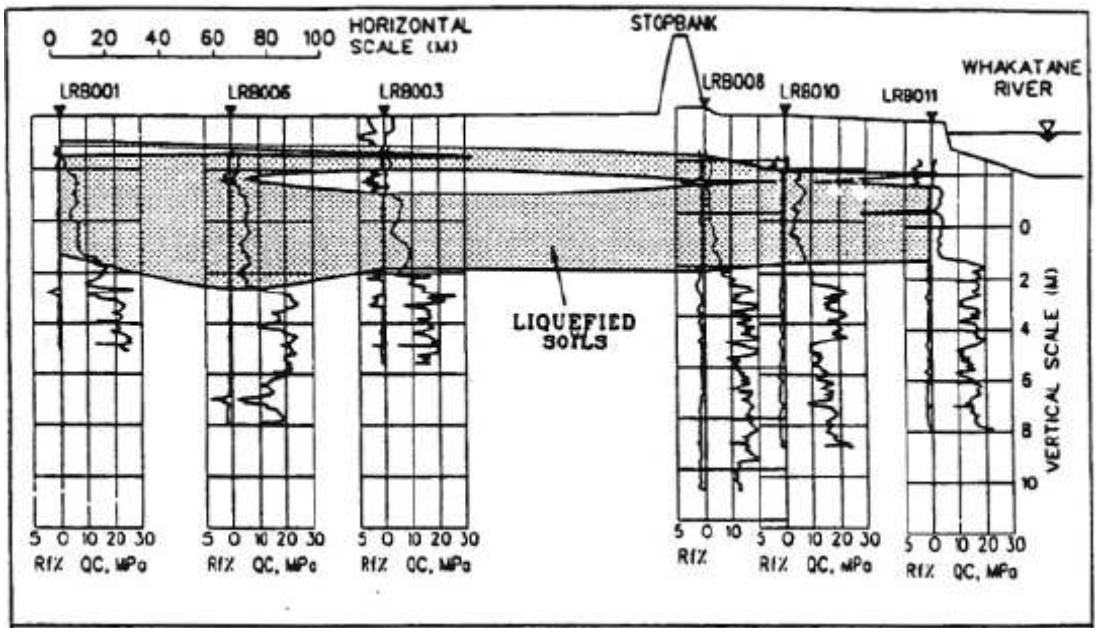

Figure 2-14: Cross Section at Landing Load Bridge showing the estimated Liquefied Strata (Berrill et. al, 1997)

At the piers on the left bank, soil had mounded up on the landward sides of the piers and gaps of up to 600 mm formed on the river side, suggesting passive failures in the soil crust above the water table. The bridge superstructure did not undergo any significant distress. Compression along the axis of the bridge was indicated in one instance by the buckling of a pair of concrete footpath slabs.

Excavation to about one meter at the northern abutment showed that the front raked piles were cracked on the river side. These cracks extended through 75% of the width of the piles. There was no indication of cracking on the other side of the piles. Piles beneath the internal piers were not inspected at the time, since the pile caps were both buried and below the water table. Soil at the northern abutment settled 300 to 500 mm, exposing the piles. At the time of the earthquake this abutment was thought to have rotated. This observation was supported in 1994 with the measurement of ½ degree rotation of the bottom of the abutment face towards the river. The south-eastern abutment was not inspected after the earthquake. In 1992 it was found by observation that the tops of the first two piers from the northern abutment were leaning towards the river by about 1 degree, while the remaining piers appeared vertical.

Horizontal cracks near the base of the piers H and J were not noticed until some years after the earthquake but were considered to have occurred as a result of it. This cracking is consistent with the lateral spreading loads being transmitted both

downwards through the raked pile system and upwards through the slab piers to the superstructure. The superstructure would thus carry a compressive load through to the fixed south abutment, constructed in the older and denser sands and gravels which had not been affected by mitigation of the river channel. Some of this compressive load, originating from the left bank piers, would be shed to the strengthened piers in mid-stream due to their greater stiffness.

Keenan calculated the total horizontal force required to initiate collapse of the substructure to be 1000-1100 kN per pier. Since this force was at the same order as the rough estimates of the passive load, trenching was undertaken to inspect the tops of the piles for cracking. Keenan reported that since the piers were still very near vertical, it was clear that a full collapse mechanism had not developed, but it was possible that cracking had started at potential plastic hinges. The most critical point is at the top of the northern piles; the outside face at the top of the southern row of piles.

The potential collapse mechanism of the substructure is shown below (Figure 2-15):

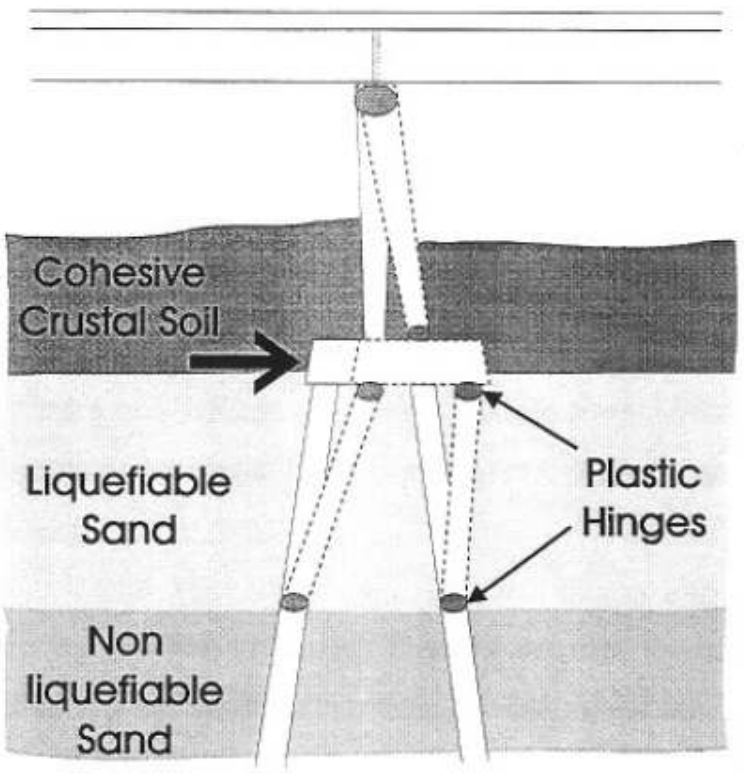

Figure 2-15: Potential Collapse Mechanism for Landing Load Bridge (Keenan, 1996)

Trenching at two piers on the flood plain of the left bank revealed slip surfaces in the 1·5 m thick non-liquefied crustal layer, consistent with passive failure as the buried piers and raked piles resisted its displacement towards the river channel. The passive force on the buried portion of the slab piers is estimated at 850–1000 kN per pier. The "collapse load" of the foundation system is estimated to be about 1200 kN, according to Keenan. Thus according to him, the force imposed by the non-liquefied crust was close to the ultimate capacity of the foundation. He reported that clear evidence was found of passive failure as the crust drove against the buried pier, piled through to firm ground. Since the bridge was still standing after the earthquake, very

close to plumb, and since no major cracking was found at the base of the pier nor at the top of the riverward piles, it is clear that a collapsed mechanism did not form. However given the passive force and the collapse load cited previously, it is likely that collapse was only narrowly avoided.

Unliquified crust will be present wherever there is granular material above the water table, or with cohesive soil regardless of the position of the water table. In these circumstances, where lateral spreading is likely, according to Keenan, passive loads from this unliquified crust constitute an important design loading.

2.3. The Kobe Earthquake

The 1995 Hyogoken-Nambu Earthquake, or Kobe earthquake as it is more commonly known overseas, was an earthquake in Japan (Great Hanshin earthquake, 2008) that measured 7.3 on the Richter magnitude scale and 6.8 on the Moment magnitude scale. It occurred on Tuesday January 17, 1995 at 5:46 a.m. in the southern part of Hyōgo Prefecture and lasted for approximately 20 seconds. The focus of the earthquake was located 16km beneath its epicenter, on the northern end of Awaji Island, 20 km away from the city of Kobe with a population of 1.5 million. This is in the middle of the fault zone of the Pacific, the Eurasian and the Philippine tectonic plates.

Three crustal plates (Figure 2-16) meet near to the coast of Japan. Close to Kobe, the denser oceanic Philippines Plate is being subducted beneath the lighter continental Eurasian Plate at a rate of about 10 centimeters per year. The Japanese island arc has been formed from the molten magma released by the melting Philippines Plate. Earthquakes are very common here and happen because of the friction resulting from the two plates colliding along this destructive margin.

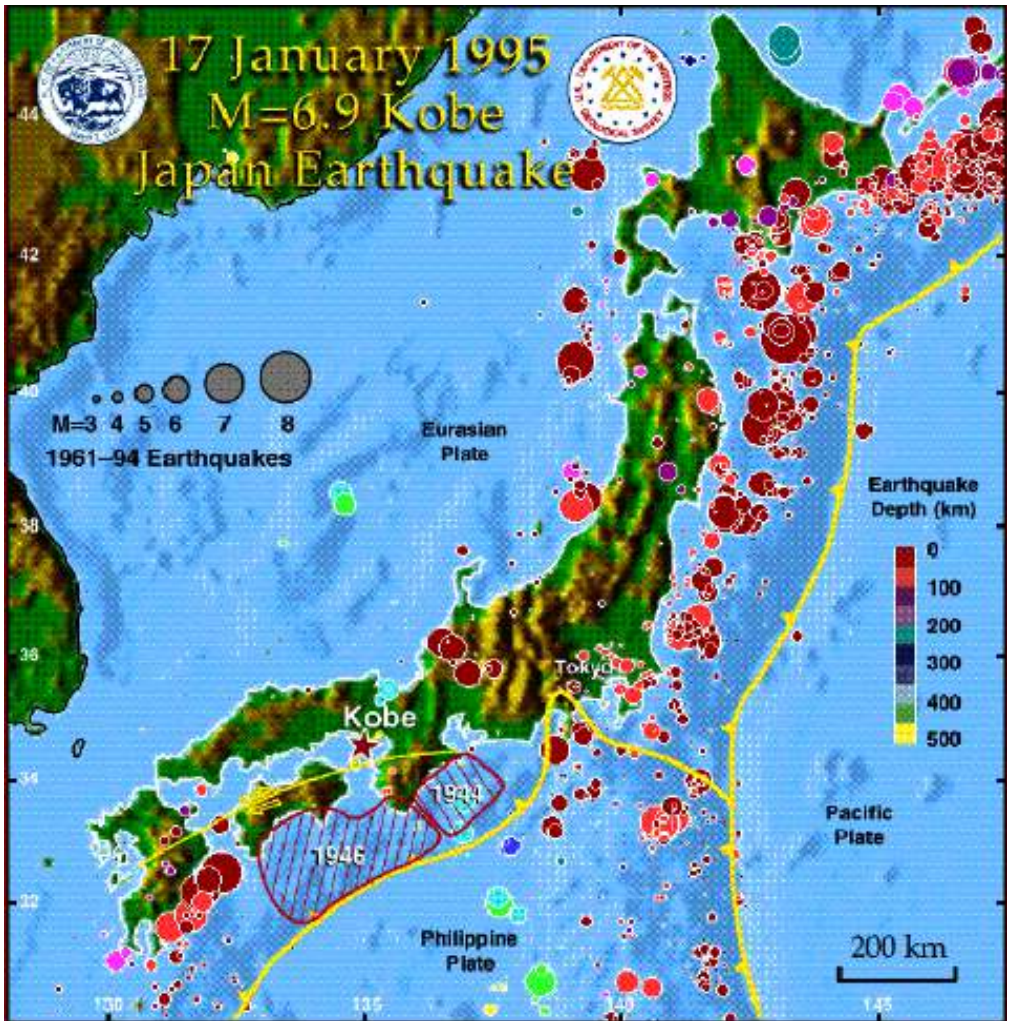

Figure 2-16: Tectonic Setting of Kobe Earthquake (Nevada Seismological Laboratory)

Approximately 6,434 people (final estimate as of 2006), mainly in Kobe, lost their lives as a result of the earthquake. Because Kobe was the closest major city to the epicenter of the earthquake, it was hit by the strongest shock waves; the earthquake was felt less strongly in cities further away. It was the worst earthquake in Japan since the Great Kantō earthquake in 1923, which claimed 140,000 lives. It caused approximately ten trillion yen or $200 billion USD in damage.

The maximum observed horizontal acceleration was 818 gal in Kobe City. (Shibata, et.al, 1996) Figure 2-17 shows a map of the peak horizontal accelerations recorded during the earthquake.

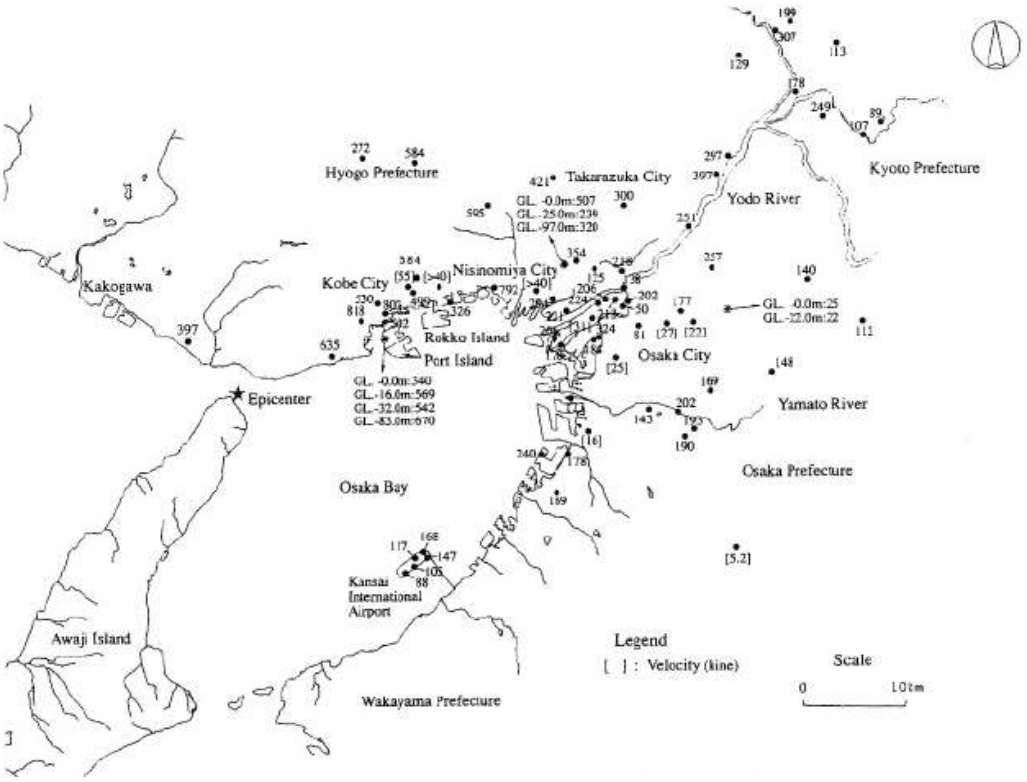

Figure 2-17: Map of observed horizontal peak acceleration (Ishihara, 2003)

The 1995 Kobe Earthquake (Hamada et. al, 1996) caused severed soil liquefaction in extensive areas of reclaimed land in Kobe and its neighboring cities. The soil liquefaction also included large ground displacements in the horizontal direction, which resulted in serious damage to foundations of structures. The Kobe Earthquake induced large ground displacements in large reclaimed land areas, and caused devastating damage to “lifelines” including to foundations of bridges.

An overall feature of the geological setting in the region of Osaka Bay is depicted in Figure 2-18.

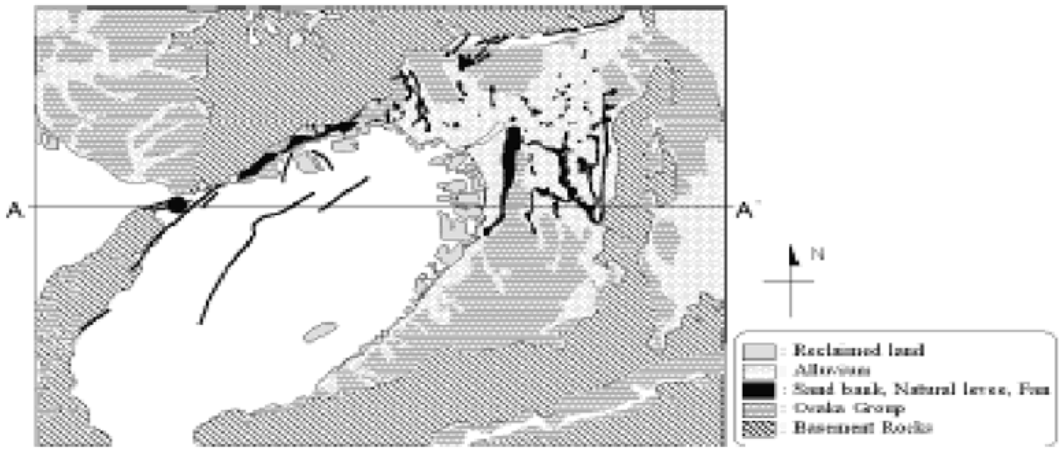

Figure 2-18: Geological Setting of Osaka Bay Region (Ishihara, 2003)

A cross section A-A’ in the west to east is shown in Figure 2-19 , where it can be seen that sedimentary deposits of different geological eras exist in a bowl-shaped basin with a maximum depth of about 2km. It can be seen that there exist several offsets in the underlying rock formation indicating presence of fault rupture zones. They are considered to be sources of historical earthquakes in the long geological

past. Kobe and its neighboring cities such as Ashiya and Nishinomiva lie on the north-western side of Osaka Bay.

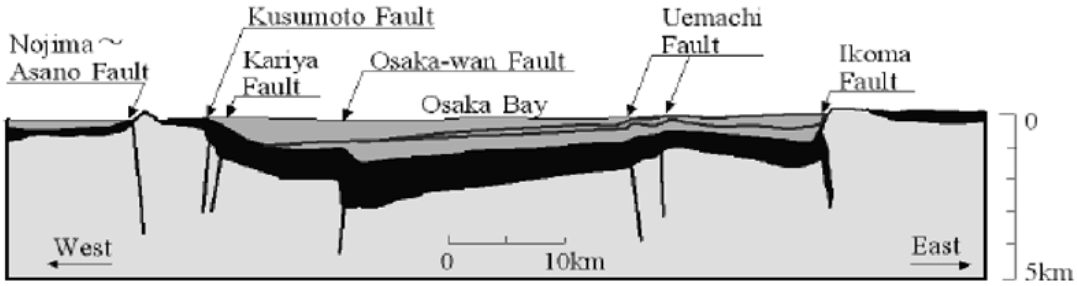

Figure 2-19: Faulting near or around Kobe (Ishihara, 2003)

As shown in Figure 2-20, they are located in the lowlands extending southwards from the foot of the Rokko Mountain Chain which consists of several fault blocks with deep escarpments dipping towards the sea. The mountain areas with an elevation in excess of 300m are essentially composed of base rock such as granite and granodiorite. The formation of the lowland extending from the mountain to the coast is a consequence of water run-off, which created a narrow flood belt and zones of numerous inter-connecting alluvial fans as illustrated in Figure 2-20.

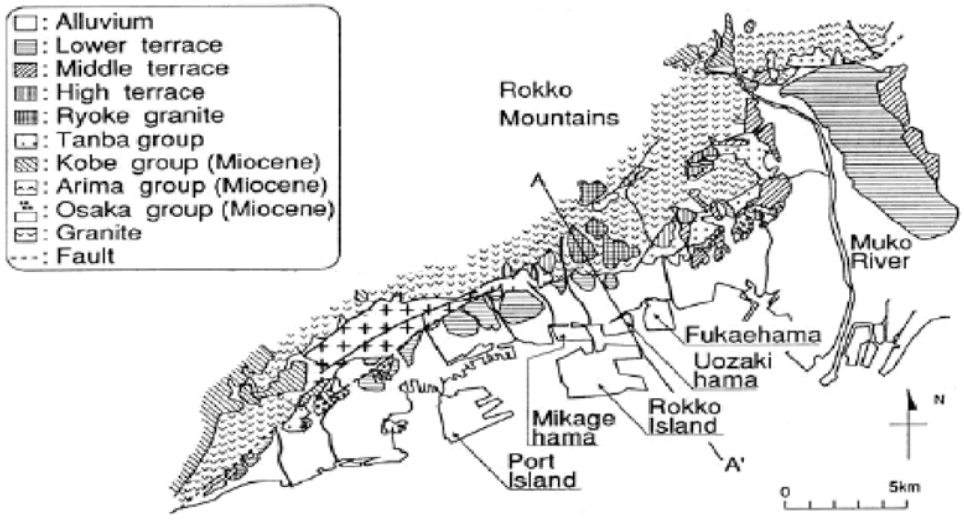

Figure 2-20: Alluvial fans near or around Kobe (Ishihara, 2003)

Terrace deposits of Pleistocene origin are shown to exist in the area south of the Rokko Mountain. The Pleistocene deposits are overlain by Holocene alluvium composed of sand, gravel and clay, which forms a relatively flat and narrow corridor of land on which the city of Kobe developed. A cross sectional view in the cross section A-A' in Figure 2-21 is shown.

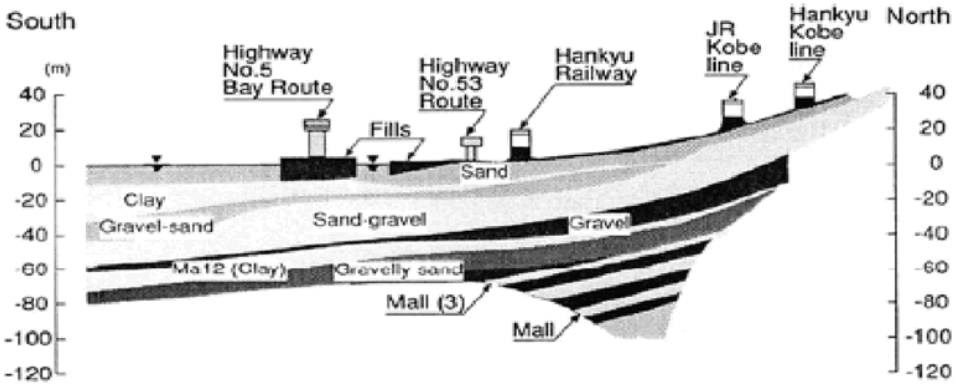

Figure 2-21: Subsurface geology near or around Kobe (Ishihara, 2003)

It may be seen that several southward dipping layers of sand, gravel and clay do exist with overlying reclaimed fills near the surface. The clay rich deposits under the man-made fills is the seabed sediment before the reclamation was conducted.

The fills beneath several islands in the port area of Kobe were constructed using residual soil formed by weathering of granite rocks. The soil dubbed Masado was obtained from borrow sites in the Rokko Mountain and brought to the site through a combination of conveyor belts and push-barges.

A large number of buildings, storage tanks and bridge piers on pile foundations were located within the lateral spreading zone, thus subjecting the piles of these structures to very large kinematic loads caused by the lateral ground movement. Many of these piles were damaged or collapsed during the quake and the excessive lateral ground movement was identified as a key factor in the damage to the piles. In order to inspect the damage to piles, detailed investigations were conducted on selected piles by means of several field inspection techniques. For example, development of cracks were investigated by lowering a borehole video camera down the length of the embedded piles while a survey of pile deformation was carried out by using an inclinometer. In some cases, the top part of the pile foundation was exposed by excavating the surface soils and visual inspection of the damage to the pile head was carried out.

2.3.1. Uozakihama Bridge

Characteristic damage features of piles for Uozakihama Bridge (Cubrinovski, 2006) located within the lateral spreading zone are briefly described below on the example of the foundation.of Pier 211 of the Hanshin Bay Route No. 5 (Figure 2-22).

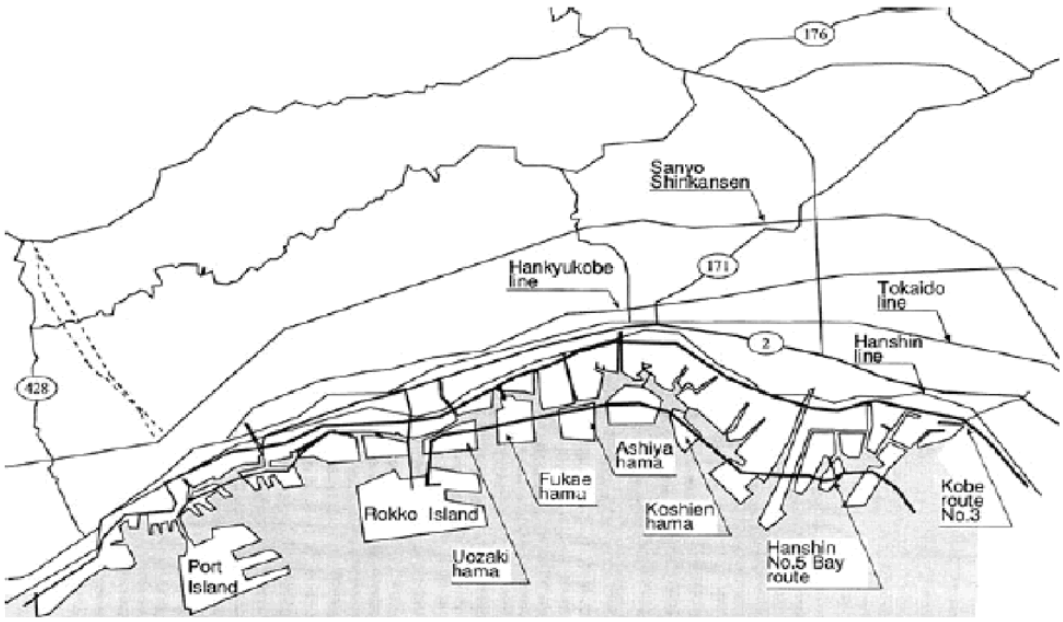

Figure 2-22: Highway System in the Osaka-Kobe District (Ishihara and Cubrinovski, 1998)

Side views of Pier 211 and a plan view of its foundation are shown in Figure 2-23a. The pier was supported on 22 cast-in-place reinforced concrete piles, 1.5 m in diameter and 41.5 m long. The damage to the piles summarized from borehole camera recordings of two inspected piles is shown in Figure 2-23b where cracks are seen at the pile head and predominantly at depths corresponding to the interface

between the liquefied layer and the underlying non-liquefied layer. The water table is 2.0 m below the ground surface and the upper 20 m of this site consists of Masado sand.

The damage pattern shown in Fig. 2-23 b was typical for many of the inspected piles in the waterfront area and can be summarized as follows.

1. Piles in the zone of large lateral spreading displacements were consistently damaged at depths corresponding to the interface between the liquefied layer and the underlying non-liquefied layer. Since this damage was at large depths where inertial effects from the superstructure are known to be less significant, this damage can be attributed to the lateral loads arising from the excessive ground movement due to spreading.
2. Damage at the pile head was encountered both for piles in the free field and piles located within the lateral spreading zone indicating that both inertial loads from the superstructure and kinematic loads caused by the lateral ground movement contributed to the damage at the pile head.

(a)

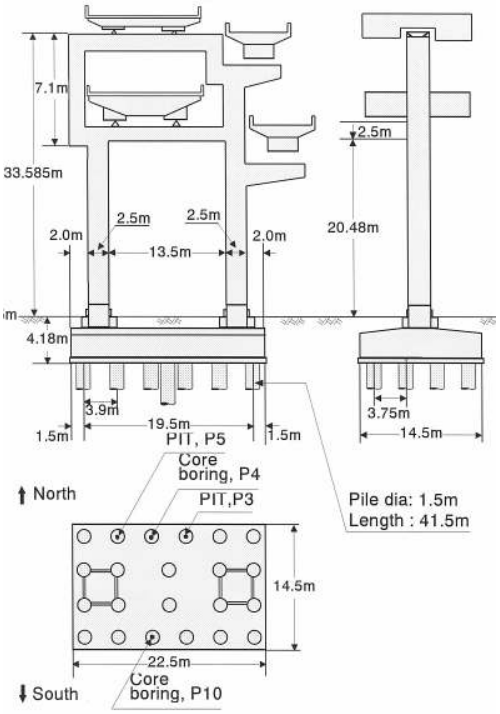

(b)

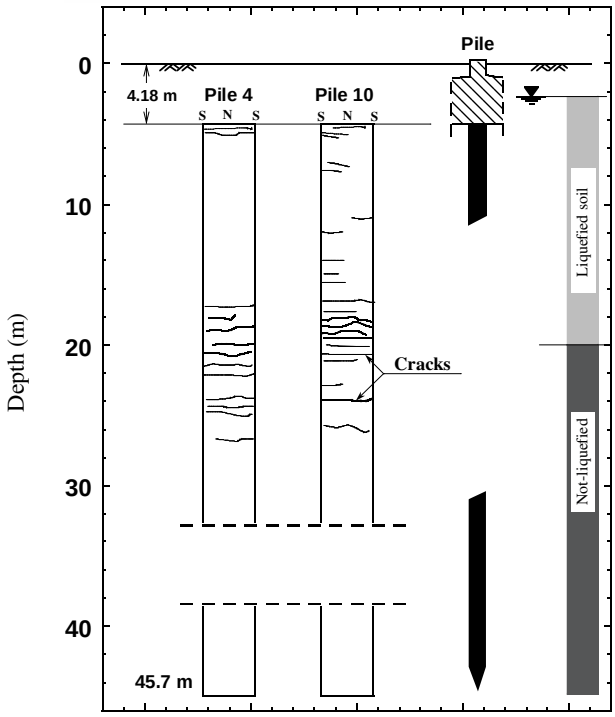

Figure 2-23. Uozakihama Bridge Pier 211: (a) Side view of the pier and plan view of the foundation; (b) Observed damage to piles (Hanshin Highway Authority, 1996)

For the investigation of piles supporting Pier 211, excavation was executed to a depth of 6m at the northeast corner of the footing, by enclosing a 3.2 m by 4.5 m section using sheet piles. Visual observation at the pile head disclosed several vertical and horizontal cracks a few millimeters wide. In the second method of in-situ investigation, a borehole 7 cm in diameter was drilled by the method of coring from the top surface through the footing slab down into the pile. If it happened to hit the reinforcement midway, another hole was drilled to reach a desired depth of 34m. A total of 2 holes were drilled to a depth of 34 m for inspection of the damage in the foundation of Pier 211. A video camera was lowered into the holes to examine feature of cracking around the walls. By and large, cracks were predominantly observed at depths corresponding to the boundary in soil deposits where liquefaction did and did not develop.

The outcome of the in-situ investigations as above revealed the fact that, generally speaking, the pile damage has taken place around the three depths illustrated in Figure 2-24.

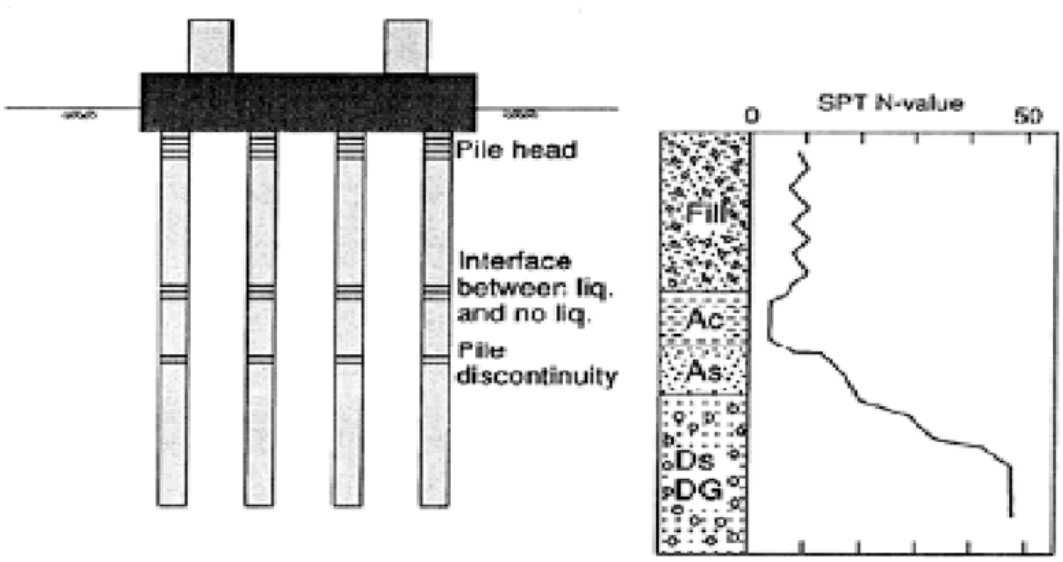

Figure 2-24: In-Situ Investigation, Uozakihama Bridge Pier 211, (Ishihara, 2003)

In practically all the piles investigated, cracks were detected at depths below 0-3 m below the bottom of the footing slab. The damage of the pile head was supposedly caused by a high bending moment resulting from the inertia force from the superstructure during intense shaking at the time of the earthquake. The cracks near the interface between the liquefied and unliquefied deposits were observed mainly in the piers located near the waterfront. The cracks were also observed at the depths of discontinuity where the cross sectional area or reinforcement was changed. This type of damage was intensified, by and large, in the case of the piles located in proximity to the waterfront. Thus, it may be considered highly likely that the cracks at some depths were caused by the lateral spreading of the surrounding soils that had liquefied during the main shaking of the earthquake.

The picture of lateral displacements obtained for the southern part of Uozakihama is displayed in figure 2-25, where it may be seen that in the area near the revetment line the lateral displacement is directed southwards to the waterfront with its maximum of 186cm. Note that the lateral displacement of the bridge pier, P211, closest to the revetment was 62cm, a value which is significantly smaller than the surrounding ground.

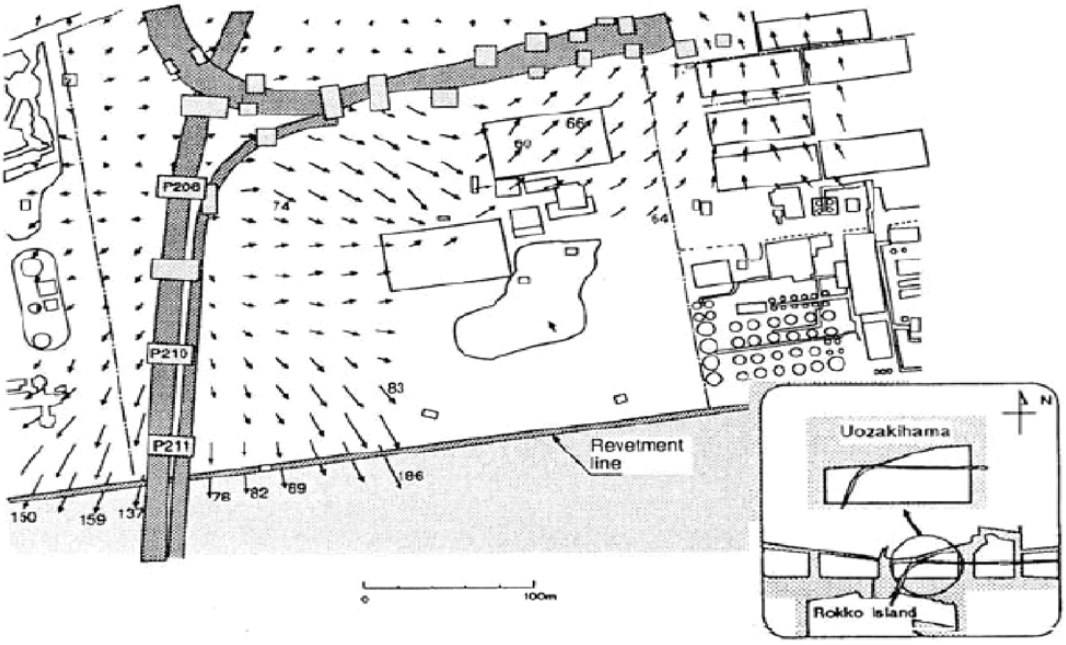

Figure 2-25: Ground Displacements in the South part of Uozakihama Island (Ishihara, 2003)

2.4. The Luzon Earthquake

The 1990 Luzon earthquake (1990 Luzon earthquake, 2008) occurred on Monday, July 16, 1990, at 4:26 PM local time in the Philippines at the densely populated island of Luzon, located about 110 km north of the capital, Manila. The magnitude of the event was among the greatest to have occurred in the Philippine Archipelago in recent decades. The magnitude of earthquake was 7.8 M_s (surface-wave magnitude). The earthquake produced a 125 km-long ground rupture that stretched from Dingalan, Aurora to Kayapa, Nueva Vizcaya as a result of strike-slip movements along the Philippine Fault Zone and the Digdig Fault. The earthquake epicenter was placed at 15º 42' N and 121º 7' E near the town of Rizal, Nueva Ecija, northeast of Cabanatuan City.

The earthquake caused damage in an area of about 20,000 square kilometers, from northwest of Manila through the Central Luzon and into the mountains of the Cordillera Administrative Region. About 1,600 people were killed, mostly in the central Luzon and Cordillera region. This was one of the deadliest and costliest natural disasters in the Philippines.

The earthquake was accompanied by a slip along a 110 km-long segment of the Philippine fault (Figure 2-26) that ruptured the Earth's crust to a depth of about 25 km. The ruptured segment is located in the northern-most edge of the 1200 km-long Philippine fault extending northerly from Mindanao Island and veering

northwestward in the middle of the Archipelago. The ground rupture appeared on the surface of the southern-most end near Dingalan and extended to the north terminating in the mountain east of Baguio, the rupture on the fault was left lateral type producing a horizontal displacement of the order of 3-6 m in the segment north of Rizal and of the order of 2-3 m in the southern segment. The vertical offsets differed significantly from one place to another and there was no coherent pattern indicating uplifting or subsidence of the land on either side.

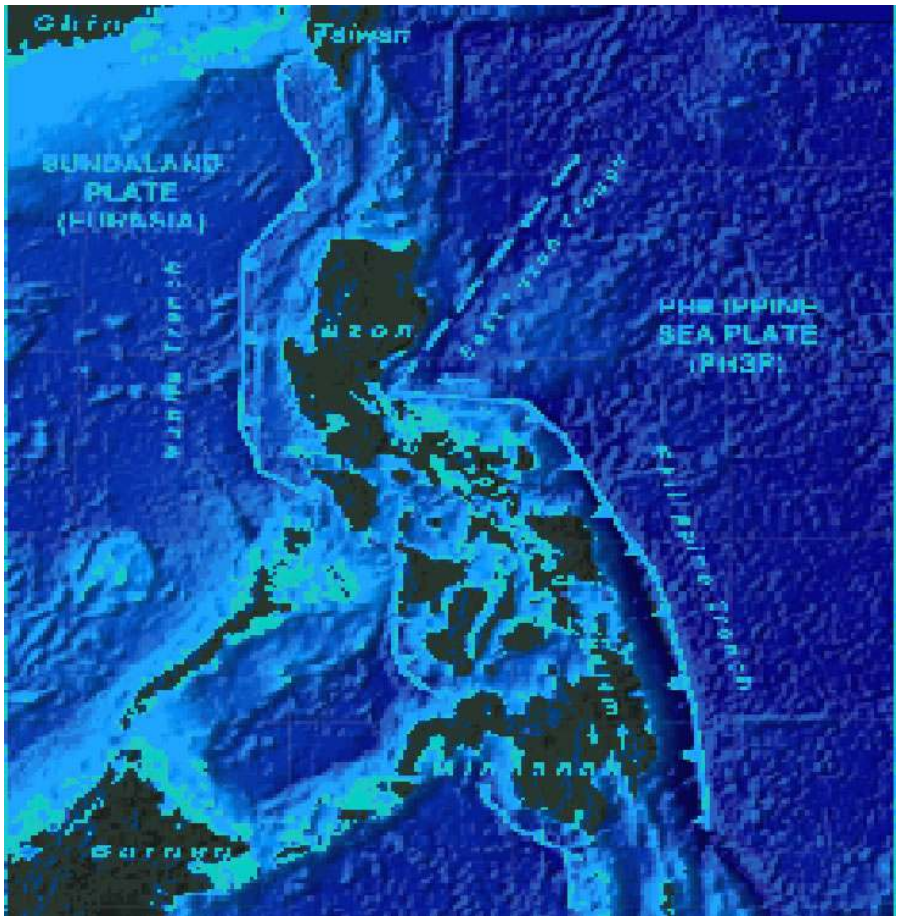

Figure 2-26: Physical Map of the Philippines, Showing Topography and Major Philippines Fault System (Galgana et. al, 2007)

In the absence of any records on the motions, an effort was made to roughly estimate the magnitude of accelerations on the basis of observed performances of rigid objects such as concrete fences or benches. The outcome of this effort led to an estimate of the acceleration magnitude of 0.4g.

The city of Dagupan, which is the chief port and commercial and financial center of Northern Luzon; was devastated by the extensive liquefaction which occurred in the sandy deposits prevailing in the city area along the Pantal river. Physical evidences of liquefaction such as sand boiling and lateral flow of the ground were seen everywhere in the city.

Figure 2-27 shows the area where apparent signs of liquefaction were observed during the 1990 July earthquake.

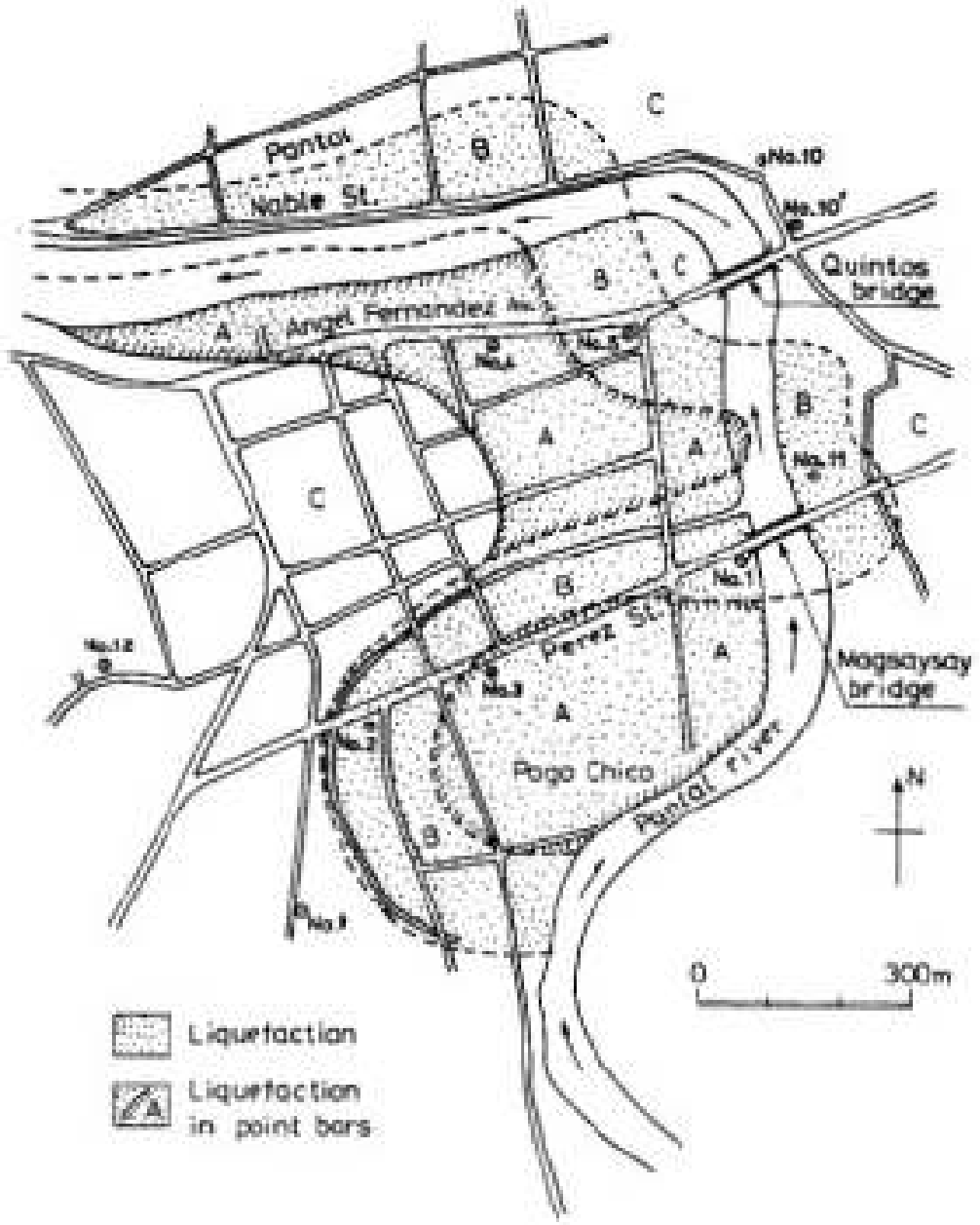

Figure 2-27: City area of Dagupan affected by liquefaction (Wakamatsu et. al, 1991)

Figure 2-28 shows the locations of liquefaction in central part of Luzon, during the July 16th, 1990 earthquake.

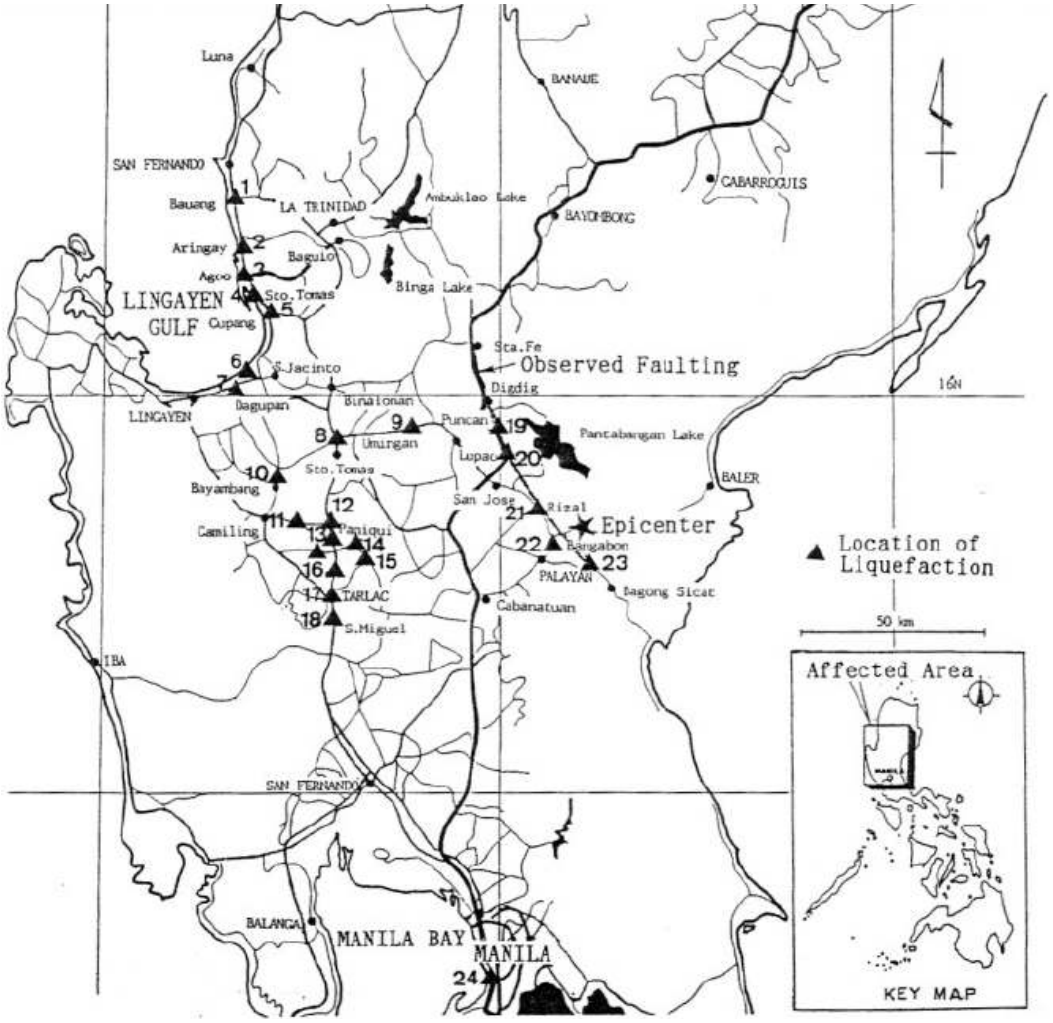

Figure 2-28: Map of Central Part of Luzon showing the region affected by the July 16, 1990 Earthquake and Locations of Liquefaction (Wakamatsu et. al, 1991)

2.4.1. Magsaysay Bridge

Among the structures suffering damage due to liquefaction induced lateral spread was Magsaysay bridge crossing the Pantal river, which collapsed as a result of excessive sinking of piers. The failure mode consisted of the collapse of four simple supported spans induced by about 2 meters of lateral spread at the west abutment, shown in Figure 2-29.

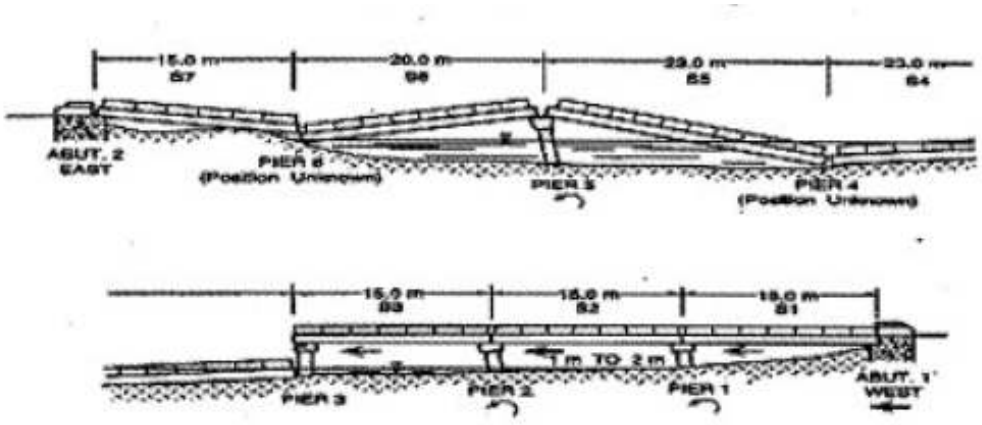

Figure 2-29: Sketch of Magsaysay Bridge Damage during the 1990 Luzon Earthquake (Hall and Scott, 1995)

Figure 2-30 shows features of this bridge prior to and after the earthquake. As indicated, this bridge 144 meters long was comprised of 8 simply supported reinforced concrete girders resting on piers supported by concrete piles about 10 m in length.

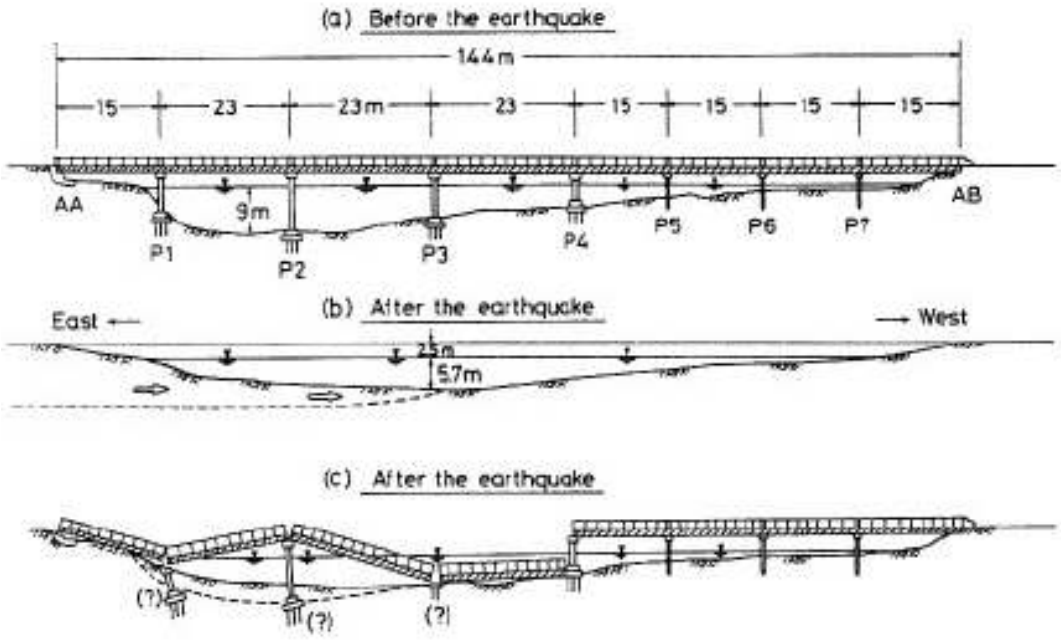

Figure 2-30: Side Views of Magsaysay Bridge Before and After Earthquake (Ishihara et. al, 1993)

The locations and approximate values of lateral displacements are indicated in Fig 2-31, where it can be clearly seen that practically all the areas behind the present river bank had suffered a lateral deformation of the order of 1 to 6 m.

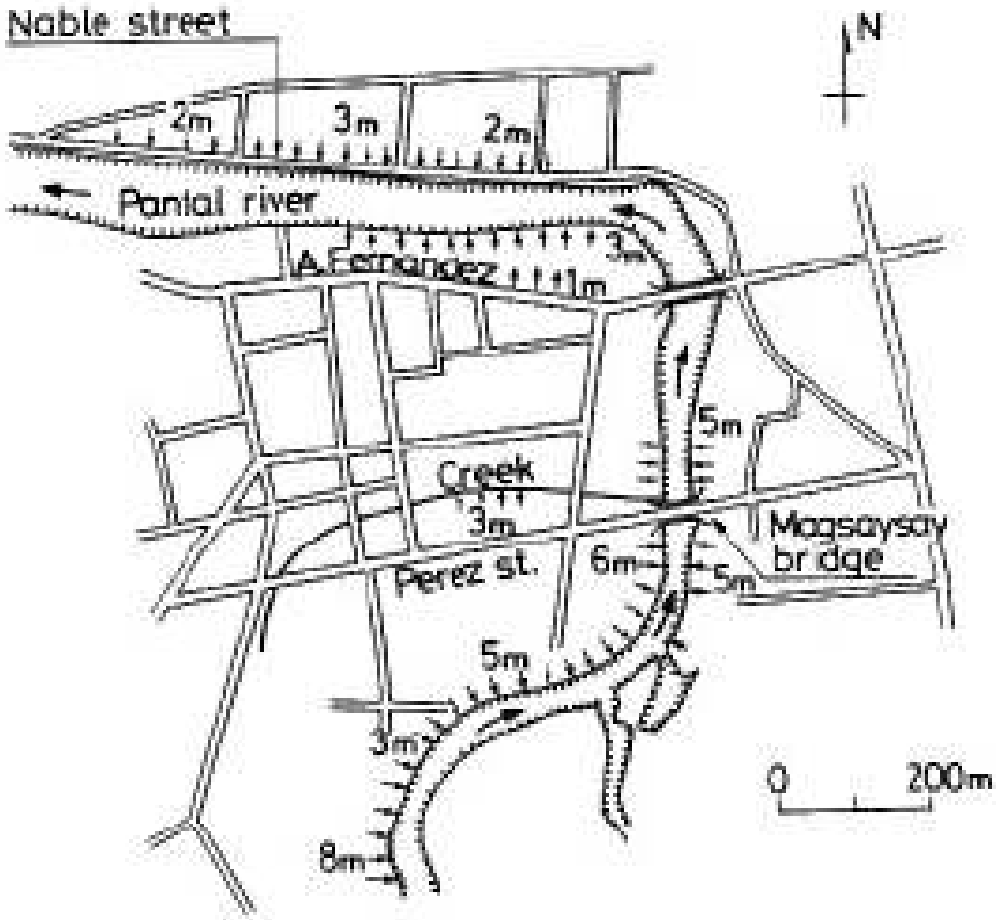

Figure 2-31: Lateral Flow along the River Side (Ishihara et al, 1993)

To illustrate, the road on the Nable street in the district of Pantal moved by 1 to 3 m towards the river as a consequence of liquefaction developed in the sandy deposits. The right bank of the Pantal river in the vicinity of the Magsaysay bridge is underlain by sandy deposits and consequently developed extensive liquefaction accompanied by a lateral flow amounting to about 5 m.

The city area of the Dagupan, had developed over the lowlands in the lower reaches of the Pantal river which has a complexly meandering pattern as shown in Figure 2-32.

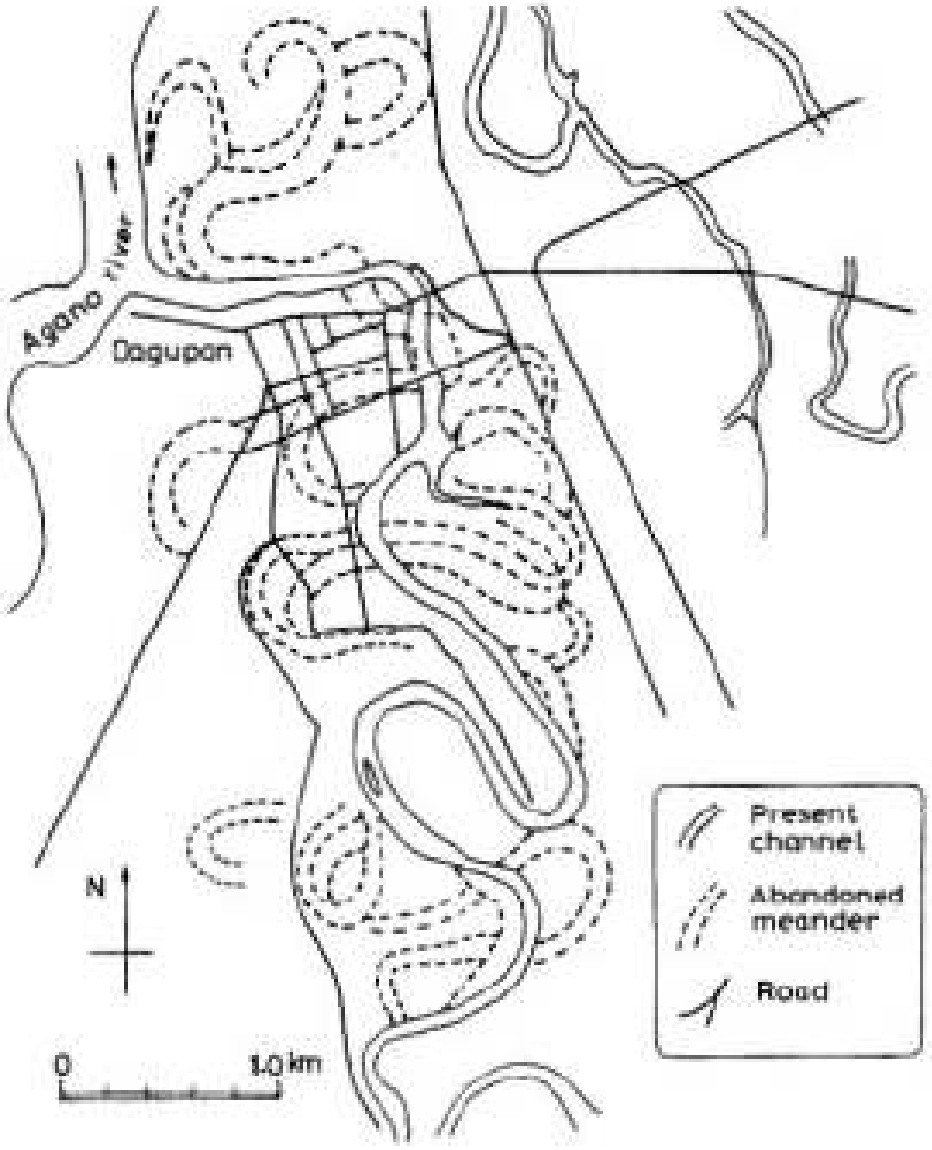

Figure 2-32: Meandering Patterns of Old and Present River Channels (Ishihara et al, 1993)

The shift of the river courses is purported to have taken place naturally for a long geological era, and therefore the abandoned portion of the river channel indicated in figure above is not man-made fills, but was created probably by transport of sediments during flooding and inundation. It is generally believed with good reason that the area of old river channels is composed of loose deposits of silts and sands, whether it is of natural sediments or man-made fills, and thus susceptible to liquefaction during earthquakes. According to Ishihara, judging from the depth of current river channel, the naturally formed fills appear to extend down to a depth of about 5 to 10 m.

The subsurface soil condition consists of a crust comprised of reclaimed fills with blow counts between 2 and 7, but considered non liquefiable due to the large amount of fine contents, generally more than 40 percent fines. The crust is underplayed by a liquefiable sand layer comprised of liquefiable upper half with blow count of less than 15 and a non liquefiable lower half with blow count beyond 30. Underneath the sand layer there exists a clay or silt-rich deposit having a N-value varying between 10 and 30, as indicated in Figures 2-33 (a) and 2-33 (b). This clayey layer appears to be of diluvial origin and accordingly possesses high stiffness. Groundwater was 0.5 m below ground surface.

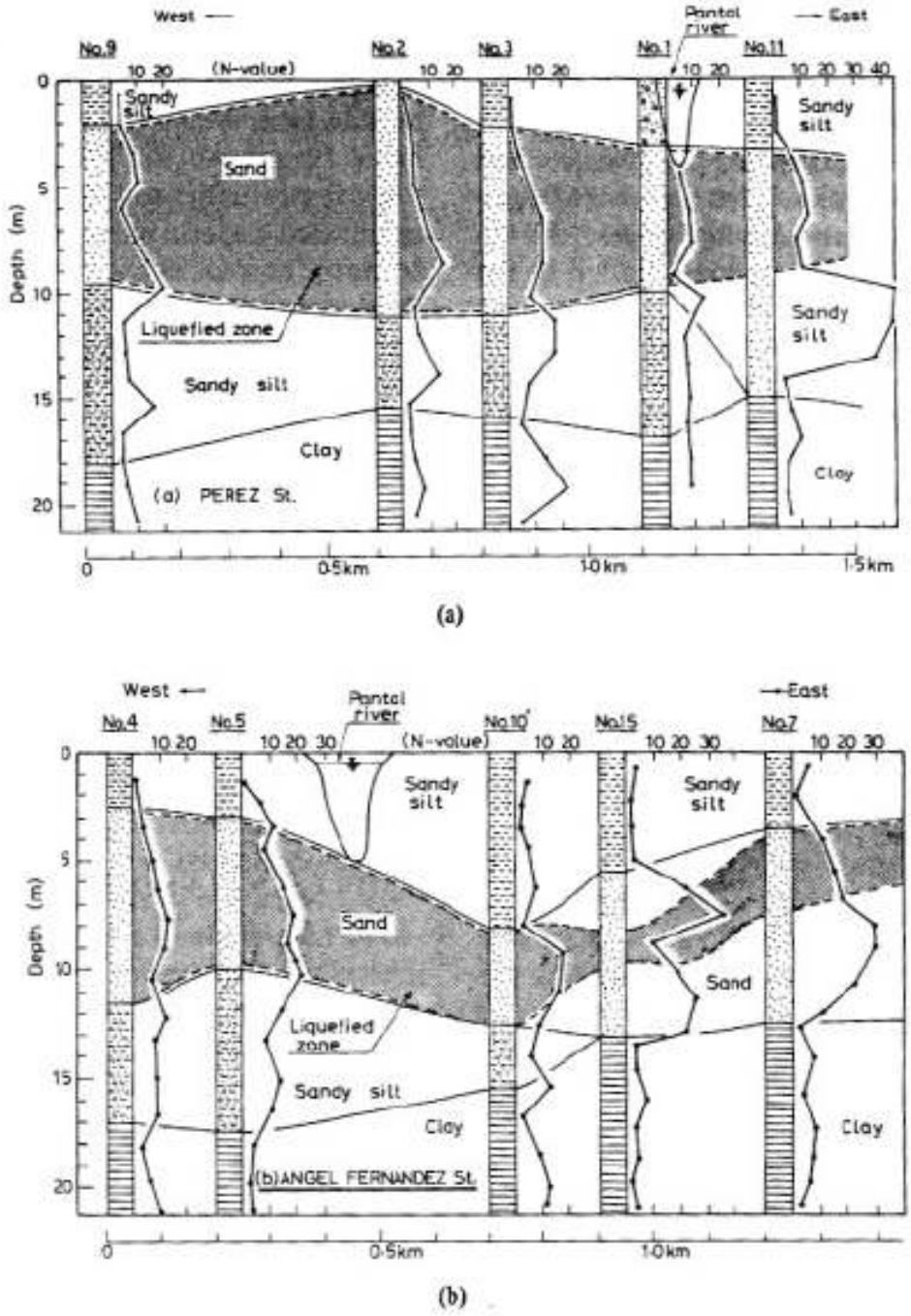

Figure 2-33: Soil Profile along Major Streets (Ishihara et al, 1993)

Large amount of lateral spreading occurred toward the Pantal River near the Magsaysay Bridge as shown in photo below (Figure 2-34), which caused severe damage.

Figure 2-34: Lateral Spreading of Right Bank which pushed the wooden house into river (Wakamatsu et al, 1991)

The Magsaysay bridge is a 7 span concrete bridge across the Pantal River. It is one of the two bridges that spanned a major river that flows through Dagupan. This route provides access to the northeast coast and to two roads to Baguio. The bridge is located on North Road in downtown Dagupan at the north edge of an eight-square-block portion of the city that sustained major damage from soil liquefaction.

The seven-span bridge was supported by six piers and the two abutments. The bridge structure was supported by concrete piles about 10 m long. There was no indication of settlement of the north abutment or of significant settlement of the soil adjacent to the abutment. Referencing piers and spans from the north side of the river, the first pier failed and was below the water line. The second pier had tilted to the north, but continued to support its ends of the second and third spans. The pier cap was over a meter wide. The third pier failed and was below the water line. The fourth span fell from the fourth pier and was resting with its roadway about 0.5 meters above the river surface. While the fourth pier did not totally fail, it was tilting to the north. The fourth, fifth and sixth piers tilted to the north. The remaining spans did not fall from their supports, the fifth and sixth piers have much smaller pier caps, but they were adequate to support their spans. The southern abutment failed and the soil adjacent to the abutment settled about a meter. Observers reported that near the south abutment, gas started coming out of soil and pavement joints and then muddy water containing sand started flowing. The approach slab was broken and separated by as much as 15 to 20 cm.

2.5. The Niigata Earthquake

The June 16, 1964 Niigata earthquake (Figure 2-35) with the moment magnitude of 7.5, occurred at 1:01 PM. The epicenter of this Japanese earthquake was located near Awa Island in the Japan Sea, 22 km off the coast with the focus 40 km deep, about

50 km from the Niigata city. In terms of human loss, twenty six people lost their lives (Auckland Regional Government, 2008).

The Niigata Earthquake caused extensive soil liquefaction in Niigata City and the surrounding areas. Many buildings and lifeline structures such as bridges suffered severe damage. The maximum acceleration recorded in the basement of a four story concrete building in Niigata City was about 160 gal., suggesting that the earthquake motion was not particularly strong and that most of the damage was caused by liquefaction rather than by ground motion. (Hamada et. al, 1986).

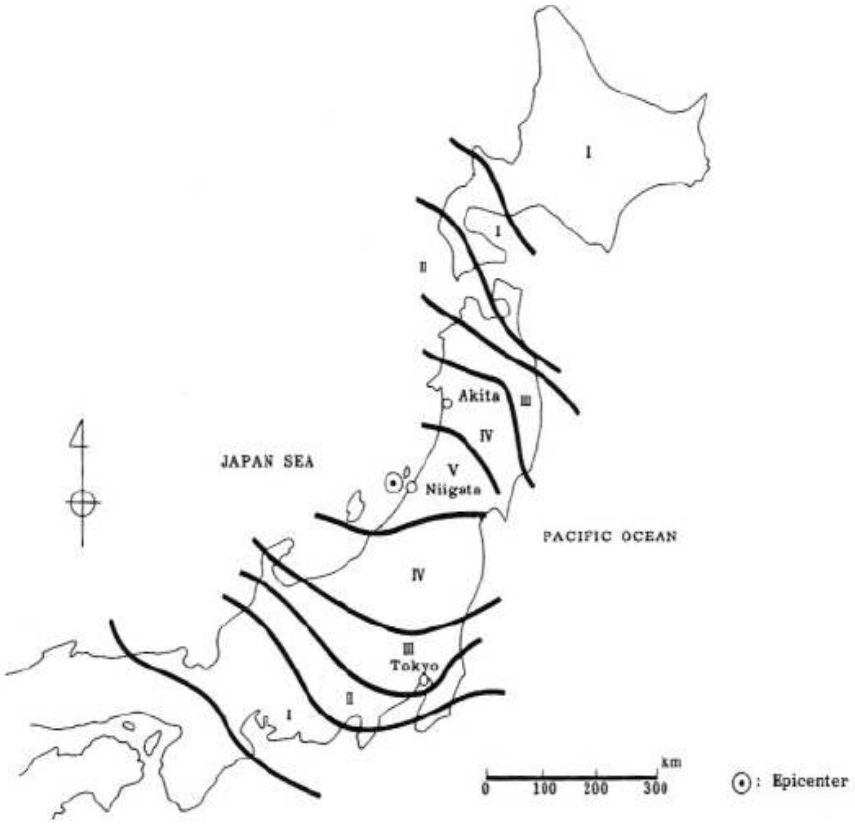

Figure 2-35: Epicenter and Seismic Intensity of 1964 Niigata Earthquake (Hamada, 1992)

Liquefaction reportedly occurred mostly in reclaimed former channels of the Shinano and Tsusen Rivers in Niigata City. Permanent ground displacement was measured by the aerial photograph survey. Figure 2-36 shows the horizontal vectors of the permanent ground displacements.

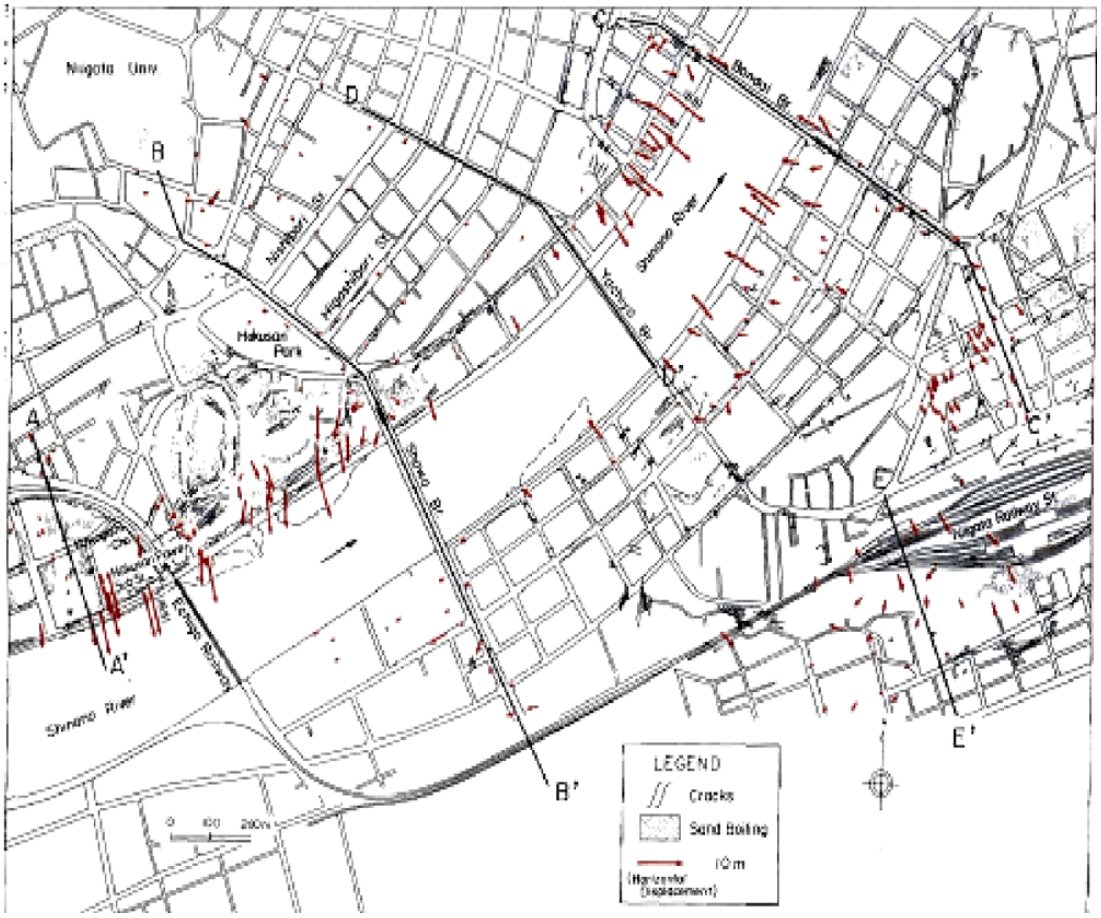

Figure 2-36: Permanent horizontal ground displacements in Niigata City during the 1964 Niigata earthquake (Hamada et. al, 1986)

Horizontal ground displacements of above 8m occurred in the area along the Shinano River toward the center of the river. It was reported that the revetment of the left bank between the Bandai Bridge and the Echigo Railway bridge, which consisted of steel sheet piles of 8m length, collapsed toward the river and the revetment line developed a zigzag shape with considerable subsidence and tilting.

2.5.1. Showa Bridge

The collapse of the Showa Bridge (Figure 2-37) was one of the worst instances of damage to structures during the Niigata earthquake.

Figure 2-37: Showa Bridge Collapse (Kramer and Elgamal, 2001)

As shown in Figure 2-38, five simple steel girders of about 28m span between piers P2 and P7 collapsed.

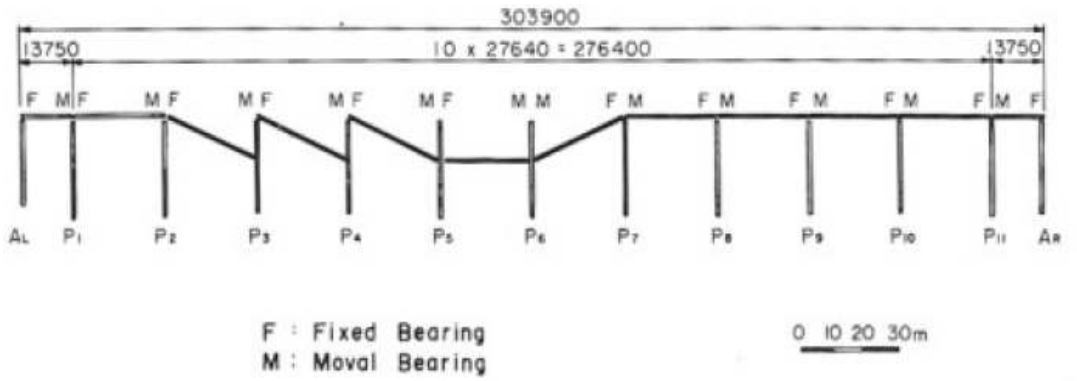

Figure 2-38: Collapse of Showa Bridge during the Niigata Earthquake (Hamada et al, 1986)

There were obvious signs that a violent collision had occurred between the girders themselves and between the girders and the abutment on the left bank. There were also signs that the bridge pier foundations on the left bank had moved toward the center of the river (Figure 2-39). In particular, pier P6 had tilted considerably toward the right bank. Such movement of the bridge pier foundations contributed to the collapse.

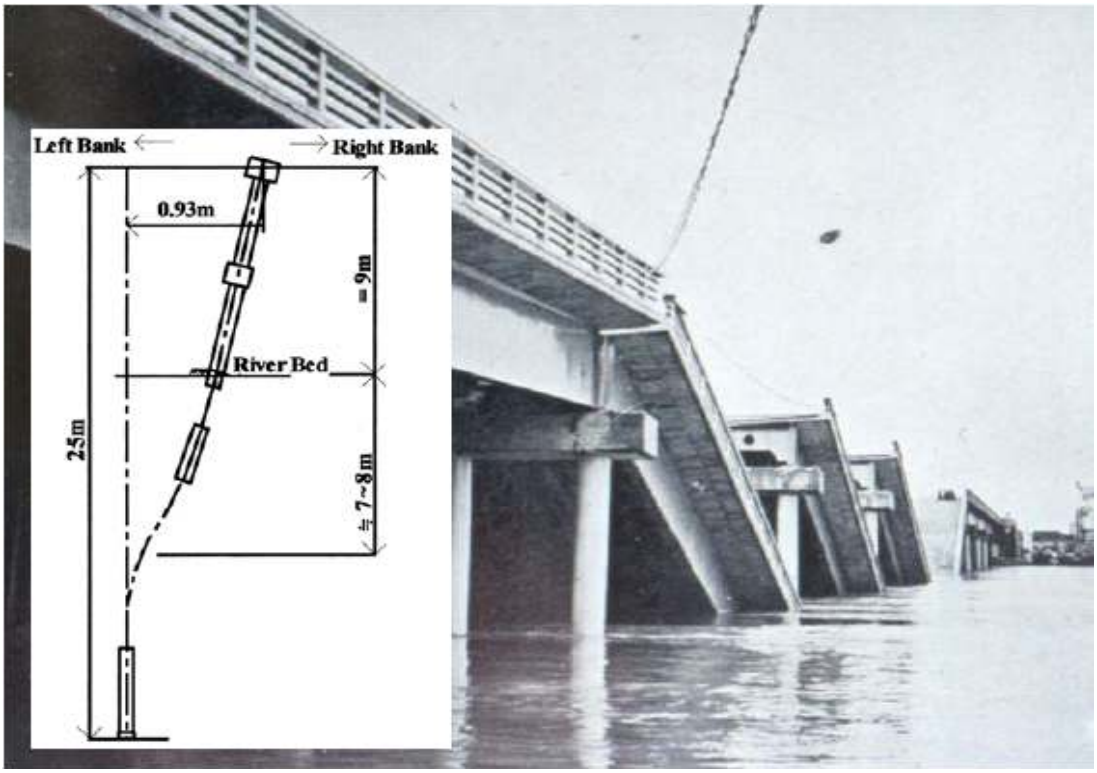

Figure 2-39: Showa Bridge Foundation's Lateral Movement (Yasuda and Berrill, 2000)

Figure 2-40 shows the deformation of the steel pipe piles of pier P4 that was extracted after the earthquake. The steel pipe piles were bent toward the right bank at a position 7 to 8 m below the river bed.

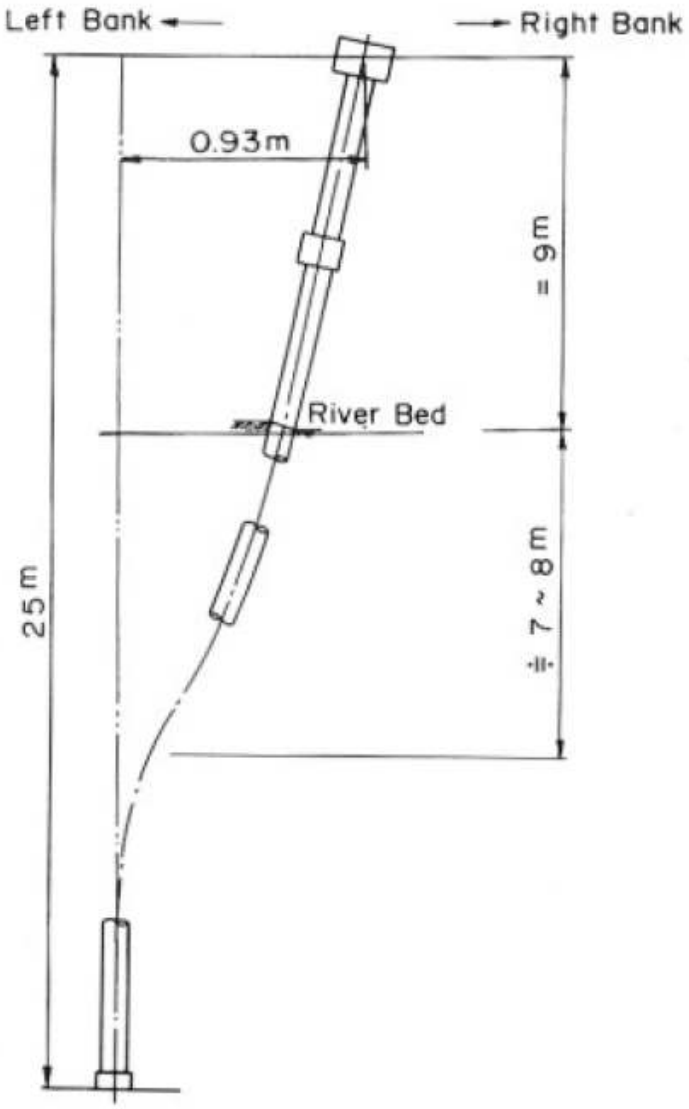

Figure 2-40: Damage to Steel Pipe Piles of Pier P4 of Showa Bridge (Hamada et. al, 1986)

The collapse of the bridge was mainly due to the lateral spread of about 10m thick layer of sand causing a large ground displacement toward the river, causing damage to the steel pipe piles of the piers. Inertia was not the primary cause of the damage since the latter did not occur during the main earthquake event, eyewitnesses

reported that the collapse occurred somewhat later. The amplitude of the ground displacement vector at the end of the access road that is near the bridge abutment, was about 2.0 m, (see Figure 2-41) and the displacement component in the direction of the bridge axis was about 1.6m.

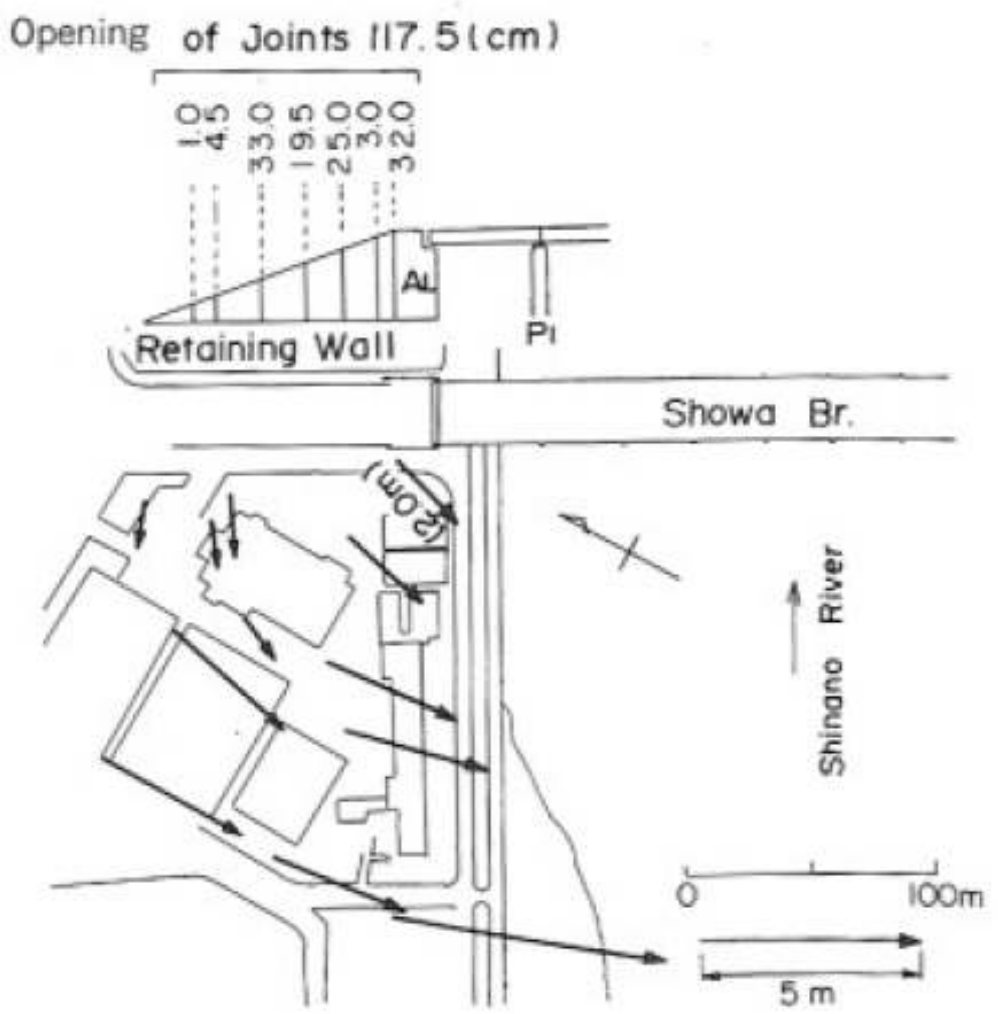

Figure 2-41: Damage to Retaining Wall of Access Road of Showa Bridge (Hamada et. al, 1986)

2.5.2. Yachiyo Bridge

The bridge consists of a fourteen (14) span, made of pre-stressed concrete slab and composite girders, approximately 304 m long and 10 m wide[1]. Its substructure was damaged during the 1964 Niigata earthquake. Figures 2-42 and 2-43 show the damage to the abutment and the piers of the Yachiyo Bridge on the left bank. The foundation of the abutment and piers P1 and P2 had been constructed of RC piles with diameter of 300 mm. The cause of the damage was the liquefaction induced lateral spread.

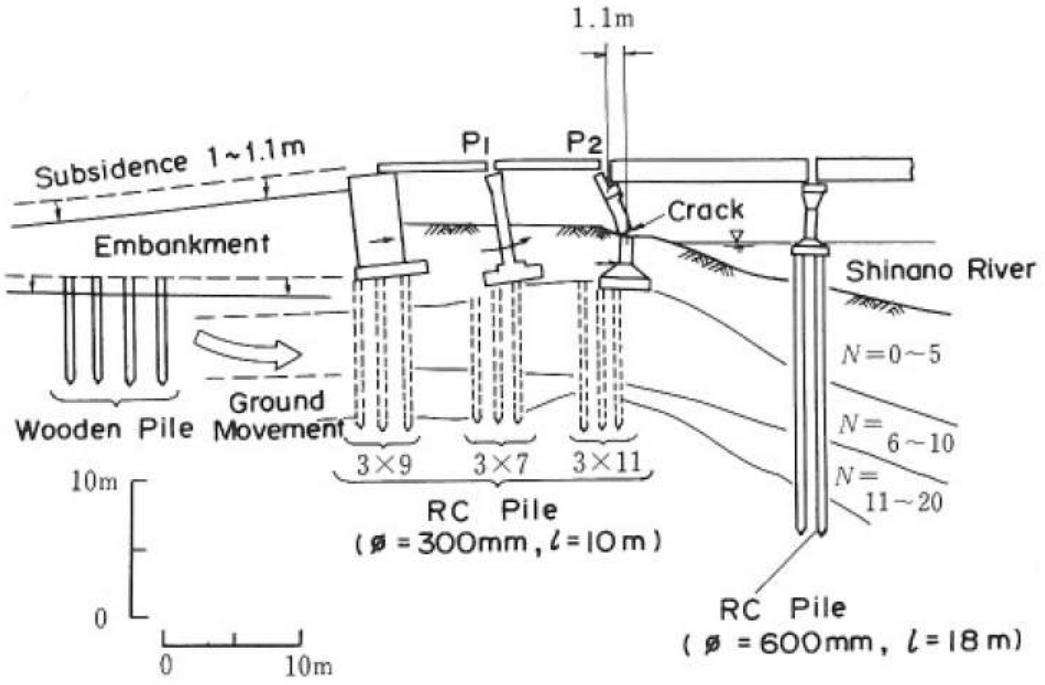

Figure 2-42: Damage to the Abutments and Piers of Yachiyo Bridge on the Left Bank (Hamada et. al, 1986)

[1] Personal communication with Dr. Takao Okada, PWRI of Japan (2008)

Figure 2-43: Damage to the Abutments and Piers of Yachiyo Bridge on the Left Bank (Hamada et. al, 1986)

Pier 2 was broken in the middle, the permanent deformation between the bridge seat center and the lower part of the pier being 1.1 m. Similar damage was reported to the abutment and the piers on the right bank. The permanent ground displacements on both banks were 2 to 4 m towards the river, causing damage to the abutments and the piers.

2.5.3. East Bridge over the Railway

The East Bridge over the railway (Hamada, 1992) was located to the east of Niigata Railway Station, at point 4 in figure 2-44 below.

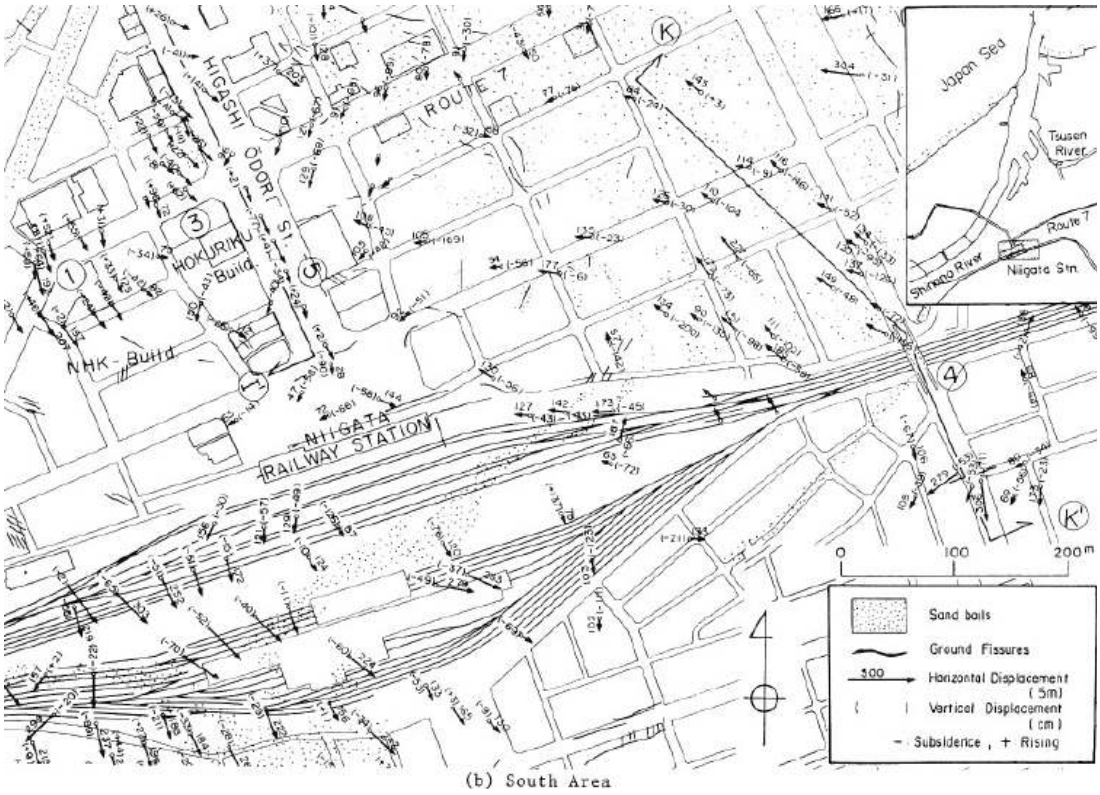

Figure 2-44: Permanent Ground Displacement at Niigata Station and its Surroundings (Hamada, 1992)

A simply supported steel girder with a span of 26.6 m fell because of the earthquake, as shown in Figure 2-45 below and crushed a locomotive. The two piers which supported the girder stood on concrete piles of diameter 30 cm and length about 7m.Cracks caused by the bending moment were found not only on the upper portion, but also towards the bottom. Cracks were caused by the liquefaction induced lateral spread and the influence of inertia was ruled out, since the cracks occurred on only one side of the piers.

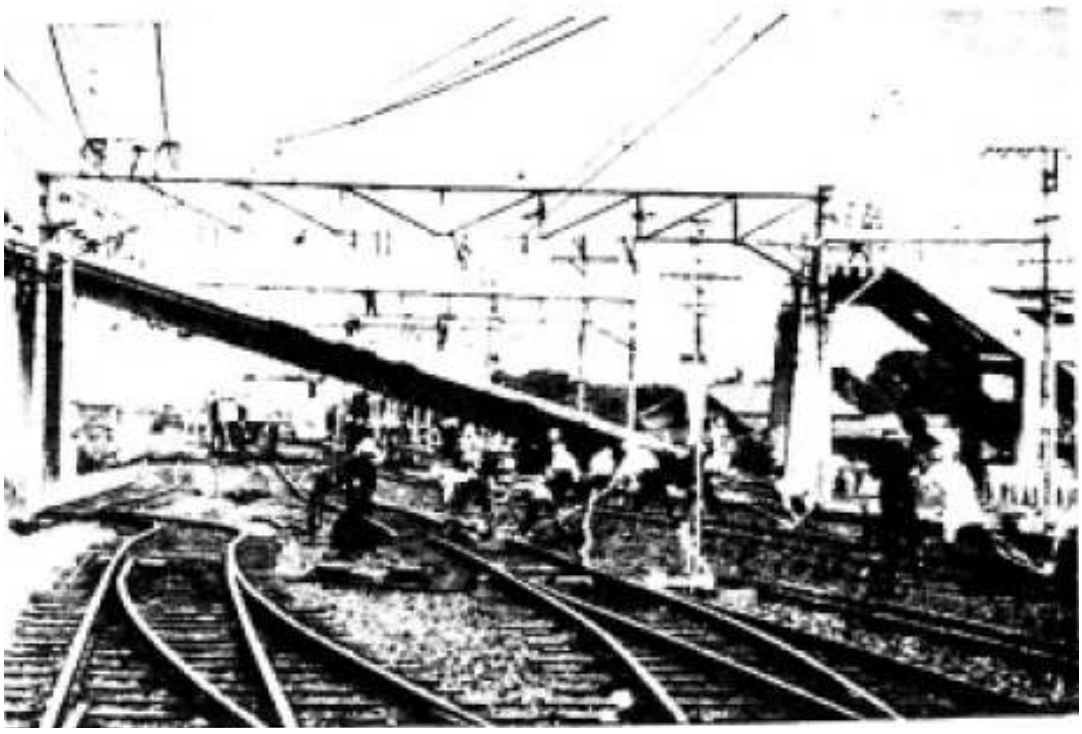

Figure 2-45: Collapse of the East Bridge over Railway (Hamada, 1986)

Figure 2-46 shows the horizontal permanent ground displacements in the area around the collapsed bridge. To the north of the bridge, the ground moved in a northwest direction, mostly parallel to the bridge axis. South of the bridge, however the ground moved in a southwest direction, perpendicular to the bridge axis. According to (Hamada, 1992) this caused a tensile strain in the ground resulting in an increase in distance between the two piers.

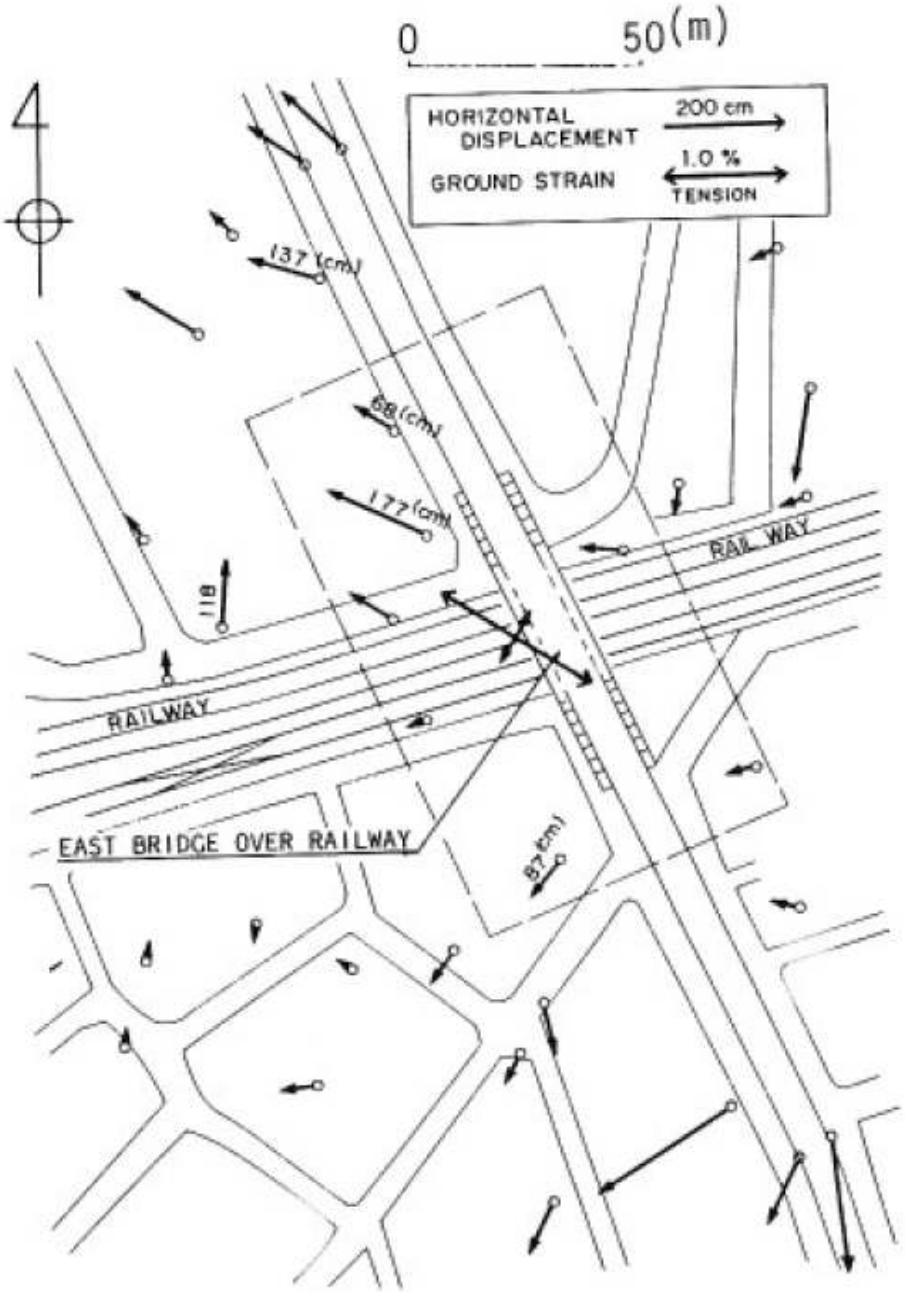

Figure 2-46: Horizontal Ground Displacement in the Vicinity of the East Bridge over Railway (Hamada, 1992)

The 1964 Niigata earthquake demonstrated that bridge structures founded on piles in liquefiable soils can be damaged due to liquefaction induced lateral spread. The damage as described in examples above did lead in some cases to the collapse of the bridge structures. The significance of the 1964 Niigata earthquake was further emphasis on the destructiveness of liquefaction induced lateral spread and the corresponding earthquake response and of bridge structures and their pile foundations.

CHAPTER 3: EVALUATION OF LIQUEFACTION INDUCED LATERAL SPREAD

The following describes the steps required for evaluation of liquefaction induced lateral spread. The first step is to assess the liquefaction potential at a given site, given the subsurface site conditions and the design earthquake magnitude. The following step is to evaluate the residual strength of the liquefied material needed to assess post liquefaction deformations. The final step is to assess the liquefaction induced lateral spread displacements. The Newmark procedure is commonly used to perform the latter step.

3.1. Liquefaction Potential Assessment

Liquefaction (Kramer, 1996) is one of the most important, interesting, complex topics in geotechnical earthquake engineering. Following devastating earthquakes of Alaska in United States and Niigata, Japan in 1964 that caused severe damage as discussed in previous chapter, liquefaction has been studied extensively.

In the 1960s and 1970s, many advances in the state of knowledge of liquefaction phenomena resulted from the pioneering work of H.B. Seed and his colleagues. The most basic procedure used in engineering practice for assessment of site liquefaction potential is that of the "Simplified Procedure" originally developed by Seed and Idriss (1971, 1982). Later refinements to the latter procedure were made by by Seed et. al (1983), Seed et al. (1985), Seed and De Alba (1986) and Seed and Harder

(1990). That procedure essentially compares the cyclic resistance ratio (CRR) [the cyclic stress ratio required to induce liquefaction for a cohesionless soil stratum at a given depth] with the earthquake-induced cyclic stress ratio (CSR) at that depth from a specified design earthquake (defined by peak ground surface acceleration and an associated earthquake moment magnitude).

Values of CRR were originally established from empirical correlations using extensive databases for sites that did or did not liquefy during past earthquakes where values of $(N_1)_{60}$ could be correlated with liquefied strata. The current version of the baseline chart defining values of CRR as a function of $(N_1)_{60}$ for moment magnitude 7.5 earthquakes is shown on Figure 3.1. The chart was established by a consensus at the 1996 NCEER workshop (Youd and Idriss, 1997). A corresponding chart documenting revised magnitude scaling factors was also developed, and is shown on Figure 3.2.

For estimating values of the earthquake-induced cyclic stress ratio, CSR, the NCEER Workshop recommended essentially no change to the original simplified procedure (Seed and Idriss,1971), where the use of a mean r_d factor defining the reduction in CSR with depth is usually adopted for routine engineering practice.

The above procedure should be regarded as the minimum requirement for evaluating site liquefaction potential, where SPT data are used as a basis for determining

liquefaction strengths. However, the use of the CPT is now recognized as one of the preferred investigation tools to estimate liquefaction strengths, especially as the database of case histories grows. It has the advantage of providing continuous data with depth, and the relatively low cost of performing multiple soundings over a site enable continuity of liquefied strata to be assessed.

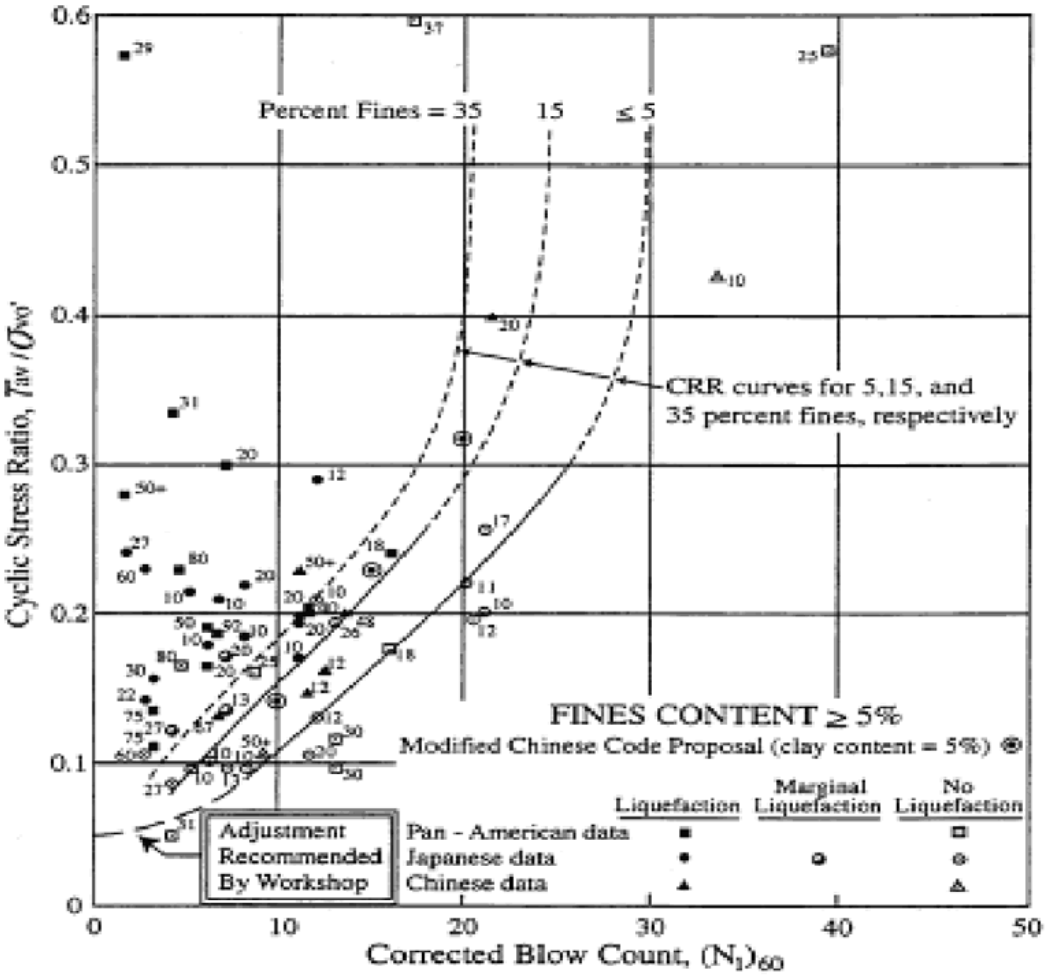

Figure 3-1: Empirical Relationship between the Cyclic Stress Ratio Initiating Liquefaction and $(N_1)_{60}$ Values for Silty Sands in M 7.5 Earthquakes (Youd and Idriss 1997; after Seed, 1979)

Figure 3-1 summarizes a very large database of case history performance, and represents the most robust basis currently available for assessment of in situ liquefaction resistance. With respect to the influence of fines content on the boundary curves shown in the figure, it has been suggested that further increases in fines content beyond about 35% results in no further changes in the relationship between CRR and $(N1)_{60}$. The trend of increased liquefaction resistance with increased fines content should not be extrapolated beyond the relationship in the figure.

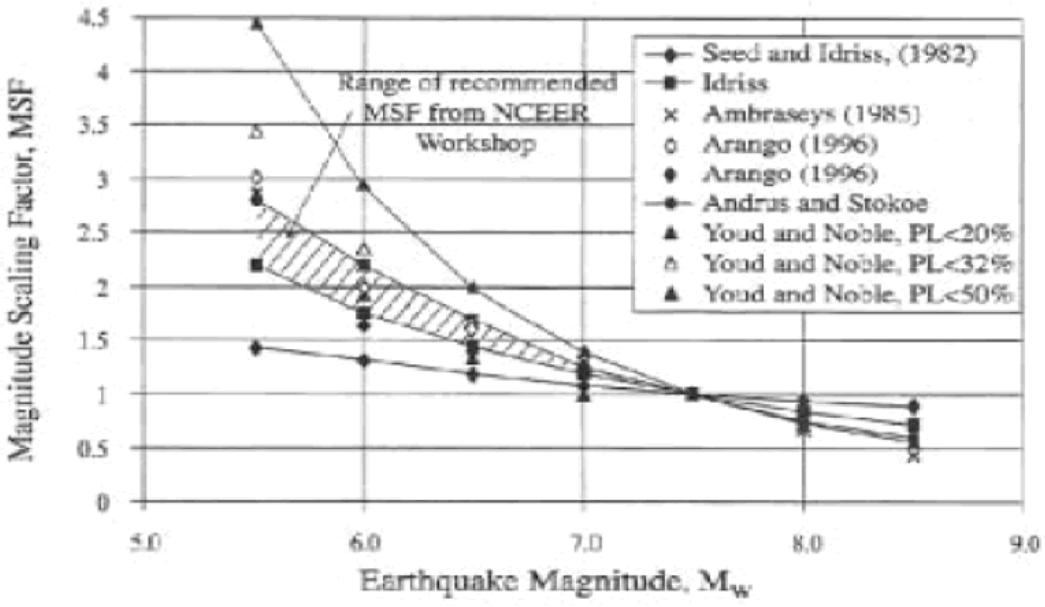

Figure 3-2: Magnitude Scaling Factors Derived by Various Investigators (Youd and Idriss 1997)

The value of CRR determined from figure 3.1 can be corrected to account for the magnitude of interest by means of the following formula:

$$\mathbf{CRR_{(M)} = CRR_{(M7.5)} (MSF)}$$

Seed and Harder (1990) suggest correcting the CRR value for two additional factors, K_σ and K_α which are used to account for the influence of soil depth and the presence of static shear stress (sloping ground condition), respectively. The factor K_σ is used to correct CRR for the effects of large overburden pressures that are typically found beneath embankments, dams and deep fills. As the overburden pressure increases, the CSR required to cause liquefaction (CSRL) effectively decreases. For liquefiable materials at shallow depths (less than 12 m) where most lateral spreads occur, the K_σ correction factor is generally near 1.0 (figure 3-3 below).

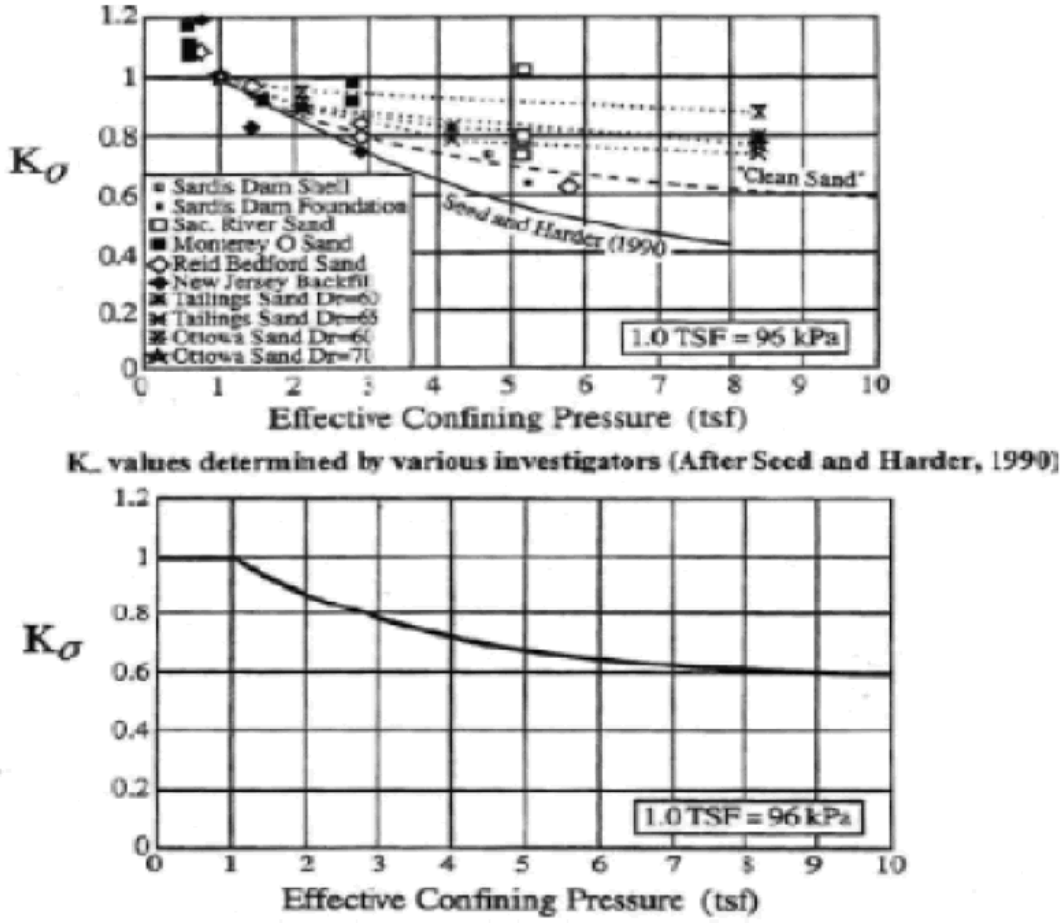

Figure 3-3: Minimum Values for K_σ Recommended for Clean Sands, Silty Sands and Gravels (Youd and Idriss 1997, after Seed and Harder 1990)

Recent recommendations pertaining to the correction factors have been summarized by Youd and Idriss (1997).

An additional correction has been proposed for the simplified liquefaction procedure. The second correction factor, K_α, is used to account for conditions other than level ground, such as the case with bridge embankments. For level ground conditions,

there are no static driving shear stresses acting on a horizontal plane in the soil. When sloping ground conditions exist, the generation of pore pressures and accumulation of shear strains under cyclic loading can be significantly affected by the presence of static driving shear stresses and must be accounted for in analysis of liquefaction resistance. Recent studies have shown that the presence of static driving shear stresses in loose, contractive soils can decrease the liquefaction resistance of the soil (Seed and Harder 1990). To account for the effects of static driving shear stresses, the following equation should be used:

$$\mathbf{CSR_{L\ (\alpha = \alpha)} = CSR_{L\ (\alpha = 0)}\ K_{\alpha}}$$

A relationship between K_{α} and α is presented in figure 3-4 below:

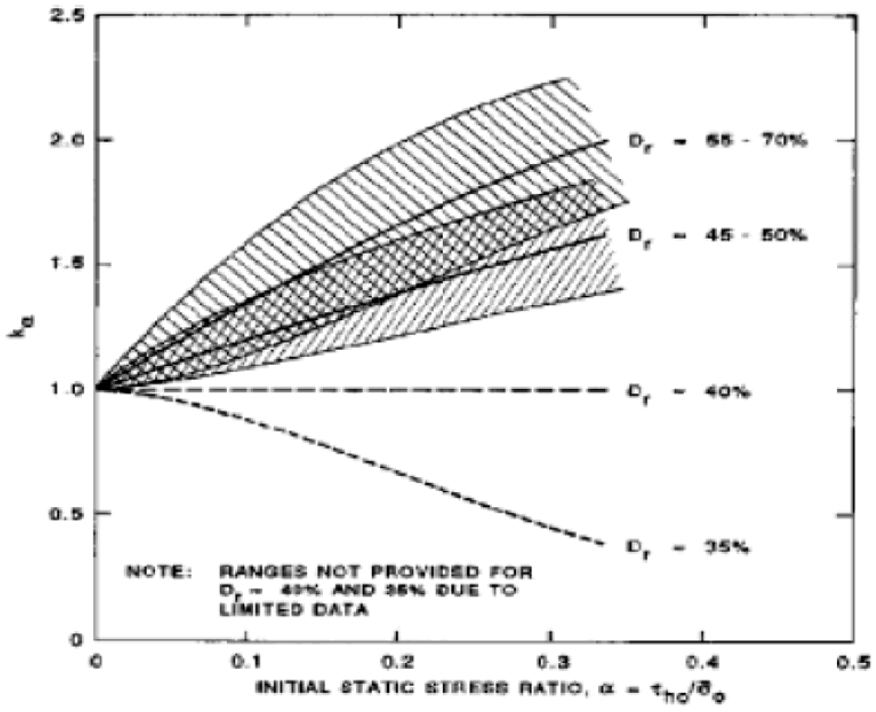

Figure 3-4: Correction Factors K_{α} for Static Shear Ratios α (Marcuson et al.1992)

This relationship has been discussed in several workshops (Youd and Idriss 1997) and the current consensus recommendation is that the use of this factor is not advisable.

As an alternative to the use of SPT N-values, CPT tip resistance (q_c) values may be used as a basis for evaluation of in situ liquefaction resistance. In the "Proceedings of the NCEER Workshop on Evaluation of Liquefaction Resistance of Soils" (Youd and Idriss 1997), workshop participants were unable to reach a consensus on a single, preferred CPT-based criterion for evaluating liquefaction resistance. Figure 3-5 shows a chart developed by Robertson and Wride (Youd and Idriss, 1997) for determining liquefaction strengths for clean sands (fines content, FC, less than or equal to 5%) from CPT data. The NCEER Workshop Proceedings provide an explicit commentary on how the new Robertson and Wride CPT procedure should be used for liquefaction evaluations.

A chart (figure 3.6), relating the cone resistance and friction ratio to the soil behavior type allows for approximate soil classification based on the normalized CPT data.

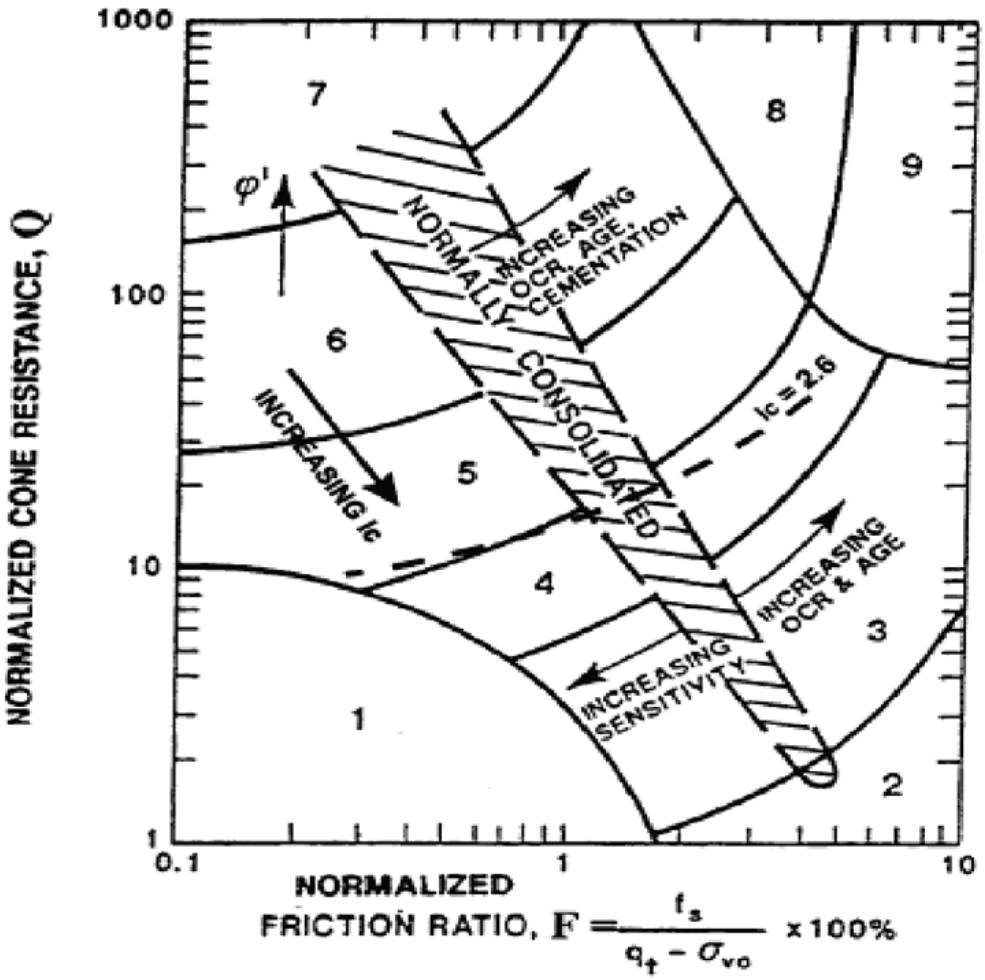

Figure 3-5: Normalized CPT Soil Behavior Type Chart (after Robertson and Wride 1997a,b)

1- Sensitive, fine grained

2- Organic soils-peats

3- Clays-silty clay to clay

4- Silt mixtures-clayey silt to silty clay

5- Sand Mixtures-silty sand to sandy silt

6- Sands-clean sand to silty sand

7- Gravelly sand to dense sand

8- Very stiff sand to clayey sand*

9- Very stiff, fine grained*

* Heavily overconsolidated or cemented

The CRR is scaled for the design-level earthquake motion(s) using the appropriate MSFs (Figure 3.2). The recommended design chart is shown in Figure 3.6, below:

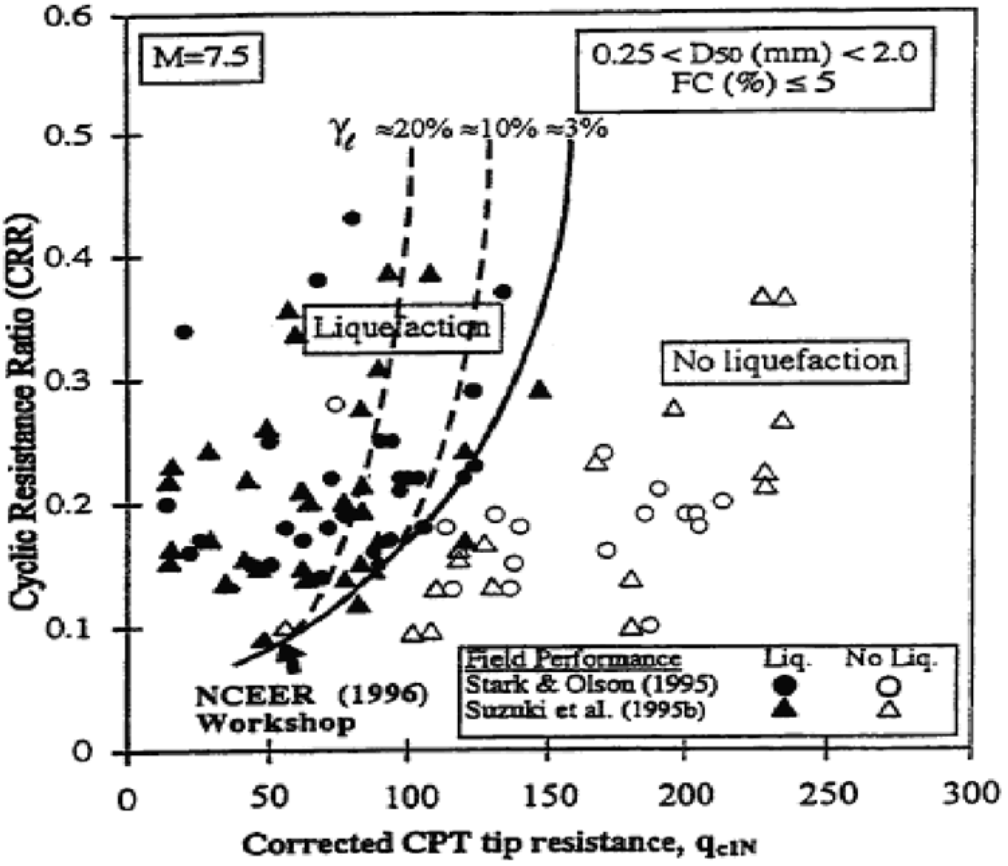

Figure 3-6: Recommended Cyclic Resistance Ratio (CRR) for Clean Sands under Level Ground Conditions Based on CPT (Robertson and Wride 1997a, b)

It should be noted that for Ic>35% (i.e. FC>35%) the soil is considered to be non-liquefiable by Robertson and Wride. They add that this general guideline should be checked using independent methods of analysis.

3.1.1. Evaluating Seismic Behavior of Plastic Fine-Grained Soils

Evaluating the seismic behavior of soil, whether sand or clay, requires addressing the potential for significant strains or strength loss that can contribute to ground deformations or instability during or following the occurrence of an earthquake.

The Chinese Criteria were described by Wang (1979) and reported by Seed and Idriss (1982) as a means for identifying fine-grained soils that might be susceptible to "liquefaction". To make the distinction between "cohesive" soils and " cohesionless" soils, the Chinese Criteria or similar index test-based criteria (e.g. Andrews and Martin 2000) should be used in conjunction with the behavior observed in consolidation tests, monotonic undrained shear strength tests, cyclic tests, and vane shear tests, for example.

Chinese criteria specify that liquefaction can only occur if all three of the following conditions are met:

1. Weight fraction smaller than 5 μm (i.e. clay fraction CF < 15%
2. Liquid limit LL < 35% and
3. Natural water content (wa) > 0.9LL

Andrews and Martin (2000) state that silty soils are susceptible to liquefaction if both LL < 32% and the amount finer than 2 μm < 10%. Recent studies summarized in Boulanger and Idriss (2006) indicate that the Chinese criteria may be unconservative in some situations, and alternative methods need to be considered.

3.2. Residual Strength of Liquefied Soil

In order to assess the seismic stability of earth structures and foundations, it is necessary to estimate the post liquefaction residual undrained shear strength (S_r) of the liquefied soil during and after seismic loading. The shear strength of liquefied soils has been an area of considerable interest over the past 20 years.

Several investigators have proposed procedures to estimate the shear strength of liquefied soils (Castro 1975, Poulos 1981, Poulos et al. 1985; Seed 1987; Seed and Harder 1990; Stark and Mesri 1992; Ishihara 1993; Konrad and Watts 1995; Fear and Robertson 1995; among others). The most widely used of these procedures in practice are those developed by Seed and Harder (1990), Stark and Mesri (1992) and Olsen and Stark (2002).

These approaches are based on evaluating the residual strength of a liquefied soil by correlation with in-situ test data, either by the comparison of in situ soil properties based on penetration resistance with residual strengths back-calculated from case histories of flow failures or estimation of undrained residual strength ratios

(undrained strength divided by the pre-earthquake vertical effective stress) back-calculated from case histories of flow failures.

These approaches are described further in Para. 3.2.2. Laboratory tests have also been used as described in Para. 3.2.1.

Note that the residual strengths for liquefied soils based on Case Histories have been back calculated from large deformation flow histories, whereas limited deformation earthquake induced lateral spreads occur as a result of a progressive racheting mechanism associated with relatively small cyclic strains. However, recent studies by Olson and Johnson (2008) back analyzing thirty nine lateral spread case histories using the Newmark sliding block methods appear to support the use of residual strengths to calculate lateral spread incremental displacements, as described in para. 3.3.

3.2.1. The Strength of Liquefied Sand from Laboratory Testing

When tested under undrained conditions at sufficiently low densities, saturated sands exhibit peak shear strength at relatively small strains, followed by a subsequent reduction in shear strength as deformations continue. This decline in strength results from the increasing pore pressures generated in response to the contractive tendency of the soil when sheared. During this period of strain, softening the strength continues to decrease until, at large strains, the deforming sand reaches a state at

which there is no further tendency for volume change. As a result, the pore pressure, effective stress, and shear strength remain constant as the sample continues to deform. This residual condition has been termed the "Steady state of deformation" (Castro 1975; Poulos 1981). Research has supported the concept that for a given material, the stresses existing at the steady state are solely a function of the deforming soil's density. Since the steady state strength has been suggested to be the minimum undrained shear strength of a contractive deposit at its in situ density (Poulos et al 1985), the steady state approach has potential applications in the analysis of seismic stability and deformations of deposits potentially subject to liquefaction. If the driving stresses within the a soil mass are less than the undrained steady-state shear strength, then the soil mass is considered not to be susceptible to liquefaction failure associated with large deformations.

There are two basic assumptions when applying the steady-state concept.

(1) the steady-state residual strength and effective stress conditions are reasonably unique functions of initial void ratio, and
(2) their relationship with initial void ratio can be evaluated by specific triaxial testing procedures.

Unfortunately, the steady state strength is very sensitive to void ratio and changes in density due to sampling, handling, and consolidation in the laboratory. Therefore, minor variations in material and procedure have large impacts on the test results.

Correction factors, which require a great deal of engineering judgment, must be applied to strengths measured directly upon undisturbed samples. The steady state analysis method, including the correction procedures and factors affecting post-liquefaction strength assessments, are provided by Poulos and others (1985) and Seed and Jong (1987).

Laboratory tests have been used to estimate undrained strength ratios for sands and silty sands (Ishihara 1993, 1996; Baziar and Dobry 1995; Amini and Qi 2000). These studies provide valuable summaries of available data and demonstrate that undrained strength ratios obtained in the laboratory for loose sands and silty sands (Sr/σ_c' ~%0.1 to 0.2, where σ_c' is the effective consolidation stress) compare favorably with the values back-calculated from case histories of ground failure. The influence of the plasticity index on this relationship is shown in Figure 3-7 below.

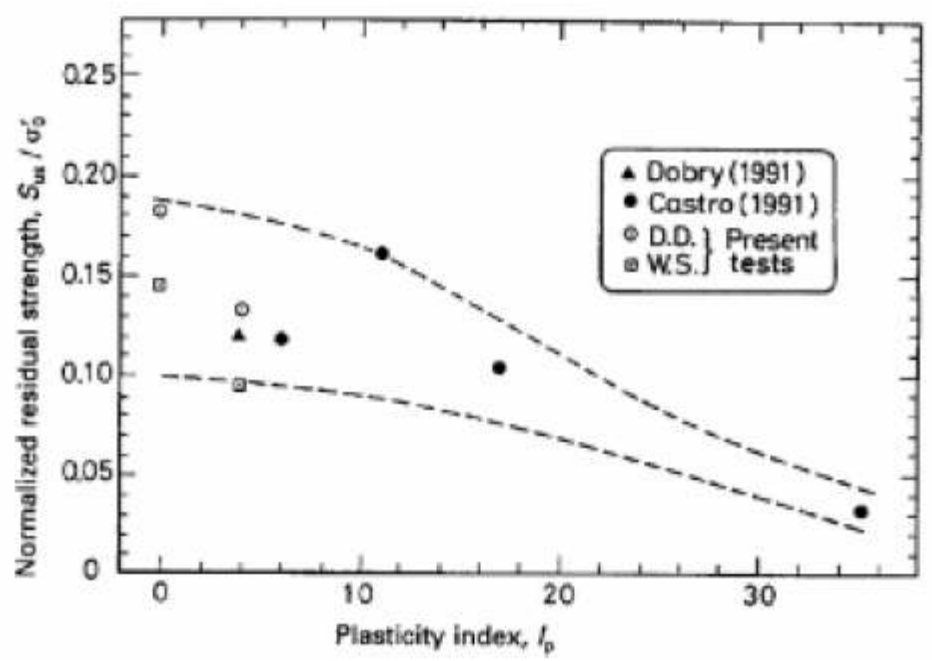

Figure 3-7: Normalized Residual Strength Plotted Against Plasticity Index (Ishihara 1996)

The post-liquefaction strength of silty soils has been investigated in the laboratory by cyclically loading the soil until ru = 100%, then monotonically loading the soil undrained. It is interesting to note that numerous investigators have found that liquefied silty sands and silts are dilative when sheared following liquefaction (Stark et al 1997, Boulanger et al 1998, Dickenson et al 2000). This behavior indicates that once the soil liquefies, large strain can be mobilized at sloping sites and at large strain the strength of the soil increases. This scenario assumes that the loading is fully undrained. In light of the limitations associated with sampling cohesionless soils and laboratory testing of the post-liquefaction behavior of soil, it is not recommended that the strength gain due to dilation be incorporated into design.

3.2.2. The Strength of Liquefied Sand from In-Situ Test Data

Recognizing the difficulties associated with laboratory testing of cohesionless soil, alternative methods have been proposed for evaluating the residual shear strength of a fully liquefied deposit. Two procedures that are commonly used are:

1) residual strength ratio methods (Stark and Mesri 1992; Baziar and Dobry 1995); and Olsen and Stark (2002).
2) a procedure which is independent of the in situ vertical effective stress (Seed and Harder 1990).

3.2.2.1. Baziar & Dobry (1995)

The relationship between SPT data, $(N_1)_{60}$ and residual shear strength (Sr) with vertical effective overburden pressure (σ_{vo}') for silty soil deposits developed by Baziar and Dobry (1995) is shown in Figures 3-8(a)(b) below.

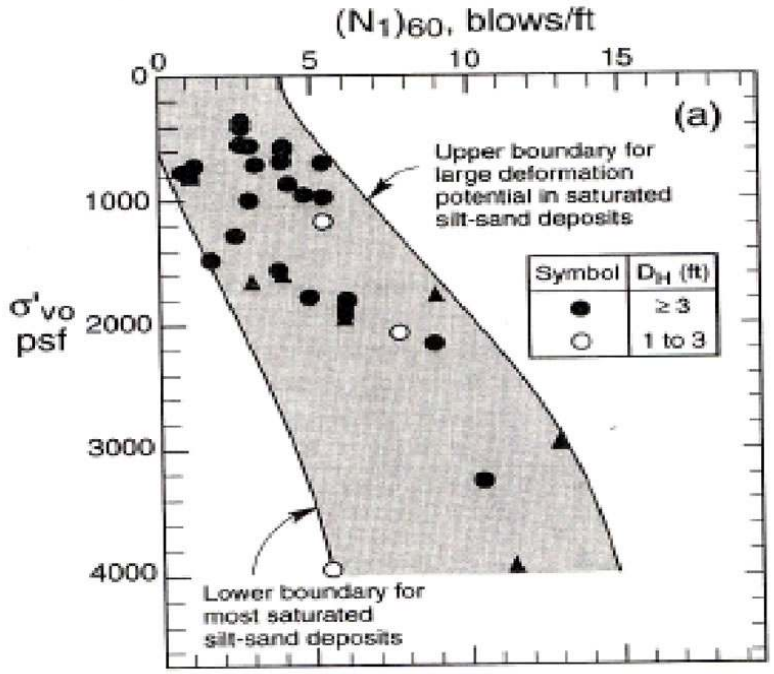

Figure 3-8(a): Chart Relating Normalized Standard Penetration Resistance $(N_1)_{60}$ (Baziar and Dobry, 1995)

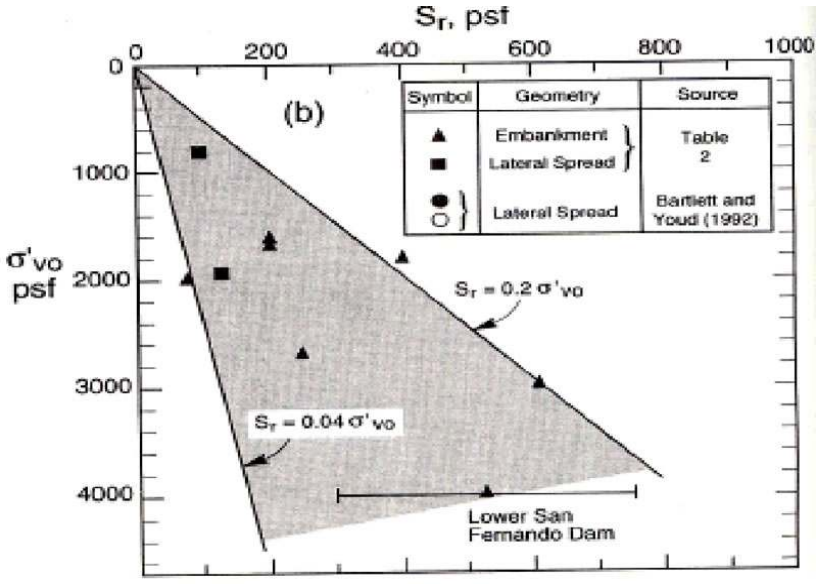

Figure 3-8 (b): Chart Relating Residual Shear Strength S_r to Vertical Effective Overburden Pressure σ_{vo}', for Saturated Non-gravelly Silt-Sand Deposits that have Experienced Large Deformations (Baziar and Dobry, 1995)

The curves were developed from the back-calculation of residual sand shear strengths from case studies where liquefaction flow failures had occurred. Nearly all of the case histories were selected based on previous work by Stark and Mesri (1992). The evaluation procedure developed by Baziar and Dobry is based on the use of the SPT to evaluate the potential for large deformations during earthquakes in saturated loose sandy silt and silty sand deposits and slopes. The method is based on laboratory tests and case histories corresponding to earthquakes of less than Mw 8.0 Charts relating the normalized standard penetration resistance and residual shear strength to vertical effective overburden pressure have been developed for use as screening tools in liquefaction hazard evaluations. (figure 3-8)

Figure 3-8 can be used to evaluate the large ground deformation potential during earthquakes due to shearing of saturated, non-gravelly silt-sand deposits having at least 10% fines. The figure is applicable to slopes, embankments, and level or almost level sites prone to lateral spreading. Figure 3-8(a) suggests that silty soils with a measured $(N_1)_{60}$ versus σ_{vo}' profile plotting to the right of the chart cannot experience flow failure due to their dilative behavior, and that lateral spreading generally cannot experience flow failure due their dilative behavior, and that lateral spreading generally cannot exceed 0.3 to 1.0 m (1 to 3 ft) for earthquakes of less than Mw 8.0. Figure 3-8(b) indicates that for silty deposits that have experienced large deformations or flow failures, the Sr/ σ_{vo}' ranges from about 0.04 to 0.20. The average value of Sr/ σ_{vo}' is 0.12.

3.2.2.2. Stark & Mesri (1992)

Similar to Baziar and Dobry, Stark and Mesri (1992) related the normalized clean sand blow count value, $(N_1)_{60cs}$ to the residual undrained critical strength ratio for magnitude 7.5 earthquakes. As illustrated in figure 3-9 below, the post-liquefaction strength of the soil is provided for two conditions: the yield strength and the critical strength. The steeper curve represents the yield, or mobilized undrained shear strength. The flatter curve represents the critical undrained shear strength curve. Stark and Mesri recommend that the yield curve be used only for cases where the post-cyclic shearing is drained. If the drainage conditions cannot be verified, the critical undrained shear strength curve should be used. The relationship derived for the undrained critical strength on the basis of case history data is provided in Equation below:

Undrained critical strength / initial vertical effective stress = 0.0055 $(N_1)_{60\text{-}CS}$

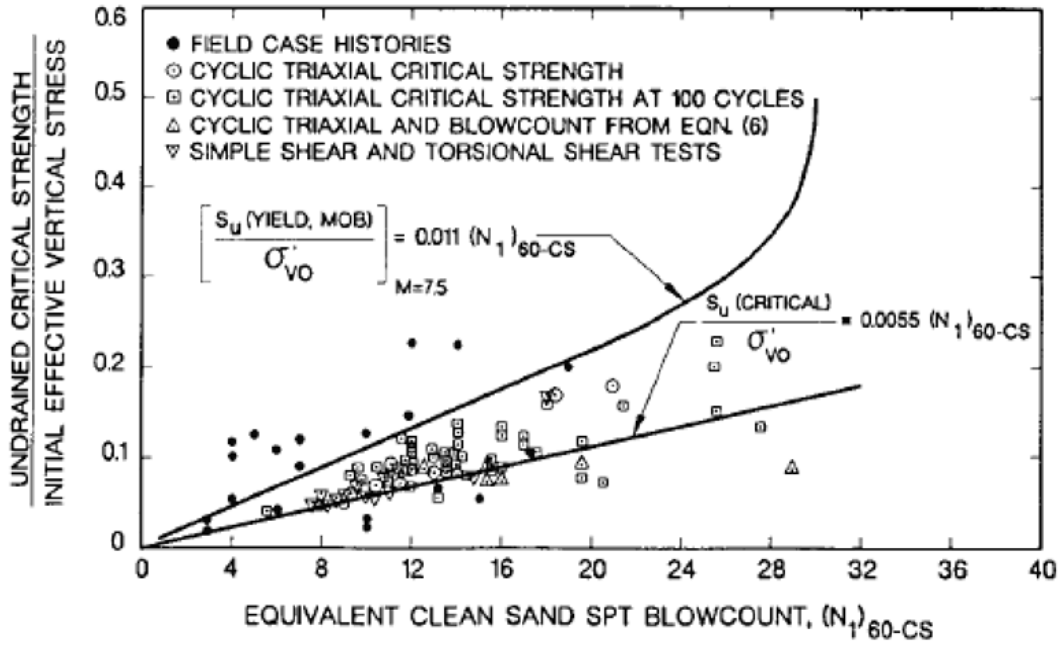

Figure 3-9: Undrained Critical Strength Ratio versus Equivalent Clean Sand Blow Count (Stark and Mesri, 1992)

It should be noted that the $(N_1)_{60\text{-}CS}$ used in the residual undrained shear strength evaluation is not the same as the fines corrected penetration resistance used in the liquefaction triggering analyses. The $(N_1)_{60\text{-}CS}$ is calculated using the data from Figure 3-10 and Equation below.

$$\mathbf{(N_1)_{60\text{-}CS} = (N_1)_{60} + N_{corr}}$$

% FINES	N_{corr} (blows / 30 cm)
0	0.0
10	2.5
15	4.0
20	5.0
25	6.0
30	6.5
35+	7.0

Figure 3-10: Recommended Fines Correction for Estimating of Residual Undrained Strength (Stark and Mesri, 1992)

For the sake of comparison, the yield strength curve developed by Stark and Mesri provides residual strengths that are in good agreement with the results of the work by Baziar and Dobry (1995) and Ishihara (1996).

3.2.2.3. Olson & Stark (2002)

The liquefied shear strength: S_u(LIQ) is the shear strength mobilized at large deformations after liquefaction is triggered in saturated, contractive, sandy soils. (Olson &Stark, 2002). The shear strength of liquefied soil, S_u(LIQ) mobilizing during a liquefaction flow failure is normalized with respect to the vertical effective stress (σ_{vo}') prior to failure to evaluate the liquefied strength ratio, S_u(LIQ)/ (σ_{vo}'). Liquefied strength ratios mobilized during 33 cases of liquefaction flow failure are estimated using a procedure developed to directly back-analyze the liquefied strength ratio. Using liquefied strength ratios back-calculated from case histories,

relationships between liquefied strength ratio and normalized standard penetration test blow count and cone penetration test tip resistance are proposed. These relationships indicate approximately linear correlations between liquefied strength ratio and penetration resistance up to values of q_{c1} and $(N_1)_{60}$ of 6.5 Mpa. and 12 blows/ft (i.e., blows/0.3 m), respectively. Figure 3-11 below, presents the "best estimate" liquefied strength ratios and mean q_{c1} values for each of the cases.

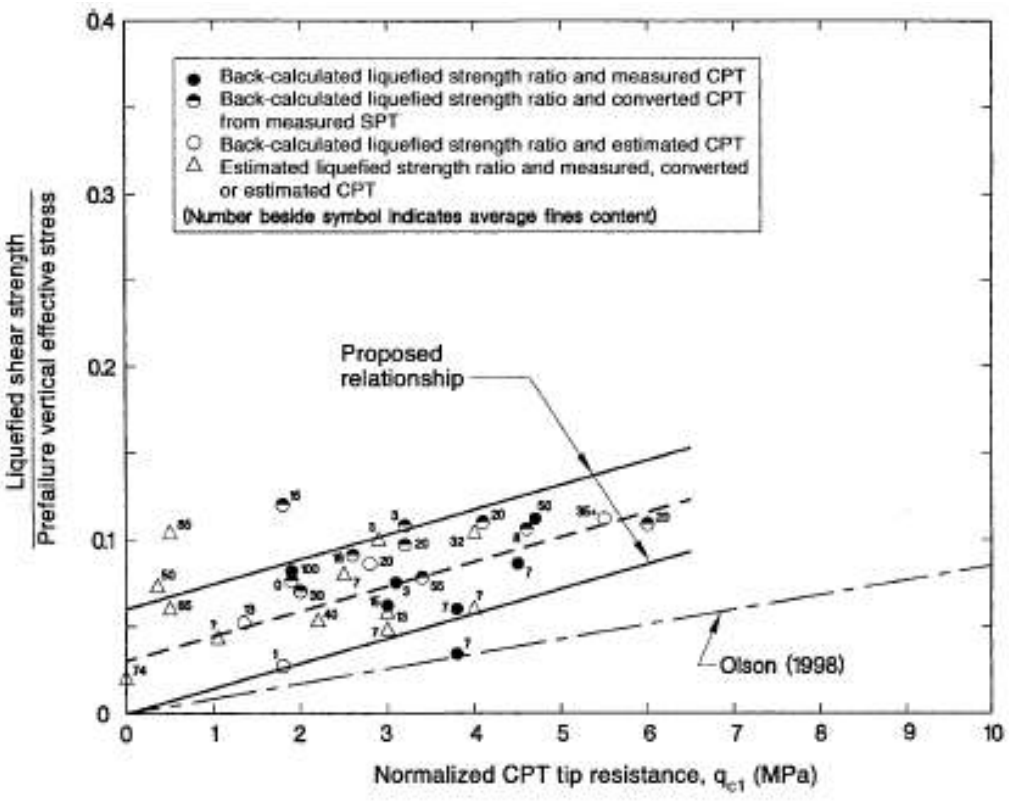

Figure 3-11: A Comparison of Liquefied Strength Ratio Relationships Based on Normalized CPT Tip Resistance (Olson and Stark, 2002)

3.2.2.4. Seed & Harder (1990)

Drawing from the original procedure developed by Seed (1987), Seed and Harder (1990) analyzed a number of case studies where liquefaction-induced flow had occurred and established a correlation between equivalent clean sand blow count, $(N_1)_{60\text{-}CS}$ and back-calculated residual shear strength (figure 3-12) below. The calculated values of $(N_1)_{60\text{-}CS}$ are slightly different than that of Stark and Mesri because of the different fines content correction recommended by Seed and Harder (Figure 3-13)

The residual strength values obtained by the Seed and Harder relationship are typically more conservative than those from Stark and Mesri, even when using the curve bounding the upper limit of the data in Figure 3-12.

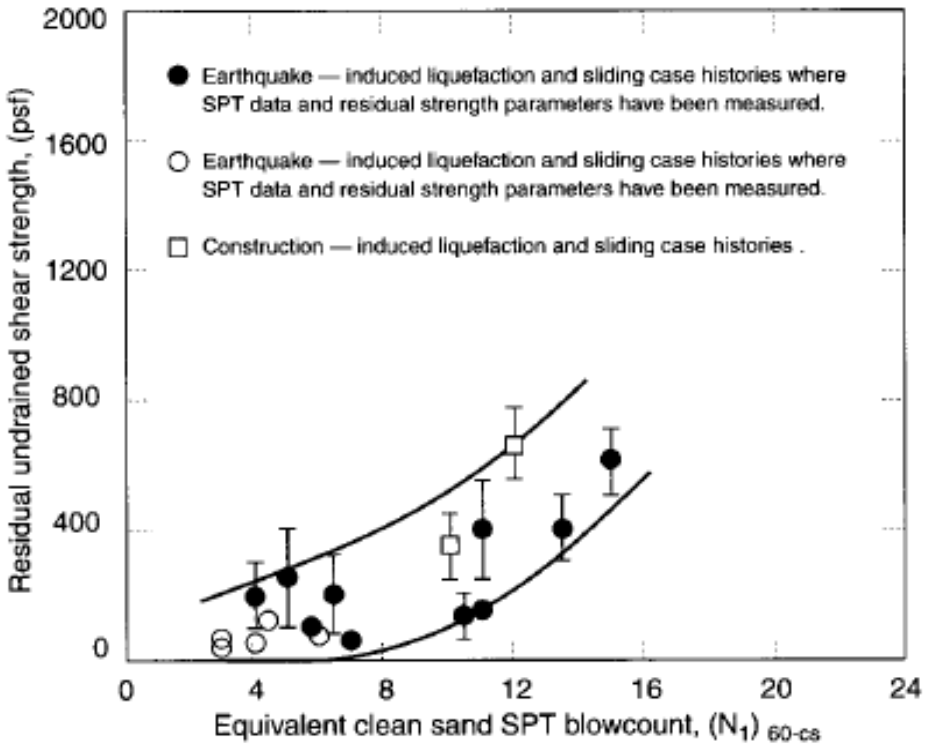

Figure 3-12: Relationship between Residual Strength and Corrected SPT Resistance (Seed and Harder, 1990)

% FINES	N_{corr} (blows/30 cm)
10	1.0
25	2.0
50	4.0
75	5.0

Figure 3-13: Recommended Fines Correction for Estimation of Residual Undrained Strength

3.3. Newmark Sliding Block Analysis

The pseudo-static method of slope stability analysis, like all limit equilibrium methods, provides an stability index (the factor of safety) but no information on deformations associated with slope failure. Since the serviceability of a slope after an earthquake is controlled by deformations, analyses that predict slope displacements provide a more useful indication of seismic slope stability. Since earthquake-induced accelerations vary with time, the pseudo-static factor of safety will vary throughout an earthquake. If the initial forces acting on a potential failure mass become large enough that the total (static plus dynamic) driving forces exceed the available resisting forces, the factor of safety will drop below 1.0. Newmark (1965) considered the behavior of a slope under such conditions. When the factor of safety is less than 1.0, the potential failure mass is no longer in equilibrium; consequently, it will be accelerated by the unbalanced force. The situation is analogous to that of a block resting on an inclined plane as shown in Figure 3-14. (Kramer, 1996)

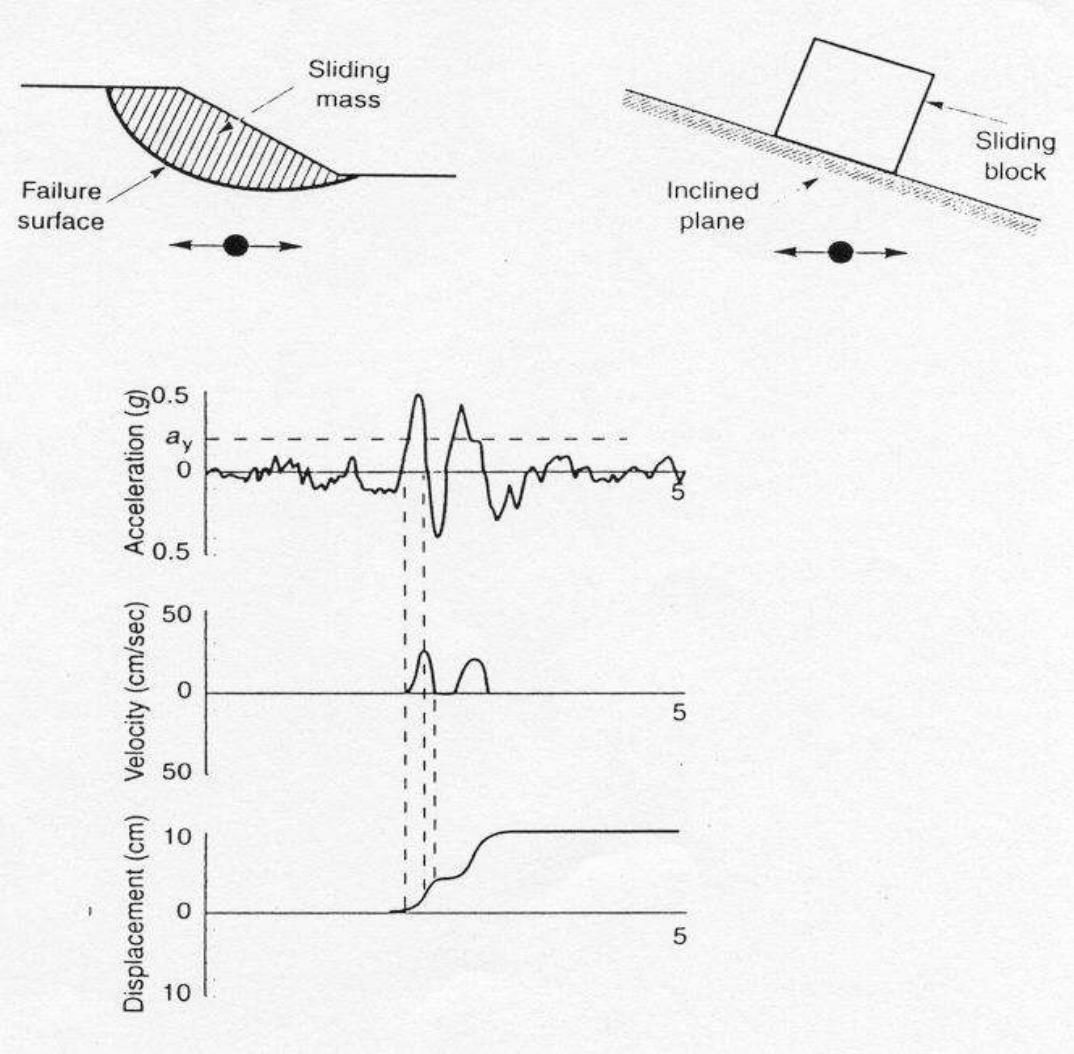

Figure 3-14: Newmark Analogy (Kramer, 1996)

Newmark used this analogy to develop a method for prediction of the permanent displacement of a slope subjected to any ground motion.

Consider the block in stable, static equilibrium on the inclined place of Figure 3-15b. Under static conditions, equilibrium of the block (in the direction parallel to the

plane) requires that the available static resisting force, Rs, exceed the static driving force, Ds (Figure 3-15a).

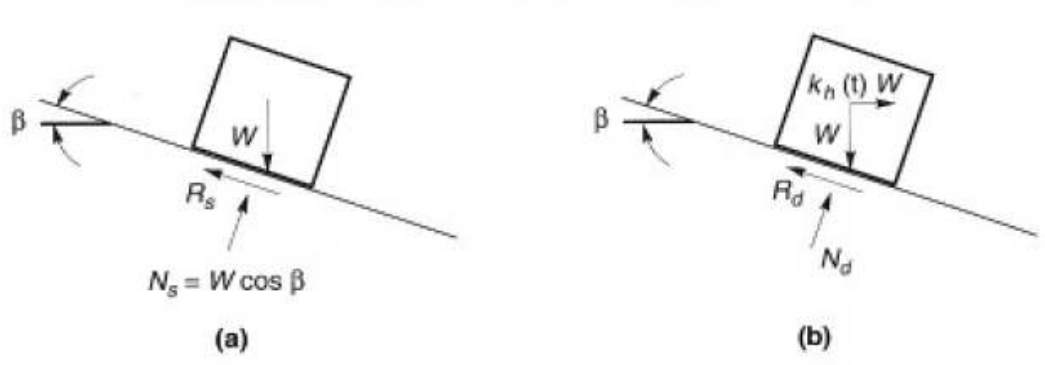

Figure 3-15: Forces Acting on a Block Resting on an Inclined Plane (a) Static Conditions (b) Dynamic Conditions (Kramer, 1996)

Assuming that the block's resistance to sliding is purely frictional (c=0), where phi is the angle of friction between the block and the plane. Now consider the effect if inertial forces transmitted to the block by horizontal vibration of the inclined plane with acceleration, $a_h(t) = k_h(t)g$ (the effects of vertical accelerations will be neglected for simplicity). At a particular instant of time, horizontal acceleration of the block will induce a horizontal inertial force, k_hW (figure 3-15b). When the inertial force acts in the down slope direction, resolving forces perpendicular to the inclined plane gives $FS_d(t)$ = available resisting force/ pseudostatic driving force = $R_d(t) / D_d(t) = [\cos \beta - k_h(t) \sin\beta] \tan \Phi / [\sin\beta + k_h(t) \cos\beta]$

Obviously, the dynamic factor of safety decreases as k_h, increases and there will be (for a statically stable block) some positive value of k_h that will produce a factor of safety of 1.0 (figure 3-16)

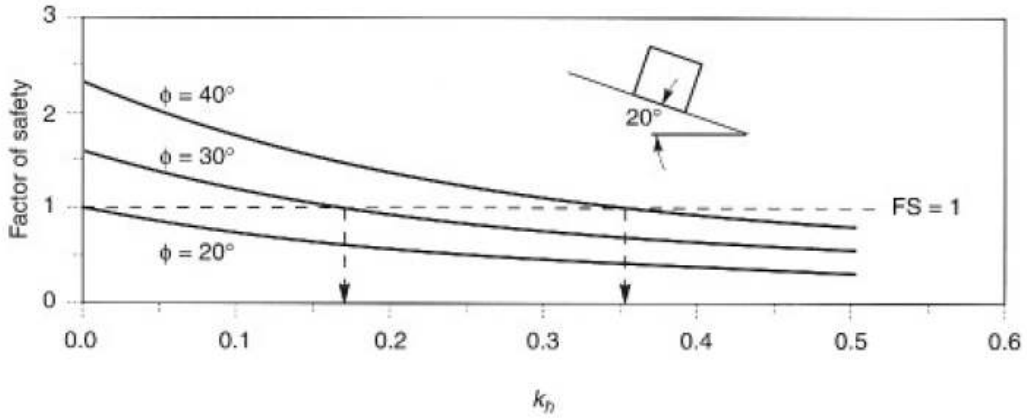

Figure 3-16: Variation of pseudo-static factor of safety with horizontal pseudo-static coefficient for block on plane inclined at 20 degree. For ϕ = 20 degree, block is at the point of failure (FS=1) under static conditions, so the yield coefficient is zero. For ϕ = 30 degree and ϕ = 40 degree, yield coefficients are 0.17 and 0.36 respectively. (Kramer, 1996)

This coefficient, termed the yield coefficient, k_y, corresponds to the yield acceleration, $a_y = k_y g$. The yield acceleration is the minimum pseudo-static acceleration required to produce instability of the block, for the block of Figure 3-15, for sliding in the down slope direction.

$$k_y = \tan (\Phi - \beta)$$

Obviously, the sliding block model will predict zero permanent slope displacement if earthquake-induced accelerations never exceed the yield acceleration (ay/amax.1.0) as illustrated in Figure 3-17.

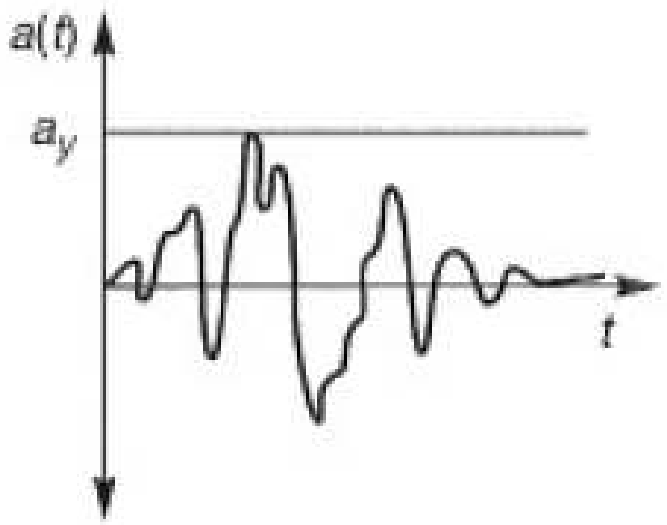

Figure 3-17: Zero Displacement for a_y/a_{max} =1 (Kramer, 1996)

Since the permanent displacement is obtained by double integration of the excess acceleration, the computed displacements for a slope with a relatively low yield acceleration (small a_y/a_{max}) will be greater than that of a slope with a higher yield acceleration (Figure 3-18a,b).

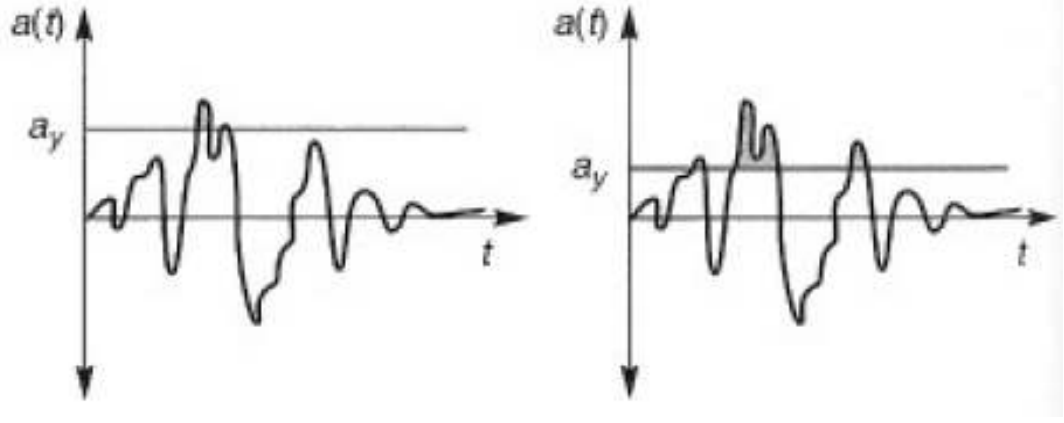

Figure 3-18 (a,b): Computed Displacement for relatively high and low yield acceleration (Kramer, 1996)

The relationship between slope displacement and a_y/a_{max} has been investigated by a number of researchers.

Newmark (1965) related single-pulse slope displacement to peak base velocity, νmax by

$$d_{rel} = (v^2_{max} / 2a_y) ((1- a_y)/A)$$

Analysis of several earthquake motions normalized to peak accelerations of 0.5g and peak velocities of 30in/sec (76cm/sec) suggested that the effective number of pulses in an earthquake motion could be approximated by A/a_y. Newmark found that a reasonable upper bound to the permanent displacements produced by these earthquake motions was given by

$$d_{max} = (v^2_{max} / 2a_y) (a_{max} / a_y)$$

Where $a_y/a_{max} > 0.17$.

Figure 3-19 depicts the Chart by WES.

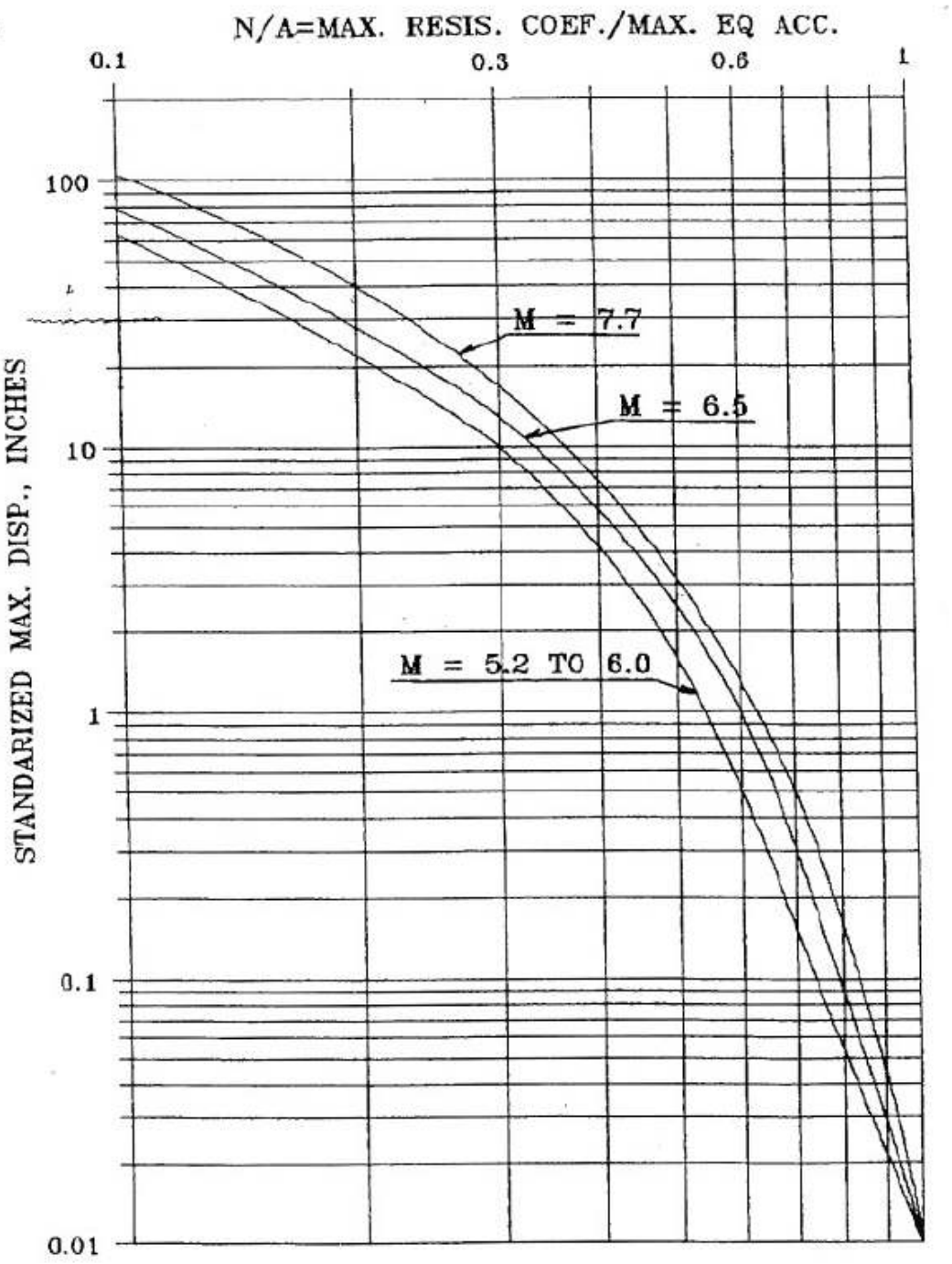

Figure 3-19: Mean Permanent Displacement For Different Magnitudes of Erathquakes (Soil Sites). (WES)

Charts have been developed by number of individuals (Franklin and Chang, 1977); Hynes and Franklin (1984); Wong and Whitman, 1982; and Martin and Qiu, 1994) using large databases of earthquake records and the Newmark Time History Analysis method. These charts allow deformations during seismic loading to be estimated using relationships between the acceleration ratio (i.e., ratio of yield acceleration (k_y) to the peak ground acceleration (k_{max}) occurring at the base of the sliding mass) to ground displacement. The Martin and Qiu charts (recommended in the (NCHRP 12-49, 2002) document) includes peak ground acceleration and peak ground velocity as additional regression parameters, resulting in the displacement equation:

$$d = 6.82 \, (k_y/k_{max})^{-0.55} \, (1-k_y/k_{max})^{5.08} \, A^{-0.86} \, V^{1.66}$$

where A is in in/sec^2 and V is in in/sec. Martin and Qiu note that magnitude was not a statistically significant parameter for the range of magnitudes (M6 to M7.5) used in their evaluation. The following figures 3-20 and 3-21 depicts the Martin and Qiu Charts for two values of peak ground velocity.

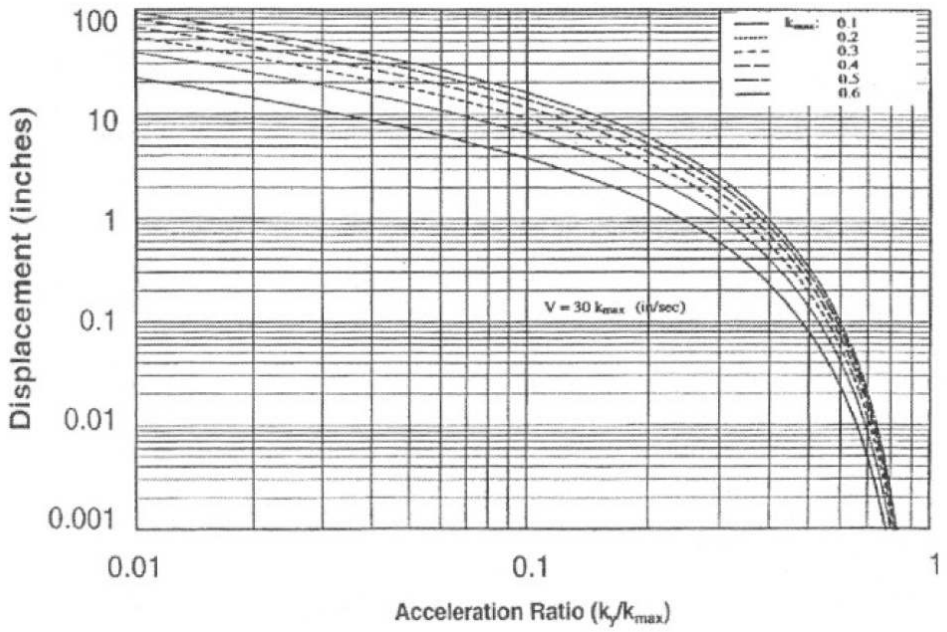

Figure 3-20: Simplified Displacement Chart for velocity-acceleration ratio of 30 (Martin and Qiu, 1994)

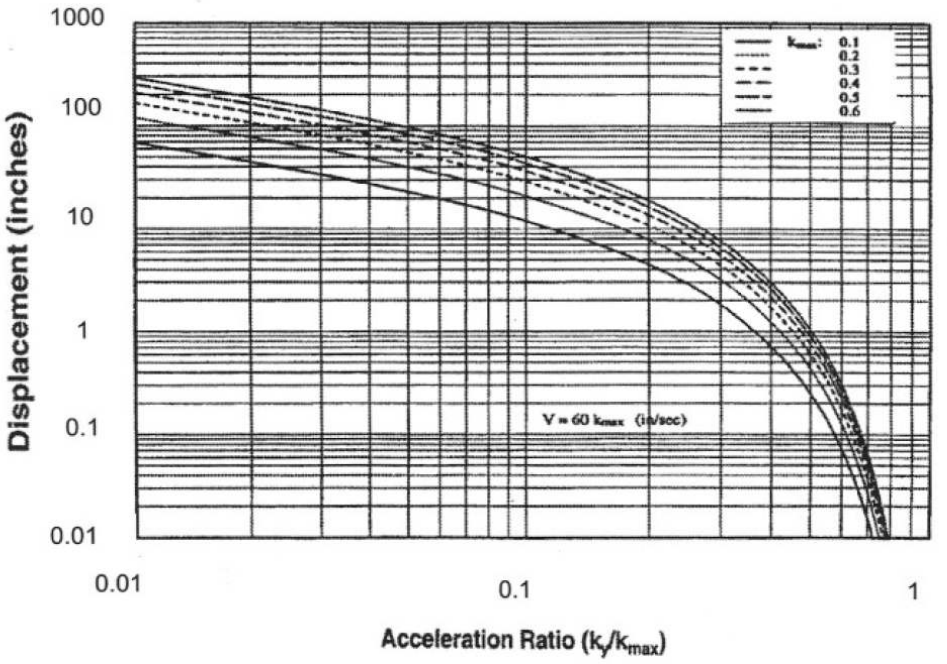

Figure 3-21: Simplified Displacement Chart for velocity-acceleration ratio of 60 (Martin and Qiu, 1994)

In practice values of k_y are determined by performing pseudo-static slope stability runs with a given horizontal ground acceleration. The horizontal acceleration value which yields a factor of safety of 1.0 for the pseudo-static slope stability is the yield acceleration. k_y is the yield seismic coefficient which is defined as the ratio of the yield acceleration to the gravity (g).

NCHRP recommendations for evaluating the seismic yield coefficient for sites prone to liquefaction is to calculate k_y corresponding to the liquefiable layer with the lowest factor of safety against liquefaction for a site with multiple liquefiable layers. Use of residual strength and Newmark concepts for determination of lateral spread deformations are discussed further in Chapter 5.

CHAPTER 4: MODELING CONCEPTS FOR PILES SUBJECT TO LATERAL SPREAD

The modeling concepts used in the past research for piles subject to lateral spread can be divided into two major categories:

1) Analytical Methods
2) Centrifuge Laboratory Test Methods

The following is comprised of three (3) sections. Section 4.1 presents design methods and analytical models used in assessing the response of piles to lateral spread. Following the latter, a presentation on centrifuge modeling and its role in assessing the pile response to lateral spread is given in Section 4.2. Finally, section 4.3 presents a summary of past analytical and centrifuge studies on piles subject to lateral spread, conducted by various researchers in the last decade.

4.1 Design Methods and Analytical Models

To design piles to survive lateral spreading one needs to be able to predict the bending moments and shear forces induced in them by permanent ground displacement. Approaches that have been proposed include:

(a) Estimating the lateral pressure acting on the pile by the lateral spread and then evaluating the consequent pile response.

(b) First estimating the ground displacement within the free-field soil profile, and then applying this displacement profile to the pile through a Winkler soil model.

(c) Treating the displacing soil as a viscous fluid, and computing the resultant pile actions.

4.1.1. The Specified Earth Pressure Method

The first method was adopted by the Japanese Road Association (JRA) in 1996, following the Kobe investigations. The JRA design stresses are illustrated in figure 4-1.

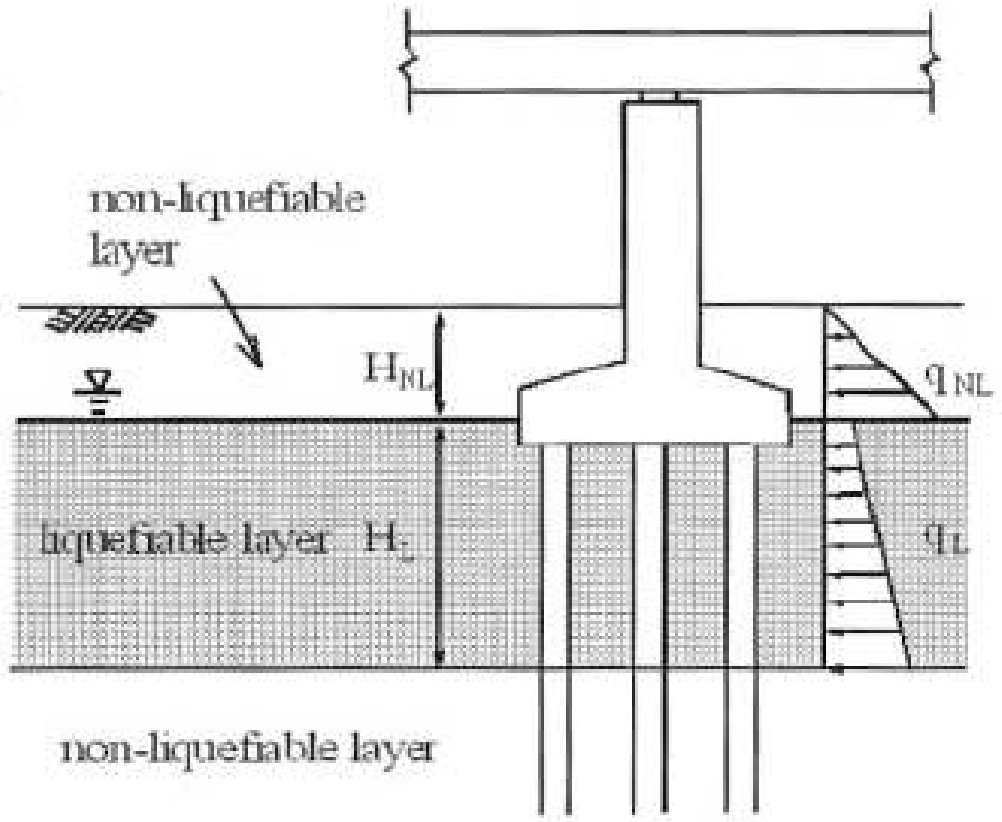

Figure 4-1: Earth Pressure Considered in the 1996 JRA Design Specifications (Berrill and Yasuda, 2002)

The values were calibrated against Kobe damage. Forces from a non-liquefied crust are correctly taken to be the passive values. Stresses imposed by the liquefiable layer depend on coefficients for distance from a quay wall and for absolute stress level. These can be modified, as more information from a wider range of soil conditions becomes available.

At present, the JRA rules specify a lateral stress equal to 30% of the total overburden stress on the projected area of pile when the piles are within 160 feet of a quay wall higher than 16 feet, and 15% when the pile is between 160 and 320 feet of quay wall. This approach is not widely used in the United States and is not discussed further.

4.1.2. The Seismic Displacement Method

In the seismic displacement method adopted for this research study, the free-field deformed shape of the soil profile must first be evaluated. The nonlinear spring stiffness (p-y curves) of the liquefied soil are then evaluated and a soil-pile interaction analysis performed to evaluate pile bending moments and shears.

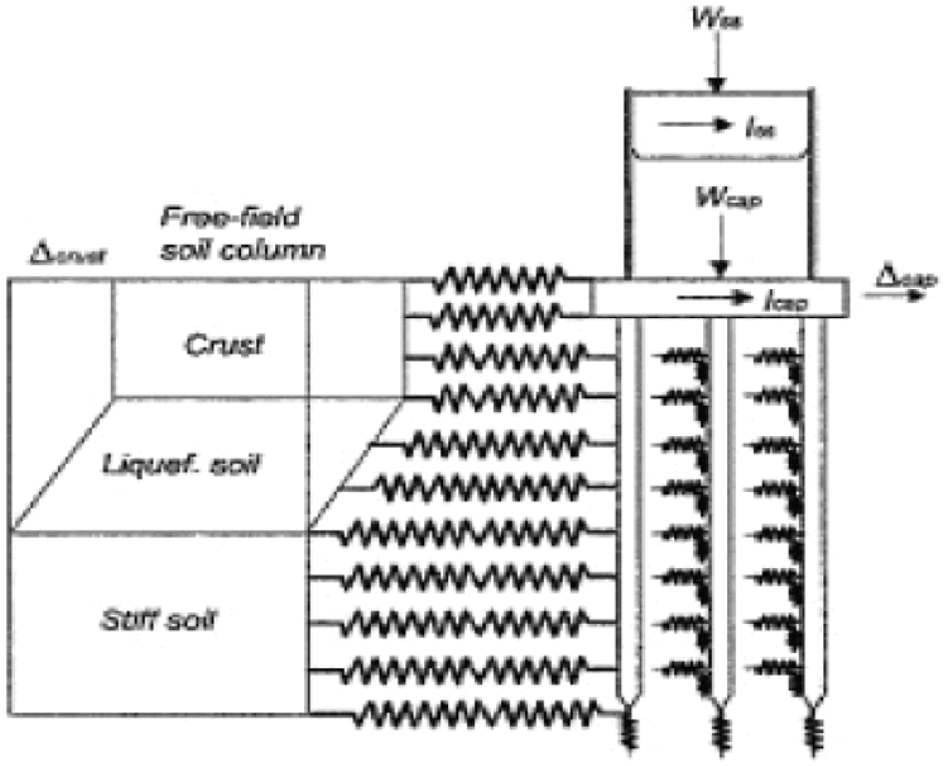

Figure 4-2: The Seismic Deformation Model (Boulanger et al., 2007)

As a foundation problem, the analysis of a pile under lateral loading is complicated since the soil reaction (resistance) at any point along a pile is a function of pile deflection. The pile deflection on the other hand, is dependent on the soil resistance; therefore, solving for the response of a pile under lateral loading can be classified as soil-structure interaction problem. The conditions of compatibility and equilibrium must be satisfied between the pile and soil and between the pile and superstructure.

Further discussion of p-y models and adoption to moving soil solutions are given below.

4.1.2.1. The LPILE Program and Soil P-Y Curves

The model shown in figure 4-7 represents the one utilized by the software program LPILE version 5 (Ensoft) used for this research. The loading on the pile is generally for the two-dimensional case (no torsion or out-of-plane bending). The LPILE software was originally developed for pile top loading as shown in figure 4-3 but subsequently modified for lateral spread loading as discussed later. The horizontal lines across the pile are meant to show that it is made up of different sections; for example a steel pipe could be used with changes in wall thickness. The finite difference method is employed for the solution of the beam-column equation to allow the different values of bending stiffness with respect to the bending moment that is computed during iteration. An axial load is indicated and is considered in the solution with respect to its effect on bending and not in respect to axial settlement.

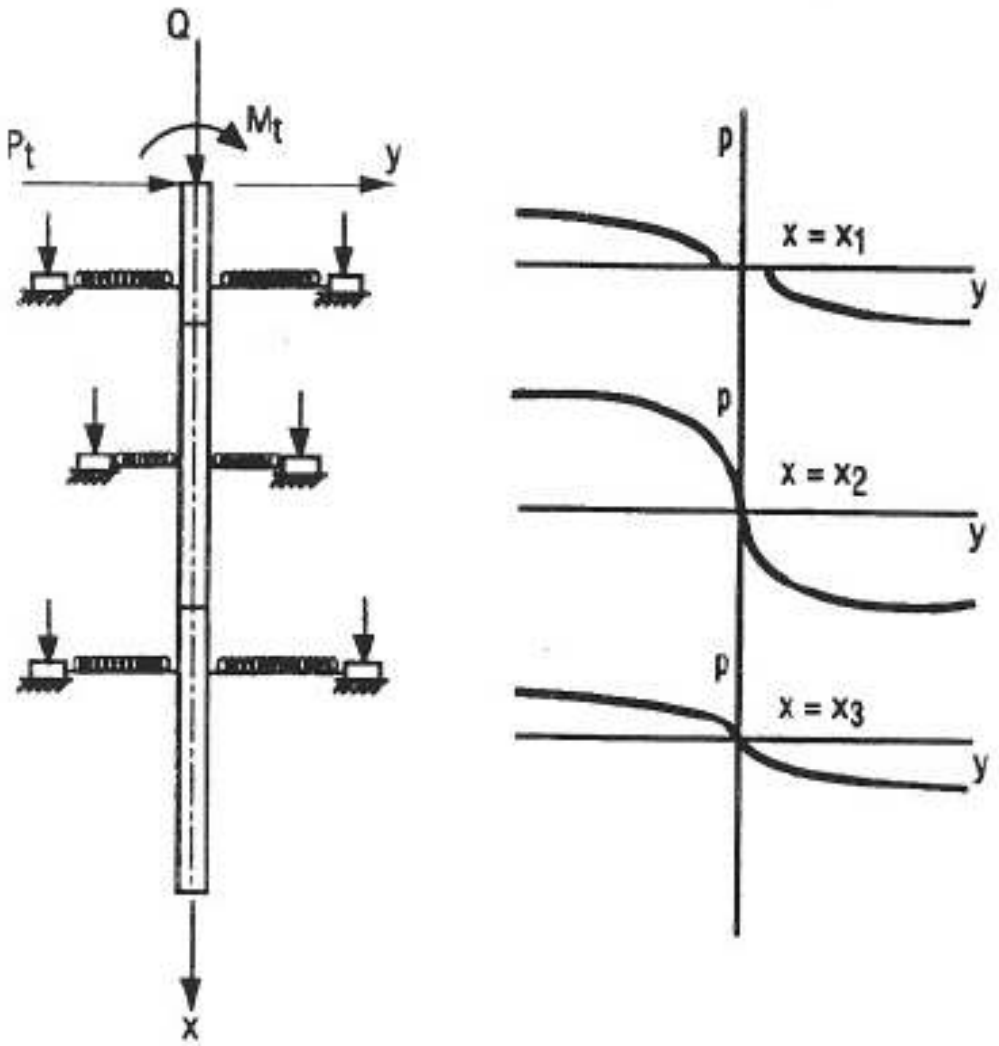

Figure 4-3: Model for Pile under Lateral Loading With p-y Curves (LPILE 2004)

The soil around the pile is replaced by a set of mechanisms that merely indicate that the soil resistance p is a nonlinear function of pile deflection y. The p-y curves are fully nonlinear with respect to distance x along the pile and pile deflection y.

The p-y method is versatile and provides a practical means for design. The method was suggested over fifty years ago (McClelland and Focht, 1958). Two developments during the 1950's made the method possible: the digital computer for solving nonlinear, fourth-order differential equation; and the remote-reading strain gauge for use in obtaining soil-response (p-y) curves from experiment.

4.1.2.2. Definition of P-Y

Figure 4-4 below shows a uniform distribution of unit stresses, normal to the wall of a cylindrical pile. The distribution is correct for the case of a pile that has been installed without bending. (figure 4-4a)

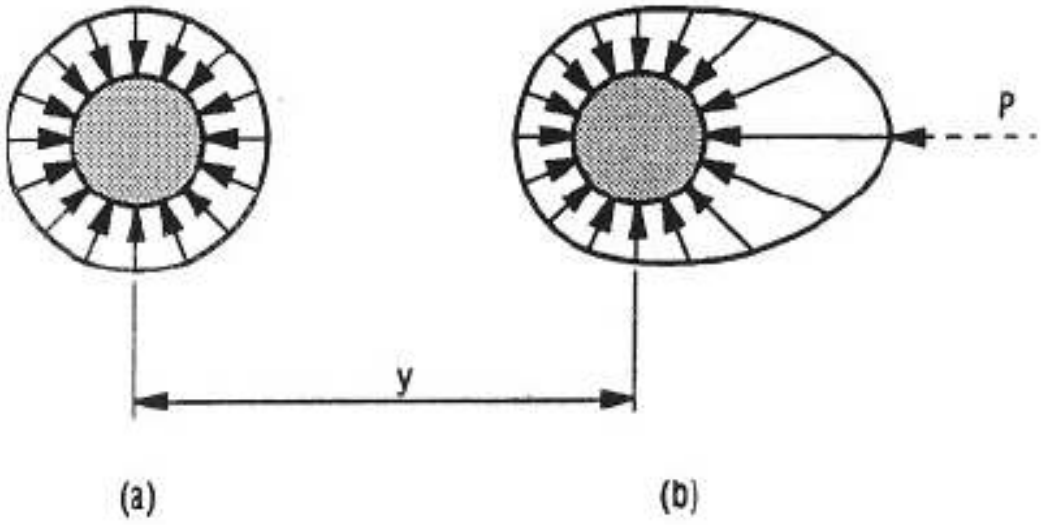

Figure 4-4: Distribution of Unit Stresses against a Pile Before and After Lateral Deflection (LPILE 2004)

If the pile is caused to deflect a distance y (exaggerated in the sketch for clarity), the distribution of unit stresses will be similar to that shown in Figure 4-4 (b). The

stresses will have decreased on the back side of the pile and increased on the front side. Some of the unit stresses have both a normal and a shearing component. Integration of the unit stresses results in the quantity p which acts opposite in direction to y. the dimensions of p are load per unit length of the pile. These definitions of p and y are convenient in the solution of the differential equation.

4.1.2.3. Derivation of Differential Equation for the Beam-Column

The derivation for the differential equation for the beam-column on a foundation was given by Hetenyi (1946). The assumption is made that a bar on an elastic foundation is subjected not only to the vertical loading, but also to the pair of horizontal compressive forces Q acting in the center of gravity of the end cross-sections of the bar.

If an infinitely small unloaded element, bounded by two verticals a distance dx apart, is cut out of this bar (figure 4-5), the equilibrium of moments (ignoring second-order terms) leads to the equation

$$(M + dM) - M + Qdy - V_v dx = 0$$

or

$$dM/dx + Qdy/dx - V_v = 0$$

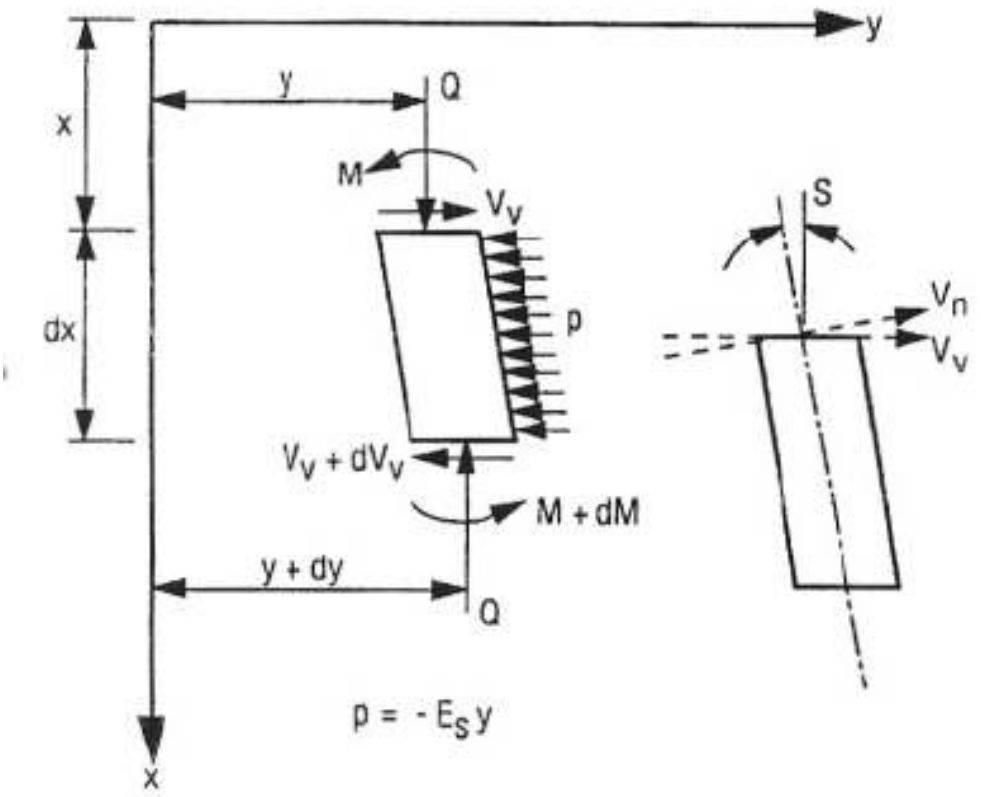

Figure 4-5: Element form beam-column (after Hetenyi, 1946) (LPILE 2004)

Differentiating equation above with respect to z, the following equation is obtained

$$d^2M/dx^2 + Q\, d^2\, y/\, dx^2 - d\, V_v/dx = 0$$

The following identities are noted:

$$d^2M/dx^2 = EI\, d^4\, y/\, dx^4$$

$$d\, V_v/dx = p$$

$$p = -E_s\, y$$

where E_s is equal to the secant modulus of the soil-response curve. Making the indicated substitutions, we have:

$$EI\, d^4\, y/\, dx^4 + Q\, d^2\, y/\, dx^2 + E_s\, y = 0$$

The ability to allow a distributed force W per unit of length along the upper portion of a pile is convenient in the solution of a number of practical problems. The differential equation then becomes as shown below:

$$EI\, d^4 y/ dx^4 + Q\, d^2 y/ dx^2 - p + W = 0$$

Where;

Q = axial load on the pile

y = lateral deflection of the pile at a point x along the length of the pile,

p = soil reaction per unit length

EI = flexural rigidity, and

W = distributed load along the length of the pile

Other beam formulas that are needed in analyzing piles under lateral loads are:

$$EI\, d^3 y/ dx^3 + Q\, d\, y/ dx = V_v$$

$$EI\, d^2 y/ dx^2 = M$$

and,

$$d\, y/ dx = S$$

where

V = shear in the pile

M = bending moment in the pile, and

S = slope of the elastic curve defined by the axis of the pile

4.1.2.4. Solution by Finite Difference Equations

The solution of the fourth degree differential equation needs to be found in order to assess the lateral response of the pile. The formulation of the differential equation in finite difference form and a solution by iteration mandates a computer program. In the finite difference formulations, the derivative terms are replaced by algebraic expressions. The following central difference expressions have errors proportional to the square of the increment length h.

$$dy/dx = (y_{m-1} + y_{m+1})/2h$$

$$d^2y/dx^2 = (y_{m-1}-2y_m+y_{m+1})/h^2$$

$$d^3y/dx^3 = (-y_{m-2}+2y_{m-1}-2y_{m+1}+y_{m+2})/2h^3$$

$$d^4y/dx^4 = (y_{m-2}-4y_{m-1}+6y_m-4y_{m+1}+y_{m+2})/h^4$$

If the pile is subdivided in increments of length h, as shown in figure 4-6 below.

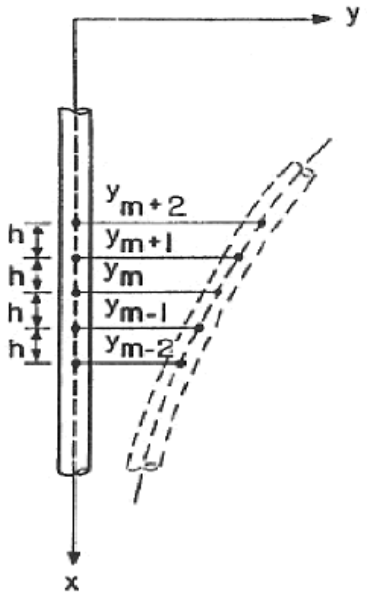

Figure 4-6: Representation of Deflected Pile (LPILE 2004)

The governing differential equation in difference form is as follows:

$$y_{m-2}R_{m-1}+$$

$$y_{m-1}(-2R_{m-1}-2R_m+Qh^2)+$$

$$y_m(R_{m-1}+4R_m+R_{m+1}-2Qh^2+k_mhH^4)+$$

$$y_{m+1}(-2R_m-2R_{m+1}+Qh^2)+$$

$$y_{m+2}R_{m+1}Wh^4 = 0$$

Where

$R_m = E_m I_m$ (flexural rigidity of pile at point m) and

$k_m = E_{sm}$

If the pile is divided into n increments, n+1 equations of the sort as equation above can be written. There will be n+5 unknowns because two imaginary points will be introduced above the top of the pile and two will be introduced below the bottom of the pile. If two equations giving boundary conditions are written at the bottom and two at the top, there will be n+5 equations to solve simultaneously for the n+5 unknowns. The set of algebraic equations can be solved by matrix methods in any convenient way.

4.1.2.5. Response of Pile to the Moving Soil

LPILE4 (version 4) did not have the capacity of incorporating moving soil profile in analysis of the pile to lateral loading. LPILE4M version incorporated the latter followed by LPILE Plus v.5 (version 5) which included the moving soil and non

linear flexural stiffness (EI) aspects of the pile. If piles are situated in a soil layer undergoing lateral movement, it is evident that horizontal pressures are developed against the piles. The net soil reaction on piles depends on the relative movement of the pile and soil. The soil resistance versus the pile deflection for a given soil movement is shown in Fig. 4-7. As may be seen, the soil-resistance curve is not symmetric with respect to the y-axis, and the entire curve is shifted according to the amount of soil movement. The whole soil-resistance curve is offset and becomes symmetric to line AA. The p-y curve in figure below is drawn in the first and fourth quadrants for convenience; however, p is opposite in sign to y. if the pile deflection y_1 is less than the soil movement y_s at certain layers, the surrounding soil gives the pile a driving force instead of a resistance force, as indicated in figure below. If the pile deflection at some depth is y_2 and the soil movement is again y_s, the soil is now resisting the pile movement.

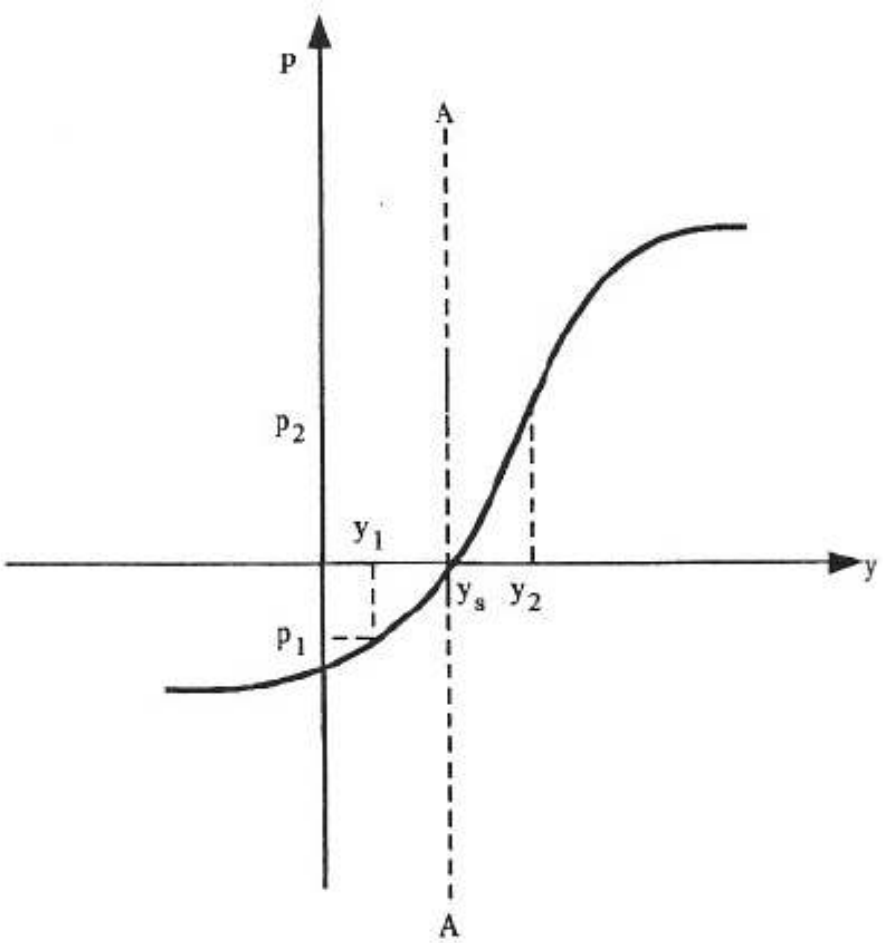

Figure 4-7: Soil Resistance versus the Pile Deflection for a Given Soil Movement (LPILE 2004)

4.1.2.6. Modeling the Interaction between Piles and Soil due to Relative Movement

If the governing equation for the case where the soil does not move, the soil resistance is represented as p = ky (curve 1 in figure 4-8).

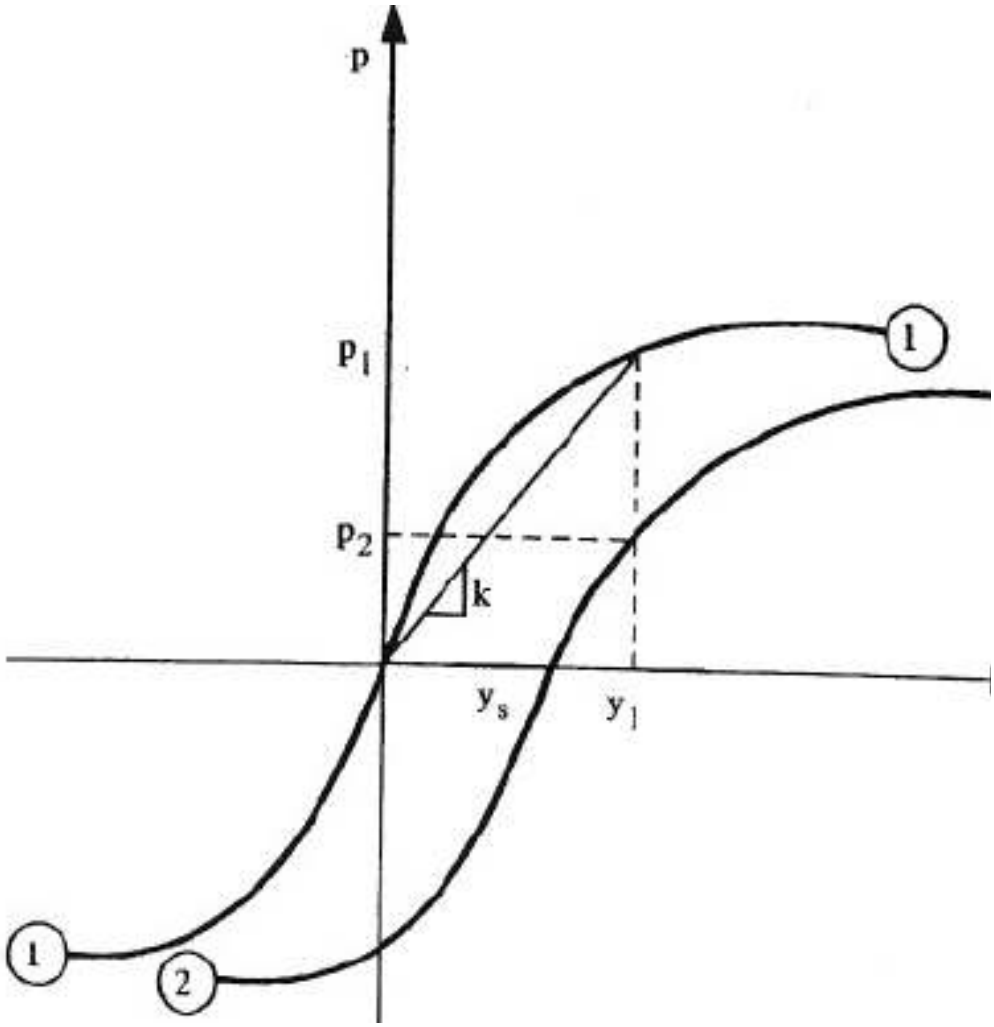

Figure 4-8: Pile Response Due to Relative Soil Movement (LPILE 2004)

To account for the change of the soil resistance, the relative displacement between the pile and soils, needs to be included in the difference equation as:

$$EI\, d^4 y/ dx^4 + Q\, d^2 y/ dx^2 - p(y-y_s) + W = 0$$

Where y_s = free-field soil movement

4.1.2.7. P-Y Curves for Liquefied Soil

Two sets of p-y curves are usually used for bridge design purposes. The first set corresponds to a non-liquefied soil state while the second set includes the effect of liquefaction. There is no general consensus in the engineering community as to what constitutes an appropriate way to model liquefied soil by means of p-y curves. Field and model evidence indicate that the shape of p-y curves for liquefied soils is substantially different than that of monotonic static p-y curves. Current practice, however, consists of modifying existing monotonic p-y curves. These modifications usually involve a reduction in the magnitude of the p value while conserving the original shape of the static p-y curve.

Several procedures are usually used for specifying p-y curves for liquefied sands.

- The liquefied sand is presented as undrained material with a representative undrained residual strength. The p-y curves are assumed to be similar to those developed for soft clays (i.e., Matlock, 1970), with the ultimate undrained strength defined by the residual strength of the liquefied sand Sr as suggested by Wang and Reese (1998). Incorporation of the effects of liquefaction is done by using the residual strength of the liquefied soil instead of the undrained shear strength of the clay.
- The p-y curves for liquefied sands are also modeled using available relations (i.e. API, 1993, Reese et al, 1974) for non-liquefied sands. The effect of

liquefaction is implemented by multiplying the p values by a reduction factor mp. The reduction factor is usually assumed to range between 0.1 and 0.5.

- Assumption that the liquefied sand provided no resistance to lateral movement. In employing the first method cited above, the residual strength of the liquefied sand is determined from a correlation with SPT blow count developed by Seed and Harder (1990).
- P-Y curves in liquefied sand are characterized by a concave-up load-displacement shape where the slope of the curve increases as displacement increases. (Rollins et. al, 2005). The p-y curves stiffen with depth and following liquefaction, p-y curves in sand become progressively stiffer as excess pore water pressure dissipate.

4.1.2.8. Pile Ductile Response

Pile ductile response is based on the evaluation of the pile ductile capacity and its comparison to the lateral displacement demand. Pile is modeled as elastic perfectly plastic element with the moment curvature either evaluated or imported. The pile ductile response is according to the moment curvature capacity of the pile section and the demand exerted by the moving soil. At each incremental point along the pile length, the bending moment and flexural stiffness of the pile is computed. The pile is pushed to the ultimate point and well past the plastic limit tracking along the ductile response of the pile.

A each point along the pile, the curvature demand is calculated based on the ratio of the bending moment and the flexural stiffness. The latter is then compared to the curvature capacity of the pile. The pile has the ability to go well past the plastic hinge based on the structural and geotechnical characteristics of the soil-pile elements and the lateral spread displacement demand.

The following presents what is ductility and how is defined mathematically, followed by a mathematical evaluation of the moment curvature and lastly the stress strain models for reinforced concrete and steel used in evaluation of the moment curvature.

4.1.2.8.1. Ductility

The program LPILE plus v.5 can evaluate the pile ductile response due to liquefaction induced displacement demands by assessing the pile curvature along its entire length. Ductility is defined as the capacity of a structure element to displace inelastically through several cycles of response without significant degradation of strength or stiffness. Ductility is defined mathematically as shown in figure 4-9 below.

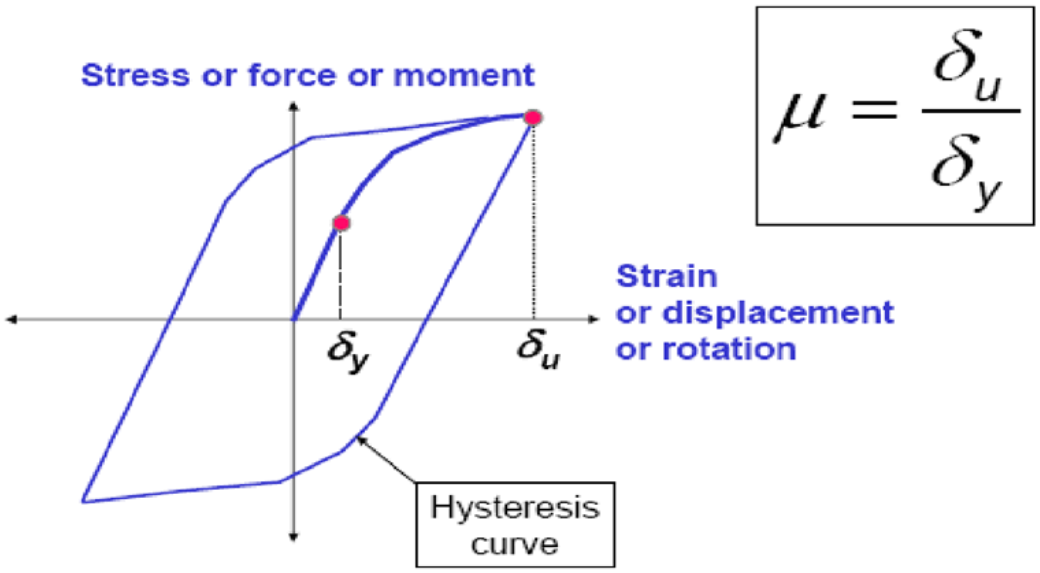

Figure 4-9: Definition of Ductility (FEMA)

The ductility ratio (μ) is the ratio of the ultimate displacement (δ_u) to the yield displacement (δ_y). Although the ductility ratio refers to displacements, curvature ductility ratios relating ultimate and yield curvatures at critical sections are also frequently defined. Curvature ductility relates to the response of an individual section and depends on its reinforcement and axial load level. Displacement ductility relates to overall structural response.

4.1.2.8.2. Moment-Curvature Evaluation

To determine the pile ductile capacity, the moment-curvature relationship must be evaluated. It is important that the concrete stress-strain relationship distinguish between cover concrete and confined concrete with allowance for the different

compression strength and strain capacities of these two components, when moment curvature analysis is carried out. Thus with reference to the figure 4-10 below:

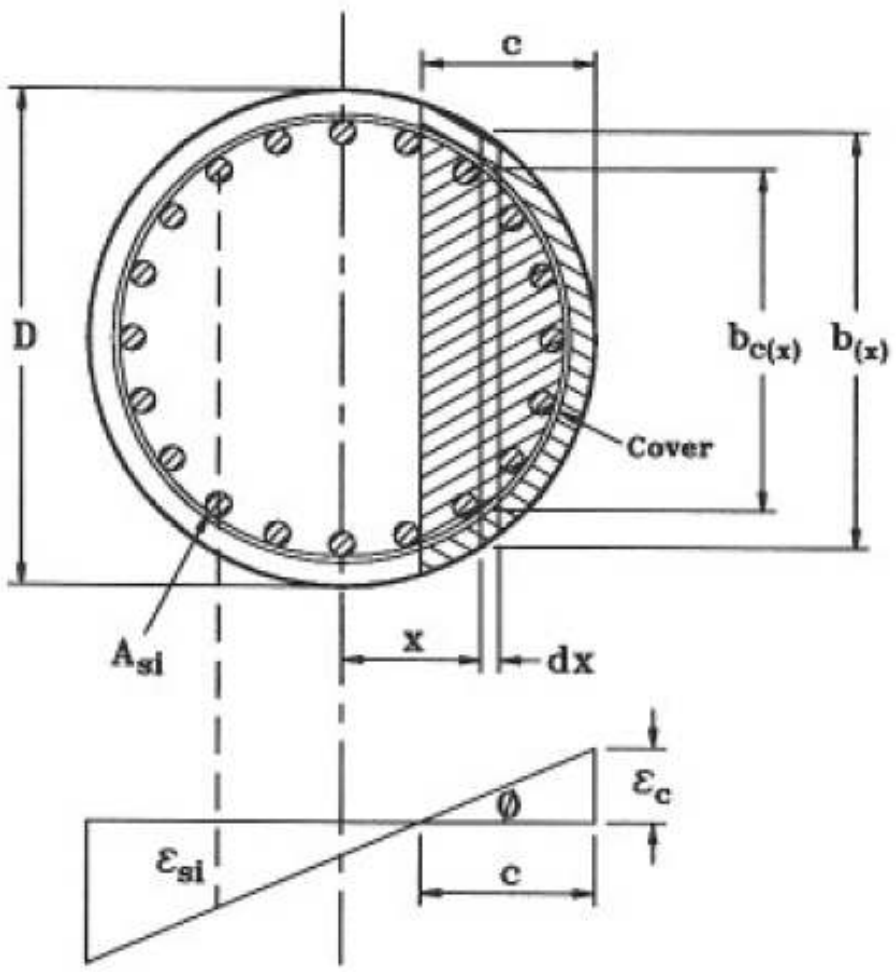

Figure 4-10: Moment Curvature Analysis for Circular Column (Priestley et al, 1996)

The moment curvature curve for a circular column may be generated for specified values of extreme fiber compression strain ε_c by considerations of axial and moment equilibrium. Considering axial equilibrium:

$$P = \int_{x=(D/2)-c}^{D/2} [b_{c(x)} f_{c(\varepsilon_x)} + (b_{(x)} - b_{c(x)}) f_{cu(\varepsilon_x)}]\, dx + \sum_{i=1}^{n} A_{si} f_{s(\varepsilon_{xi})} \quad \textbf{(EQ.4-1)}$$

Where

$$\varepsilon_x = \frac{\varepsilon_c}{c}(x - 0.5D + c) \quad \textbf{(EQ. 4-2)}$$

From consideration of moment equilibrium,

$$M = \int_{x=(D/2)-c}^{D/2} [b_{c(x)} f_{c(\varepsilon_x)} + (b_{(x)} - b_{c(x)}) f_{cu(\varepsilon_x)}] x\, dx + \sum_{i=1}^{n} A_{si} f_{s(\varepsilon_{xi})} x_i \quad \textbf{(EQ. 4-3)}$$

and the curvature is

$$\phi = \frac{\varepsilon_c}{c} \quad \textbf{(EQ.4-4)}$$

Where $f_c(\varepsilon)$, $f_{cu}(\varepsilon)$, and $f_s(\varepsilon)$ are the stress-strain relationships for confined concrete, unconfined concrete , and reinforcing steel, respectively, and A_{si} is the area of a reinforcing bar with distance x_i from the centroidal axis. Other nomenclature is defined in Figure 4-11.

The equation 4-1 is solved for c by trial and error using the known axial load level P and the specified extreme fiber compression strain. This enables the moment M and curvature ϕ to be calculated directly from Eqs. 4-3 and 4-4. The entire moment

curvature is generated by specifying a sequence of ε_c values up to the ultimate compression strain.

Substituting $b_{(x)} = b$ and $b_{c(x)} = b_c$, eqs 4-1, 4-3 and 4-4 also apply to rectangular sections, using the nomenclature of figure 4-11

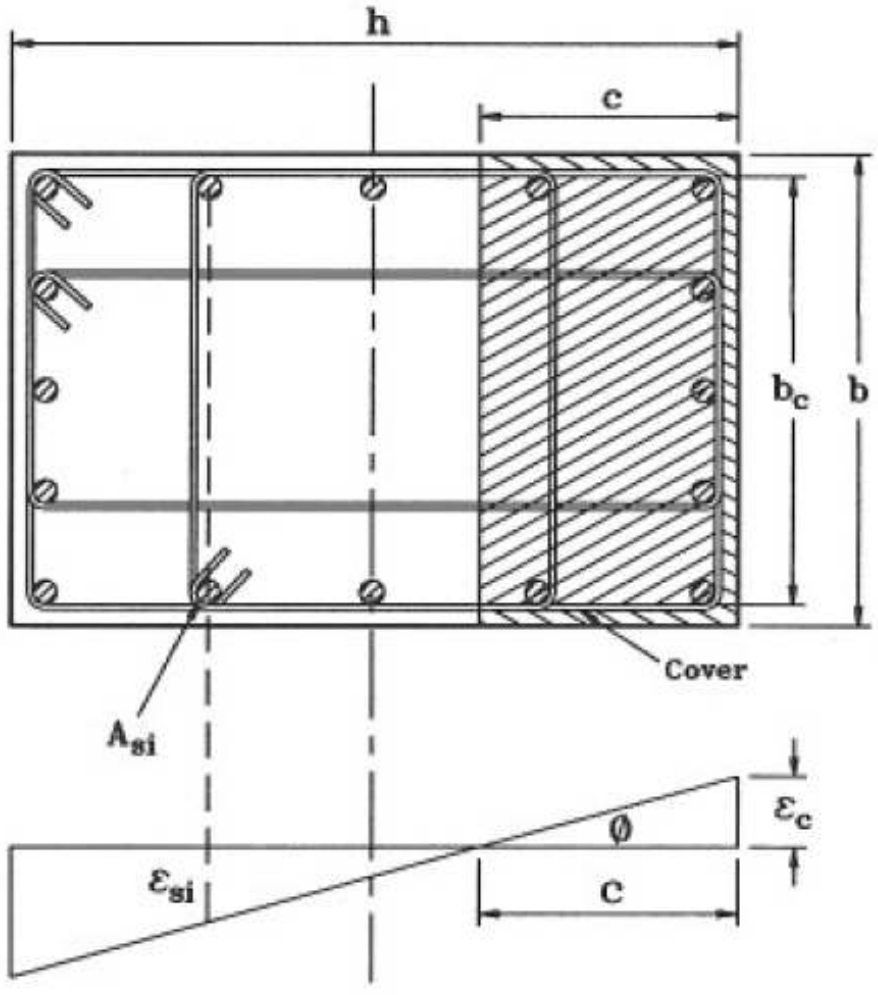

Figure 4-11: Moment Curvature Analysis for Rectangular Column (Priestley et al, 1996)

The moment curvature calculations described above are suitable for inclusion in computer codes and are used as the basis for most analysis using models for stress-strain curves of confined and unconfined concrete and reinforcing steel described below.

4.1.2.8.3. Non Linear Concrete and Reinforcing Steel Models for Ductile Reinforced Concrete Member

Non linear stress-strain concrete model for confined and unconfined concrete for the ductile reinforced concrete pile is used in the analysis to determine the local capacity of the ductile pile. The initial ascending curve may be represented by the same equation for both the confined and unconfined model since the confining steel has no effect in this range of strains. As the curve approaches the compressive strength of the unconfined concrete, the unconfined stress begins to fall to an unconfined strain level before rapidly degrading to zero at the spalling strain ε_{sp}, typically $\varepsilon_{sp} = 0.005$. The confined concrete model continues to ascend until the confined compressive strength f'_{cc} is reached. This segment is followed by a descending curve dependent on the parameters of the confining steel. The ultimate strain ε_{cu} is the point where strain energy equilibrium is reached between the concrete and the confinement steel. A commonly used model is Mander's stress strain model for confined concrete which is also used in this study (Mander et al., 1988) shown in figure 4-12.

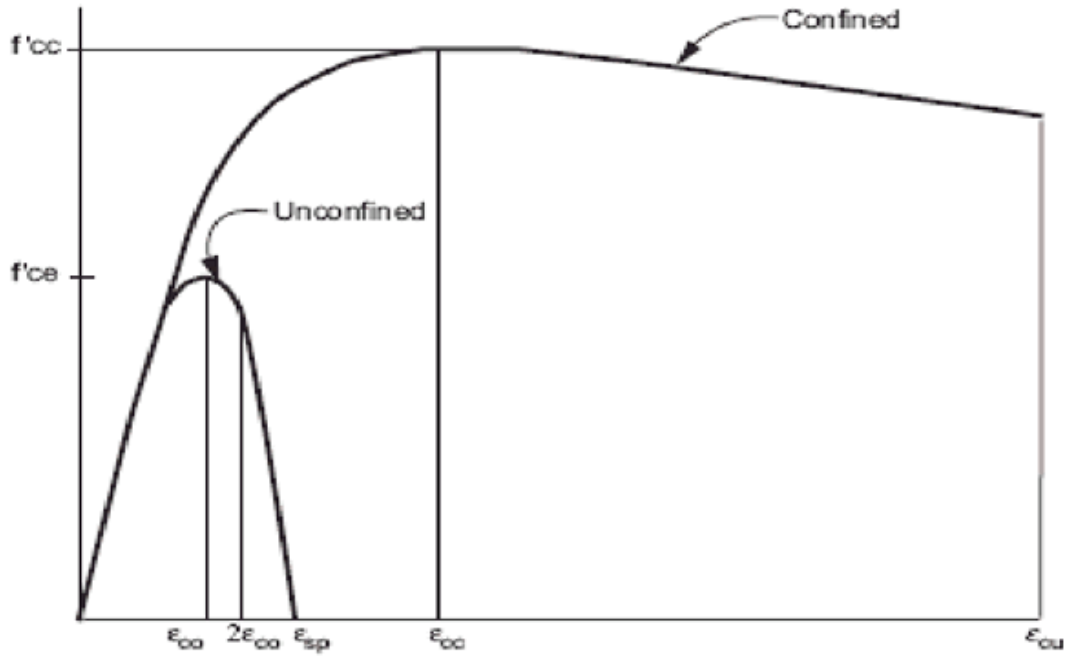

Figure 4-12: Concrete Stress Strain Model (Mander, 1988)

Non Linear Reinforcing steel model used for ductile reinforced concrete pile is modeled with a stress-strain relationship that exhibits an initial linear elastic portion, a yield plateau, and a strain hardening range in which the stress increases with strain. The yield point is defined by the expected yield stress of the steel f_{ye} . The length of the yield plateau is a function of the steel length and bar size. The strain-hardening curve can be modeled as a parabola or other non-linear relationship and should terminate at the ultimate tensile strain ε_{su}. The ultimate strain is set at the point where the stress begins to drop with increased strain as the bar approaches fracture. The commonly used steel model is shown in Figure 4.13.

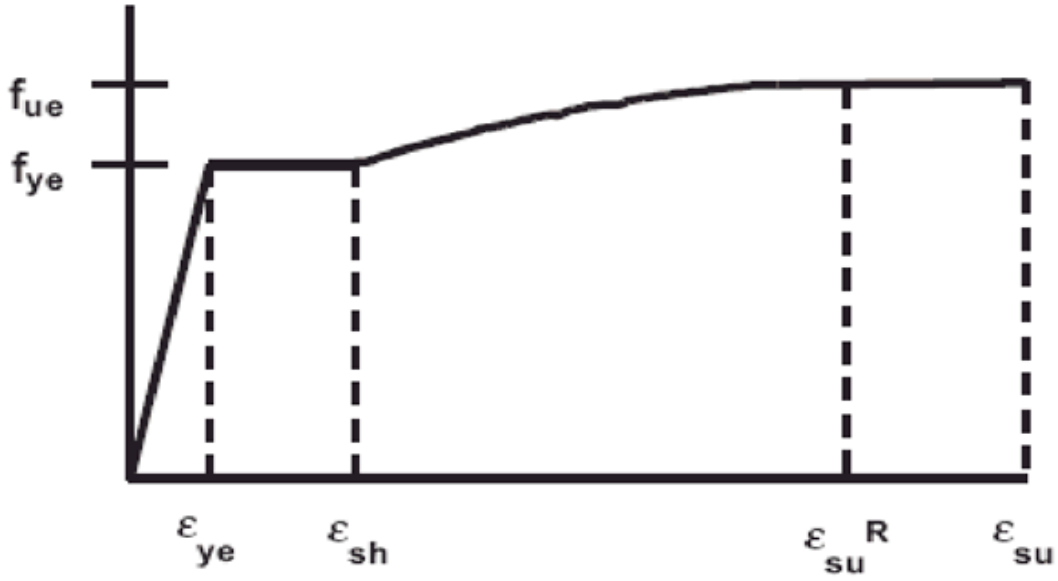

Figure 4-13: Steel Stress Strain Model (SDC, 2006)

4.1.2.8.4 The XTRACT Program

The software XTRACT (Imbsen) was used in this research to evaluate moment curvature relationships for piles, required as input to LPILE5. Non linear concrete for both confined and unconfined and steel models cited above are incorporated into the XTRACT program (Imbsen) based on the Equations shown in section 4.1.2.8.2 to perform the cross sectional analysis of the structural component and to evaluate the moment curvature relationship. As earthquake engineering design is more and more based on a displacement based design methodology, realistic assessment of the nonlinear behavior of systems is required. A very important parameter for reinforced concrete elements subject to inelastic deformation demands is the ultimate curvature. The latter, in part, determines the ultimate rotations as well as the ultimate

displacement capacity. In determining this value for different axial loads, a series of moment curvature analyses are typically performed and the last point calculated within a moment curvature relation is taken as the ultimate curvature corresponding that particular axial load. XTRACT is capable to do the latter and the moment curvature is then incorporated into the LPILE program.

4.2. Centrifuge Modeling

Most of the liquefaction failures have occurred at sites which were not instrumented. The corresponding lack of quantitative observations has slowed down the development of reliable techniques to evaluate the consequences of soil liquefaction at depth. The advent of the geotechnical centrifuge physical modeling methodology has helped in this respect, by offering the ability to create fairly realistic full-scale stress with uniform and measurable soil and foundation properties. The centrifuge testing is effectively used to study the mechanism behind lateral spread and liquefaction as well as to validate numerical codes, both for free field and soil-pile interaction conditions. The VELACS (Verification of Liquefaction Analysis by Centrifuge Studies) project sponsored by the National Science Foundation and involving the cooperative effort of seven universities was particularly useful to the modeling of lateral spreading.

In a centrifuge test, A 1/N scale model located at a distance, r, from the axis of a centrifuge is rotated at a rotational speed which is sufficient to raise the acceleration

field at the location of the model to N times the acceleration of gravity. In principle, the stress conditions at any point in the model should then be identical to those at the corresponding point in the full scale prototype. The overall behavior (e.g. displacements, failure mechanisms, etc…) should also be identical. The following figure 4-14 illustrates the concept:

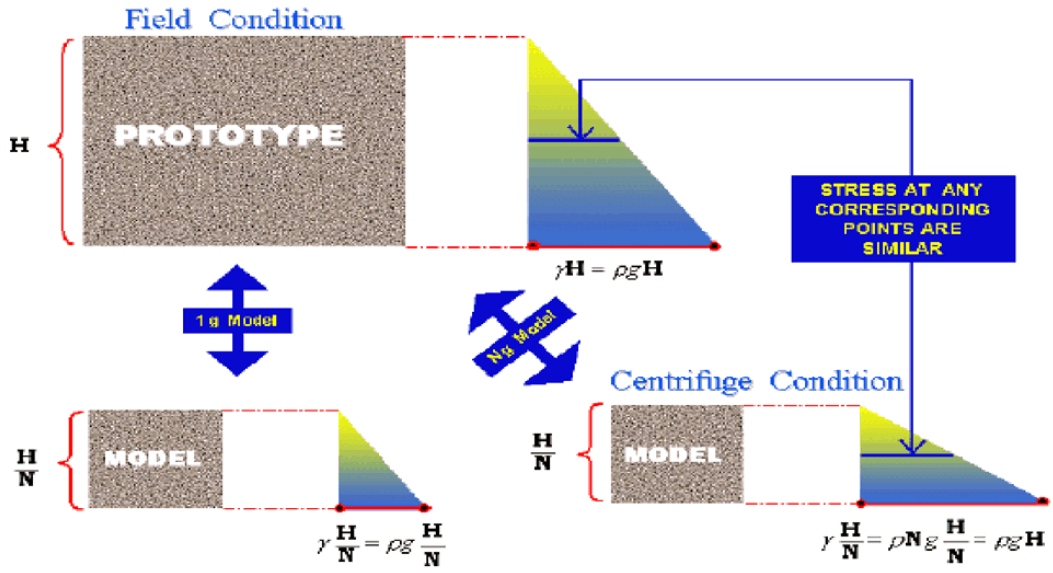

Figure 4-14: Centrifuge Modeling Concept (http://nees.rpi.edu)

The effect of permanent lateral ground displacements due to seismically induced liquefaction and lateral spreading on both single piles and pile groups has been investigated by several researchers using centrifuge modeling.

The centrifuge studies by various researchers cited later in this chapter were performed by RPI and UC Davis Centrifuges. (Figures 4-15 and 4-16)

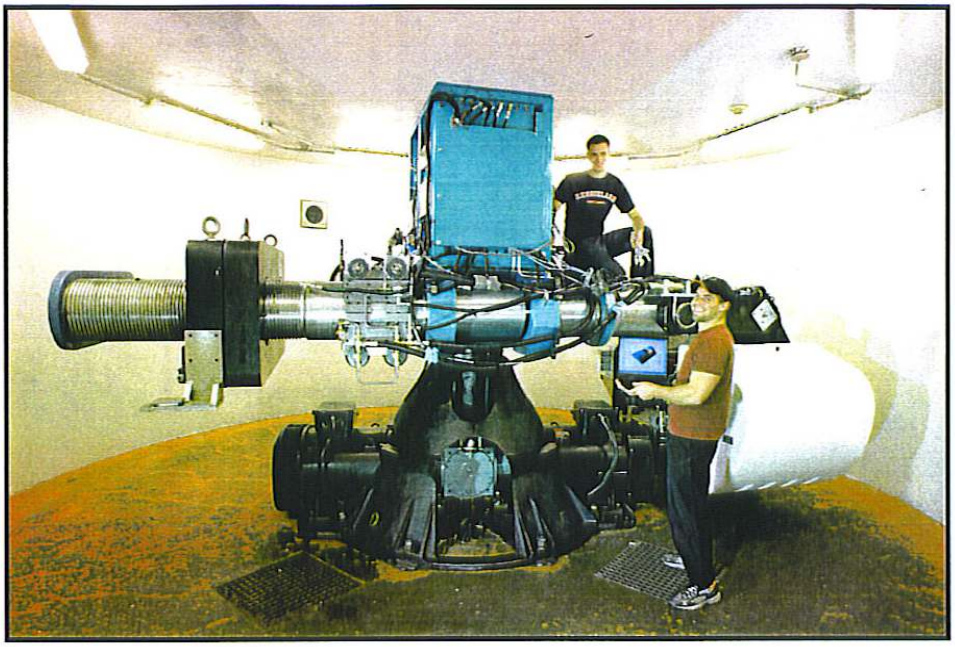

Figure 4-15: RPI Centrifuge (3.0 m radius and 100 g-tonnes)

Figure 4-16: UC Davis Centrifuge (9.1 m radius and 240 g-tonnes)

4.3. Past Analytical and Centrifuge Studies on Piles Subject to Lateral Spread

Several researchers have contributed to the study of piles subject to liquefaction induced lateral spread. (Hamada,1992; Meyersohn,1994; Abdoun,1997; Berrill et al., 1997; Chaudhuri, 1998; Ramos, 1999; Tokimatsu, 1999; Wilson, 2000; Goh,2001; Abdoun et.al ,2003; Lagos,2005, Brandenberg,2005; Cubronovski and Ishihara,2005; Blandon, 2007; Lam et.al, 2007; Rajaparthy et al, 2008; Armstrong, 2008; Ledezma and Bray, 2008). The following provides an overview of the work by several of these researchers:

4.3.1. Research by Meyersohn (1994)

Meyersohn's research dealt with the response of pile foundations to ground displacements caused by soil liquefaction. Methods were developed to estimate failure modes of single piles to liquefaction-induced lateral spread and to assess maximum levels of soil displacement to cause pile failure. A finite element model was developed to study the response of single piles and pile groups to horizontal ground displacements associated with soil liquefaction.

Pile failure modes caused by liquefaction-induced lateral spread were evaluated by means of parametric studies. Three failure mechanisms were recognized under lateral spread conditions.

The pile was modeled using beam elements, while soil reactions in the axial and transverse directions of the pile are represented by means of spring-slider elements, representing p-y curves. The numerical model was implemented in a FORTRAN-77 computer program called B-STRUCT. The program has the capability of simulating the geomaterial as well as material nonlinearities of pile and soil. Geomaterial nonlinearities allows handling large displacements. Material nonlinearities are taken into account by means of spring-slider elements for the soil and rotational springs elements of the pile.

Flexural characteristics of reinforced concrete piles are introduced in B-STRUCT by means of moment-curvature relationships, which are obtained by appropriate selection of stress-strain curves of concrete under compressive and tensile stresses. The stress-strain relationship for concrete in compression proposed by Mander,et al (1988) was adopted in Meyersohn's work. Tensile response of reinforced concrete was modeled according to the expressions suggested by Mier (1987) and Marzouk and Chen (1993) for tension stiffening effects of normal and high strength concrete respectively.

Moment curvature relationships were generated by the adopted concrete models. B-STRUCT did generate moment rotation and the relationship between curvature and angle of rotation was used to generate the curvature, whereby pile rotation can

be found given the pile displacement and once the displacement is found, the curvature can be calculated.

4.3.2. Research by Abdoun (1997)

Abdoun studied the seismically induced lateral spreading of multi-layered soil and its effect on pile foundations. He performed eight centrifuge tests at RPI including a total of 9 different cases. The prototype piles simulated had a bending stiffness of 8000 kN-m^2 and a diameter d =0.6m. The piles were instrumented with strain gauges to measure the bending moment. He proposed a limit equilibrium procedure to predict the maximum bending moments along the pile when the soil is subjected to liquefaction and lateral spreading. The prototype being simulated involved a single pile of diameter 24 inch, length 32 feet , free at the top; embedded in a three-layer soil system. The prototype profile includes a bottom layer of slightly cemented sand, followed by a layer of uniform Nevada sand placed at a relative density of about 40%, topped by a layer of the same slightly cemented sand. The top slightly cemented sand was pervious and was intended to simulate approximately a free-draining, dense, non liquefiable layer. The soil profile is fully saturated. (Abdoun and Dobry, 1997).

4.3.3. Research by Chaudhuri (1998)

Chaudhuri's main research outcome was developing a method for estimating p-y curves for liquefied soil for analyzing soil-pile interaction during lateral spread. A

series of centrifuge test were conducted to verify the method. Liquefaction was modeled based on collapse behavior of sand to include the strain-softening of p-y curves of liquefied soil.

Chaudhuri is of the opinion that load transfer occurs principally on the upstream side, so that the triaxial extension test is the more appropriate test to characterize soil-pile interaction under lateral spread and large horizontal displacements of the soil mass. Chaudhuri stated in his research that soil yield pressure of liquefied soil on the pile decrease as the flow progresses. The maximum yield pressure would correspond to the peak undrained strength of the soil, and the minimum strength would correspond to the steady-state strength of the soil. He stated a need for several p-y curves to describe the state of the soil during lateral spread and flow. As the soil state transitions, the soil response shifts from the stiffer p-y curve to the softer p-y curve. He then proposed to use a trilinear p-y curve constructed based on four parameters and they are peak soil reaction, steady state soil reaction and the corresponding pile displacements for peak and steady state. He suggested that soil displacements corresponding to 1% -1.5% of the pile diameter and 4%-5% of the pile diameter for peak and steady state respectively. Chaudhuri assumed soil strains from monotonic soil-pile interaction only and to develop the simplified p-y curve, transient and monotonic soil responses were uncoupled.

4.3.4. Research by Ramos (1999)

Ramos used Centrifuge modeling as the main tool to study the restraining effect of the superstructure above ground on the response of a single pile to lateral spreading. Two and three layer soil profiles were used with free and fixed head conditions for the pile. The superstructure horizontal stiffness was modeled by a horizontal spring attached to the top of the pile having a stiffness varying between very flexible to very stiff. Pile bending moments and displacements were monitored, as well as displacement of the restraint and accelerations, displacements and excess pore pressures in the soil.

Ramos modeled end bearing single piles, some with pile caps using centrifuge testing. Fundamentally, his work continued Abdoun (1997) work and uses the centrifuge technologies developed at RPI. He recommended that to better predict the pile behavior subject to lateral spread, in the case of the pile embedded in non liquefiable soil, the rotational flexibility of the bottom non liquefiable soil must be considered. He concluded that the equivalent superstructure's horizontal and rotational stiffnesses must be used as part of the calculations of bending moments and displacements of a pile foundation system.

4.3.5. Research by Wilson (2000)

Wilson (2000) conducted a series of dynamic centrifuge tests of pile supported structures in soft clay and liquefying sand during strong shaking, at UC Davis. The

observed dynamic p-y curves were back-calculated from the time histories of bending moments and accelerations of the soil profile. The soil displacements and the pile displacements were determined independently. Pile displacements were calculated by double integrating the bending moment distribution at each time step.

These dynamic model tests were performed by using the 9m radius centrifuge test at UC Davis. These testes were performed using several different structural models, different earthquake motions and different soil profiles. The experiments were performed with the upper soil layer being either saturated sand or soft, normally consolidated clay. Wilson is of the pinion that based on his research the simple p multipliers on the API recommended p-y curves for drained loading can not represent adequately the observed dynamic p-y curves in his study. He states that factors such as relative density, p-y history, pore pressure generation, strain rate, partial drainage and others inherent in undrained behavior of soil, can be ideally accounted for in dynamic p-y soil response. One of the model setups is shown in figure 4-17

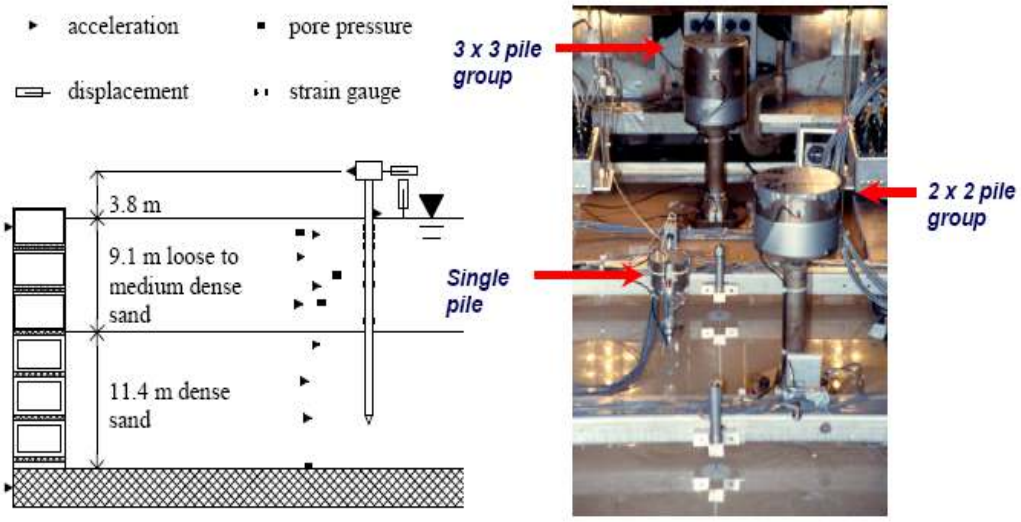

Figure 4-17: Centrifuge Model Setup (Wilson, 2000)

4.3.6. Research by Goh (2001)

Goh further studied the strain-softening p-y approach proposed by Chaudhuri (1998).He undertook a program of undrained triaxial testing to help characterize the behavior of liquefied soil and quantify parameters that influence soil-pile interaction during lateral spread. Using the strength and deformation parameters determined from the triaxial tests, strain-softening p-y relationships were generated and then utilized in finite element analyses to model soil-pile interaction under conditions of significant lateral ground deformation.

4.3.7. Research by Abdoun et al. (2003)

Abdoun et.al developed Limit equilibrium methods using the results of six centrifuge models of instrumented single pile foundations subjected to lateral spreading. (see Figure 4-18) These six models simulate single reinforced concrete piles in two-and three-layer soil profiles, mostly end bearing but including also one floating pile, with and without a reinforced concrete pile cap, and one model where the liquefiable sand layer was densified locally around the pile to simulate the effect of pile driving.

In order to simultaneously measure the pile head displacement and the maximum bending moment, a rotational spring k_r representing the flexibility of the bottom nonliquefiable layer was introduced.

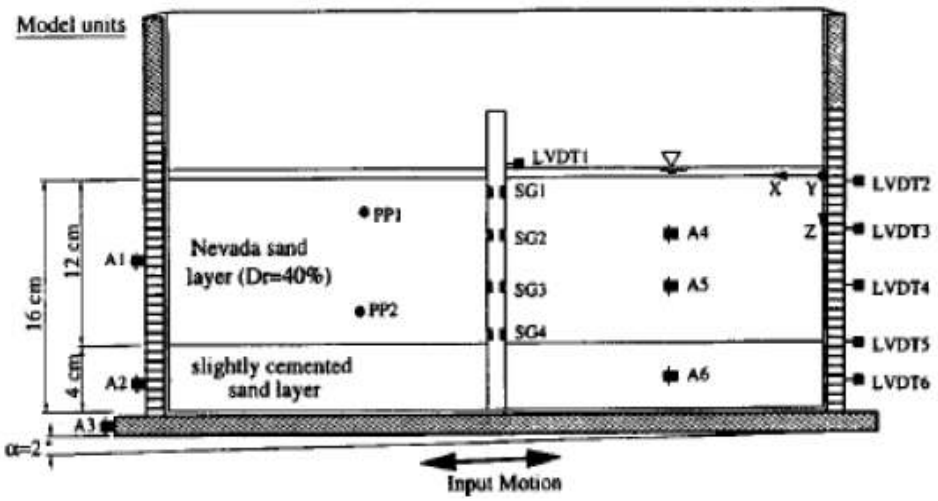

Figure 4-18: Centrifuge Model Setup (Abdoun, 2003)

4.3.8. Research by Lagos (2005)

Lagos work was based on the modeling the permeability and pinning reinforcement effects on pile response to lateral spreading. He conducted a series of centrifuge modeling tests using the 150 g-ton RPI centrifuge to investigate the effects of single piles and pile groups subjected to liquefaction induced lateral spreading. The models consisting of different pile configurations were tested using water as the pore fluid, simulating a loose layer of coarse sand. These models were then repeated using the same fine sand, but saturated with a viscous fluid (metulose), hence simulating a loose layer of fine sand.

Consequently, these centrifuge tests simulated deposits of wide different permeability in the field.

Lagos work showed that when pile models were in the water saturated soil, the pile lateral displacements and associated bending moments reached a maximum value after a few seconds of shaking, decreasing afterwards. However, in the low permeability models (saturated with viscous fluid), the pile lateral displacements and associated moments increased gradually, reaching at the end of the excitation values as large as 6 times the ones observed in the models saturated with water. He suggested that the bending moments and lateral displacements for a pile foundation installed in silty sand in the field could be much higher than those measured in the same foundation installed in clean sand, due to lower permeability of the silty sand.

Pile pinning effect was studied by a series of four centrifuge tests conducted at the 150 g-ton RPI centrifuge facility. The response of 3x2, 6x2, and 3x1 pile group was simulated by centrifuge tests. The pile group pinning effect with non-liquefied crust riding on top of the liquefied soil showed that the largest reduction in lateral spread was caused by the 6x2. Before soil failure, the reduction appeared to be proportional to the pile group stiffness. However, once the passive failure developed, the additional reduction seemed to be proportional to the effective area subjected to passive pressure. Lagos also recommended that the separation between piles should be large enough to ensure that the confinement around the piles does not decrease significantly due to the frame effect.

4.3.9. Research by Brandenberg (2005)

Brandenberg conducted a series of dynamic centrifuge model experiments performed by UC Davis 9-m radius centrifuge testing instrument, to improve the knowledge on the behavior of pile foundations in liquefied and laterally spreading ground. Models consisted of single and group piles, soil consisting of a nonliquefiable clay crust overlying liquefiable loose sand over dense sand. He back-calculated the fundamental engineering behaviors from the raw recorded data. He stated that inertia forces and lateral spreading displacements need to be considered simultaneously to accurately predict bending moments and pile cap displacements. Based on his work, he is of the opinion that friction components of the nonliquefiable crusts must be considered to accurately analyze the pile response and predict peak bending

moments and pile cap displacements. Rotational flexibility at the connection between the pile and pile cap can be important, if pile cap displacement is excessive.

4.3.10. Research by Blandon (2007)

Blandon carried a set of analyses in order to check the displacement capacity of piles supporting wharves for inertial and kinematic loading based on the material strains in the structural element. Some of the strain values defined for the plastic hinging in the pile section below ground historically not verified were found by performing full scale test to validate current values.

Most of the wharf related damages have occurred due to large permanent displacements that in most cases have been caused by liquefaction of soil layers inside the profile where the piles are embedded (Blandon, 2007). As part of his research, Blandon studied the kinematic loading effect of a thin sliding layer on the displacement capacity of a typical Port of Los Angeles (POLA) , 2 feet diameter prestressed pile. Pile moment curvature was obtained by OPENSEES, using a Fiber Model and the pile response to the sliding layer was obtained using a Finite Element program with the soil modeled based on p-y curves following the API methodology. OPENSEES (Open System for Earthquake Engineering Simulation) is a software framework for developing applications to simulate the performance of structural and geotechnical systems subjected to earthquakes. Priestley (2005) proposed a procedure based on assumptions of the plastic hinge length, elastic distance to fixity

and plastic hinge location for a 2 feet sliding layer. The ground above sliding surface is assumed to be competent and moves as a rigid body on top of the liquefiable layer. Plastic hinge formation occurs some distance above and below the sliding layer interfaces. Studying the problem, Blandon concluded that the piles can have a shear failure before rupturing the longitudinal reinforcement. The analyses also showed that the shear force demand and displacement capacity is a function of the depth (confinement stress) to the sliding layer. Blandon study showed that the location of the liquefiable layer is a relevant factor for the pile response analyses. His research is discussed further in Section 7.1.2.

4.3.11. Research by Lam et. al (2008)

Lam et. al studied the soil-pile interaction under lateral spread loading using Opensees. Reference was made to the problems associated with displacement input for uncoupled models, distinguishing between far-field and near-field displacement. Problems associated with formulating Winkler Springs were also discussed. They proposed procedures for sliding layer soil-pile interaction problem, where a characteristic parameter that is a function of thickness of the liquefiable layer, outer diameter, flexural rigidity and elastic modulus of pile is formulated. The study concluded that the current approach in analyzing the pile response using Winkler springs leads to conservative results, unless appropriate corrections are made.

CHAPTER 5: RECOMMENDED NCHRP 12-49 DESIGN APPROACH

5-1. Background

The 1971 San Fernando earthquake was a major turning point in the development of seismic design criteria for bridges in the United States. Prior to 1971, the American Association of State Highway and Transportation Officials (AASHTO) specifications for the seismic design of bridges were based in part on the lateral forces requirements for buildings that had been developed by the Structural Engineers Association of California. In 1973, the California Department of Transportation (Caltrans) introduced new seismic design criteria for bridges, which included the relationship of the site to active faults, the seismic response of the soils at the site and the dynamic response characteristics of the bridge. AASHTO adopted Interim Specifications in 1975 which were a slightly modified version of the 1973 Caltrans provisions, and made them applicable to all regions of the United States. In addition to these code changes, the 1971 San Fernando earthquake stimulated research activity on seismic problems related to bridges.

In the light of these research findings, the Federal Highway Administration awarded a contract in 1978 to the Applied Technology Council (ATC) to evaluate current criteria used for seismic design of highway bridges, develop new and improved seismic design guidelines for highway bridges applicable to all regions of United States. The guidelines from this ATC project, known as ATC-6, *Seismic Design*

Guidelines for Highway Bridges (ATC, 1981), were first adopted by AASHTO as a Guide Specification in 1983. They were later adopted as seismic provisions within the AASHTO *Standard Specifications for Highway Bridges* as Division I-A in 1991.

After damaging earthquakes occurred in California (1989), Costa Rica (1991) and the Philippines (1991), AASHTO requested the Transportation Research Board (TRB) to review these criteria and prepare revised specifications as appropriate. Funded through the AASHTO sponsored National Cooperative Highway Research Program (NCHRP) under NCHRP Project 20-7, Task 45, the Multidisciplinary Center for Earthquake Engineering Research (MCEER, formerly known as NCEER) prepared an updated set of seismic design provisions which closely followed the previous criteria but removed ambiguities and introduced limited new material that was based on field experience and new research findings. The updated provisions were adopted into both the AASHTO *Standard Specifications* and the first and second editions of AASHTO *LRFD Bridge Design Specifications.* However, the technical basis for the updated provisions was essentially the same as that of the ATC-6 provisions which were initially published in 1981.

In 1998, the NCHRP initiated a subsequent study under NCHRP Project 12-49 to develop a new set of seismic design provisions for highway bridges, compatible with the AASHTO *LRFD Bridge Design Specifications*. NCHRP Project 12-49, which was conducted by a joint venture of the Applied Technology Council and the

Multidisciplinary Center for Earthquake Engineering Research (the ATC/MCEER Joint Venture), had as its primary objective the development of seismic design provisions that reflected the latest design philosophies and design approaches that would result in highway bridges with a high level of seismic performance. (MCEER/ATC 49, 2003a)

In 2003, the ATC/MCEER Joint Venture, published a set of documents, *Recommended LRFD Guidelines for the Seismic Design of Highway Bridges, Part I, Specifications, and Part II, Commentary and Appendices*. NCHRP Project 12-49 also included a companion study to investigate the effects of liquefaction. The liquefaction study is documented in the MCEER/ATC-49-1 Report, *Liquefaction Study Report, Recommended LRFD Guidelines for the Seismic Design of Highway Bridges*, and the design examples are provided in the companion MCEER/ATC-49-2 Report, Design Examples, *Recommended LRFD Guidelines for the Seismic Design of Highway Bridges.* (MCEER/ATC 49-1, 2003). These guidelines formed the starting point for the research described in this study, and are summarized below.

5.2. NCHRP Design Approach for Bridge Piles Subject to Earthquake Induced Lateral Spread

The NCHRP design approach has new concepts and major modifications to the existing provisions such as the treatment of liquefaction in the capacity of pile foundations.

Liquefaction has been one of the most significant causes of damage to bridge structures during past earthquakes. Most of the damage has been related to lateral movement of soil at the bridge abutments. However, cases involving the loss of lateral and vertical bearing support of foundations for central piers of a bridge have also occurred. The NCHRP design approach outline procedures for estimating liquefaction potential using methods developed in 1997, as part of a national workshop on the evaluation of liquefaction. Procedures for quantifying the consequences of liquefaction, such as lateral flow or spreading of approach fills and settlement of liquefied soils, are also given. The provisions also provide specific reference to methods for treating deep foundations extending through soils that are spreading or flowing laterally as a result of liquefaction. (MCEER/ATC 49, 2003a)

When liquefaction occurs, inertial bridge response and permanent lateral spread movement occur simultaneously during a seismic event. The recommended methodology in the NCHRP provisions is to consider the two effects independently; i.e., de-coupled.

In the case of the lateral flow occurrence, significant movement of the abutment and foundation systems can result and this can be a difficult problem to mitigate. The range of design options include (1) designing the piles for the flow forces to (2) an acceptance of the predicted lateral flow movements, provided inelastic hinge rotations in the piles remain within a specified limit. The acceptance of plastic

hinging in the piles is a deviation from past provisions in that damage to piles is accepted when lateral flow occurs, thereby acknowledging that the bridge may need to be replaced if this option is selected. (MCEER/ATC 49, 2003a)

In support of the NCHRP 12-49 study to develop the next generation of seismic design guidelines for new bridges, a detailed study of design approaches to evaluate and mitigate liquefaction induced lateral spread deformations was undertaken. The design approaches as documented in the recommended LRFD Guidelines for the Seismic Design of Highway Bridges were summarized in Martin et al (2002) paper, where the beneficial effects of considering the resistance that the bridge substructure offers to lateral displacements of soil via a "pinning" action was discussed. In addition the benefits of allowing inelastic behavior of pile foundations under the action of lateral spread of ground were discussed. (Martin,G.R., Marsh, L.M., Anderson, D.G., Mayes, R.L, Power, M.S., 2002).

5.2.1. Methodology for Lateral Spread Impact Assessment and Design for Bridges

Martin et al, (2002) summarized the design approaches cited above and outlined case studies of two liquefaction prone sites and their respective bridge structures which were in Washington State and Missouri. In their study the importance of pile pinning effects in reducing lateral ground deformations was identified together with the need

to recognize the importance of pile ductility and its acceptance in MCE life safety events.

The NCHRP methodology involves the following four basic steps:

1. Slope stability analyses are conducted to determine the minimum yield acceleration, and associated failure surface (normally associated with the deepest soil layer showing liquefaction potential (FOS,1). Pinning effects of the piles may be included or an increase in resistance of the soil site due to ground improvement.
2. Newmark sliding block are performed to estimate displacements of the soil-pile system
3. The passive force that can ultimately develop against a pile or foundation as soil movement occurs is estimated, and
4. The likely plastic mechanisms that may develop in the foundations and substitute due to lateral spread are evaluated.

The rationale behind the proposed method is to assess the ability of the structure to both accommodate this movement and/or potentially limit the movement. The framework of a simplified approach to the design problem using the above concepts and adopted in the LRFD guidelines, is outlined below:

To design for the impact of the earthquake induced lateral spread on bridge pile foundations, LRFD approach consists of the following steps:

- Step 1: the soil layers that are likely to liquefy are identified.
- Step 2: Residual undrained strengths are assigned for layers that liquefy A pseudo-static seismic stability analysis is conducted to determine the minimum yield acceleration k_y. This defines the depths of soil likely to move and the extent of the likely-soil failure block.(Figure 5.1) The slope stability is calculated using limit equilibrium method. The block failure due to the movement of the upper non liquefiable layer on top of the liquefiable layer constitutes the mode of failure. The failure plane corresponding to the lowest factor of safety against liquefaction is also shown in Figure 5.1

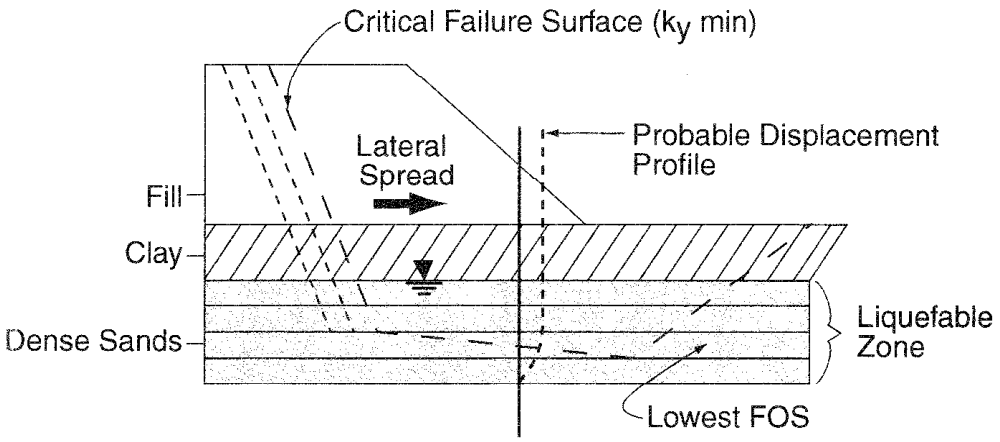

Figure 5-1: Movement of the Slope due to Lateral Spread (Martin et al., 2002)

- Step 3: the maximum displacement of the soil is estimated. This can be accomplished using the simplified Newmark charts or the Newmark Time History.
- Step 4: An assessment is made whether soil moves past the foundation or movement of the foundation occurs in concert with the soil. This assessment requires a comparison between the estimated passive soil forces that can be exerted on the foundation and the ultimate structural resistances that can be developed by the structure. In cases where a crust of non-liquefied material may exist at the ground surface, the full structural resistance may be less than the displacement-induced passive forces and, in such cases; the foundation is likely to continue to move with the soil. Schematic illustrations of the two cases are shown (figures 5-2 and 5-3)

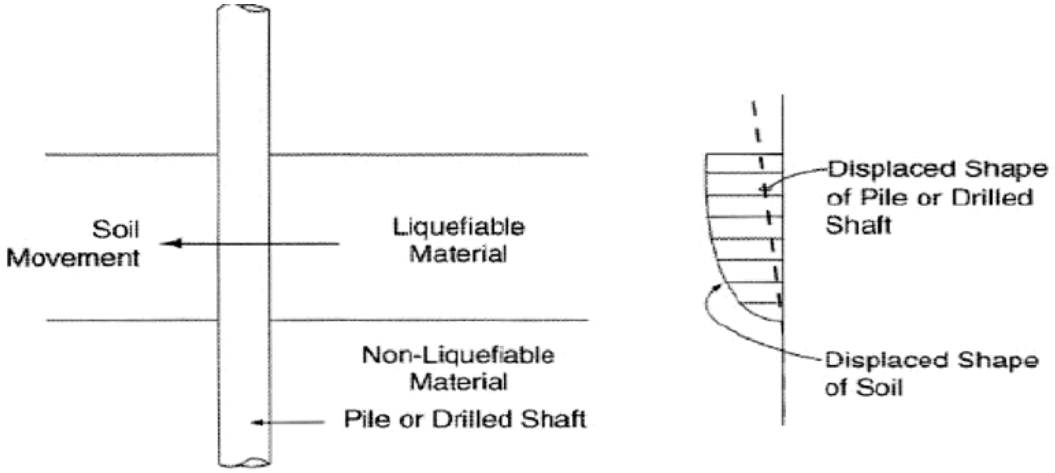

Figure 5-2: Movement of Liquefiable Soil Passed Pile or Drilled Shaft (Martin et al., 2002)

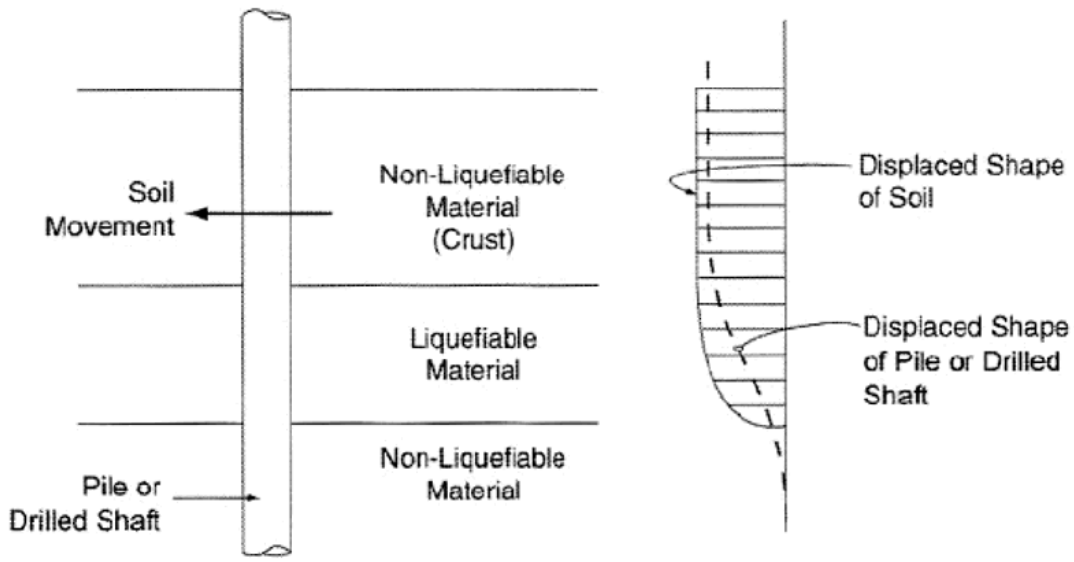

Figure 5-3: Movement of Liquefiable Soil with Crust with Pile or Drilled Shaft (Martin et al., 2002)

- Step 5: If movement of soil around the structure is indicated, then the foundation is designed to withstand the passive pressures created by the soil moving around the structure. The induced forces are effectively the largest forces that the structure will experience and, for this reason, it is conservative to design a structure for such forces.
- Step 6: If on the other hand, the assessment indicates that movement of the foundation is likely to occur in concert with the soil, then the structure must be evaluated for adequacy at the maximum expected displacement. The implication of this assessment is that for relatively large ground movements, soil displacements are likely to induce similar magnitude movements of the foundation. In this context, "large" is taken relative to the structural yield resistance. The resulting induced movements of the foundations may produce

substantial plasticity or hinge zones in the foundations, and may induce relatively large reactions in the superstructure. For an upper level earthquake event, the recommended acceptance criterion is a plastic rotation of 0.05 radians, although values determined by rational cross section analyses are also acceptable and preferred in many cases.

- Step 7: If deformations in step 6 are not acceptable, there are realistically only two ways to restrict the foundation and substructure forces to acceptable values. The first method is to design or retrofit the foundations to resist the forces that would accompany passive flow of the soil around the foundations. The second method would be to limit the ground movement by providing either ground or structural remediation. It is the structural option that provides a potential first path, and this makes use of the "pinning" or dowel action that pile or shaft foundations contribute as they cross the potential failure plane of the moving soil. This can effectively reduce the magnitude of lateral displacement.
- Step 8: The determination of the plastic mechanism that is likely to occur in the presence of spreading should be done. Estimates of the mechanism could be based on hinge development in stable or firm soil zones above and below (by say 2 pile diameters) the liquefiable layer. Maximum "pinning" shear could then be assumed equal to $2M_p/L$, where M_P is the plastic moment and L is the distance between hinges- this assumes that the load transfer in the liquefied zone is negligible.

- Step 9: The system must be assessed for a prescribed displacement field to represent the likely soil spreading deformation. From this analysis, an estimate of the likely shear resistance the foundation will provide is estimated and this shear can then be incorporated back into the stability analysis.
- Step 10: If substantial resistance is provided, then its effect on limiting the instability driven movement of the soil block should be accounted for.
- Step 11 and 12: The overall displacement is re-calculated and once a realistic displacement is calculated, then the foundation and structural system can be assessed for this movement. It is at this point that more permissive displacements than those allowed for substructure design can be relied upon. This implies that plastic rotations may be allowed to occur in the foundation under such conditions.
- Step 13: If the behavior of the structure is acceptable then the liquefaction design is complete; if not, then the designer must assess whether to try to produce adequacy either additional piles or shafts (Note that these may not need to connect to the foundation (passive piles) or the pile cap. Alternatively, ground improvement approaches may be considered such as stone columns.

Figure 5-4 shows the flow chart for the LRFD methodology.

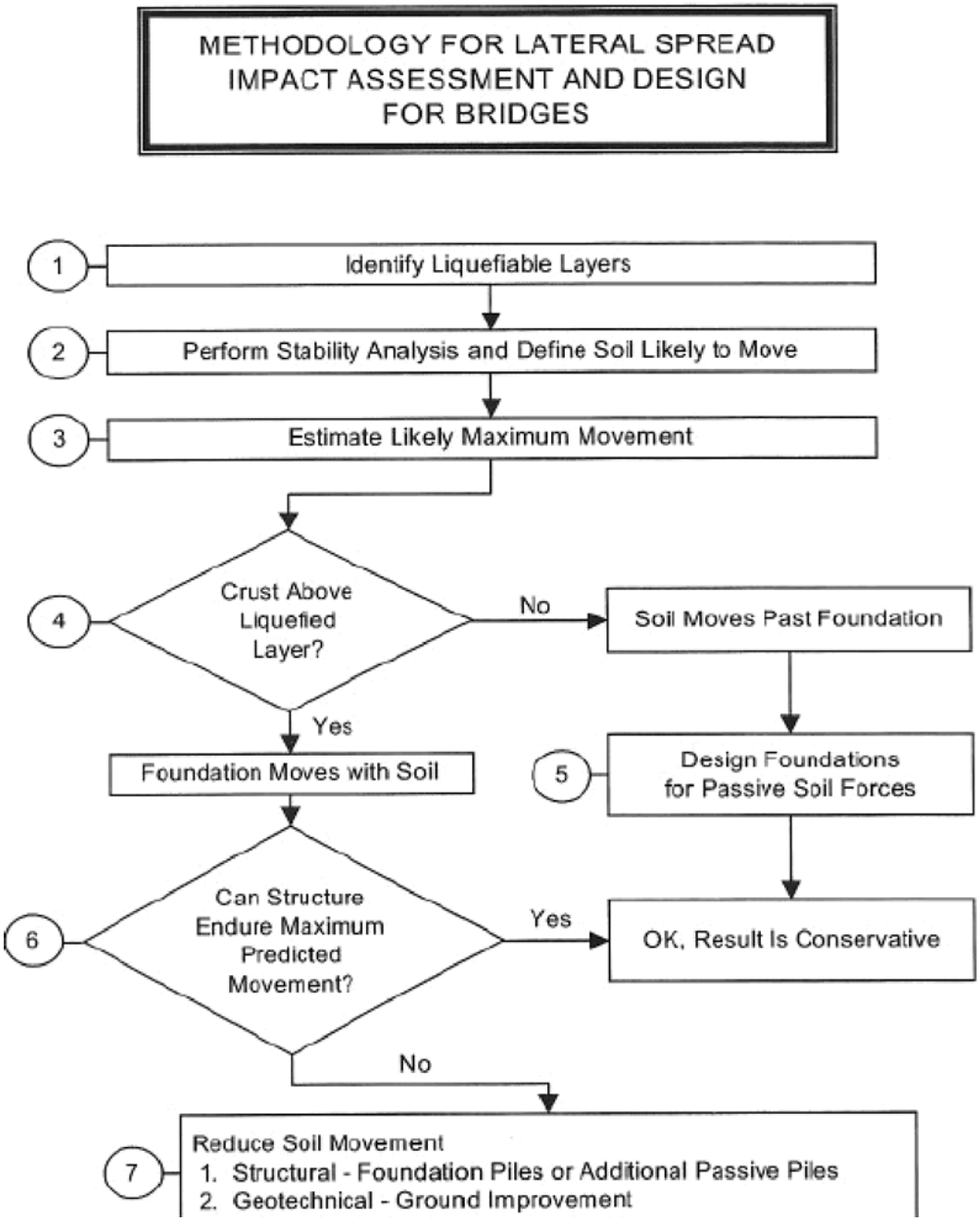

Figure 5-4 (a): Methodology for Lateral Spread Impact Assessment and Design For Bridges (MCEER/ ATC 49 (2003b))

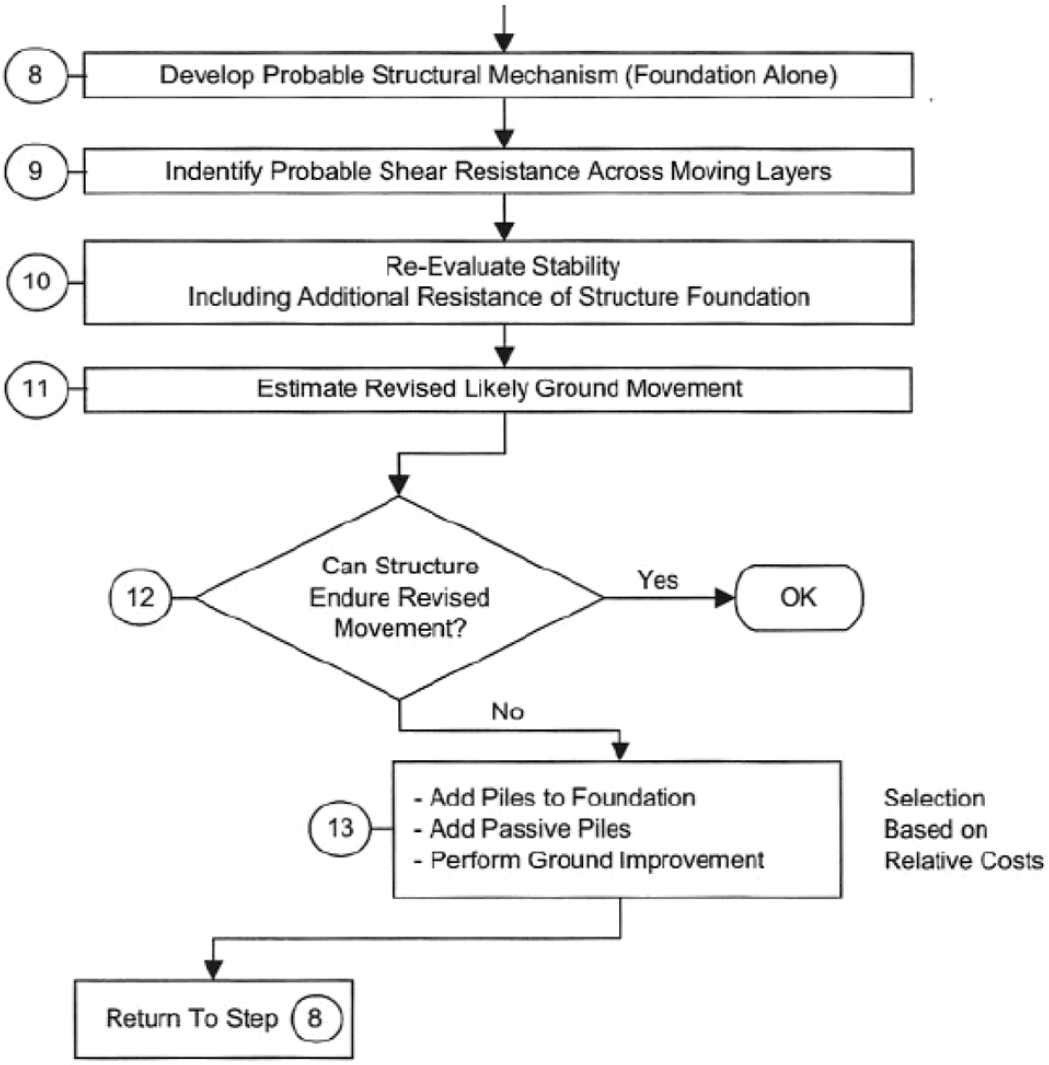

Figure 5-4 (b): Methodology for Lateral Spread Impact Assessment and Design For Bridges (MCEER/ ATC 49 (2003b))

The pinning contribution by the piles is recognized in the NCHRP 12-49. The calculation of the pinning force is based on the smearing of the pile shear along the base of the failure plane. Pile shear estimates are based on hinge development in stable or firm soil zones above and below (by say 2 pile diameters) the liquefiable layer. Maximum "pinning" shear is assumed to be equal to 2Mp/L where Mp is the

plastic moment and L the distance between hinges. The yield deflection of the piles is also based on the latter distance which makes it at best an approximation.

The plastic drift of the pile is based on the distance cited above and the plastic rotation of the pile assumed to be 0.05 radians. The latter value is based on assumptions for the plastic curvature and the plastic hinge length that can be developed for the given piles.

The primary objectives of this thesis is to develop fundamental modifications on the pinning and pile ductility evaluations which ultimately improves the pile response to lateral spread provided in the NCHRP 12-49 design approach. Details as to how these improvements are achieved are provided in Chapter 7.

5.3. Case Studies

Two case studies, Western United States Site (Washington bridge) and Mid-America Site (Missouri Bridge) are considered in the NCHRP (2003) study. These bridges were part of the latter study to evaluate NCHRP design methodology. The following presents a description of these bridges and their site characterization. These bridges are reevaluated in Chapter 7, using the *improved design methodology* described in that Chapter, together with a comparison with results using the NCHRP (2003) methodology.

5.3.1. Missouri Bridge

The bridge consists of an existing prestressed girder (Figure 5-5), three span bridge structure 180 feet long, supported on three-column bents.

The substructure is formed of 3 foot diameter columns, which support a 40 inch dropped cap beam. They are of the integral type, where the end diaphragm is integrated with the end of the girders and deck. The site is located along the western edge of the Mississippi River alluvial plane in southeastern Missouri, within the New Madrid earthquake source zone.

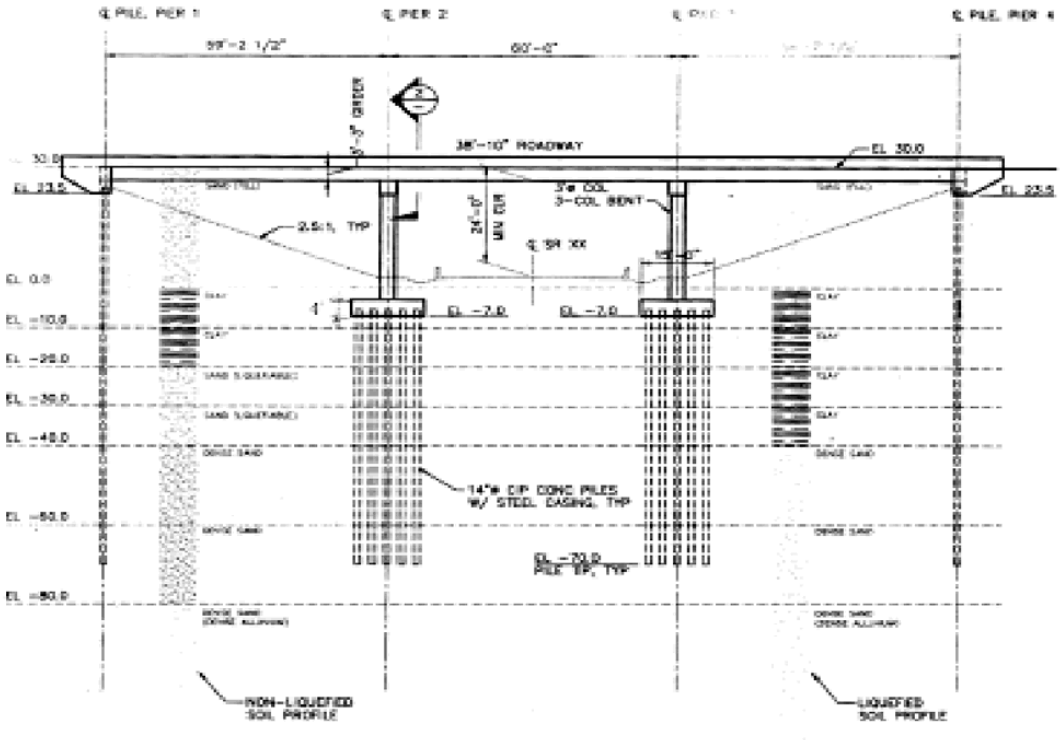

Figure 5-5: Missouri Bridge Configuration (NCHRP, 2002)

5.3.1.1. Foundation of the Bridge Structure

The foundations are comprised of 14 inch steel pipe piles (filled with concrete) that are driven into the native material. The thickness of the steel pipe shell is 0.25 inch. (See Table 5-1)

Location	Bottom of Footing Elevation (ft)	Specified Pile Tip Elevation (ft)
Pier 1 (Abutment)	23.5	-70
Pier 2 (Bent)	-7	-70
Pier 3 (Bent)	-7	-70
Pier 4 (Abutment)	23.5	-70

Table 5-1: Pile Information (Missouri Bridge)

5.3.1.2. Geotechnical Exploration Program

The geotechnical exploration program corresponding to the Missouri Bridge under study by the NCHRP has been performed by MODOT and included boreholes with SPTs to 100 feet or more below the ground surface, CPTs to depth of 40 feet, and shear wave velocity measurements in the upper 40 feet of soil profile. The following (Table 5-2) represents the simplified liquefiable soil profile:

LIQUEFIABLE SOIL PROFILE, PIER 4									
							Including Group Effects		
Elev. (ft)	Soil Type	Cohesion (psf)	Friction Angle	Eff.unit weight (pcf)	Subgrade Modulus k (pci)	Strain @ 50%	Cohesion (psf)	Friction Angle	Subgrade Modulus K (pci)
30-0	Sand (fill)	-	37	130	150	-	-	31	75
0-(-10)	Soft Clay	1000	-	110	10	0.01	500	-	5
10	Soft Clay	2000	-	110	20	0.02	1000	-	10
-20[1]-(-30)	Liquefied Sand	300	-	48	3	0.01	150	-	1.5
10	Liquefied Sand	300	-	48	3	0.01	150	-	1.5
20	Dense Sand	-	38	63	100	-	-	32	50
20	Dense Sand	-	38	63	100	-	-	32	50
-80	Dense Sand	-	40	63	200	-	-	34	100

[1] Ground Water Elevation

Table 5-2: Engineering Characteristics of Subsurface Soil at Missouri Bridge (NCHRP, 2003)

5.3.1.3. Seismicity

Peak ground acceleration (PGA) of 0.17g was used for the 475 year event with the mean earthquake magnitude of 6.6. Peak ground acceleration (PGA) of 0.53g was used for the 2,475 year event with the mean earthquake magnitude of 7.5.

5.3.1.4. Liquefaction and Lateral Spread at Pier 4

At abutment 4, the underlying soil is subject to liquefaction from elevation –20 to –30 and –30 to –40. The sloping ground underlain by liquefiable soil layers at pier 4, may cause lateral spreading of the embankment during the design earthquake. Resulting lateral displacements based on the Newmark sliding block method, were about 30 ins, for the 2475 year event and 8 in.for the 475 year event due to liquefaction lateral spread.

5.3.2. Washington Bridge

The project consists of the study of an existing concrete box girder (Figure 5.6), five span bridge structure 500 ft long, comprised of a 6 foot deep concrete box girder that is continuous between the two abutments. The intermediate piers are two-column bents. The roadway is 40 feet wide. The two 4 foot diameter columns for each pier are approximately 23 feet apart, and due to the relatively large size of the pile caps, a single combined pile cap was used for both columns at each pier. The abutments are of the overhanging stub abutment type. The site is located on the Duwamish River, approximately 4 miles south of downtown Seattle in the State of Washington.

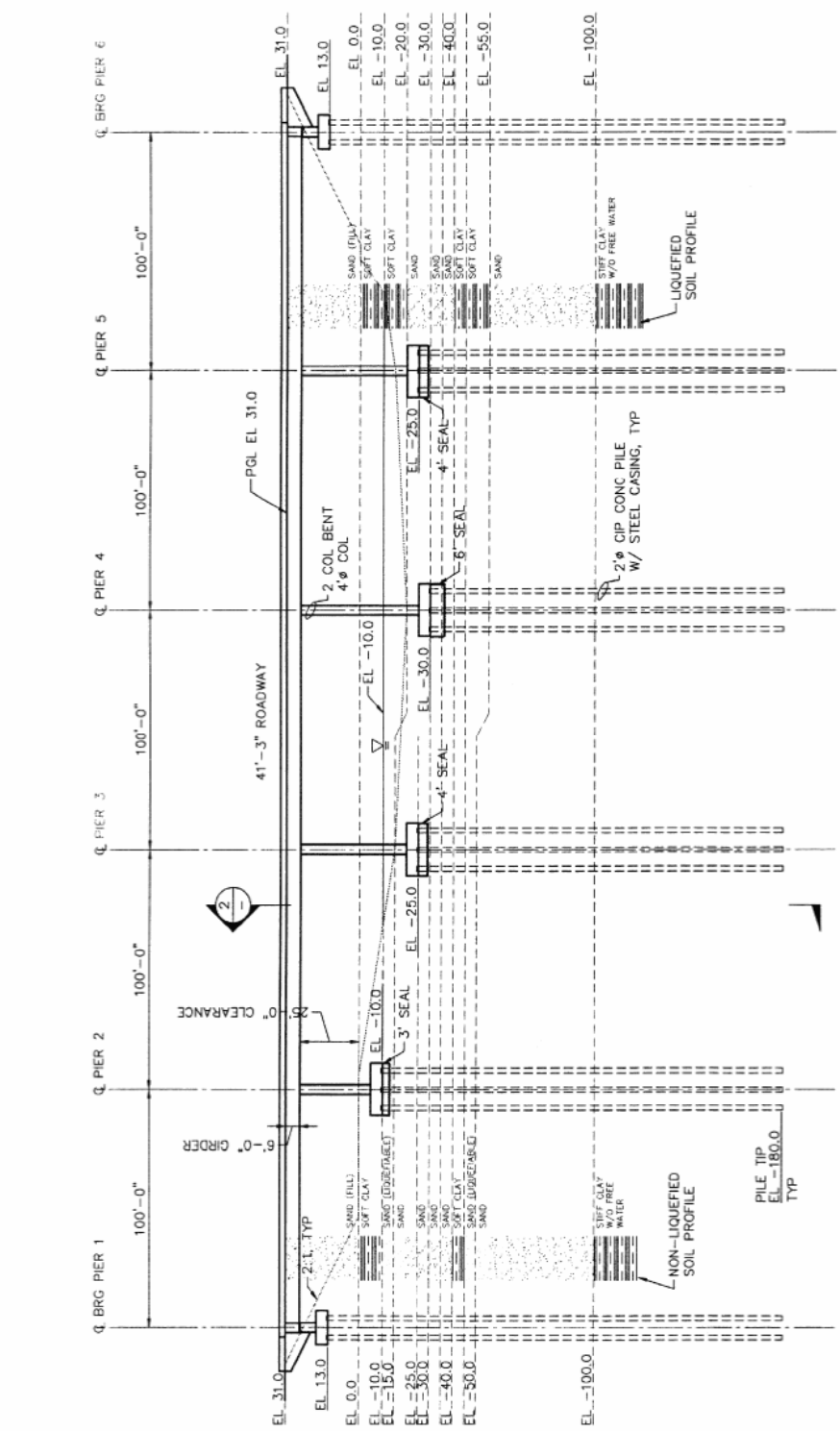

Figure 5.6: Washington Bridge Configuration (NCHRP, 2003)

5.3.2.1. Foundation of the Bridge Structure

The foundations are comprised of 24 inch steel pipe piles that are driven to a specified tip elevation (Table 5.3) into the native material. The piles are filled with reinforced concrete. The thickness of the steel pipe shell is 0.5 inch.

Location	Bottom of Footing Elevation (ft)	Specified Pile Tip Elevation (ft)
Pier 1 (Abutment)	13	-180
Pier 2 (Bent)	-10	-180
Pier 3 (Bent)	-25	-180
Pier 4 (Bent)	-30	-180
Pier 5 (Bent)	-25	-180
Pier 6 (Abutment)	13	-180

Table 5.3: Foundation Table

5.3.2.2. Geotechnical Exploration Program

The geotechnical exploration program corresponding to the Washington Bridge under study by the NCHRP was based on a prototype site that had undergone a detailed exploration by Washington Department of Transportation. This program consisted of cone penetrometer testing (CPT) with pore water pressure measurements to over 150 feet depth, standard penetration testing (SPT) to a maximum depth of 250 feet and shear wave velocity measurements to depths of 100 feet. A total of fifteen CPT's, twelve boring holes using SPT and four shear wave velocity measurements were performed.

5.3.2.3. Design Subsurface Soil Profile

At the prototype site, the soil at depths of less than 150 feet are generally alluvial deposits. At greater depths some estuarine materials exist and below about 200 feet dense glacial materials are found. The actual soil profile at the site has many layers of material with broad variations of properties and densities.

The actual site profile was simplified such that fewer layers exist and the profile is the same across the entire site (Figure 5.7). The following (tables 5.4 and 5.5) represent the simplified soil profile for both Non-Liquefied Soil and Liquefied Soil Profiles.

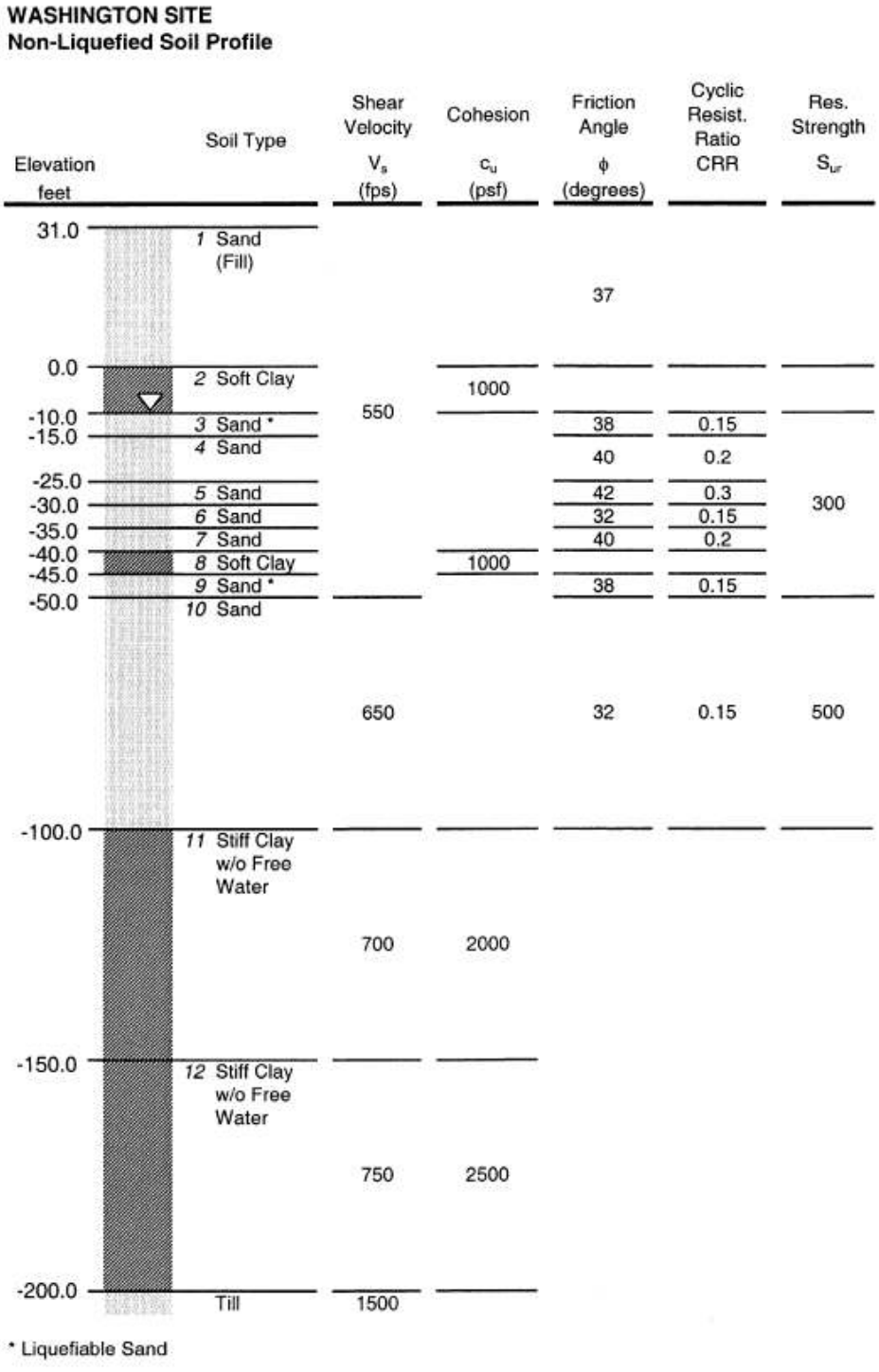

Figure 5.7: Washington Bridge Site Subsurface Profile (NCHRP, 2003)

NON-LIQUEFIABLE SOIL PROFILE									
							Including Group Effects		
Elev. (ft)	Soil Type	Cohesion (psf)	Friction Angle	Density (pcf)	Subgrade Modulus k (pci)	Strain @ 50%	Cohesion (psf)	Friction Angle	Subgrade Modulus K (pci)
31-(0)	Sand (fill)	-	37	110	150	-	-	31	75
0-(10)	Soft Clay	1000	-	120	10	0.01	500	-	5
-30	Sand	-	38?	60	50	-	-	32?	25
10	Sand	-	30	60	40	-	-	23	20
5	Sand	-	24	60	40	-	-	19	20
5	Sand	-	30	60	40	-	-	23	20
5	Soft Clay	1000	-	60	10	0.01	500	-	5
10	Sand	-	38	60	50	-	-	32	25
45	Sand	-	26	60	50	-	-	21	25
-250	Stiff Clay	2000	-	60	200	0.005	1000	-	100
50	Stiff Clay	2500	-	60	200	0.005	1250	-	100
-200	Till								

Table 5.4: Engineering Characteristics of Subsurface Soil at Washington Bridge (NCHRP, 2003)

LIQUEFIABLE SOIL PROFILE									
							Including Group Effects		
Elev. (ft)	Soil Type	Cohesion (psf)	Friction Angle	Density (pcf)	Subgrade Modulus k (pci)	Strain @ 50%	Cohesion (psf)	Friction Angle	Subgrade Modulus K (pci)
31-0	Sand (fill)	-	37	110	150	-	-	31	75
0-(-10)	Soft Clay	1000	-	120	10	0.01	500	-	5
-30	Liquefied Sand	300	-	60	3	0.02	150	-	1.5
10	Sand	-	30	60	40	-	-	23	20
5	Sand	-	24	60	40	-	-	19	20
5	Sand	-	30	60	40	-	-	23	20
5	Soft Clay	1000	-	60	10	0.01	500	-	5
10	Liquefied Sand	300	-	60	50	0.02	150	-	25
-155	Sand	-	26	60	50	-	-	21	25
-250	Stiff Clay	2000	-	60	200	0.005	1000	-	100
-350	Stiff Clay	2500	-	60	200	0.005	1250	-	100
-200	Till								

Table 5.5: Engineering Characteristics of Subsurface Soil at Washington Bridge (NCHRP, 2003)

5.3.2.4. Seismicity

Peak Ground Acceleration (PGA) was used for the 475 year event with the mean earthquake magnitude of 6.5. Peak Ground Acceleration (PGA) of 0.42g were used for the 2,475 year event with the mean earthquake magnitude of 6.5.

5.3.2.5. Liquefaction and Lateral Spread at Abutment 6 and Pier 5

Evaluations of liquefaction potential for the 2475 year event, show liquefaction in all sands without overlying fill, and with overlying fill for layers at elevations -10 to -15 ft, -30 to -35 ft and -45 to -50 ft. For the 475 year event, liquefaction occurs in sands at elevations -30 to -35 ft and -45 to -50 ft with overlying fill, but does not occur for sands below the fill.

The sloping ground underlain by liquefiable soil layers at Abutment 6, may cause lateral spreading of the embankment during the design earthquake. Pier 5 is subject to lateral spreading during the design earthquake.

Resulting lateral displacements based on the Newmark sliding block method, were about 8 ins, for the 2475 year event and 5 ins. for the 475 year event due to liquefaction lateral spread.

CHAPTER 6: CALTRANS DESIGN APPROACH

This chapter provides a summary of current Caltrans Seismic Design Approaches to provide additional background to the development of an improved methodology in Chapter 7. Comments on superstructure design are first described leading to the approach adopted for foundation and liquefaction induced lateral spread design by Caltrans.

Caltrans (SDC, 2006) uses "Ductility-based" design procedures to quantify the damage to bridge structures and to prevent collapse of California bridges as they are subjected to the maximum credible earthquake (MCE). Certain structural components, such as columns and shafts, are targeted to receive the damage and dissipate the seismic energy. All other bridge components are "capacity-protected", because they are more difficult to repair. The plastic hinges in columns and shafts limit the seismic force flowing through the bridge. Bridge foundations are seismically designed to be stronger than the columns they support and to allow bridges to have a displacement capacity greater than the displacement demand for the MCE.

6.1. Seismic Design Philosophy

The following fundamental philosophies are utilized in the seismic design of all bridges to ensure satisfactory performance during seismic events.

6.1.1. Collapse Limit State

The collapse limit state is defined as the condition where any additional deformation will potentially render a bridge incapable of resisting the loads generated by its self-weight. Structural failure or instability in one or more components usually characterizes collapse. All forces (axial, flexure, shear and torsion) and deformations (rotation and displacement) shall be considered when quantifying the collapse limit state.

All bridges shall be designed to withstand deformations imposed by the design earthquake. All structural components shall be designed to provide sufficient strength and/or ductility, with a reasonable amount of reserve capacity, to ensure collapse will not take place during the MCE.

6.1.2. Ductility

Ductility is mathematically defined as the ratio of ultimate deformation to the deformation at yield. Ductile response of structural components is characterized by several cycles of inelastic deformation without significant degradation of strength or stiffness. The most desirable type of ductile response in bridge systems is sustained hysteric force-deformation cycles that dissipate energy. This type of response can be generated either internally, within the structural members, by the deformation of flexural plastic hinges or externally with isolation bearings or external dampers. The

analytically derived deformations are limited so the structures will not exceed its inelastic deformation capacity.

Ordinary bridges are not designed to respond elastically during the design earthquakes because of economic constraints and the uncertainties in predicting seismic demands. Caltrans takes advantage of ductility and post elastic strength to meet the performance criteria with a minimum capital investment. This philosophy is based on the relatively low probability that a major earthquake will occur at a given site, and the willingness to absorb the repair cost at a future date if a major earthquake occurs.

6.1.3. Pre-Determined Locations of Damage

Inelastic behavior is limited to pre-determined locations within the bridge that can be easily inspected and repaired following an earthquake. Continuous column/pile shaft combinations are an exception since elastic behavior may occur below ground. Preferable locations for inelastic behavior on most bridges include columns, pier walls, backwalls, wingwalls, seismic isolation and damping devices, bearings, shear keys and steel end-diaphragms.

Significant inelastic response in concrete superstructures is not desirable because they are difficult to inspect and repair. Furthermore, superstructure damage may prevent the bridge from being repaired to a serviceable condition.

6.2. Seismic Design Approach

Displacement ductility approach requires the designer to ensure that the structural system and its individual components have enough capacity to withstand the deformations imposed by the design earthquake.

A bridge's displacement capacity is dependent on the structural configuration and the formation and rotational capacity of flexural hinges. The displacement capacity of a bridge can be assessed with an inelastic static "pushover" analysis that incorporates non-linear inelastic load/deformation behavior of selected components. This enables the designer to determine the location and sequence of hinging within the bridge and provide adequate ductility in the appropriate locations. The designer can control the amount of anticipated inelastic flexural behavior by limiting the allowable material strains in ductile components.

6.2.1. Seismic Demands on Structural Components

In order to evaluate the seismic demand, the displacement demand must be assessed.

6.2.1.1. Displacement Demands

The displacement demands for Ordinary bridges are estimated from a linear elastic response spectra analysis that includes the effective stiffness of its members. Estimating inelastic displacements with elastic analysis is based on the equal displacement observation for single-degree-of-freedom systems. The equal

displacement rule assumes that displacements can be reasonably estimated with linear elastic analysis for bridges with fundamental structural periods (T) that shall fall within the displacement conservation region of the elastic response spectra typically defined as the region between 0.7 seconds and 3 seconds.

6.2.2. Seismic Capacity of Structural Components

6.2.2.1. Component Capacities

Moment-curvature analysis or finite element analysis is used to calculate the strength and deformation capacity of ductile components. Strength formulas specified in the current Caltrans SDC, Bridge Design Specifications, moment curvature analysis, or finite element analysis are used to calculate the strength capacity of essentially elastic components.

6.2.2.2. Plastic Hinge Performance

The displacement ductility approach relies on a bridge's ability to undergo dependable deformation in plastic hinge regions without experiencing brittle failure. The rotation capacity of all plastic hinges shall be limited to a "safe" performance level. Plastic hinge capacity shall be based on the most probable material properties. Plastic hinge regions shall be designed and detailed to perform with minimal degradation in strength under sustained cyclic loading.

6.3. Seismic Design Practice

Caltrans seismic design practice is based on meeting a set of performance requirements for a given structure component.

6.3.1. Performance Requirements

The estimated displacement demands generated by the design earthquake shall not exceed the structure's global displacement capacity or the local displacement capacity of any of its individual components.

6.3.2. Concrete Bents

The initial sizing of concrete bents shall be based on the slenderness ratio (KL/r), bent cap depth, compressive stress ratio, and service loads. Columns must demonstrate dependable post yield displacement capacity without an appropriate loss of strength. Moment-curvature relationships that incorporate the effects of axial load should be used to optimize a column's performance under service loads and seismic loads.

In the case of column/pile shaft combinations, the designer may choose to accept inelastic behavior in the pile shaft. Alternatively, enlarged pile shafts supporting columns with smaller cross sections can be utilized to provide a well-defined location for the formation of the plastic hinge at the base of the column. Enlarged

pile shafts shall be designed to remain essentially elastic when resisting overstrength capacity of the column.

Pier walls, shall be designed to perform in a ductile manner longitudinally (about the weak axis), and to remain essentially elastic in the transverse direction (about the strong axis).

6.3.3. Foundations

Foundation components for Ordinary Standard bridges, except pile shafts and pier wall foundations in the weak direction, shall be designed to remain essentially elastic when resisting the plastic hinging moments, associated shears and axial force at the base of columns and pier walls in the strong direction. Pile shaft foundations are permitted to respond inelastically, if they are designed and detailed in a ductile manner.

The effects of foundation flexibility shall be considered in the seismic design and analysis of all bridges.

6.3.3.1. Foundation Performance

Bridge foundations shall be designed to respond to seismic loading in accordance with the seismic performance objectives outlined above. The capacity of the

foundations and their individual components to resist MCE seismic demands shall be based on ultimate structural and soil capacities.

Caltrans Foundation Seismic Design Criteria is based on ductile columns that form plastic hinges to limit the force in the foundation to less than the column's plastic moment Mp.

Therefore, instead of designing the foundation for an actual earthquake, Caltrans simply designs the foundation (using nominal capacity) for the column's plastic moment.

6.4. Seismic Design Criteria

Current Caltrans Seismic Design Criteria (SDC, 2006, Version 1.4) specify the minimum seismic design requirements that are necessary to meet the performance goals established for Ordinary bridges. The SDC applies to Ordinary Standard bridges as defined below:

A structure must meet all of the following requirements to be classified as an Ordinary Standard bridge:

- Span lengths less than 300 feet (90 m)
- Constructed with normal weight concrete girder, and column or pier elements

- Horizontal members either rigidly connected, pin connected, or supported on conventional bearings by the substructure, isolation bearings and dampers are considered nonstandard components.
- Dropped bent caps or integral bent caps terminating inside the exterior girder, C-bents, outrigger bents, and offset columns are nonstandard components.
- Foundations supported on spread footing, pile cap w/piles, or pile shafts
- Soil that is not susceptible to liquefaction, lateral spreading, or scour

6.4.1. Displacement Ductility Demand

Ductility demand in relation to column design is described below as background to applications to piles described in Chapter 7. Displacement ductility demand is a measure of the imposed post-elastic deformation on a member. Displacement ductility is mathematically defined by:

$$\mu_D = \Delta_D / \Delta_{Y(i)}$$

Where:

Δ_D = The estimated global frame displacement demand.

$\Delta_{Y(i)}$ = The yield displacement of the subsystem from its initial position to the formation of plastic hinge (i) , see figure 6-1.

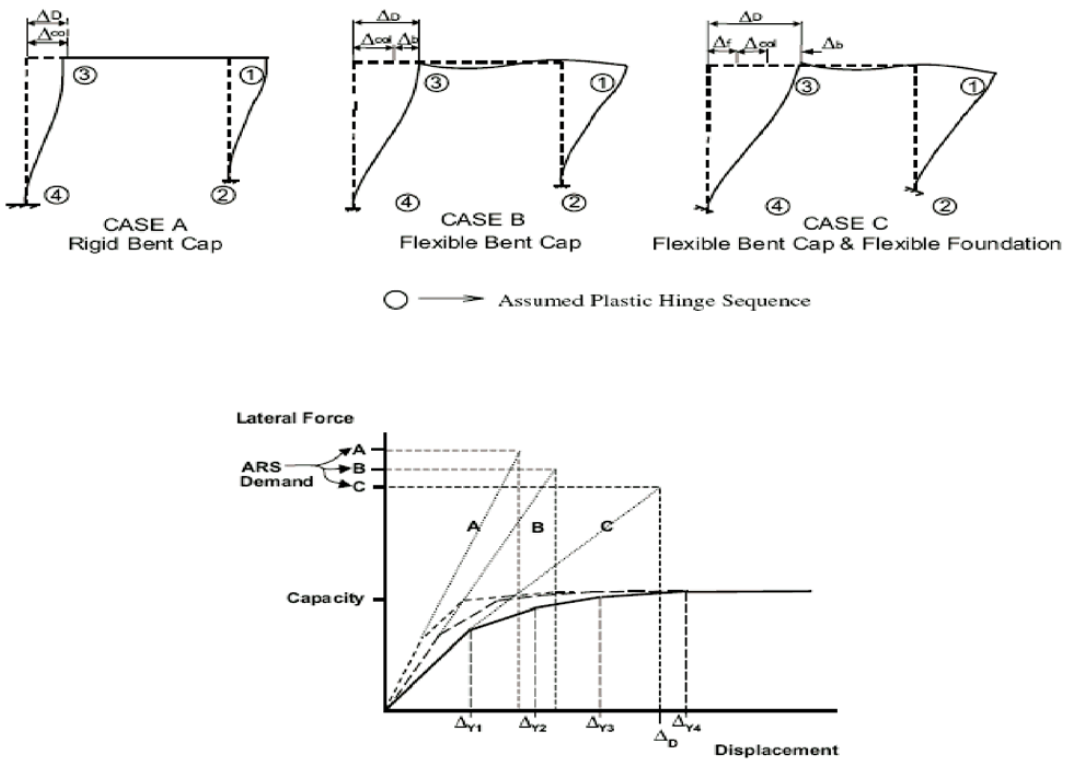

Figure 6-1: Displacement Ductility Demand (SDC, 2006)

6.4.2. Target Displacement Ductility Demand

The target displacement ductility demand values for various components are identified below. These target values have been calibrated to laboratory test results of fix-based cantilever columns where the global displacement equals the column's displacement. For Type I or Type II shafts, the global demand values listed below may not be achieved.

Single Column Bents supported on fixed foundation $\mu_D \leq 4$

Multi-Column Bents supported on fixed or pinned footings $\mu_D \leq 5$

Pier Walls (weak direction) supported on fixed or pinned footings $\mu_D \leq 5$

Pier Walls (strong direction) supported on fixed or pinned footings $\mu_D \leq 1$

6.4.3. Pile Shaft

Pile shafts are categorized into two types: Pile Shaft Type I and Pile Shaft Type II (Figure 6-2). Type I pile shafts are designed so the plastic hinge will form below ground in the pile shaft. The concrete cover and area of transverse and longitudinal reinforcement may change between the column and type I pile shaft, but the cross section of the confined core is the same for both the column and the pile shaft. The global displacement ductility demand, μ_D for a Type I pile shaft shall be less than or equal to the μ_D for the column supported by the shaft.

Type II pile shafts are designed so the plastic hinge will form at or above the shaft/column interface, thereby, containing the majority of inelastic action to the ductile column element. Type II shafts are usually enlarged pile shafts characterized by a reinforcing cage in the shaft that has a diameter larger than the column it supports. Type II pile shafts shall be designed to remain elastic; $\mu_D \leq 1$

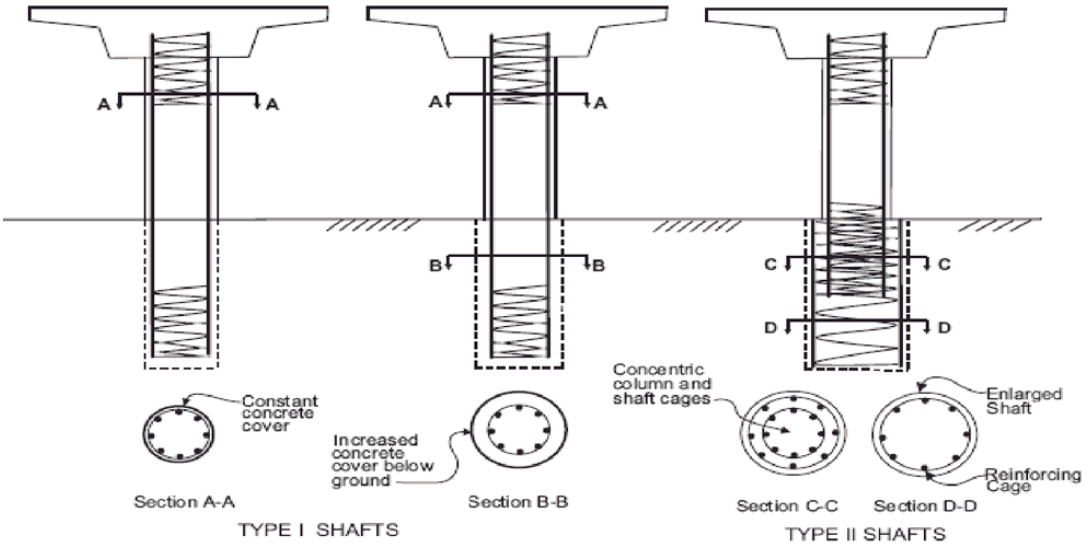

Figure 6-2: Types of Pile Shafts (SDC, 2006)

6.4.4. Displacement Capacity of Ductile Concrete Members

Local member displacement capacity, Δ_C is defined as a member's displacement capacity attributed to its elastic and plastic flexibility as defined below:

6.4.4.1. Local Member Displacement Capacity

The local displacement capacity of a member is based on its rotation capacity, which in turn is based on its curvature capacity. The curvature capacity shall be determined by M-ϕ analysis. Moment curvature analysis derives the curvatures associated with a range of moments for a cross section based on the principles of strain compatibility and equilibrium forces. The M-ϕ curve can be idealized with an elastic perfectly plastic response to estimate the plastic moment capacity of a member's cross section.

The elastic portion of the idealized curve should pass through the point marking the first reinforcing bar yield. The idealized plastic moment capacity is obtained by balancing the areas between the actual and the idealized M-ϕ curves beyond the first reinforcing bar yield point, see figure 6-3.

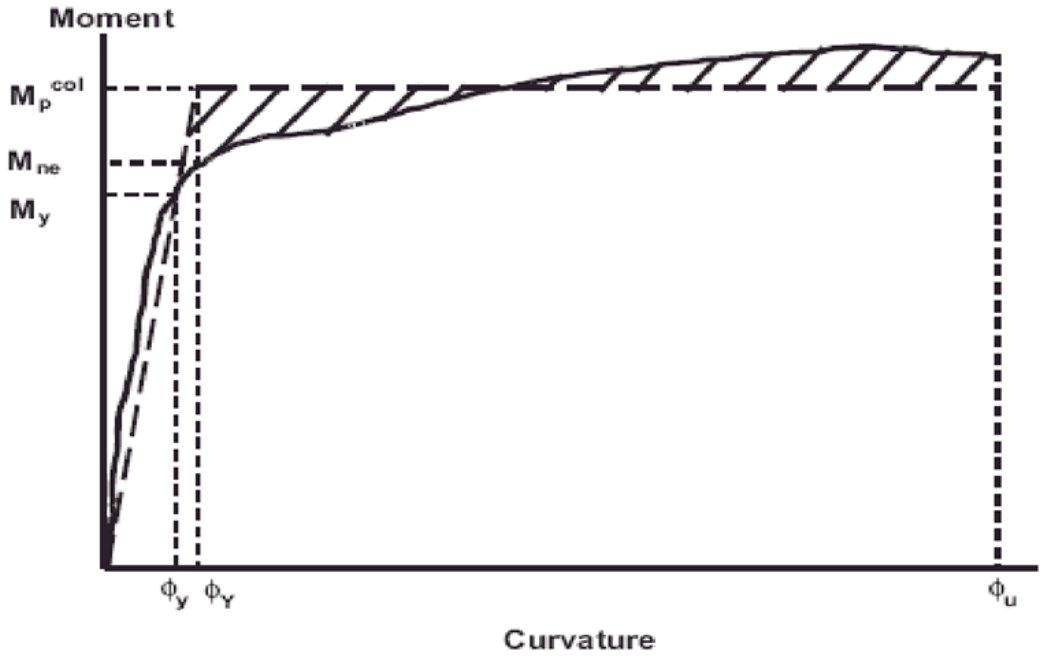

Figure 6-3: Moment Curvature Diagram Idealized (SDC, 2006)

The local displacement capacity Δ_c of any column may be idealized as one or two cantilever segments presented in equations below.

$$\Delta_c = \Delta_Y^{col} + \Delta_p$$

$$\Delta_Y^{col} = \frac{L^2}{3} \times \phi_Y$$

$$\Delta_p = \theta_p \times \left(L - \frac{L_p}{2} \right)$$

$$\theta_p = L_p \times \phi_p$$

$$\phi_p = \phi_u - \phi_Y$$

$$\Delta_{c1} = \Delta_{Y1}^{col} + \Delta_{p1} \quad , \quad \Delta_{c2} = \Delta_{Y2}^{col} + \Delta_{p2}$$

$$\Delta_{Y1}^{col} = \frac{L_1^2}{3} \times \phi_{Y1} \quad , \quad \Delta_{Y2}^{col} = \frac{L_2^2}{3} \times \phi_{Y2}$$

$$\Delta_{p1} = \theta_{p1} \times \left(L_1 - \frac{L_{p1}}{2} \right) \quad , \quad \Delta_{p2} = \theta_{p2} \times \left(L_2 - \frac{L_{p2}}{2} \right)$$

$$\theta_{p1} = L_{p1} \times \phi_{p1} \quad , \quad \theta_{p2} = L_{p2} \times \phi_{p2}$$

$$\phi_{p1} = \phi_{u1} - \phi_{Y1} \quad , \quad \phi_{p2} = \phi_{u2} - \phi_{Y2}$$

Where:

L = Distance from the point of maximum moment to the point of contra-flexure

L_P = Equivalent analytical plastic hinge length.

Δ_P = Idealized plastic displacement capacity due to rotation of the plastic hinge

Δ_Y^{col} = The idealized yield displacement of the column at the formation of the plastic hinge

ϕ_Y = Idealized yield curvature defined by an elastic-perfectly-plastic representation of the cross section's M-ϕ curve

ϕ_P = Idealized plastic curvature capacity (assumed constant over L_P)

ϕ_u = Curvature capacity at the failure Limit State, defined as the concrete strain reaching ε_{cu} or the confinement reinforcing steel reaching the reduced ultimate strain ε_{su}^{R}

θ_P = Plastic rotation capacity

See figures 6-4 and 6-5 for detail.

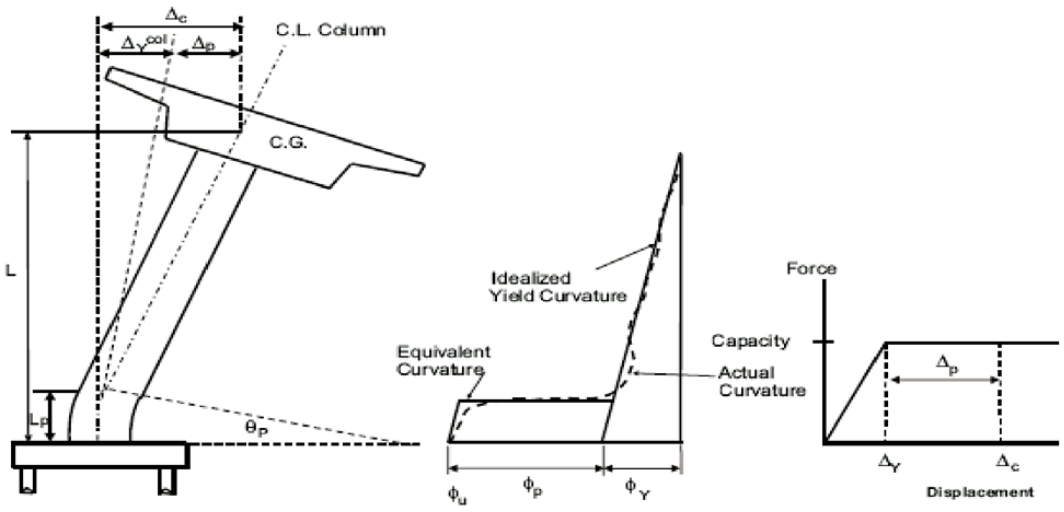

Figure 6-4: Local Displacement Capacity-Cantilever Column w/Fixed Base (SDC, 2006)

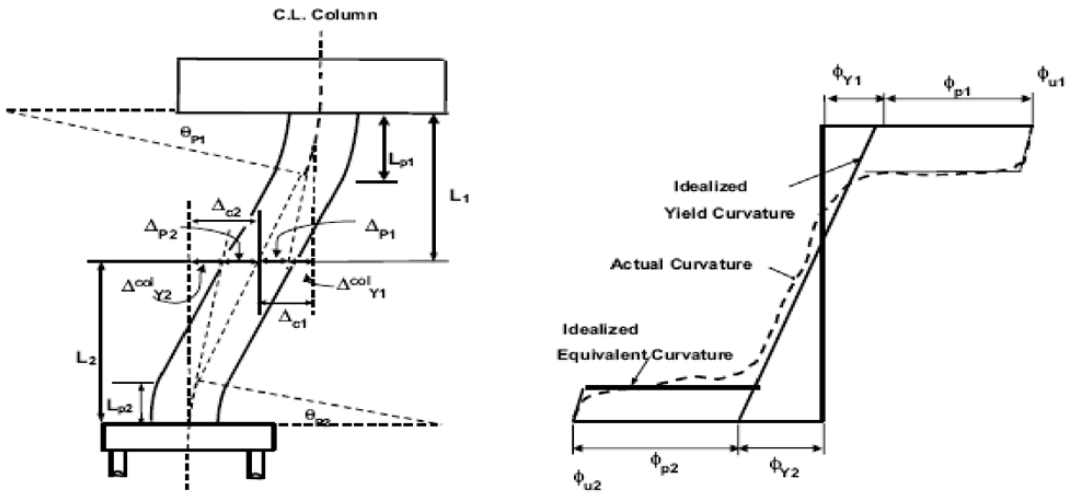

Figure 6-5: Local Displacement Capacity-Framed Column w/Fixed-Fixed (SDC, 2006)

6.4.4.2 Analytical Plastic Hinge Length

The analytical plastic hinge length is the equivalent length of column over which the plastic curvature is assumed constant for estimating plastic rotation.

For Columns and Type II Shafts:

$$L_p = \begin{cases} 0.08L + 0.15 f_{ye} d_{bl} \geq 0.3 f_{ye} d_{bl} & \text{(in, ksi)} \\ 0.08L + 0.022 f_{ye} d_{bl} \geq 0.044 f_{ye} d_{bl} & \text{(mm, MPa)} \end{cases}$$

For Non-cased Type I Pile Shafts:

$$L_p = D^* + 0.08 H_{e\text{-}max}$$

D^* = Diameter for circular shafts or the least cross section dimension for oblong shafts.

6.4.4.3. Local Member Displacement Ductility Capacity

Local displacement ductility capacity for a particular member is defined below:

$$\mu_c = \frac{\Delta_c}{\Delta_Y^{col}} \quad \text{for Cantilever columns,}$$

$$\mu_{c1} = \frac{\Delta_{c1}}{\Delta_{Y1}^{col}} \quad \& \quad \mu_{c2} = \frac{\Delta_{c2}}{\Delta_{Y2}^{col}} \text{ for fixed-fixed columns}$$

6.4.4.4. Minimum Local Displacement Ductility Capacity

Each ductile member shall have a minimum local displacement ductility capacity of $\mu_c = 3$ to ensure dependable rotational capacity in the plastic hinge regions regardless of the displacement demand imparted to that member. The local displacement ductility capacity shall be calculated for an equivalent member that approximates a fixed base cantilever element as defined in figure 6-6:

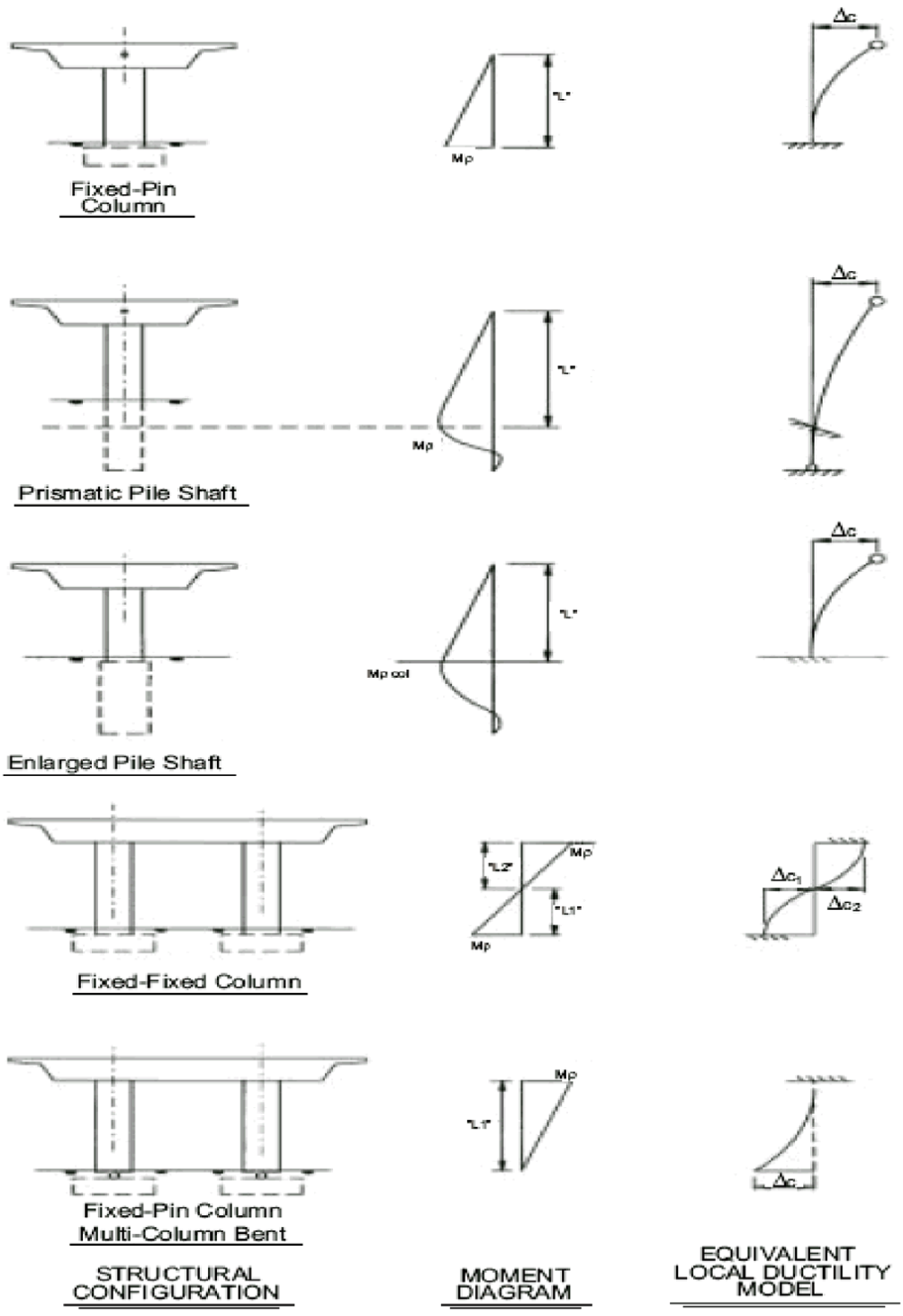

Figure 6-6: Local Ductility Assessment (SDC, 2006)

The minimum displacement ductility capacity $\mu_c = 3$ may be difficult to achieve for columns and Type I pile shafts with large diameters $D_c > 10$ ft, (3m) or components with large L/D ratios. Local displacement ductility capacity less than 3 may be allowed subject to Caltrans design approval process.

6.4.5. Non Linear Reinforcing Steel Models for Ductile Reinforced Concrete Members

Reinforcing steel shall be modeled with a stress-strain relationship that exhibits an initial linear elastic portion, a yield plateau, and a strain hardening range in which the stress increases with strain.

The yield point should be defined by the expected yield stress of the steel f_{ye}. The length of the yield plateau shall be a function of the steel length and bar size. The strain-hardening curve can be modeled as a parabola or other non-linear relationship and should terminate at the ultimate tensile strain ε_{su}. The ultimate strain should be set at the point where the stress begins to drop with increased strain as the bar approaches fracture. It is Caltrans partice to reduce the ultimate strain by up to thirty-three percent to decrease the probability of fracture of the reinforcement. The commonly used steel model is shown in Figure 6-7:

Ultimate tensile strain

$$\varepsilon_{su} = \begin{cases} 0.120 & \text{\#10 (\#32m) bars and smaller} \\ 0.090 & \text{\#11 (\#36m) bars and larger} \end{cases}$$

Reduced ultimate tensile strain

$$\varepsilon_{su}^{R} = \begin{cases} 0.090 & \text{\#10 (\#32m) bars and smaller} \\ 0.060 & \text{\#11 (\#36m) bars and larger} \end{cases}$$

Onset of strain hardening

$$\varepsilon_{sh} = \begin{cases} 0.0150 & \text{\#8 (\#25m) bars} \\ 0.0125 & \text{\#9 (\#29m) bars} \\ 0.0115 & \text{\#10 \& \#11 (\#32m \& \#36m) bars} \\ 0.0075 & \text{\#14 (\#43m) bars} \\ 0.0050 & \text{\#18 (\#57m) bars} \end{cases}$$

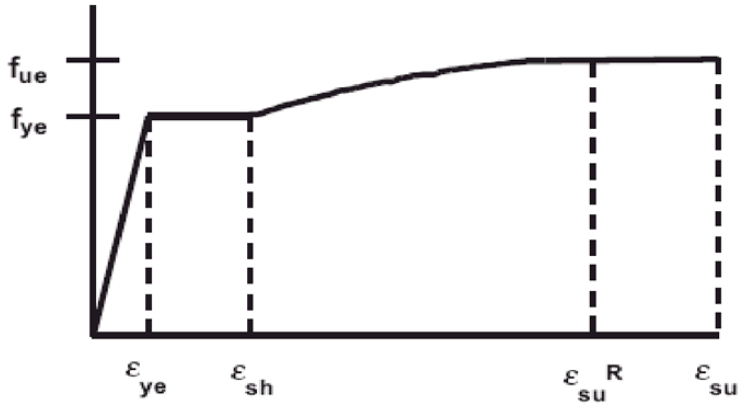

Figure 6-7: Steel Stress Strain Model (SDC, 2006)

6.4.6. Nonlinear Concrete Models for Ductile Reinforced Concrete Members

A stress-strain model for confined and unconfined concrete shall be used in the analysis to determine the local capacity of ductile concrete members. The initial ascending curve may be represented by the same equation for both the confined and unconfined model since the confining steel has no effect in this range of strains. As the curve approaches the compressive strength of the unconfined concrete, the unconfined stress begins to fall to an unconfined strain level before rapidly

degrading to zero at the spalling strain ε_{sp}, typically $\varepsilon_{sp} = 0.005$. The confined concrete model should continue to ascend until the confined compressive strength f'_{cc} is reached. This segment should be followed by a descending curve dependent on the parameters of the confining steel. The ultimate strain ε_{cu} should be the point where strain energy equilibrium is reached between the concrete and the confinement steel. A commonly used model is Mander's stress strain model for confined concrete (Mander et al., 1988) shown in figure 6-8:

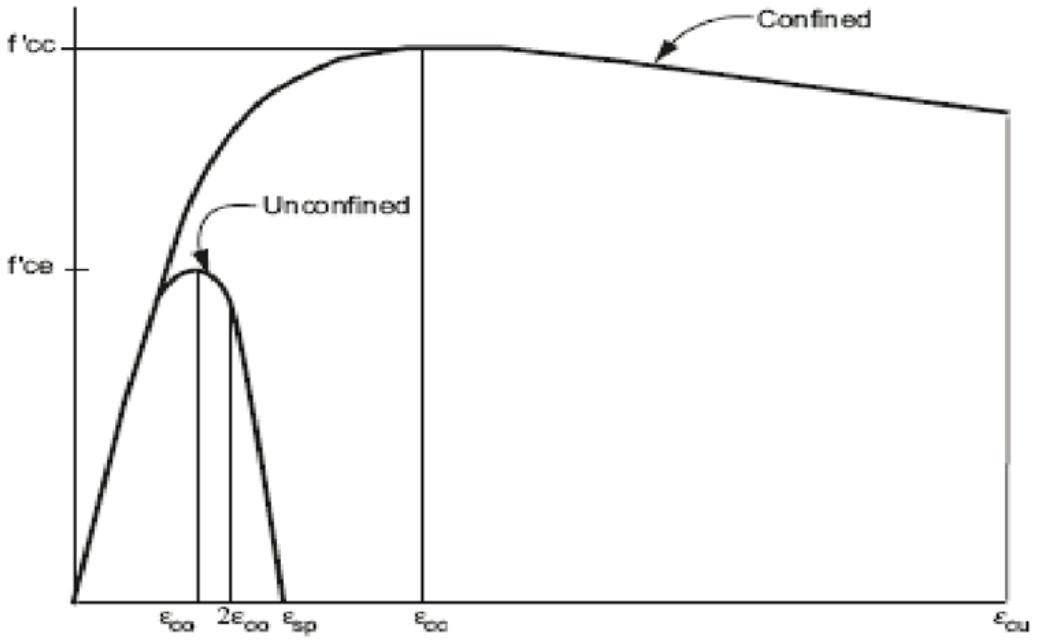

Figure 6-8: Concrete Stress Strain Model (SDC, 2006)

6.5. Effects of Liquefaction Induced Lateral Spread on Bridge Foundations, Caltrans Approach

The following captures in essence what is essentially the state of practice in approaching the design of piles due to lateral spread in Caltrans. The department uses a force-based approach for design and evaluation. The magnitude of forces generated by the moving ground are first estimated by geotechnical engineers and then transmitted to structure bridge engineers who then incorporate them in the design. The way in which the forces generated by the ground (Kinematic loading) and the forces generated during seismic loading (inertial loading) are combined for design is still a debated topic.

Structural design and evaluation of bridge foundations under lateral loading normally involves a pushover type of analysis. The formation analysis between piles and the surrounding soil is performed by means of Beam on Non-linear Winkler Foundation (BNWF) models using of p-y curves. The pushover analysis incorporates, directly or indirectly, estimated ground displacements and associated soil pressures.

Current implementation of a force-based procedure to account for the effects of liquefaction-induced ground displacement standard requires an explicit evaluation of the design ground forces. This evaluation involves nonetheless a quantification of the magnitude, direction and distribution of the expected ground displacements. The first step is to perform a standard liquefaction potential assessment using simplified

liquefaction analysis procedures (e.g., Youd et al., 2001) Liquefiable layers are identified and their lateral extent assessed based on existing subsurface and surface information. The potential for developing permanent ground displacements is assessed and the magnitude of such displacements estimated. Lateral forces that may act upon bridge foundation systems as a result of the estimated displacements are then evaluated and pressure distributions along portions of foundations affected by ground displacements are calculated and provided to bridge engineers. P-y curves along portions of the piles affected by lateral ground displacements are replaced by the calculated pressure distributions. The effects of soil liquefaction on the lateral capacity of piles where lateral ground displacements are unlikely to occur are evaluated using modified p-y curves for the liquefied layers. The overall effect is a net reduction in the lateral-load carrying capacity of the pile foundations.

Caltrans Structure Design approach for piles in liquefiable soils in general and dealing with lateral spread are as follows:

6.5.1. Bent Analysis

If lateral spreading is present, push-over analysis is performed with liquefaction and with the lateral spreading force calculated on the basis of passive pressure (Figure 6-9). Use 100% of the Lateral Spreading Force (LSF) for single-column bents on pile shafts and 67% of LSF for all other cases (i.e. single-column bents on pile groups,

multi-column bents on shafts or pile groups, and pier walls), then proceed with as follows for the appropriate foundation system:

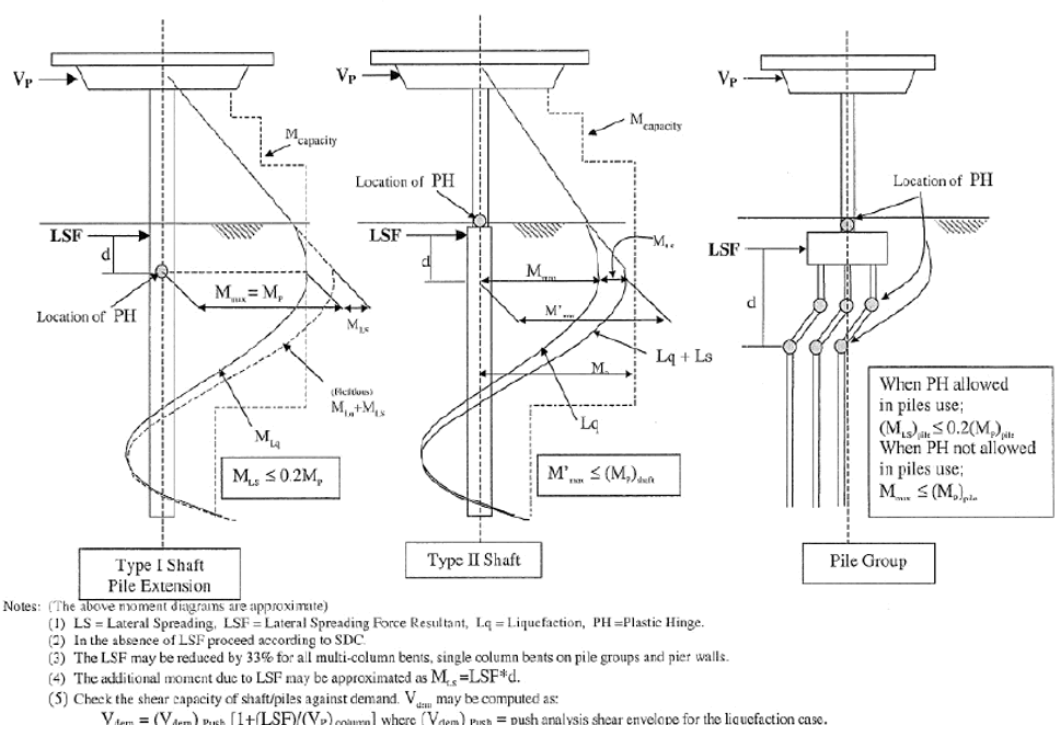

Notes: (The above moment diagrams are approximate)
(1) LS = Lateral Spreading, LSF = Lateral Spreading Force Resultant, Lq = Liquefaction, PH =Plastic Hinge.
(2) In the absence of LSF proceed according to SDC.
(3) The LSF may be reduced by 33% for all multi-column bents, single column bents on pile groups and pier walls.
(4) The additional moment due to LSF may be approximated as M_{LS} =LSF*d.
(5) Check the shear capacity of shaft/piles against demand. V_{dem} may be computed as:
$V_{dem} = (V_{dem})_{Push}\,[1+(LSF)/(V_P)_{column}]$ where $(V_{dem})_{Push}$ = push analysis shear envelope for the liquefaction case.

Figure 6-9: Lateral Spreading Force on Piles

6.5.1.1. Type-I Pile Shafts

If the moment demand on the shaft due to LSF alone is less than 20% of Mp of the shaft then check the shaft shear and end the process; if the moment demand due to LSF alone is greater than 20% but less than 30% of Mp then redesign (i.e. increase shaft strength,…) and repeat the process. However, if the moment demand is greater than 30% of Mp consider using Type-II instead of Type-I shaft.

6.5.1.2. Type-II Pile Shafts

If the total moment demand on the shaft due to Mp of the column and LSF, is less than Mp of the shaft, then check the draft shear and end the process, otherwise redesign (i.e. increase shaft strength) and repeat the process.

The following (Figure 6-10) shows the plastic hinging related to Caltrans Pile Shafts

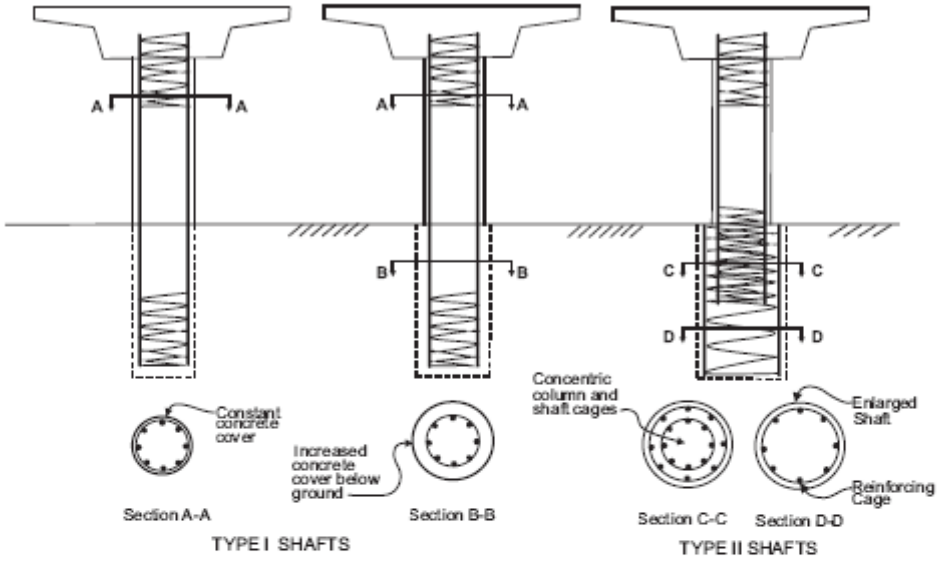

Type I Pile Shafts

Type I pile shafts are designed so the plastic hinge will form below ground in the pile shaft. The concrete cover and area of transverse and longitudinal reinforcement may change between the column and Type I pile shaft, but the cross section of the confined core is the same for both the column and the pile shaft. The global displacement ductility demand, μ_D for a Type I pile shaft shall be less than or equal to the μ_D for the column supported by the shaft.

Type II Pile Shafts

Type II pile shafts are designed so the plastic hinge will form at or above the shaft/column interface, thereby, containing the majority of inelastic action to the ductile column element. Type II shafts are usually enlarged pile shafts characterized by a reinforcing cage in the shaft that has a diameter larger than the column it supports. Type II pile shafts shall be designed to remain elastic, $\mu_D \leq 1$. See Section 7.7.3.2 for design requirements for Type II pile shafts.

Figure 6-10: Plastic Hinging Along Caltrans Pile Shafts (SDC 2006)

6.5.1.3. Pile Groups Where Plastic Hinging Is Not Allowed

If the total moment demand on the pile due to Mp of the column, and LSF, is less than Mp of the pile then check the pile shear and end the process, otherwise redesign (i.e. increase pile strength) and repeat the process.

6.5.1.4. Pile Groups Where Pile Plastic Hinging Is Allowed

Formation of plastic hinges in piles is not desirable according to Caltrans current design practice. However, if the specific design criteria allows plastic hinging in the piles, and if the moment demand on the pile due to LSF alone is less than 20% of Mp of the pile, then check the pile shear and end the process, otherwise redesign(i.e. increase pile strength) and repeat the process or consider alternative foundation type.

When lateral spreading is present, the shear demand calculation can be complicated (nonlinear behavior, particularly for Type-I shafts) and time consuming given the current state-of-the-practice and analysis tools. In lieu of the more complicated calculation, the process cited above provides a simplified and approximate expression that may be used for computing shear demand at the bents.

6.5.2. Abutment Analysis

When liquefaction/lateral spreading is identified at the abutment, the Geotechnical Designer performs the entire abutment-soil liquefaction/lateral spreading analysis and provides the designer with a pressure distribution on the abutment/pile. The

designer should then include 67% of this pressure distribution with other abutment loads for the design of the abutment piles. These piles may be isolated and analyzed separately with the lateral spreading loads distribution included with other resultant abutment loads at top of pile. When plastic hinging is not allowed in abutment piles, the maximum pile moment demand should be less than Mp of the pile. When plastic hinging is allowed in the piles (not recommended), the maximum pile moment should be within 120% of Mp of the pile.

6.5.3. Requirements for Capacity Protected Components

Capacity protected concrete components such as footings, TYPE II pile shafts, bent cap beams, joints, and superstructures shall be designed flexurally to remain essentially elastic when the column reaches its overstrength capacity, Mo = 1.2 Mp.

The expected nominal moment capacity Mne for capacity protected concrete components determined by either M-ϕ or strength design, is the minimum requirement for essentially elastic (capacity protected) behavior. However, shear is always designed using nominal values.

Caltrans approach is not to ever allow plastic hinge in the pile cap (PGFSR 2007). It is desirable to have a plastic hinge form at the bottom with no plastic hinging in the piles. However, when the column has formed a plastic hinge, sometimes project specific criteria may allow some plastic hinging at the top of the piles, with a

displacement ductility demand in the range of 1.5 to 2.5. The formation of a second hinge, at some distance below the bottom of the footing, should be avoided.

CHAPTER 7: DEVELOPMENT OF IMPROVED DESIGN METHODOLOGY

This chapter is comprised of five main sections. The first section describes the improved methodology and its development and draws a comparison with the NCHRP 12-49 design approach. The second section is an independent simulation of pile response to a sliding layer loading, where the improved methodology in this research is used to study pile response. The third section is the reevaluation of pile response for the NCHRP Missouri and Washington bridge structures, using the improved design methodology. The fourth section is revisiting two case histories of previously damaged bridge pile foundations due to liquefaction induced lateral spread displacement demand during past earthquakes followed by fifth and final section on the summary (illustrated as a flow chart) of the proposed methodology for earthquake response of bridge pile foundation to liquefaction induced lateral spread.

7.1. Outline of Improved Methodology

The NCHRP 12-49 design approach as discussed in Chapter 5 recognizes pile pinning effect and ductility in assessing the response of the pile to lateral spread loading. The contribution of pinning force (determined by assumed plastic hinge locations) to the reduction in lateral spread displacement demand is made possible by using the smearing method where the resistance per unit width is converted into equivalent shear strength along the shear plane in the liquefied zone and the equivalent strength is added to the residual shear strength.. Pile shear estimates are

based on hinge development in stable or firm soil zones above and below (by say 2 pile diameters) the liquefiable layer. Maximum "pinning" shear is assumed to be equal to 2Mp/H where Mp is the plastic moment and H the distance between hinges. The yield deflection of the piles is based on the latter distance, where Δ_y is equal to Mp $H^2/6EI_{cr}$, no plastic hinge length: L_p is considered and the plastic hinge is assumed to be a point. The same distance H is also used to calculate the plastic displacement of the pile Δ_p which is equal to H θ_p, where. θ_p is assumed to be 0.05 radians as discussed later. Figure 7-1 illustrates the plastic mechanism of piles supporting an end diaphragm. The shear forces by strutting effect due to resistance of superstructure and other piers, passive force developed against end diaphragm and the PΔ effect are all considered.

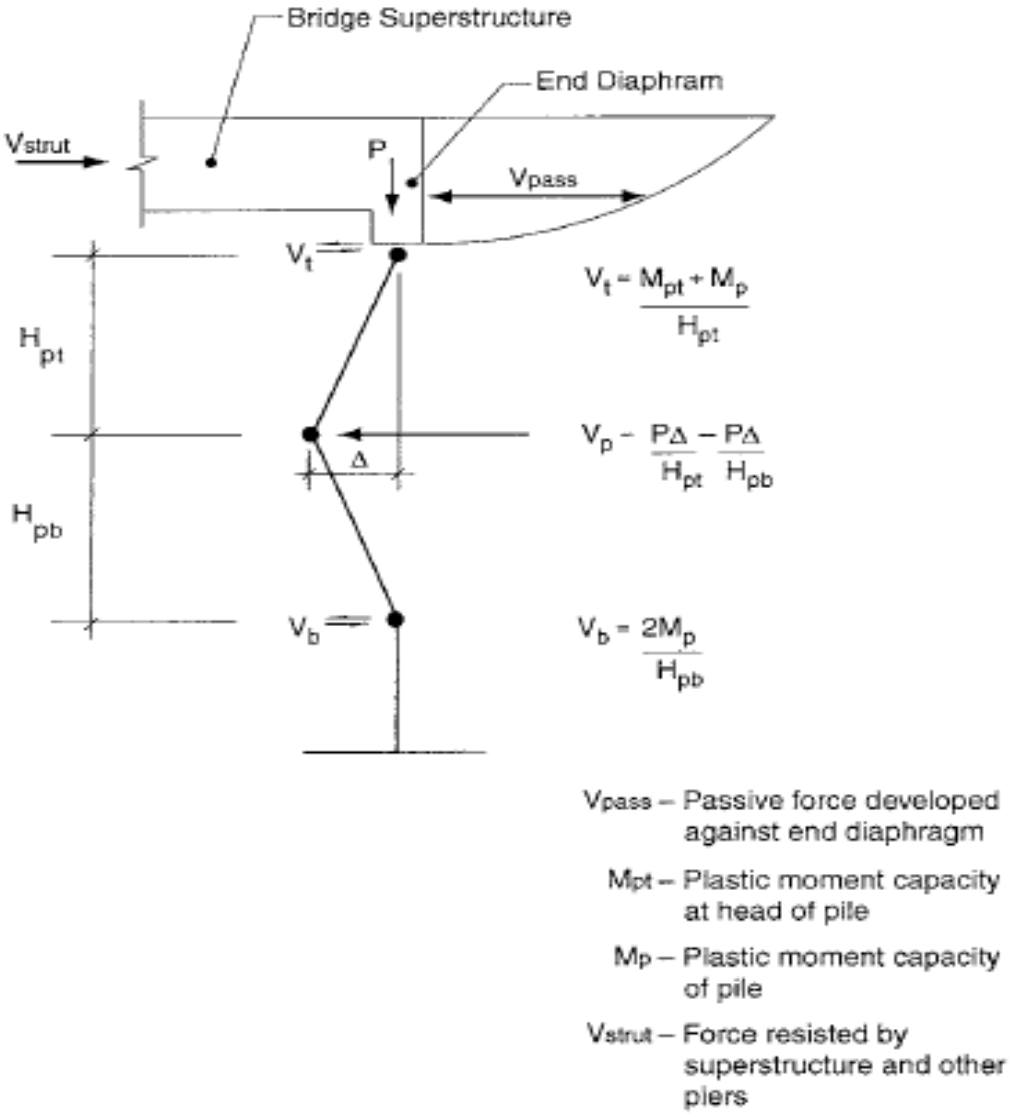

Figure 7-1 Plastic Mechanism for an Integral Abutment Supported on Piles (NCHRP 2003)

On the capacity side of the equation, NCHRP 12-49 design considers that if the pile response due to lateral spread during an earthquake event leads to yielding, it is reasonable to assume that the pile plastic hinge occurs at 2D above and below the liquefiable layer for both shallow and deep liquefaction. To allow for potential

softening (i.e. less than 100% pore pressure increase) in the sand above and below the liquefiable layer, the approach uses 5D in examples. The calculation of the plastic rotation capacity of the pile is also assumed to be 0.05 radians, which leads to assumptions on arbitrary values for plastic hinge length and plastic curvature of the pile. Clearly there is room for improvements for the NCHRP 12-49 design approach on the both aspects of the pinning and pile ductility.

The recommended design methodology in this research improves on the NCHRP 12-49 design approach by utilizing the displacement compatibility of the soil/pile structure interaction using the finite difference method and incorporating the relative displacement between pile structure and the soil (see Figure 7-2), in the calculation of the pinning force and reduced soil movement. Although the pinning force can be computed by the improved method, it is the reduced lateral spread soil movement due to the pinning effect that plays a direct and important role in ultimately assessing the pile response. The lateral spread displacement demand is incorporated into LPILE5 as a soil movement profile. There are no forces to be calculated and applied to the pile structure, hence in the latter context it can be defined as a displacement method of analysis and not a force method. Inherent in the improved methodology is the utilization of site and pile structure specific geotechnical data and structural data respectively for the assessment of lateral spread displacement demand and pile inelastic response designed to support a bridge structure. The estimation of the pile response to lateral spread loading is done considering the ‘Pinning Effect” of piles

due to soil movement and the “ductility” of the pile foundation. The performance of the piles is evaluated by assessing the pile curvature ductility demand using LPILE5 software. The pile moment-curvature relationship for a given pile is determined using the XTRACT software.

The relative movement of the pile and soil forms the basis of the net soil reaction on piles. The free field soil movement due to lateral spread accounts for the change of the soil resistance. The Newmark model evaluates the free field movement due to lateral spread. The Finite difference method is employed in the LPILE5 program that is used to assess the soil resistance. The change in the soil resistance is accounted for by including the relative displacement between the pile and soils in the governing differential equation.

The following depicts the steps taken to determine the pile pinning and the computation of the reduced liquefaction induced lateral spread displacement due to the pinning.

1. Incremental soil movements are prescribed to the embankment to determine the pile shear forces on the critical failure plane due to the prescribed soil movements. The software program LPILE5 is used to evaluate the corresponding shear forces for the piles, due to these soil movements. Shear forces (for plastic hinging forces) are found for various soil movements (Curve designated as LPILE5 in Figure 7-2)

2. Evaluate the pile pinning effect that is the resistance to the soil movement and can be considered as the added shear strength of the soil. The initial shear strength of the liquefiable soil may be found based on the Seed and Harder (1990) or Olson and Stark (2002) charts. Incremental increases in shear strength along the failure surface are assumed and yield accelerations are determined for the additional shear strength increments, resulting in incremental reductions in Newmark displacements. (Curve designated as Newmark Analysis (Martin and Qiu) curve in Figure 7-2.
3. Where the two curves converge, is the assumed value for the displacement of the embankment soil due to lateral spread, including the pile pinning effect.

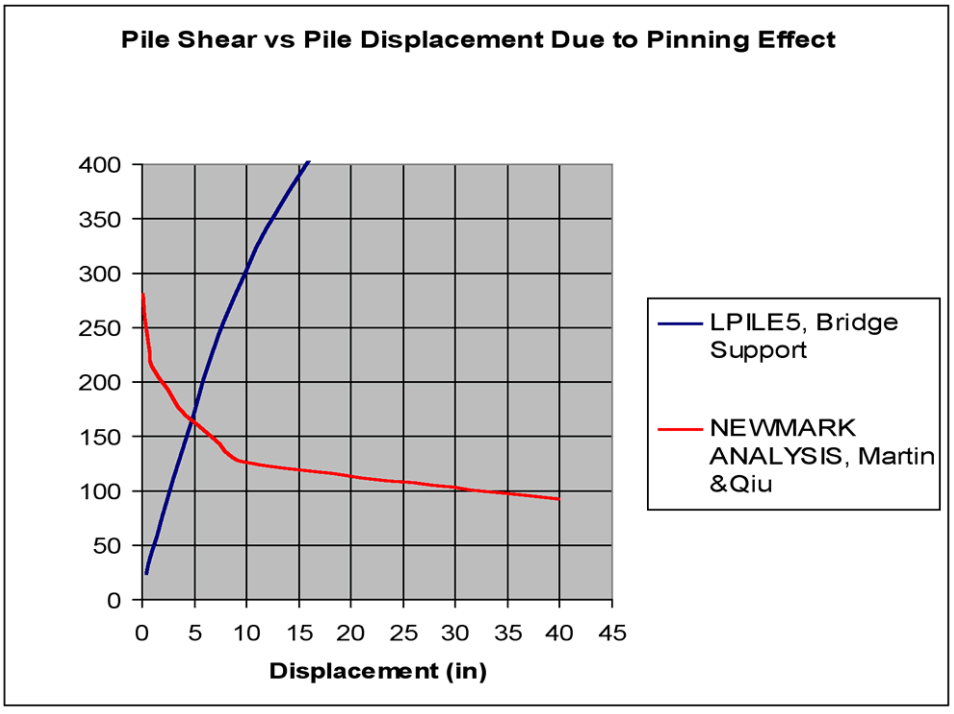

Figure 7-2: Pile Pinning Effect Based on Displacement Compatibility

The following assumptions are made:

- The yield acceleration following liquefaction is assumed constant, starting at time t=0
- Whereas the displacement compatible pile pinning effect is assumed, the pile shear force will be progressively mobilized as displacement is increased. However the latter apparent non conservative assumption is offset by the liquefaction at the time t = 0 assumption. The strut effect due to abutment and piers resisting the movement of the embankment should also be considered in the improved methodology, where appropriate.
- The soil movement due to the lateral spread in the generalized three layer subsurface configuration is assumed constant along the top (crust or non liquefiable layers), varying along the liquefiable layer and none at the top of the bottom non liquefiable layer as shown in figure 7-3.

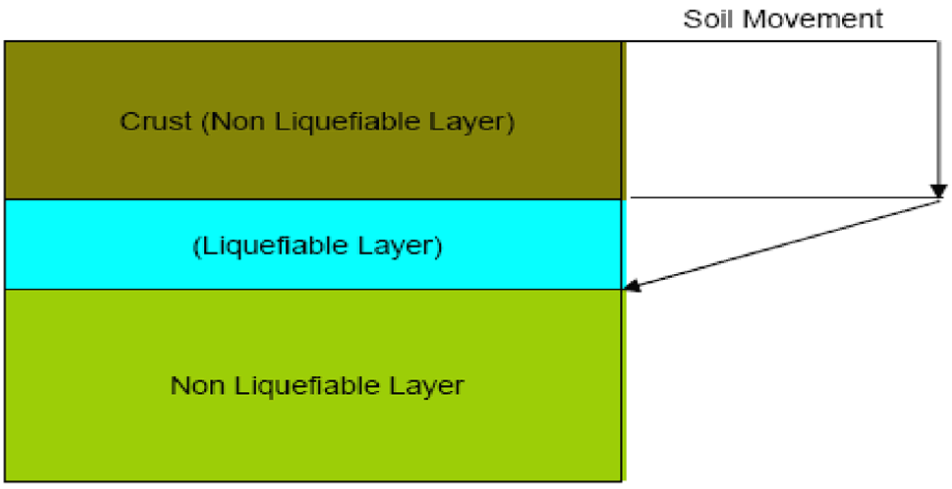

Figure 7-3: Soil Movement due to Lateral Spread

The non-linear response of the pile structural component is determined by assessing its yield curvature. It is the latter that determines in part the plastic rotation as well as plastic displacement capacity. To determine the plastic curvature for a given design axial load, the software program XTRACT (Imbsen) is used. The pile curvature demand due to lateral spread displacement computed by LPILE5 is then compared to the pile curvature capacity.

The improvements as incorporated in the thesis research may be summarized as follows:

- The push-over analysis (demand side) of the piles due to lateral spread in the thesis is based on the displacement compatibility approach of pinning forces, which leads to assigning a realistic soil movement profile based on the pile-soil relative movement. The pile/soil relative movement due to lateral spread is incorporated into LPILE5 software and the soil movement reduced by pinning effects is directly input into the program.
- On the capacity side, the actual pile ductility based on the inherent and specific characteristics of a given pile type is evaluated. The software program XTRACT is used to evaluate the moment curvature of the pile by incorporating the pile structure configuration, confined and unconfined concrete model, steel model and the transverse and longitudinal reinforcement. The moment curvature evaluated is then incorporated into the LPILE5 software.

- The pile ductile response is based on assessing the pile curvature along the pile and clearly shows where the pile is subject to plastic hinging.
- By assessing the pile curvature demand directly using the site specific soil and pile attributes incorporated into the LPILE5 soil/structure interaction model, one can evaluate whether the pile exceeds the pile yield or the plastic or ultimate curvature capacity.
- Pile Lateral Response due to lateral spread is also influenced by the axial load applied to the pile during the earthquake. The thesis incorporates the value of the axial load into the analysis by assessing the pile curvature capacity given an axial load, using XTRACT.
- The impact of soil confinement on the pile displacement curvature capacity can be approximated by modifying the confined concrete and cover concrete strength. Not considering the soil confinement would yield conservative results, since soil confinement increases the pile displacement capacity.

7.2. Independent Simulation of Pile Response to Sliding Layer Loading

The following presents a pile response simulation of a Port of Los Angeles (POLA) Pile to an idealized deformation profile using the Finite Difference Model by LPILE5 incorporating the moment curvature of the pile that is already available. The latter pile response has also been evaluated using OPENSEES (Open System for Earthquake Engineering Simulation) by Blandon (2007) as part of his PhD dissertation at UC San Diego and the Rose School of Pavia, Italy.

OPENSEES is an object-oriented software framework for simulation applications in earthquake engineering using finite element methods. The purpose of the pile simulation is to draw a comparison between the results of Blandon's analysis using a finite element model of the piles and the simplified beam column element simulation used in LPILE5.

7.2.1. Background

Most of port wharf earthquake related damage have occurred due to large soil permanent displacements that in most cases have been caused by liquefaction of soil layers within the profile where the piles are embedded (Blandon, 2007) The seismic analysis and design of pile supported wharves is the title of a Doctorate research dissertation by Carlos Blandon of UCSD and the Rose School, where he analyzed the kinematic loading on an embedded pile in a soil profile with a sliding layer (figure 7-4). His objective was to evaluate the effect of this sliding layer on the displacement capacity of a pile passing through a liquefied layer. Some previous efforts have been carried out in the past in order to define a methodology and criteria which would allow the simplification of the design procedure. Priestley (2005), proposed a procedure based on assumptions of the plastic hinge length, elastic distance to fixity and plastic hinge location for a 2 feet sliding layer. The ground above the sliding layer is assumed to be competent and moves as a deformable body on top of the liquefied layer. P-y springs are used to characterize the soil above and below the sliding layer.

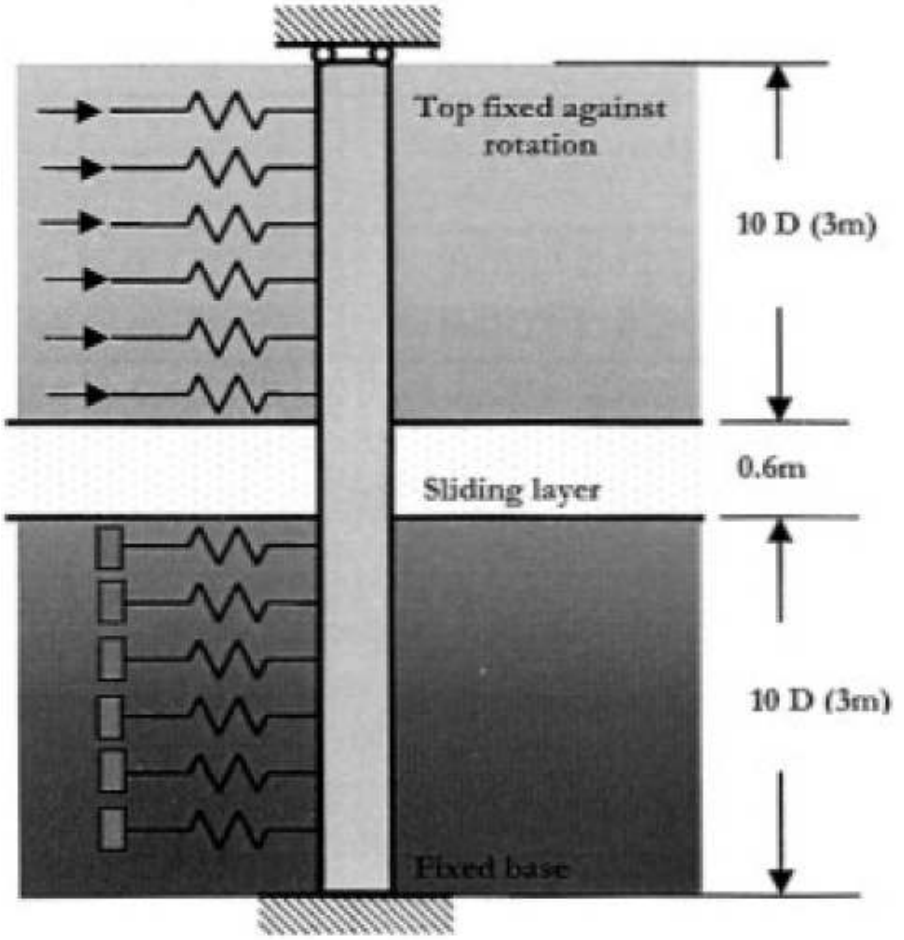

Figure 7-4: Pile Model Setup (Blandon, 2007)

7.2.2. Blandon's Model Setup

The pile consisted of an octagonal prestressed pile having a 24 inch internal diameter, and are reinforced with 16 – 0.6 in strands. The ultimate strand strength is 270 Ksi and the stress after losses is 150 Ksi giving an effective prestressing force of 516 kips. The pile has a cover of 3.0 inch to the transverse reinforcement (figure 7-5). The concrete has an estimated compressive strength of 7.0 Ksi. The transverse

reinforcement at the depth of the liquefiable layer studied consists of a W11 with a pitch of 3 inch and yield strength of 70 Ksi. The Port of Los Angeles typically uses the piles with above cited characteristics for construction.

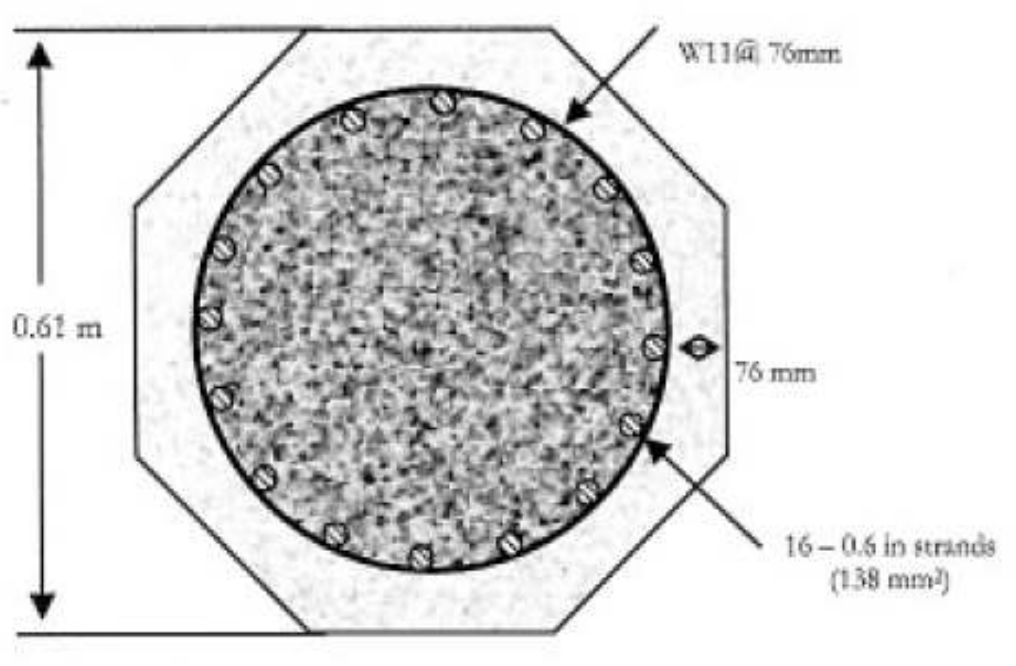

Figure 7-5: Transverse Section of Prestressed Pile (Blandon, 2007)

The concrete model is defined by the compressive strength, strain at compressive strength, crushing strength and strain at crushing strain following Mander's concrete model. Blandon used slightly increased crushing strain compared to the value that would be used for unconfined concrete without soil confinement, to capture the confinement effect of the soil into the concrete cover. The strain value of 0.008 at zero stress was used to define the crushing of the unconfined cover concrete of the pile.

The prestressing strands are defined by the Young's modulus of elasticity, strain at yielding and initial strain for modeling the prestressing. Table 7-1 shows the parameters corresponding to the prestressed pile section.

Concrete model	Compressive strength (MPa)	Strain at compressive strength	Crushing Strength (ksi)	Strain at crushing strength
Confined	59.5	0.005	52.5	0.018
Unconfined	45.5	0.002	3.5	0.008
Steel Model	**Modulus of Elasticity (GPa)**	**Initial strain**	**Strain at yielding**	
Elastoplastic	200.0	0.005	0.008	

Table 7-1: Blandon's Pile Prestressed Section Material Properties (Blandon, 2007)

The moment curvature relationship obtained by Blandon for the modeled section is shown in Figure 7-6.

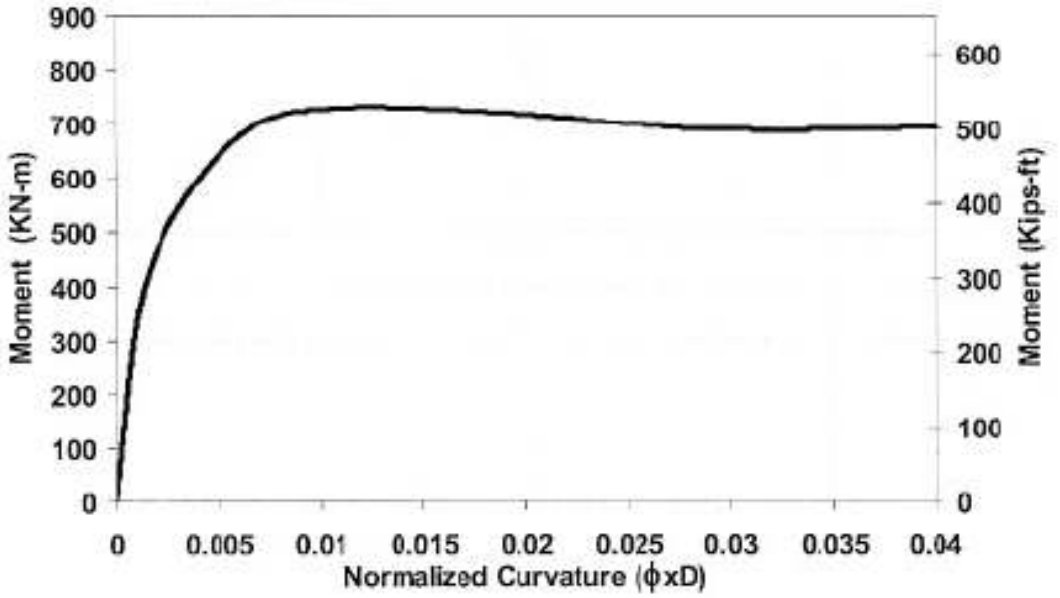

Figure 7-6: Pile Moment Curvature (Blandon, 2007)

Blandon modeled the pile using a finite element program. The pile is discretized in 12 inch length element and the soil is modeled with P-Y curves defined at e ach node above and below the sliding layer using the methodology recommended by API for a medium dense to dense sands (ϕ= 35°). Two different depth of the sliding layer were used in order to represent shallow and deep liquefaction corresponding to different possible cases of kinematic interaction. Once corresponds to the sliding layer at depth of 9m (30 feet) and the other at the depth of 15m.(50 feet). The pile top is allowed to move in the horizontal direction but rotation is restrained; at the bottom.

The 24 inch thick layer is assumed to liquefy due to the seismic event, which at the same time causes the top soil layer to move horizontally as a deformable body. No p-

y curves were included for the liquefiable layer (i.e. zero resistance) by Blandon. A second model was analyzed in order to observe the effect of the pile discritization on the overall response of the pile. The results of Blandon's analysis for the 0.5D pile segment discritization are shown in table 7-2, figures 7-7 and 7-8:

Sliding Layer Depth	Plastic hinge depth	Distance to interface	Distance between hinges
9 m	9.0 D (5.5 m) 12.5 D (7.6 m)	1.0 D (0.6 m) 1.5 D (0.91 m)	3.5 D (2.1 m)
15 m	9.0 D (5.5 m) 12.0 (7.3 m)D	1.0 D (0.6 m) 1.0 D (0.6 m)	3.0 D (1.8 m)

Table 7-2: Plastic Hinging in Blandon's Model Pile Response (Blandon, 2007)

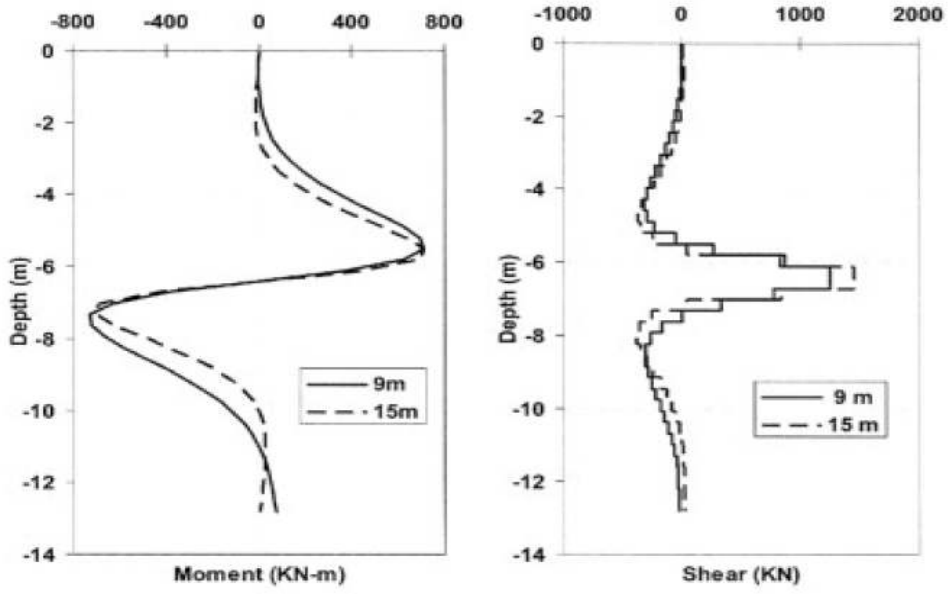

Figure 7-7: Blandon's Model Pile Response (Bending Moment & Shear) (Blandon, C.A, 2007)

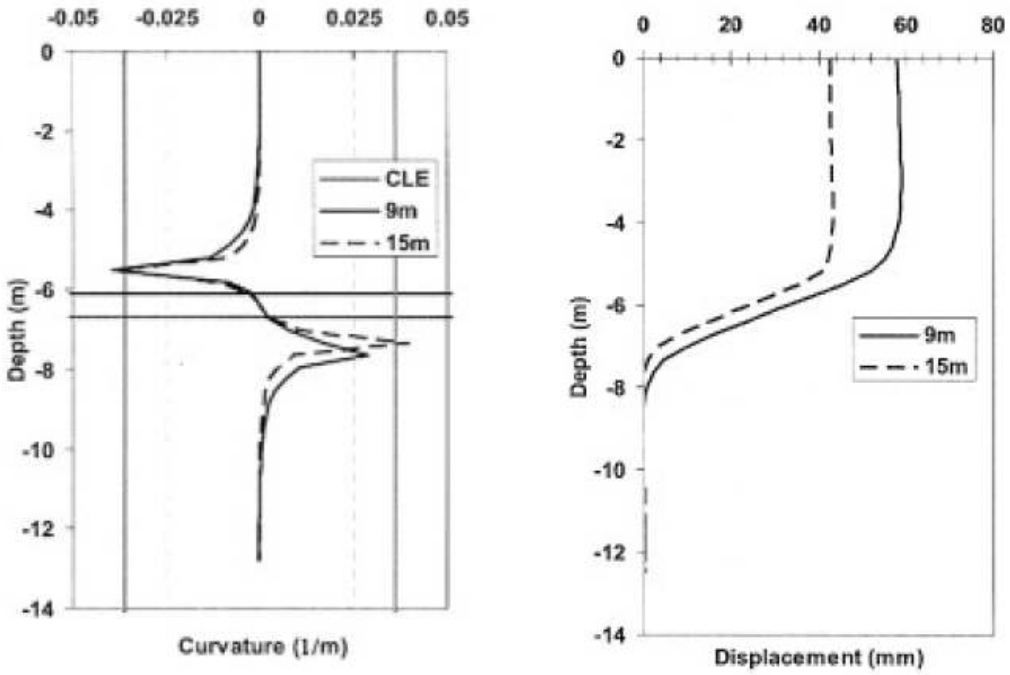

Figure 7-8: Blandon's Model Pile Response (Curvature & Displacement) (Blandon, C.A, 2007)

7.2.3. Independent Pile Simulation

The response of the POLA (Port of Los Angeles) pile modeled by Blandon as discussed above was simulated independently by LPILE5 (ENSOFT) using the finite difference model, previously described. The following (Figures 7-9,7-10, 7-11, 7-12, 7-13 and 7-14) show the results of the pile simulation.

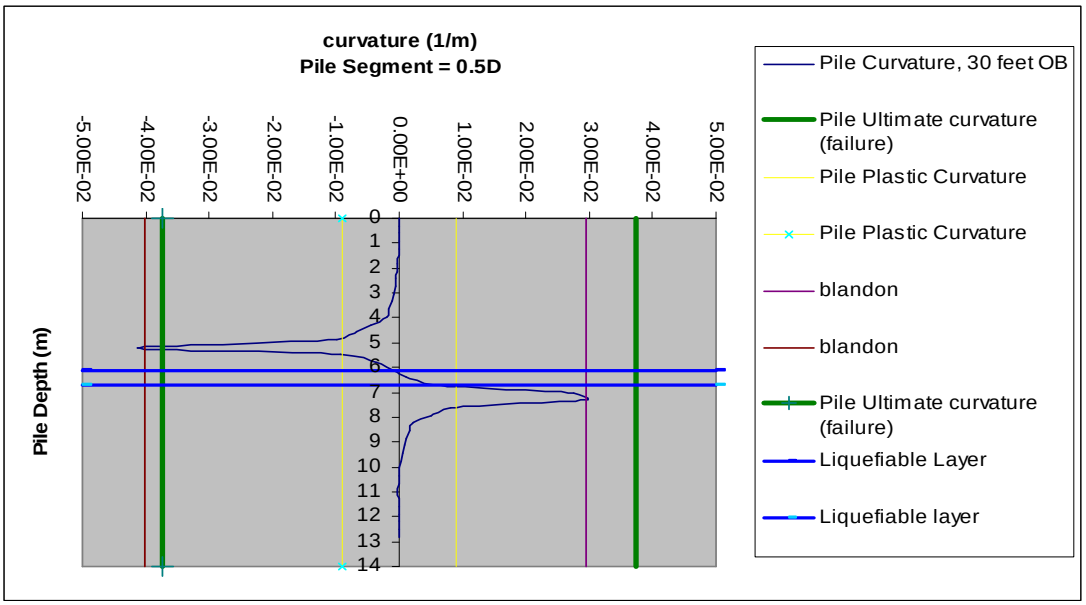

Figure 7-9: Curvature Response Simulation for Blandon's Pile

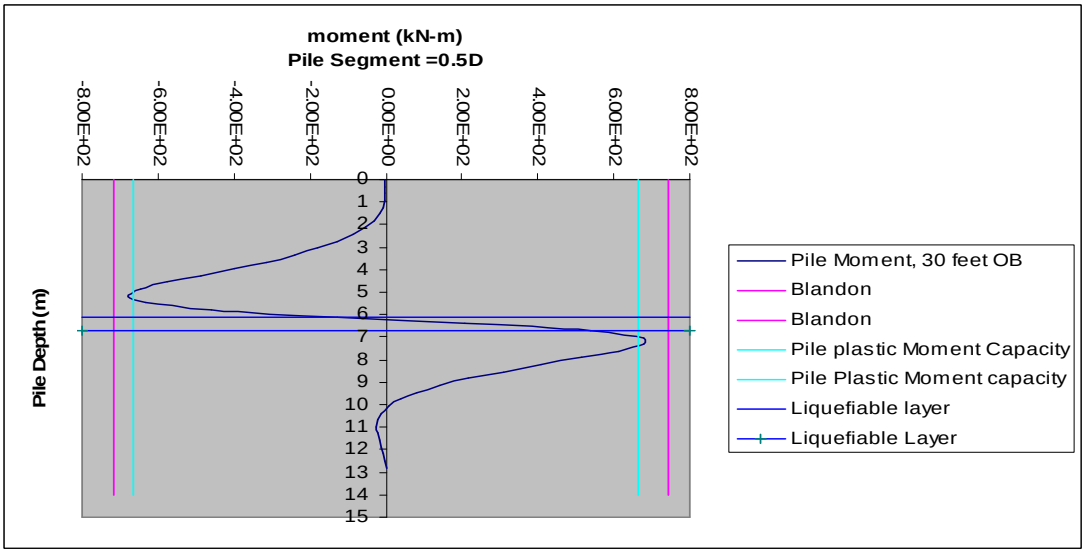

Figure 7-10: Bending Moment Response Simulation for Blandon's Pile

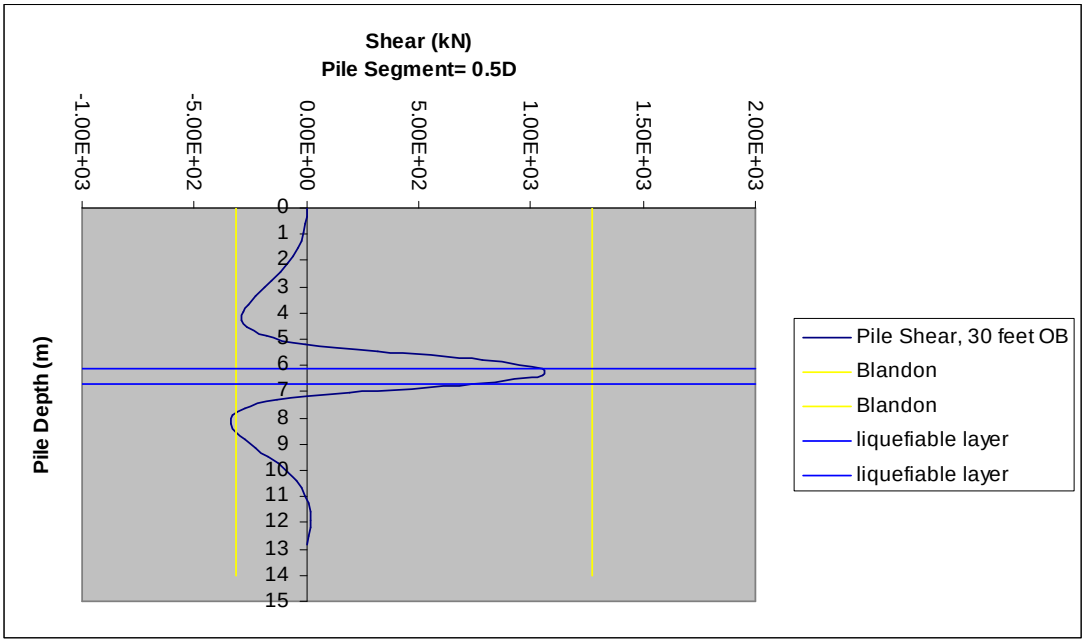

Figure 7-11: Shear Response Simulation for Blandon's Pile

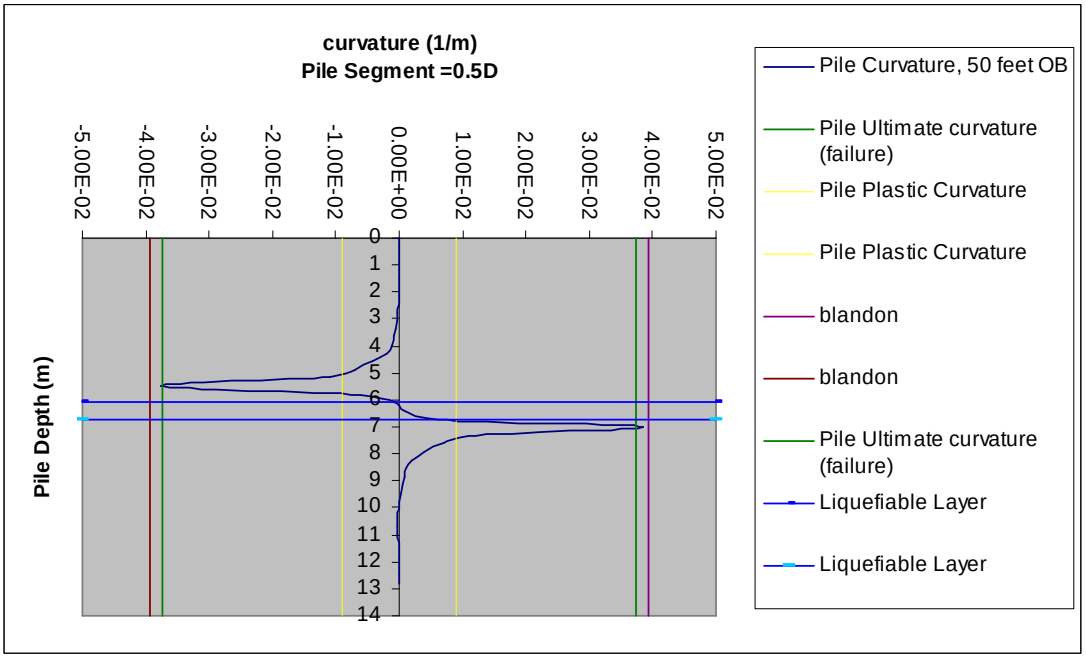

Figure 7-12: Curvature Response Simulation for Blandon's Pile

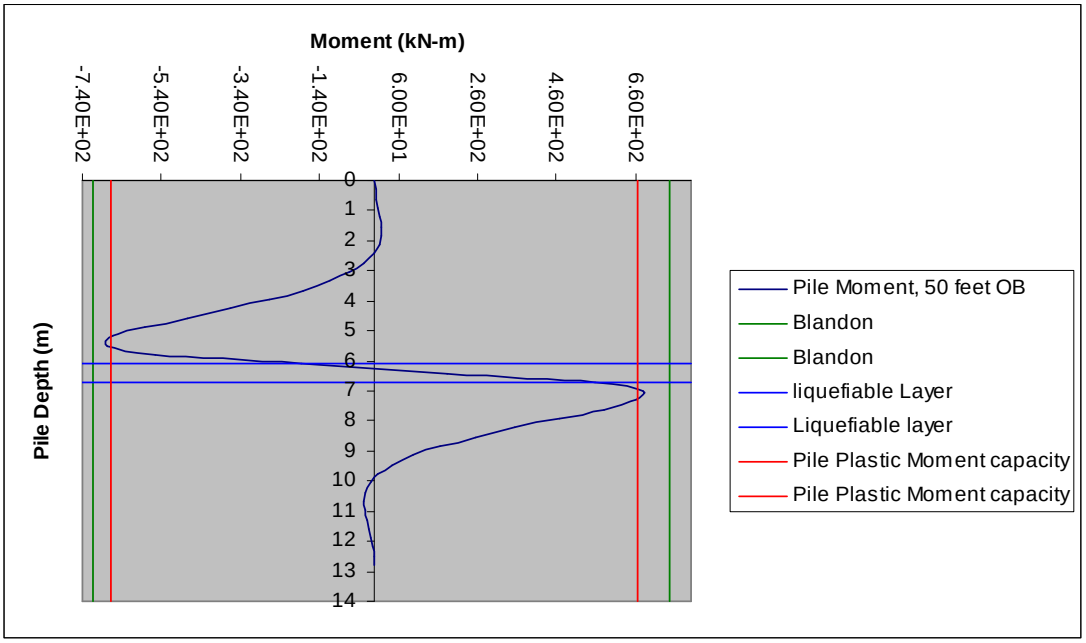

Figure 7-13: Bending Moment Response Simulation for Blandon's Pile

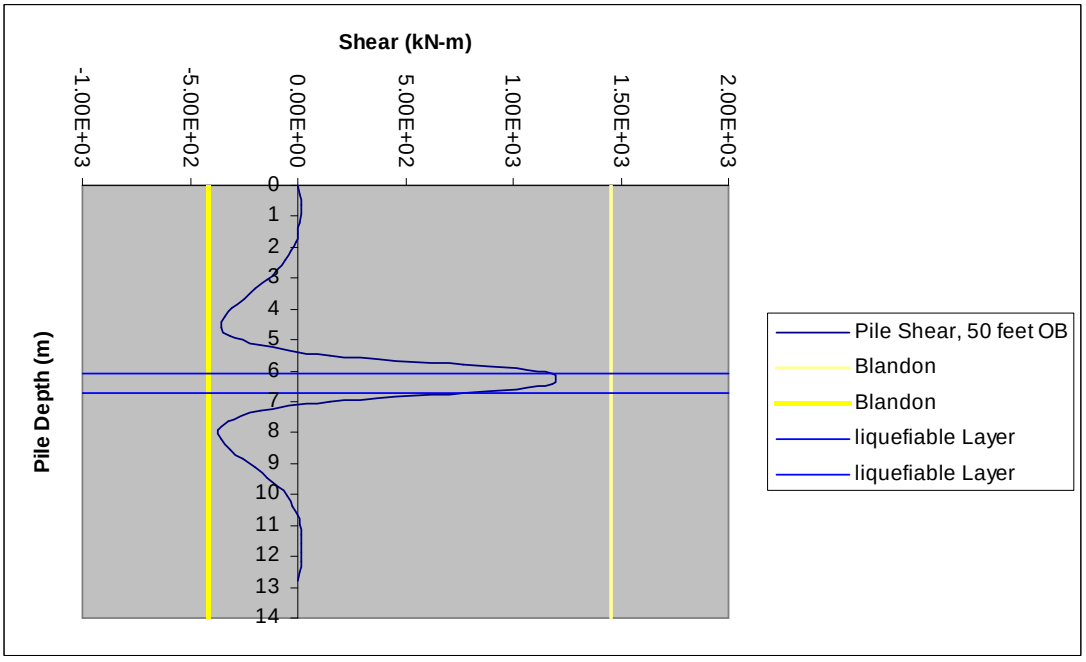

Figure 7-14: Shear Response Simulation for Blandon's Pile

A shown above there is a very good agreement between the LPILE5 simulation for curvature and Blandon's results. The Port of Los Angeles pile would undergo plastic hinging for both cases of 30 feet and 50 feet overburden at 2.2 and 1.6 inch of soil displacement respectively for the upper non liquefiable soil.

In the case of the 30 feet overburden the Port of Los Angeles pile would reach ultimate curvature (failure) above the liquefiable layer, but does not reach the failure curvature below the liquefiable layer.

In the case of the 50 feet overburden, the pile would reach ultimate curvature (failure) at both above and below the liquefiable layer.

The following (table 7-3) summarizes the results of the independent pile curvature simulation at the plastic hinges and at pile failure for both 30 and 50 feet overburden.

Sliding Layer Depth	Plastic Hinge Depth	Distance to interface	Plastic Hinge Length	Distance between Hinges	Ultimate Curvature Depth
50 feet ABOVE LIQ. LAYER	Upper: 200 inch	40			
	Lower: 225 inch	15	25 inch		216 inch
BELOW LIQ. LAYER	Upper: 265 inch	1			
	Lower: 293 inch	29	28 inch	93 inch	276 inch
30 feet ABOVE LIQ. LAYER	Upper: 190 inch	50			
	Lower: 218 inch	22	28		204 inch
BELOW LIQ. LAYER	Upper: 265 inch	1			
	Lower: 300 inch	36	35	110 inch	288 inch

Table 7-3: Pile Curvature at Plastic Hinges and Failure Points: Pile Simulation for Blandon's Pile

7.3. Re-Evaluation of NCHRP Bridge Foundation Response

The following presents a reevaluation of the NCHRP approach for earthquake response of bridge foundation analysis subject to lateral spread, using examples presented in the NCHRP (2002) reports. The representative bridges in Missouri and Washington States at liquefiable sites were used to illustrate the NCHRP approach in the reports. Assumptions did not include "Strut effect" and just looked at pile pinning. Martin and Qiu (V= 30 in/sec) and WES graphs are used for analysis. The

NCHRP approach for pile inelastic response is presented, together with the approach using the previously described methodology.

7.3.1. Case I: Missouri Bridge (475 Year Event)

The NCHRP design approach for the foundation lateral capacity of a three span pre-stressed girder bridge structure founded on a liquefiable soil layer and subject to lateral spread was documented in the NCHRP (2003) reports.

An independent analysis was performed to evaluate the loading caused by lateral spread on pile foundation for pier 4 of the Missouri Bridge, using the improved methodology.

The results of this analysis are then compared with the analysis performed and documented in the subject report (NCHRP, 2003).

Specifically, the pinning effect of piles and the pile response forming plastic hinges are re-evaluated and a comparative study with the result in the subject report is performed.

7.3.1.1. Embankment Stability

The slope stability performed for the embankment for pier 4, reveals that the slope is not stable during the design earthquake. The factor of safety for pseudo-static case

considering a horizontal ground acceleration of 0.15g leads to a value of 0.753, considering the liquefiable soil layers. This value is less than 1.1 which requires an evaluation of the slope displacement using the Newmark method. The design shear strength parameters used in the slope stability were based on the data made available to the author by the NCHRP report. For liquefiable layers, the value of the shear strength was based on the latter and was evaluated to be 300 psf.

The stability of the slope embankment during the design earthquake event where pier 4 is located, was analyzed, using XTSABL5 software program. The failure surface was designated as a block failure, with the base of the failure block passing through the liquefiable layer, at elevation –20 through –40.

The slope stability calculation for the embankment for pier 4 led to factor of safety (FOS) of 1.724. for static condition corresponding to the wedge failure through the liquefiable layer, considering post liquefaction case. The FOS is more than 1.0 which does not lead to flow condition.

The factor of safety for pseudo-static case considering a horizontal ground acceleration of 0.17g leads to a value of 0.699, considering the liquefiable soil layers. This value is less than 1.1 which requires an evaluation of the slope displacement using the Newmark method.

7.3.1.2. Yield Acceleration & Newmark Analysis

The anticipated slope displacement due to the design earthquake is evaluated using the Newmark Method. The displacement is anticipated to be in the order of 3 inch, considering the liquefiable soil layers and given a yield acceleration of 0.085.

7.3.1.3. Lateral Demand/Capacity of the Pile Foundation

The lateral demand on the pile foundation was evaluated using the LPILE4M software program (ENSOFT, version 4).

For the liquefiable layer, the strength of the liquefiable soil was increased incrementally and the corresponding yield acceleration and the slope displacement during the design earthquake was evaluated (table 7-4 below). The displacement of the embankment during the earthquake was calculated using Martin and Qiu (1994) Newmark graph.

Newmark Analysis, Missouri Bridge, Pier 4

Initial Cohesion[1] (psf)	Increase in Cohesion (psf)	Cohesion[2] (psf)	Length of Failure Surface (ft)	Pile Spacing (ft)	Width of Footing (ft)	# of Piles	Abutment Force (kips)	Total Shear Force[3] (kips)	Shear Force, top (kips)	Shear Force, bottom (kips)	Yield acceleration	Max. Acceleration	Ay/Amax	Displacement (in)[4]
300	140	440	90	4.75	43	9	520	2	1	2	0.105	0.17	0.62	1
300	160	460	90	4.75	43	9	520	11	4	7	0.108	0.17	0.64	0.7
300	180	480	90	4.75	43	9	520	20	7	13	0.11	0.17	0.65	0.5
300	355	555	90	4.75	43	9	520	95	32	63	0.145	0.17	0.85	0.05
300	500	800	90	4.75	43	9	520	157	52	105	0.165	0.17	0.97	0.015
300	600	900	90	4.75	43	9	520	200	67	133	0.185	0.17	1.09	0.01
300	700	1000	90	4.75	43	9	520	243	81	162	0.202	0.17	1.19	0.008
300	800	1100	90	4.75	43	9	520	286	95	191	0.215	0.17	1.26	0.0067
300	900	1200	90	4.75	43	9	520	329	110	219	0.230	0.17	1.35	0.005
300	1000	1300	90	4.75	43	9	520	372	124	248	0.250	0.17	1.47	0.004
300	1100	1400	90	4.75	43	9	520	415	138	277	0.265	0.17	1.56	0.0035
300	1200	1500	90	4.75	43	9	520	458	153	305	0.280	0.17	1.65	0.001

1: Initial cohesion corresponds to the shear strength of liquefiable soil, where the failure surface is located
2: Cohesion corresponds to the shear strength of the liquefiable soil after the increase in cohesion is introduced.
It is used for the embankment stability and Newmark analysis
3: Total Shear Force = (Increase In Cohesion x Length of Failure Surface x Pile Spacing) minus the abutment force
4: Displacement based on the Newmark, 1977 (WES)

Table 7-4: Newmark Analysis Results For Missouri Bridge, (475 Year Event) Pier 4

7.3.1.4. Expected Displacement of the Embankment Considering Pile Pinning Effect

When the embankment soil is moving against the piles at pier 4, considering the liquefiable layers under the design seismic event, the piles will resist the movement of the soil by producing shearing forces. These forces would provide some form of resistance against lateral spreading.

A two-front approach is used to assess the lateral spread loading on the piles and is as follows:

In this case, only pier 4 is subject to lateral spread loading. Various soil movements were prescribed to the embankment to determine the pile shear forces found due to these prescribed soil movements. The software program LPILE4M was used to prescribe various soil movements and to evaluate the corresponding shear forces for the pier 4 piles, due to these soil movements. Shear forces are found for soil movements of 0.5 through a maximum of 40 inches (Table 7-5 and Curve designated as LPILE4M in Figure 7-15)

LPILE4M (Missouri Bridge)

PILE TYPE [1]	PILE DIAMETER (in)	PILE LENGTH (ft)	MOMENT OF INERTIA (in^4)	MODULUS OF ELASTICITY (psi)	SOIL DISPLACEMENT [2] (in)	PILE SHEAR [3] (Kips)
PIPE PILE	14	93.5	2450	3,830,000	0.5	7.78
PIPE PILE	14	93.5	2450	3,830,000	1	11.57
PIPE PILE	14	93.5	2450	3,830,000	2	18.24
PIPE PILE	14	93.5	2450	3,830,000	3	25.21
PIPE PILE	14	93.5	2450	3,830,000	4	31.67
PIPE PILE	14	93.5	2450	3,830,000	5	37.63
PIPE PILE	14	93.5	2450	3,830,000	6	43.3
PIPE PILE	14	93.5	2450	3,830,000	7	48.67
PIPE PILE	14	93.5	2450	3,830,000	8	53.86
PIPE PILE	14	93.5	2450	3,830,000	9	58.94
PIPE PILE	14	93.5	2450	3,830,000	10	63.83
PIPE PILE	14	93.5	2450	3,830,000	11	68.65
PIPE PILE	14	93.5	2450	3,830,000	12	73.42
PIPE PILE	14	93.5	2450	3,830,000	13	78.04
PIPE PILE	14	93.5	2450	3,830,000	14	82.58
PIPE PILE	14	93.5	2450	3,830,000	15	87.16
PIPE PILE	14	93.5	2450	3,830,000	16	91.61
PIPE PILE	14	93.5	2450	3,830,000	17	95.97
PIPE PILE	14	93.5	2450	3,830,000	18	100.3
PIPE PILE	14	93.5	2450	3,830,000	19	104.68
PIPE PILE	14	93.5	2450	3,830,000	20	108.96
PIPE PILE	14	93.5	2450	3,830,000	25	129.68
PIPE PILE	14	93.5	2450	3,830,000	30	148.23
PIPE PILE	14	93.5	2450	3,830,000	35	165.39
PIPE PILE	14	93.5	2450	3,830,000	40	181.67

1: Pipe pile thickness is 0.25 inch.
2: Soil displacement prescribed, to represent the lateral spread movement from the ground surface to the bottom of the liq
3: Maximum shear force developed by the pile resisting to the prescribed soil movement

Table 7-5: Pile Shear Force, Pier 4, (475 YEAR EVENT) Missouri Bridge

Evaluate the pile pinning effect that is the resistance to the soil movement and can be considered as the added shear strength of the soil. The initial shear strength of the liquefiable soil for upper and lower liquefiable layers is 300 psf. An increase of 500 psf in shear strength along the failure surface which was estimated to be 90 ft (slope

stability analysis) and the spacing of 4.75 ft for the pipe piles, would be equal to 157 kips of total pile shear force, 105 kips at the bottom and 52 kips at the top of the pile. A Newmark analysis using the value of 800 psf (the initial value being 300 psf and the increase of 500 psf would make the new shear strength to be 800 psf) would result in a Yield acceleration of 0.165 and a displacement of 0.015 inches. Various Yield accelerations are found for various additional shear strength, resulting in various displacements. (Curve designated as Newmark Analysis curve in Figure 7-15)

Where the two curves converge, is the value for the actual displacement of the embankment soil due to lateral spread and the corresponding shear force that is the pinning effect of the pipe pile for pier 4.The pinning force of the pile was evaluated based on the intersection of the curves corresponding to the LPILE4M shear values and the Newmark analysis. The graphs for these curves are shown in the following graphs.

The convergence of two curves are required (Figure 7-15) when we are calculating the pinning force of the piles and their contribution to the reduction of the soil displacement. The pinning force was evaluated to be 10 kips corresponding to soil displacement of 0.8 inch, using Newmark graph. The following depicts graphically what has been stated:

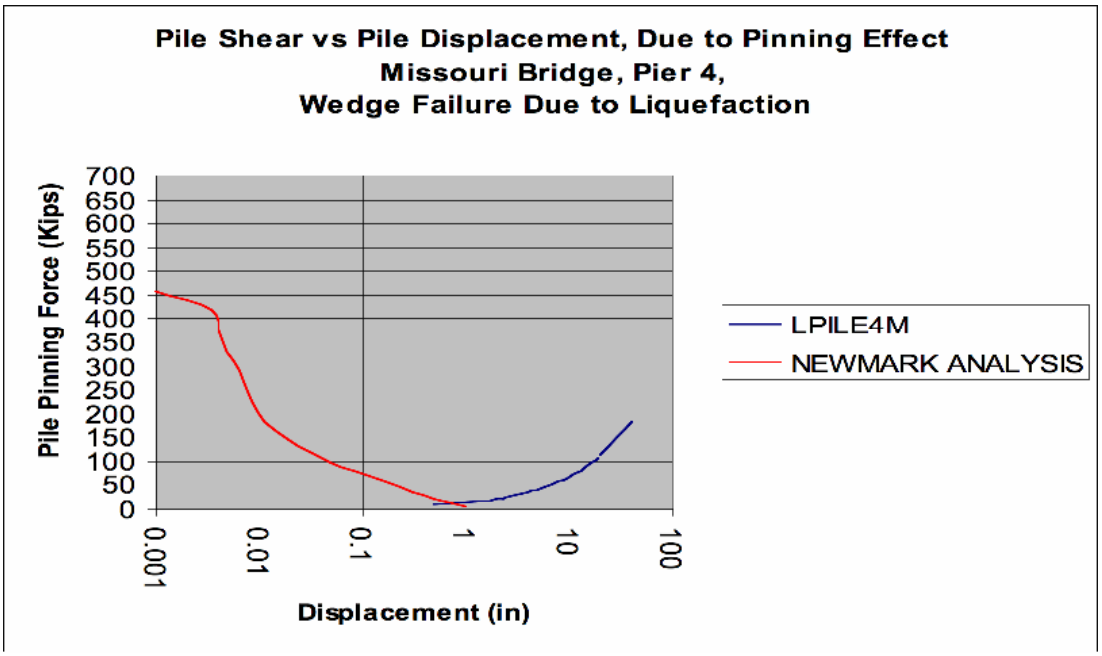

Figure 7-15: Pinning Effect on Piles, Pier 4, (475 YEAR EVENT) Missouri Bridge

7.3.1.5. Lateral Demand for the Pile Foundation (Pier 4 Only)

The lateral demand (Figures 7-16 and 7-17) using 0.8 inch of displacement (The actual displacement found due to pinning effect, is used as the free field soil movement to assess the lateral demand on the pile foundation at pier 4

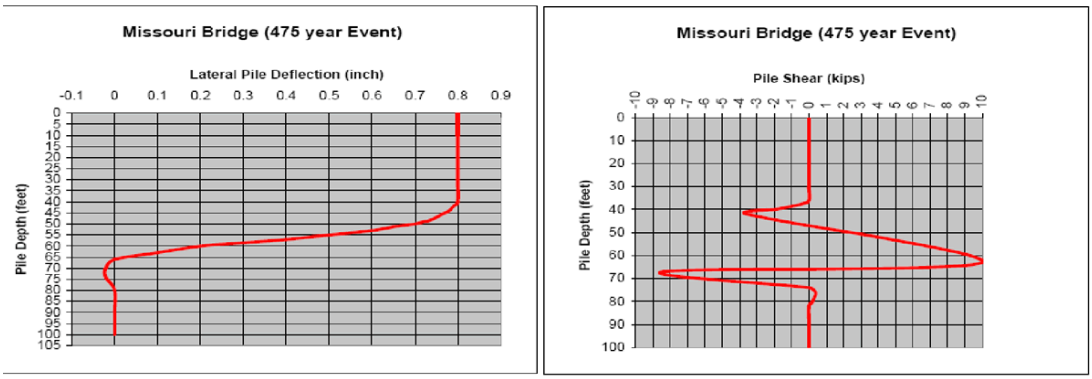

Figure 7-16: Lateral Pile Response, Missouri Bridge, (475 YEAR EVENT) Pier 4

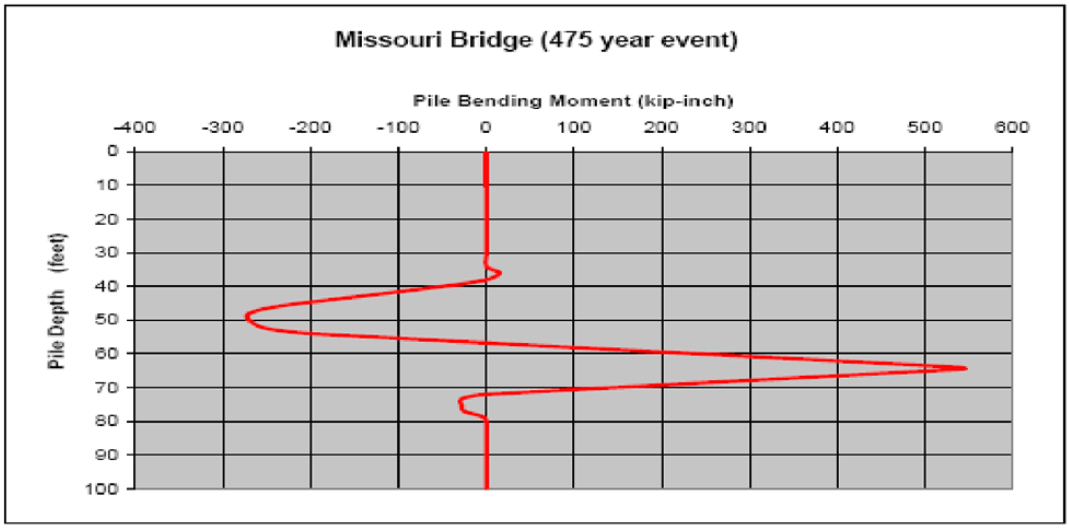

Figure 7-17: Lateral Pile Response, Missouri Bridge, (475 YEAR EVENT), Pier 4

7.3.1.6. Lateral Capacity for the Pile Foundation

The moment capacity for the pile foundation for pier 4 is based on the value stated in the NCHRP report and is computed to be 138 kip-foot. The shear capacity for the pile is calculated to be 8 kips and was based on the assumptions that the plastic

hinges develop on piles supporting pier 4, at elevations –11.3 and –46 and using the following equation:

pile shear capacity = (2 x Plastic moment capacity of pile) / (distance between plastic hinges)

$\Rightarrow$ Pile shear capacity = (2 x 138 kip-foot)/34.7 = 8 kips

7.3.1.7. Plastic Hinge Location

The following (Figure 7-18) depicts the location of the plastic hinges as shown in the referenced NCHRP report corresponding to pier 4, due to lateral spreading:

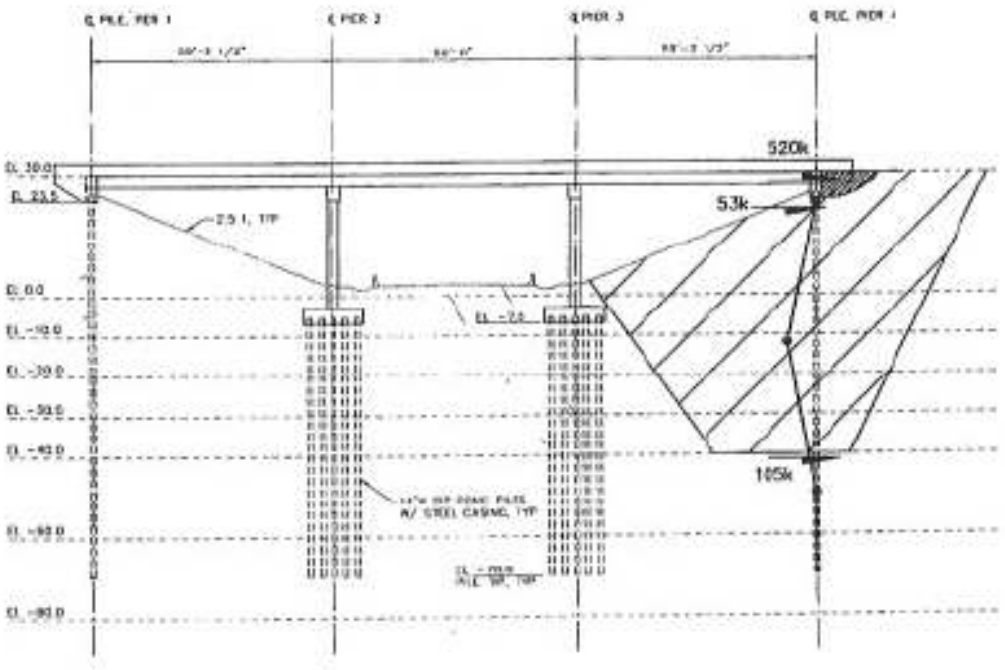

Figure 7-18: Plastic Hinge Location along the Pile, Missouri Bridge, Pier 4

The following (Figure 7-19) depicts the location of the maximum bending moments with respect to the liquefiable layers, as assessed by the author. As shown, the maximum bending moments occur at depths of 594 inch and 774 inch below the top of the pile, hence the hinge distance is 180 inch (14.9 ft).

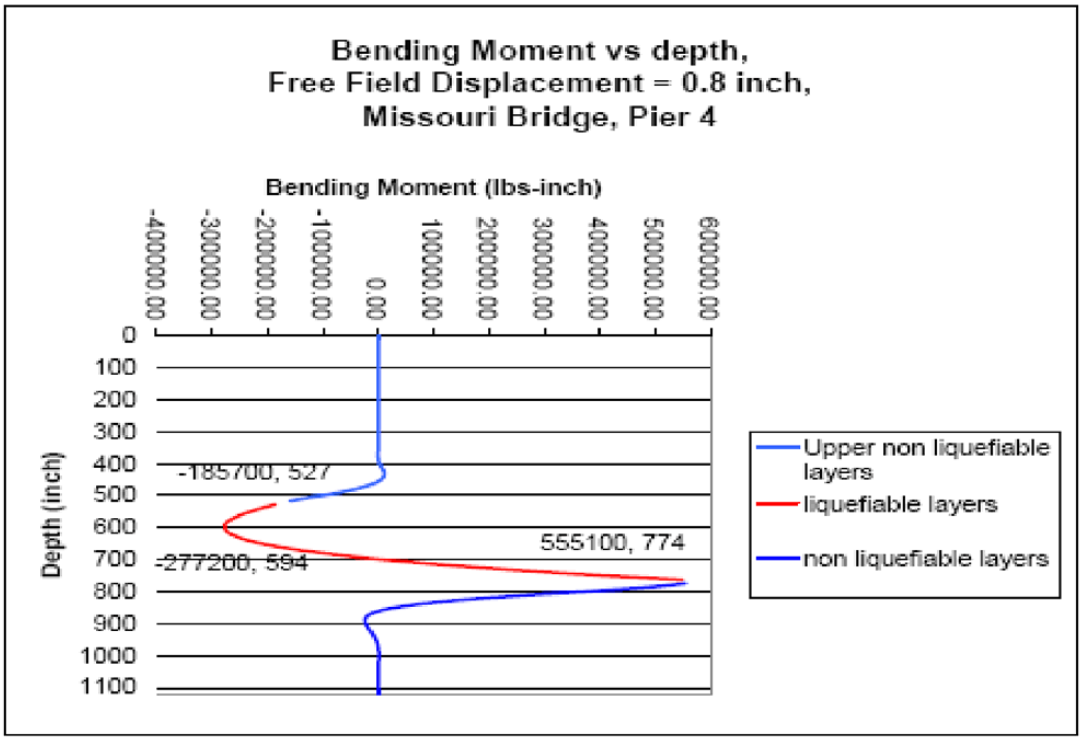

Figure 7-19: Location of the Maximum Bending Moment and Estimated Plastic Hinge Distance For Piles, pier 4, (475 YEAR EVENT) Missouri Bridge

7.2.1.8. Summary

The 14 inch pipe pile foundation for pier 4 was evaluated under lateral spread loading. The analysis showed that the effect of “pile pinning” in reducing the soil

movement due to lateral spread is relatively significant reducing the slope movement from 3 inch to 0.8 inch.

Since the pile response is dependent on the relative soil displacement with respect to the pile horizontal movement, the pile pinning effect contributed in reducing the lateral spread loading on the piles. Despite this contribution, the shear force demand due to lateral spread loading exceeded the shear capacity of 8 kips (by an amount of 2 kips) .However, the bending moment demand did not exceed the bending moment capacity of 138 kip-foot.

It is important to note that the author based the evaluation of the shear capacity on the equation shown in page 7 of this report as stated in the referenced NCHRP report. Unlike the 34.7 feet distance evaluated by the NCHRP report, the plastic hinge distance of 13.5 feet was evaluated based on the study performed by the author.

In addition, the author evaluated the pinning force due to the piles to be equal to 10 kips for pier 4 , which exceeds the value of 8 kips evaluated by the NCHRP report.

7.3.2. Missouri Bridge (2,475 Year Event)

The following is a critical review of the lateral spread loading on the existing foundation for the Missouri bridge. An independent analysis is performed for the

2,475 year event on evaluating the amount of loading caused by lateral spread on pile foundation for pier 4 of the Missouri Bridge. The result of this analysis is then compared with the analysis performed and documented in the subject report.

Specifically, the pinning effect of piles is re-evaluated and a comparative study with the result in the subject report is performed.

7.3.2.1. Embankment Stability

The slope stability performed for the embankment for pier 4, reveals that the slope is not stable during the design earthquake. The factor of safety for pseudo-static case considering a horizontal ground acceleration of 0.15g leads to a value of 0.753, considering the liquefiable soil layers. This value is less than 1.1 which requires an evaluation of the slope displacement using the Newmark method. The design shear strength parameters used in the slope stability were based on the data made available to the author by the NCHRP report. For liquefiable layers, the value of the shear strength was based on the latter and was evaluated to be 300 psf.

The stability of the slope embankment during the design earthquake event where pier 4 is located, was analyzed, using XTSABL5 software program. The failure surface was designated as a block failure, with the base of the failure block passing through the liquefiable layer, at elevation –20 through –40.

The slope stability calculation for the embankment for pier 4 led to factor of safety (FOS) of 1.724. for static condition corresponding to the wedge failure through the liquefiable layer, considering post liquefaction case. The FOS is more than 1.0 which does not lead to flow condition.

The factor of safety for pseudo-static case considering a horizontal ground acceleration of 0.17g leads to a value of 0.699, considering the liquefiable soil layers. This value is less than 1.1 which requires an evaluation of the slope displacement using the Newmark method.

7.3.2.2. Yield Acceleration & Newmark Analysis

The anticipated slope displacement due to the design earthquake is evaluated using the Newmark Method. The displacement is anticipated to be in the order of 55 inch, considering the liquefiable soil layers and given a yield acceleration of 0.085.

7.3.2.3. Lateral Demand/Capacity of the Pile Foundation

The lateral demand on the pile foundation was evaluated using the LPILE4M software program (ENSOFT, version 4). For the liquefiable layer, the strength of the liquefiable soil was increased incrementally (table 7-6 below) and the corresponding yield acceleration and the slope displacement during the design earthquake was evaluated. The displacement of the embankment during the earthquake was calculated using Martin and Qiu and Newmark graph.

Newmark Analysis, Missouri Bridge, Pier 4

Initial Cohesion[1] (psf)	Increase in Cohesion (psf)	Cohesion[2] (psf)	Length of Failure Surface (ft)	Pile Spacing (ft)	Width of Footing (ft)	# of Piles	Abutment Force (kips)	Total Shear Force[3] (kips)	Shear Force, top (kips)	Shear Force, bottom (kips)	Yield acceleration (g)	Max. Acceleration (g)	Ay/Ama x	Displacement (in)[4]	Displacement (in)[5]
300	140	440	90	4.75	43	9	520	2	1	2	0.105	0.53	0.20	38	19
300	160	460	90	4.75	43	9	520	11	4	7	0.108	0.53	0.20	36	18
300	180	480	90	4.75	43	9	520	20	7	13	0.11	0.53	0.21	34	16
300	355	655	90	4.75	43	9	520	95	32	63	0.145	0.53	0.27	22	10
300	500	800	90	4.75	43	9	520	157	52	105	0.165	0.53	0.31	17	6
300	600	900	90	4.75	43	9	520	200	67	133	0.185	0.53	0.35	10	5
300	700	1000	90	4.75	43	9	520	243	81	162	0.202	0.53	0.38	8	3.5
300	800	1100	90	4.75	43	9	520	286	95	191	0.215	0.53	0.41	6	2.5
300	900	1200	90	4.75	43	9	520	329	110	219	0.230	0.53	0.43	5	2
300	1000	1300	90	4.75	43	9	520	372	124	248	0.250	0.53	0.47	3.5	1.5
300	1100	1400	90	4.75	43	9	520	415	138	277	0.265	0.53	0.50	2.8	1
300	1200	1500	90	4.75	43	9	520	458	153	305	0.280	0.53	0.53	2	0.7

1: Initial cohesion corresponds to the shear strength of liquefiable soil, where the failure surface is located
2: Cohesion corresponds to the shear strength of the liquefiable soil after the increase in cohesion is introduced.
It is used for the embankment stability and Newmark analysis
3: Total Shear Force = [(Increase In Cohesion x Length of Failure Surface x Width of Footing)/(Pile Spacing)] minus the abutment force

Table 7-6: Newmark Analysis Results for Missouri Bridge, (2,475 Year Event), Pier 4

7.3.2.4. Expected Displacement of the Embankment Considering Pile Pinning Effect

When the embankment soil is moving against the piles at pier 4, considering the liquefiable layers under the design seismic event, the piles will resist the movement of the soil by producing shearing forces. These forces would provide some form of resistance against lateral spreading.

A two-front approach is used to assess the lateral spread loading on the piles and is as follows:

In this case, only pier 4 is subject to lateral spread loading. Various soil movements were prescribed to the embankment to determine the pile shear forces found due to these prescribed soil movements. The software program LPILE4M was used to prescribe various soil movements and to evaluate the corresponding shear forces for the pier 4 piles, due to these soil movements. Shear forces are found for soil movements of 0.5 through a maximum of 40 inches (table 7-7 And Curve designated as LPILE4M in Figures 7-20 and 7-21)

LPILE4M (Missouri Bridge)

PILE TYPE[1]	PILE DIAMETER (in)	PILE LENGTH (ft)	MOMENT OF INERTIA (in^4)	MODULUS OF ELASTICITY (psi)	SOIL DISPLACEMENT[2] (in)	PILE SHEAR[3] (Kips)
PIPE PILE	14	93.5	2450	3,630,000	0.5	7.78
PIPE PILE	14	93.5	2450	3,630,000	1	11.57
PIPE PILE	14	93.5	2450	3,630,000	2	18.24
PIPE PILE	14	93.5	2450	3,630,000	3	25.21
PIPE PILE	14	93.5	2450	3,630,000	4	31.67
PIPE PILE	14	93.5	2450	3,630,000	5	37.63
PIPE PILE	14	93.5	2450	3,630,000	6	43.3
PIPE PILE	14	93.5	2450	3,630,000	7	48.67
PIPE PILE	14	93.5	2450	3,630,000	8	53.86
PIPE PILE	14	93.5	2450	3,630,000	9	58.94
PIPE PILE	14	93.5	2450	3,630,000	10	63.83
PIPE PILE	14	93.5	2450	3,630,000	11	68.65
PIPE PILE	14	93.5	2450	3,630,000	12	73.42
PIPE PILE	14	93.5	2450	3,630,000	13	78.04
PIPE PILE	14	93.5	2450	3,630,000	14	82.58
PIPE PILE	14	93.5	2450	3,630,000	15	87.16
PIPE PILE	14	93.5	2450	3,630,000	16	91.61
PIPE PILE	14	93.5	2450	3,630,000	17	95.97
PIPE PILE	14	93.5	2450	3,630,000	18	100.3
PIPE PILE	14	93.5	2450	3,630,000	19	104.68
PIPE PILE	14	93.5	2450	3,630,000	20	108.96
PIPE PILE	14	93.5	2450	3,630,000	25	129.58
PIPE PILE	14	93.5	2450	3,630,000	30	148.23
PIPE PILE	14	93.5	2450	3,630,000	35	165.39
PIPE PILE	14	93.5	2450	3,630,000	40	181.67

1: Pipe pile thickness is 0.25 inch.
2: Soil displacement prescribed, to represent the lateral spread movement from the ground surface to the bottom of the liquefiable soil layer.
3: Maximum shear force developed by the pile resisting to the prescribed soil movement

Table 7-7: Pile Shear Force, Pier 4, (2,475 Year Event) Missouri Bridge

Evaluate the pile pinning effect that is the resistance to the soil movement and can be considered as the added shear strength of the soil. The initial shear strength of the liquefiable soil for upper and lower liquefiable layers is 300 psf. An increase of 500 psf in shear strength along the failure surface which was estimated to be 90 ft (slope stability analysis) and the spacing of 4.75 ft for the pipe piles, would be equal to 157

kips of total pile shear force, 105 kips at the bottom and 52 kips at the top of the pile. A Newmark analysis using the value of 800 psf (the initial value being 300 psf and the increase of 500 psf would make the new shear strength to be 800 psf) would result in a Yield acceleration of 0.165 and a displacement of 0.015 inches. Various Yield accelerations are found for various additional shear strength, resulting in various displacements. (Curve designated as Newmark curve in Figures 7-20 and 7-21)

Where the two curves converge, is the value for the actual displacement of the embankment soil due to lateral spread and the corresponding shear force that is the pinning effect of the pipe pile for pier 4.The pinning force of the pile was evaluated based on the intersection of the curves corresponding to the LPILE4M shear values and the Newmark analysis. The graphs for these curves are shown in the following graphs.

The convergence of two curves are required (Figures 7-20 and 7-21) when we are calculating the pinning force of the piles and their contribution to the reduction of the soil displacement. The pinning force was evaluated to be 100 kips corresponding to soil displacement of 20 inch, using Newmark graph. The following depicts graphically what has been stated:

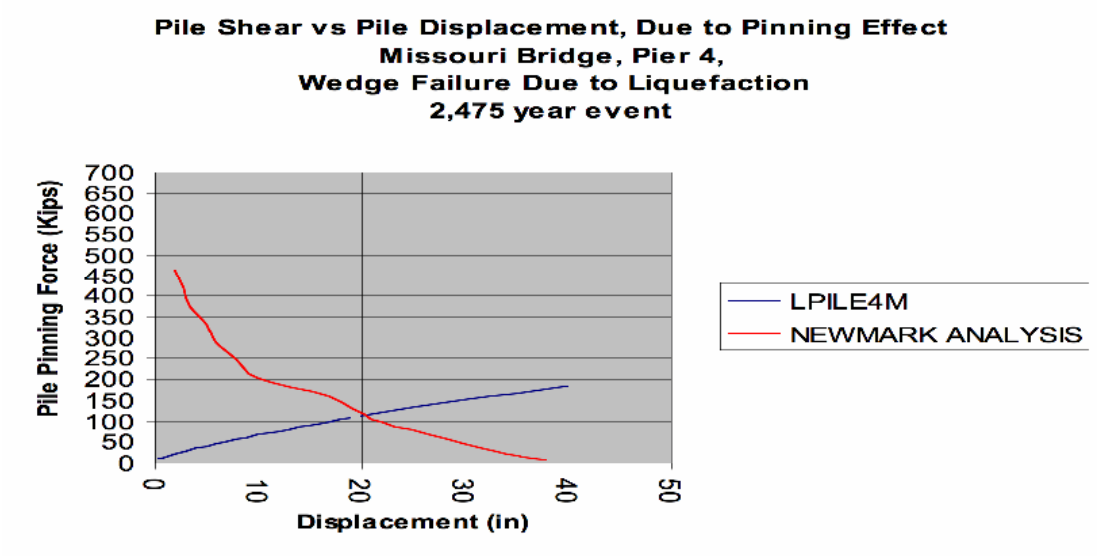

Figure 7-20: Pinning Effect on Piles, Pier 4, (2,475 YEAR EVENT) Missouri Bridge

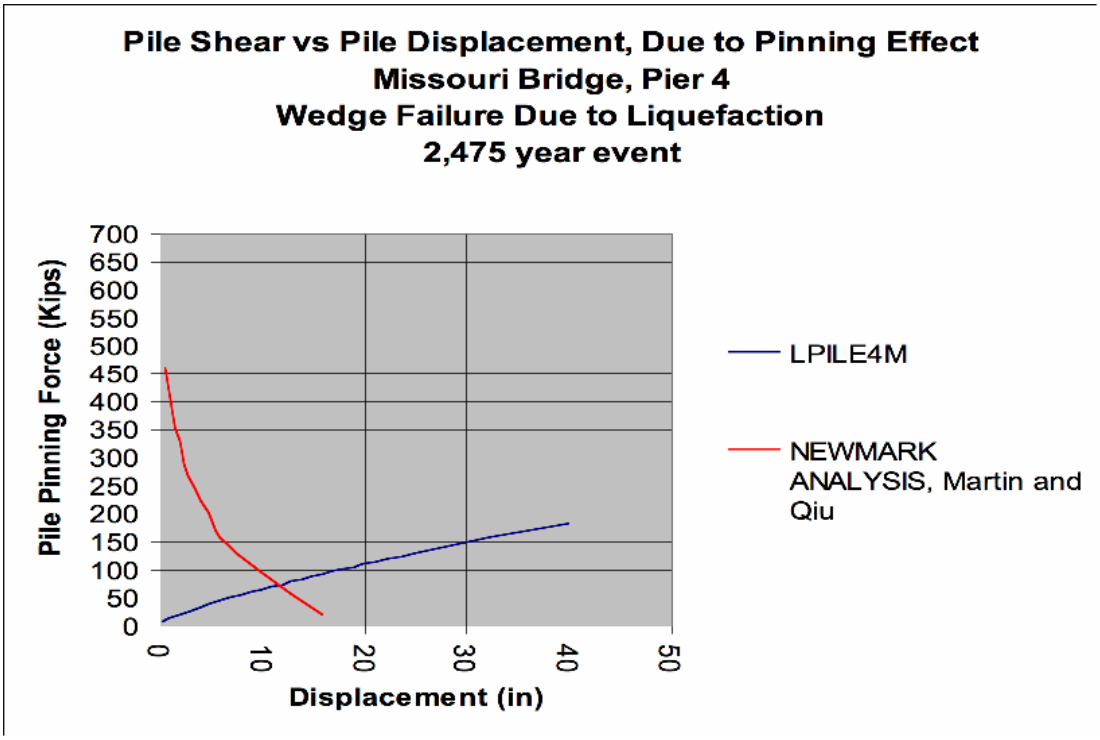

Figure 7-21: Pinning Effect on Piles, Pier 4, (2,475 YEAR EVENT), (Martin and Qiu) Missouri Bridge

7.3.2.5. Lateral Demand for the Pile Foundation (Pier 4 Only)

The lateral demand using 20 inch of displacement (Figures 7-22 and 7-23) (The actual displacement found due to pinning effect, is used as the free field soil movement to assess the lateral demand on the pile foundation at pier 4.

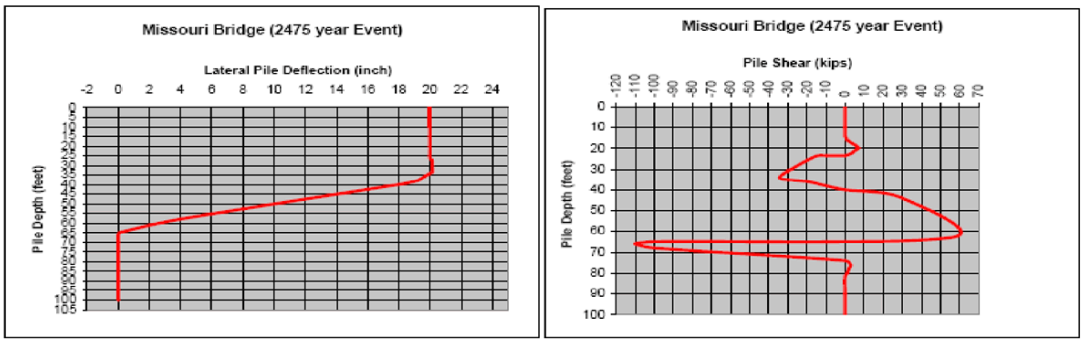

Figure 7-22: Lateral Pile Response, Missouri Bridge, (2,475 YEAR EVENT) Pier 4

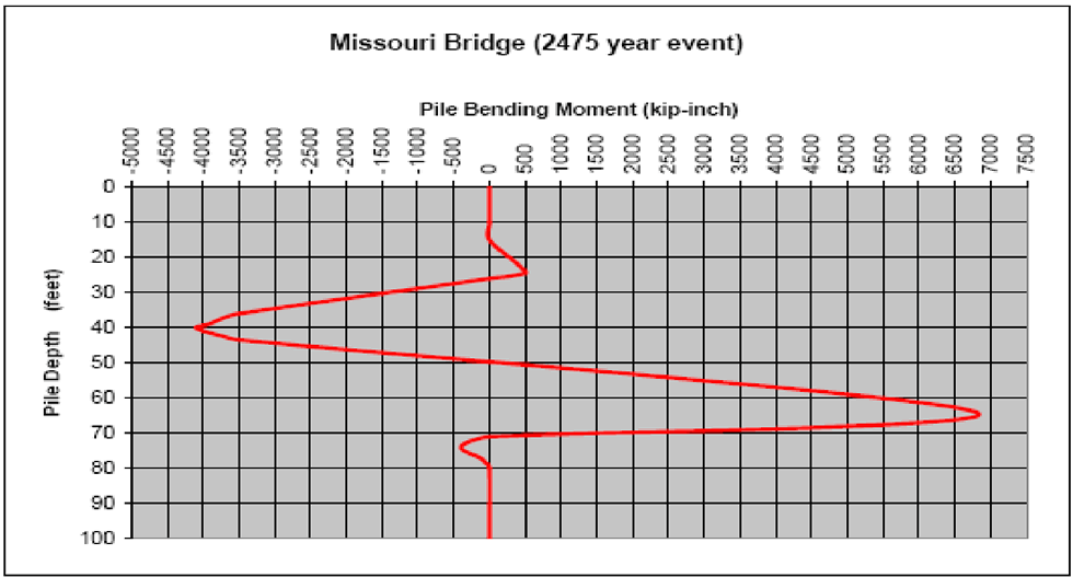

Figure 7-23: Lateral Pile Response, Missouri Bridge, (2,475 YEAR EVENT) Pier 4

7.3.2.6. Lateral Capacity for the Pile Foundation

The moment capacity for the pile foundation for pier 4 is based on the value stated in the NCHRP report and is computed to be 138 kip-foot. The shear capacity for the pile is calculated to be kips and was based on the assumptions that the plastic hinges develop on piles supporting pier 4, at elevations –11.3 and –46 and using the following equation:

pile shear capacity = (2 x Plastic moment capacity of pile) / (distance between plastic hinges)

$\Rightarrow$ Pile shear capacity = (2 x 138 kip-foot)/34.7 = 8 kips

7.3.2.7. Plastic Hinge Location

The following (Figure 7-24) depicts the location of the plastic hinges as shown in the referenced NCHRP report corresponding to pier 4, due to lateral spreading:

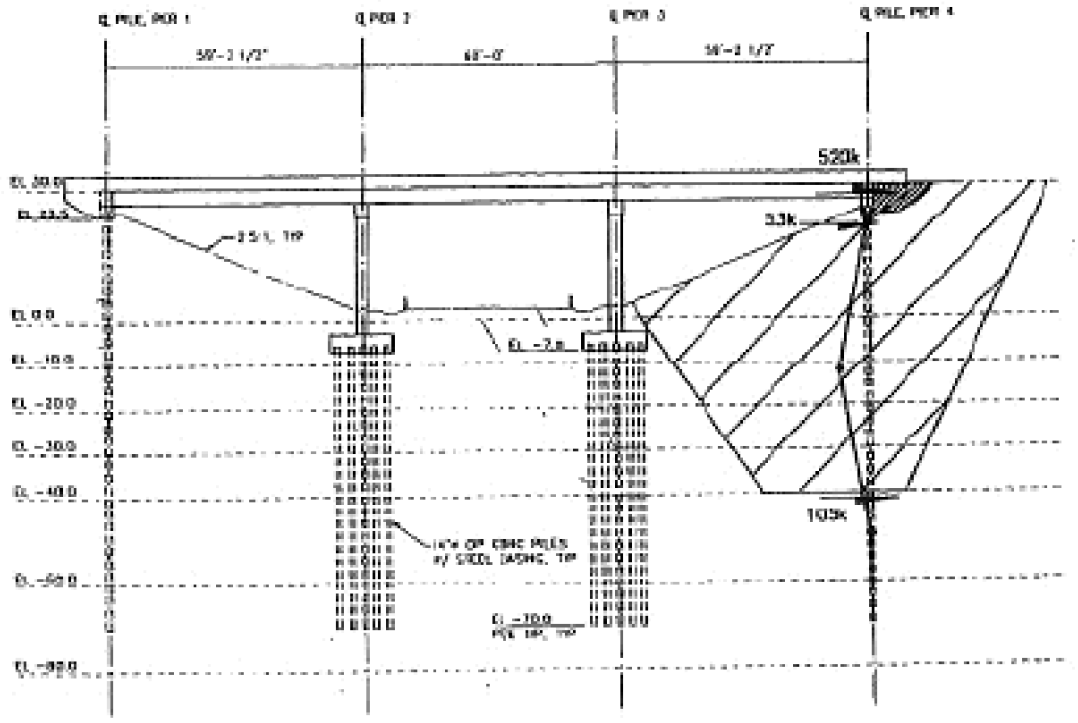

Figure 7-24: Plastic Hinge Location Along the Pile, Missouri Bridge, Pier 4

The following (Figure 7-25) depicts the location of the maximum bending moments with respect to the liquefiable layers, as assessed by the author. As shown, the maximum bending moments occur at depths of 41 ft and 64 ft below the top of the pile, hence the hinge distance is 23.0 ft. (Liquefiable layer shown in blue)

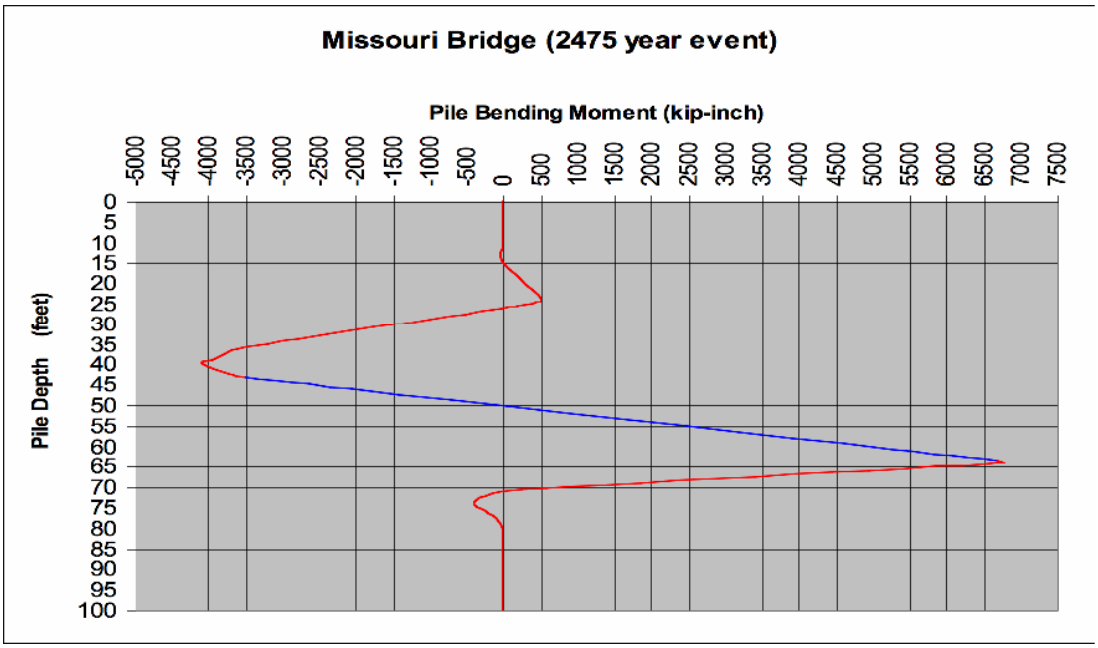

Figure 7-25: Location of the Maximum Bending Moment and Estimated Plastic Hinge Distance For Piles, pier 4, (2,475 YEAR EVENT) Missouri Bridge

7.3.2.8. Summary

The 14 inch pipe pile foundation for pier 4 was evaluated under lateral spread loading. The analysis showed that the effect of "pile pinning" in reducing the soil movement due to lateral spread is very significant reducing the slope movement from 55 inch to 20 inch. Since the pile response is dependent on the relative soil displacement with respect to the pile horizontal movement, the pile pinning effect contributed in reducing the lateral spread loading on the piles. Despite this contribution, the bending moment demand did exceed the bending moment capacity of 138 kip-foot. (by 437 kip-foot).

Unlike the 34.7 feet distance evaluated by the NCHRP report, the plastic hinge distance of 24 feet was evaluated based on the study performed by the author.

In addition, the author evaluated the pinning force due to the piles to be equal to 100 kips for pier 4 , which exceeds the value of 8 kips evaluated by the NCHRP report. No attempt in considering the free field soil movement and the impact of the pile pinning on this movement and thus the pile pinning force was made in the NCHRP report.

7.3.3. Case II: Washington Bridge (475 Year Event)

The NCHRP design approach for the foundation lateral capacity of a five span cast-in-concrete box girder bridge structure, underlayed by liquefiable soil and subject to lateral spread is as follows:

The following is a critical review of the lateral spread loading on the existing foundation for the Washington bridge. An independent analysis is performed on evaluating the amount of loading caused by lateral spread/flow on pile foundation for pier 6 and pier 5 of the Washington Bridge. The result of this analysis is then compared with the analysis performed and documented in the subject report (NCHRP, 2002).

The pinning effect of piles and the pile response forming plastic hinges are re-evaluated and a comparative study with the result in the subject report is performed.

7.3.3.1. Embankment Stability

The slope stability performed for the embankment for abutment 6 and pier 5, reveals that the slope is not stable during the design earthquake. The design shear strength parameters used in the slope stability were based on the data made available to the author by the NCHRP report. For liquefiable layers, the value of shear strength was based on the latter report and was evaluated to be 300 psf.

The stability of the slope embankment during the design earthquake event where pier 6 and pier 5 are located was analyzed, using XTSABL5 software program. The failure surface was designated as a block failure, with the base of the failure block passing through the upper liquefiable layer, at elevation –10 through –20. A separate analysis was performed , where the lower liquefiable layer, at elevation -45 through –55 was designated as the layer where the base of the block failure passes through.

The slope stability calculation for the embankment for Abutment 6 led to factors of safety (FOS) of 0.631, 0.712 and 0.692 for static condition corresponding to the wedge failure through the upper liquefiable layer, through the lower liquefiable layer and deep liquefaction respectively, considering post liquefaction case. The FOS is less than 1.0 which leads to a flow condition.

7.3.3.2. Yield Acceleration and Newmark Analysis

Normally the anticipated slope displacement due to the design earthquake is evaluated using the Newmark Method. However, this is difficult when flow failures such as the failure described above occur. Where the Newmark Chart cannot be used to compute displacements for flow conditions, hence pile pinning analyses were used to check stability.

7.3.3.3. Lateral Demand/Capacity of the Pile Foundation

The lateral demand on the pile foundation was evaluated using the LPILE4M software program (ENSOFT, version 4).

For both the upper liquefiable layer and the lower liquefiable layer, the strength of the liquefiable soil was increased incrementally and the corresponding yield acceleration and the slope displacement during the design earthquake was evaluated (Table 7-8 below). The displacement of the embankment during the earthquake was calculated using Martin and Qiu and WES graph. Result show that the flow condition would cease to exist once the strength of the liquefiable soil is increased incrementally to a value of 700 psf. for the upper liquefiable soil layer.

Newmark Analysis (upper liquefiable layer)

Initial Cohesion [1] (psf)	Increase in Cohesion [2] (psf)	Cohesion [1] (psf)	Length of Failure Surface (ft)	Pile Spacing (ft)	Width of Footing (ft)	# of Piles	Abutment Force (kips)	Shear Force [3] (kips)	Yield acceleration	Max. Acceleration	Ay/Amax	Displacement (in) [4]	Displacement (in) [5]
300	296	596	105	8	48	12	400	91	0	0.24	0.00	very large	very large
300	400	700	105	8	48	12	400	133	0.025	0.24	0.10	100	18
300	500	800	105	8	48	12	400	177	0.055	0.24	0.23	26	5
300	600	900	105	8	48	12	400	219	0.078	0.24	0.33	10	2
300	700	1000	105	8	48	12	400	261	0.103	0.24	0.43	6	0.6
300	800	1100	105	8	48	12	400	303	0.124	0.24	0.52	2	0.3
300	900	1200	105	8	48	12	400	345	0.142	0.24	0.59	1	0.1
300	1000	1300	105	8	48	12	400	387	0.160	0.24	0.67	0.3	0.03
300	1100	1400	105	8	48	12	400	429	0.178	0.24	0.74	0.18	0.001
300	1200	1500	105	8	48	12	400	471	0.194	0.24	0.81	0.1	0.0005

1: Initial cohesion corresponds to the shear strength of liquefiable soil, where the failure surface is located
2: Cohesion corresponds to the shear strength of the liquefiable soil after the increase in cohesion as introduced.
It is used for the embankment stability and Newmark analysis
3: Shear Force = (Increase In Cohesion x Length of Failure Surface x Pile Spacing) minus the abutment force
4: Displacement based on the Newmark, 1977
5: Displacement based on Martin and Qiu (1994)

Table 7-8: Newmark Analysis Results For Washington Bridge, (475 Year Event) Pier 6

7.3.3.4. Expected Displacement of the Embankment Considering Pile Pinning Effect

When the embankment soil is moving against the piles at pier 6 and pier 5 (lower liquefiable zone) and against the piles at pier 6 (upper liquefiable zone), under the design seismic event, the piles will resist the movement of the soil by producing shearing forces. These forces would provide some form of resistance against lateral spreading.

A two-front approach is used to assess the lateral spread loading on the piles and is as follows:

7.3.3.5. Upper Liquefiable Layer

In this case, only pier 6 is subject to lateral spread loading

1. Various soil movements were prescribed to the embankment to determine the pile shear forces found due to these prescribed soil movements. The software program LPILE4M was used to prescribe various soil movements and to evaluate the corresponding shear forces for the pier 6 piles, due to these soil movements. Shear forces are found for soil movements of 0.5 through a maximum of 40 inches (Table 7-9 and Curve designated as LPILE4M in Figure 7-26)

LPILE4M (UPPER LIQUEFIABLE LAYER)

Pile Type[1]	Pile Diameter (in)	Pile Length (ft)	Moment of Inertia (in^4)	Modulus of Elasticity (psi)	Soil Displacement[2] (in)	Pile Shear[3] (kips)
PIPE PILE	24	163	23197	3,830,000	0.5	20.5
PIPE PILE	24	163	23197	3,830,000	1	33.2
PIPE PILE	24	163	23197	3,830,000	2	55.2
PIPE PILE	24	163	23197	3,830,000	3	75.6
PIPE PILE	24	163	23197	3,830,000	4	95.2
PIPE PILE	24	163	23197	3,830,000	5	116.6
PIPE PILE	24	163	23197	3,830,000	6	141.8
PIPE PILE	24	163	23197	3,830,000	7	165.8
PIPE PILE	24	163	23197	3,830,000	8	189.7
PIPE PILE	24	163	23197	3,830,000	9	212.8
PIPE PILE	24	163	23197	3,830,000	10	232.6
PIPE PILE	24	163	23197	3,830,000	11	252.2
PIPE PILE	24	163	23197	3,830,000	12	272.7
PIPE PILE	24	163	23197	3,830,000	13	293.2
PIPE PILE	24	163	23197	3,830,000	14	313.5
PIPE PILE	24	163	23197	3,830,000	15	332.6
PIPE PILE	24	163	23197	3,830,000	16	351.4
PIPE PILE	24	163	23197	3,830,000	17	370.2
PIPE PILE	24	163	23197	3,830,000	18	387.5
PIPE PILE	24	163	23197	3,830,000	19	404.9
PIPE PILE	24	163	23197	3,830,000	20	422
PIPE PILE	24	163	23197	3,830,000	25	480.7
PIPE PILE	24	163	23197	3,830,000	30	519
PIPE PILE	24	163	23197	3,830,000	35	524.6
PIPE PILE	24	163	23197	3,830,000	40	518.6

1: Pipe pile thickness is 0.5 inch.
2: Soil displacement prescribed, to represent the lateral spread movement from the ground surface to the bottom of the liquefiable soil layer.
3: Maximum shear force developed by the pile resisting to the prescribed soil movement

Table 7-9: Pile Shear Force, Upper Liquefiable Layer, (475 Year Event) Washington Bridge

2. Evaluate the pile pinning effect that is the resistance to the soil movement and can be considered as the added shear strength of the soil. The initial shear strength of the liquefiable soil for upper and lower liquefiable layers is 300 psf. An increase of 296 psf in shear strength along the failure surface which was estimated to be 105 ft and 129 ft for upper and lower liquefiable layers respectively (slope stability analysis) and the spacing of 8 ft for the pipe

piles, would be equal to 91 kips of pile shear force. A Newmark analysis using the value of 596 psf (the initial value being 300 psf and the increase of 296 psf would make the new shear strength to be 596 psf) would result in a Yield acceleration of 0.0 and a displacement of 100inches. Various Yield accelerations are found for various additional shear strength, resulting in various displacements. (Curve designated as Newmark curve in Figure 7-28)

3. Where the two curves converge, is the value for the actual displacement of the embankment soil due to lateral spread and the corresponding shear force that is the pinning effect of the pipe pile for pier 6.

The pinning force of the pile was evaluated based on the intersection of the curves corresponding to the LPILE4M shear values and the Newmark analysis. The graphs for these curves are shown in the following graphs. The convergence of two curves are required (Figure 7-26) when we are evaluating the pinning force of the piles and their contribution to the reduction to the soil displacement. The pinning force was evaluated to be 225 kips corresponding to soil displacement of 9 inch, using the WES graph. The pinning force was evaluated to be 160 kips corresponding to soil displacement of 7 inch using Martin and Qiu data. (Figure 7-27)

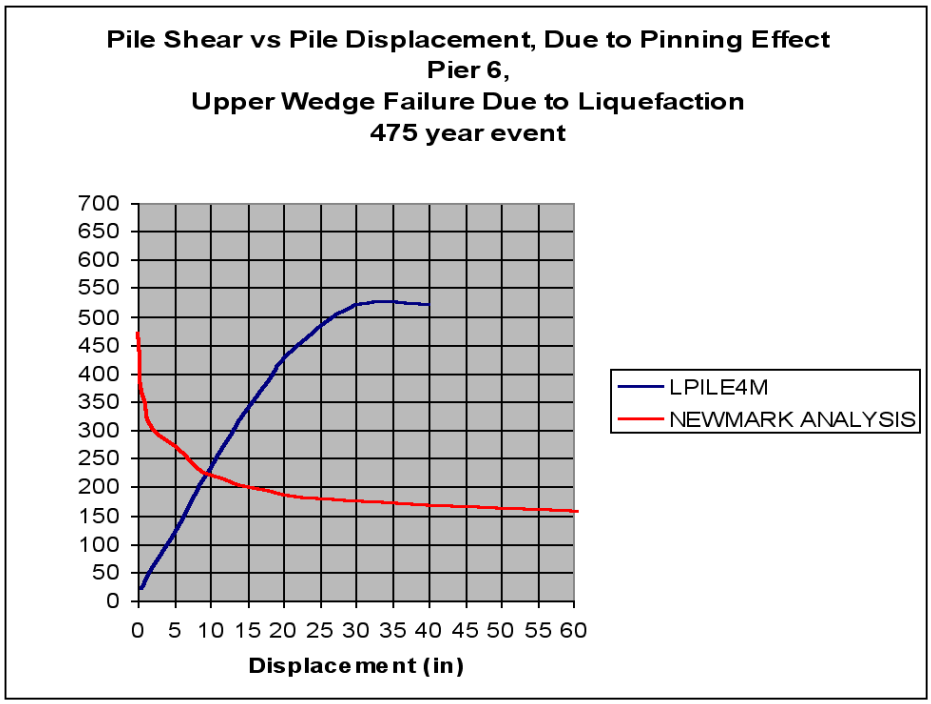

Figure 7-26: Pinning Effect on Piles, Pier 6, (475 YEAR EVENT) Washington Bridge

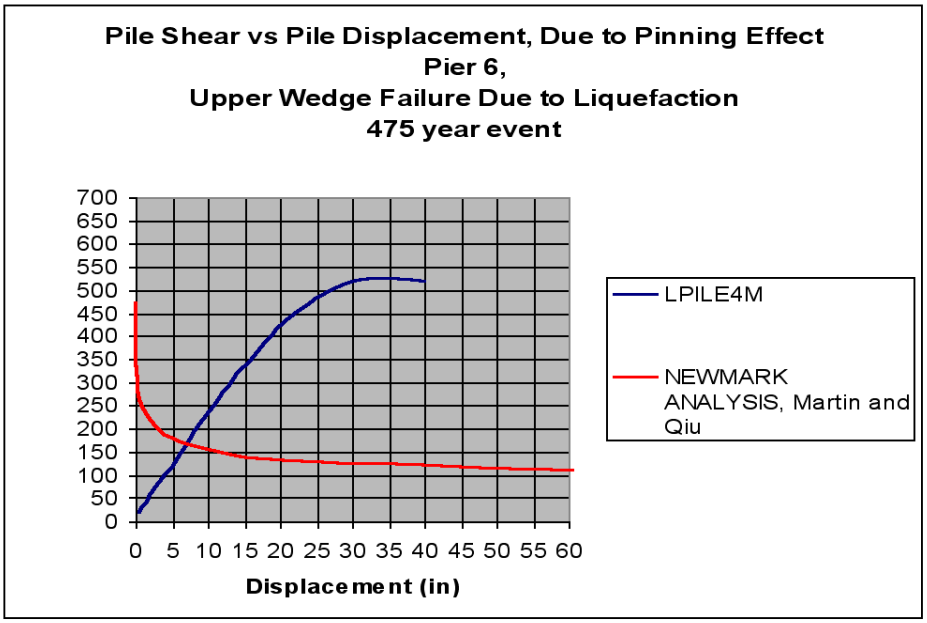

Figure 7-27: Pinning Effect on Piles, Pier 6, (475 YEAR EVENT), (Martin and Qiu) Washington Bridge

7.3.3.6. Lower Liquefiable Layer

In this case, both pier 5 and pier 6 piles are subject to lateral spread loading. Same approach was performed, except in this case, the length of failure plane through the lower liquefiable zone was 129 ft, the added resistance due to the columns was included (420 kips). In increase of 545 psf in shear strength along the failure surface would correspond to 91 kips of pile shear force. A Newmark analysis using the value of 845 psf the initial value being 300 psf and the increase of 545 would make the new shear strength to be 845 psf) would result in a yield acceleration of 0.01 and a displacement of 100 inches. Various yield accelerations are found for various additional shear strengths, resulting in various displacements (Table 7-12)

The pinning force of the pile can not be evaluated using the convergence of the two curves, since the plane of failure passing through then lower liquefiable layer, passes through the pier 6 and pier 5 pile foundations.

Unlike the upper liquefiable layer case, where the plane of failure passes through only the pier 6 pile foundation, in this case the pinning force must also consider the contribution due to the pier 5 pile foundation. In order to evaluate the pinning force due to the pier 6 and pier 5, both curves corresponding to LPILE4M for these piers are converging the Newmark curve. The software program LPILE4M was used to prescribe various soil movements and to evaluate the corresponding shear forces for the piers 5 and pier 6 piles, due to these soil movements. Shear forces are found for

soil movements of 0.5 through a maximum of 40 inches (Tables 7-10, 7-11 and Curves designated as LPILE4M in figures 7-30 and 7-31).

LPILE4M (Lower Liquefiable layer), PIER 6

PILE TYPE[1]	PILE DIAMETER (in)	PILE LENGTH (ft)	MOMENT OF INERTIA (in^4)	MODULUS OF ELASTICITY (psi)	SOIL DISPLACEMENT[2] (in)	PILE SHEAR[3] (Kips)
PIPE PILE	24	193	23197	3,830,000	0.5	23.6
PIPE PILE	24	193	23197	3,830,000	1	41.7
PIPE PILE	24	193	23197	3,830,000	2	76
PIPE PILE	24	193	23197	3,830,000	3	109
PIPE PILE	24	193	23197	3,830,000	4	140
PIPE PILE	24	193	23197	3,830,000	5	170
PIPE PILE	24	193	23197	3,830,000	6	200
PIPE PILE	24	193	23197	3,830,000	7	230
PIPE PILE	24	193	23197	3,830,000	8	256
PIPE PILE	24	193	23197	3,830,000	9	278
PIPE PILE	24	193	23197	3,830,000	10	300
PIPE PILE	24	193	23197	3,830,000	11	321
PIPE PILE	24	193	23197	3,830,000	12	340
PIPE PILE	24	193	23197	3,830,000	13	357
PIPE PILE	24	193	23197	3,830,000	14	373
PIPE PILE	24	193	23197	3,830,000	15	388
PIPE PILE	24	193	23197	3,830,000	16	403
PIPE PILE	24	193	23197	3,830,000	17	417
PIPE PILE	24	193	23197	3,830,000	18	431
PIPE PILE	24	193	23197	3,830,000	19	443
PIPE PILE	24	193	23197	3,830,000	20	455
PIPE PILE	24	193	23197	3,830,000	25	506
PIPE PILE	24	193	23197	3,830,000	30	550
PIPE PILE	24	193	23197	3,830,000	35	587
PIPE PILE	24	193	23197	3,830,000	40	622

1: Pipe pile thickness is 0.5 inch, filled with concrete
2: Soil displacement prescribed, to represent the lateral spread movement from the ground surface to the bottom of the liquefiable soil layer.
3: Maximum shear force developed by the pile resisting to the prescribed soil movement

Table 7-10: Pile Shear Force, Pier 6, (475 YEAR EVENT) Washington Bridge

LPILE4M (Lower Liquefiable layer), PIER 5

PILE TYPE[1]	PILE DIAMETER (in)	PILE LENGTH (ft)	MOMENT OF INERTIA (in^4)	MODULUS OF ELASTICITY (psi)	SOIL DISPLACEMENT[2] (in)	PILE SHEAR[3] (Kips)
PIPE PILE	24	150	23197	3,830,000	0.5	89
PIPE PILE	24	150	23197	3,830,000	1	148
PIPE PILE	24	150	23197	3,830,000	2	249
PIPE PILE	24	150	23197	3,830,000	3	320
PIPE PILE	24	150	23197	3,830,000	4	365
PIPE PILE	24	150	23197	3,830,000	5	399
PIPE PILE	24	150	23197	3,830,000	6	426
PIPE PILE	24	150	23197	3,830,000	7	450
PIPE PILE	24	150	23197	3,830,000	8	470
PIPE PILE	24	150	23197	3,830,000	9	488
PIPE PILE	24	150	23197	3,830,000	10	504
PIPE PILE	24	150	23197	3,830,000	11	
PIPE PILE	24	150	23197	3,830,000	12	
PIPE PILE	24	150	23197	3,830,000	13	
PIPE PILE	24	150	23197	3,830,000	14	
PIPE PILE	24	150	23197	3,830,000	15	
PIPE PILE	24	150	23197	3,830,000	16	
PIPE PILE	24	150	23197	3,830,000	17	
PIPE PILE	24	150	23197	3,830,000	18	
PIPE PILE	24	150	23197	3,830,000	19	
PIPE PILE	24	150	23197	3,830,000	20	
PIPE PILE	24	150	23197	3,830,000	25	
PIPE PILE	24	150	23197	3,830,000	30	
PIPE PILE	24	150	23197	3,830,000	35	
PIPE PILE	24	150	23197	3,830,000	40	

1: Pipe pile thickness is 0.5 inch, filled with concrete.
2: Soil displacement prescribed, to represent the lateral spread movement from the ground surface to the bottom of the liquefiable soil layer.
3: Maximum shear force developed by the pile resisting to the prescribed soil movement

Table 7-11: Pile Shear Force, Pier 5, (475 YEAR EVENT) Washington Bridge

Newmark Analysis (lower liquefiable layer)

Initial Cohesion[1] (psf)	Increase in Cohesion (psf)	Cohesion[2] (psf)	Length of Failure Surface (ft)	Pile Spacing (ft)	Width of Footing (ft)	# of Piles	Abutment Force (kips)	Column Force (kips)	Shear Force[3] (kips)	Yield acceleration	Max. Acceleration	Ay/Amax	Displacement (in)[4]	Displacement (in)[5]
300	545	845	129	3	48	28	400	420	91	0.01	0.24	0.04	150	40
300	600	900	129	3	48	28	400	420	103	0.015	0.24	0.06	100	28
300	700	1000	129	3	48	28	400	420	126	0.032	0.24	0.13	50	10
300	800	1100	129	3	48	28	400	420	148	0.047	0.24	0.20	30	7
300	900	1200	129	3	48	28	400	420	170	0.062	0.24	0.26	18	4
300	1000	1300	129	3	48	28	400	420	192	0.077	0.24	0.32	10	2.5
300	1100	1400	129	3	48	28	400	420	214	0.090	0.24	0.38	6	1
300	1200	1500	129	3	48	28	400	420	236	0.105	0.24	0.44	5	0.6
300	1300	1600	129	3	48	28	400	420	258	0.120	0.24	0.50	2.5	0.3
300	1400	1700	129	3	48	28	400	420	280	0.135	0.24	0.56	1.5	0.2

1 Initial cohesion corresponds to the shear strength of liquefiable soil, where the failure surface is located

2 Cohesion corresponds to the shear strength of the liquefiable soil after the increase in cohesion is introduced.

It is used for the embankment stability and Newmark analysis

3 Shear Force = [(Increase In Cohesion x Length of Failure Surface x Width of Footing)/ (Pile Spacing)] minus the abutment force-minus the column force

4 Displacement based on the Newmark, 1977

5 Displacement based on Martin and Qiu (1994)

Table 7-12: Newmark Analysis Results For Washington Bridge, (475 YEAR EVENT) Piers 5 and 6

The following (Figures 7-28 and 7-29) depict graphically the above cited cases:

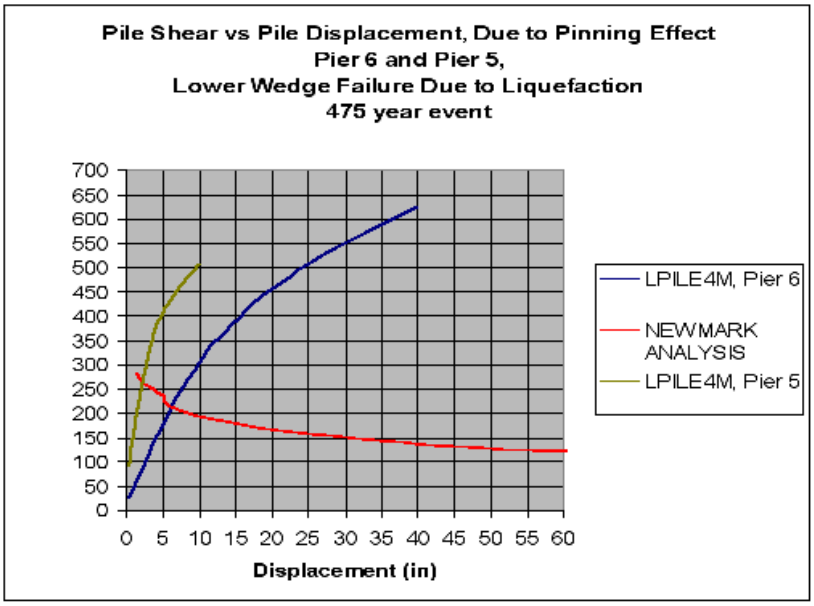

Figure 7-28: Pinning Effect on Piles, Piers 5 and 6, (475 YEAR EVENT) Washington Bridge

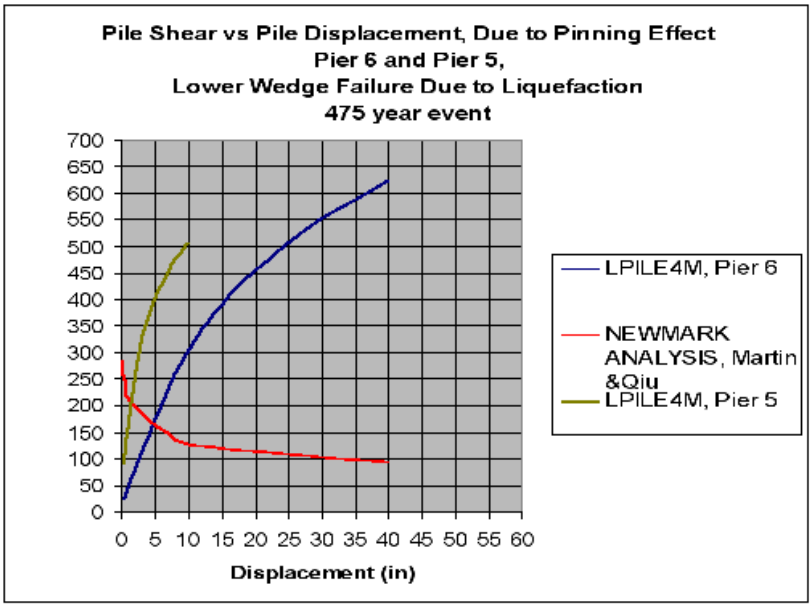

Figure 7-29: Pinning Effect on Piles, Piers 5 and 6, (475 YEAR EVENT), (Martin and Qiu) Washington Bridge

7.3.3.7. Lateral Demand for the Pile Foundation (Pier 6 Only)

The lateral demand (Figures 7-30 and 7-31) using 9 inch of displacement (The actual displacement found from step 3 described above, is used as the free field soil movement to assess the lateral demand on the pile foundation at pier 6.

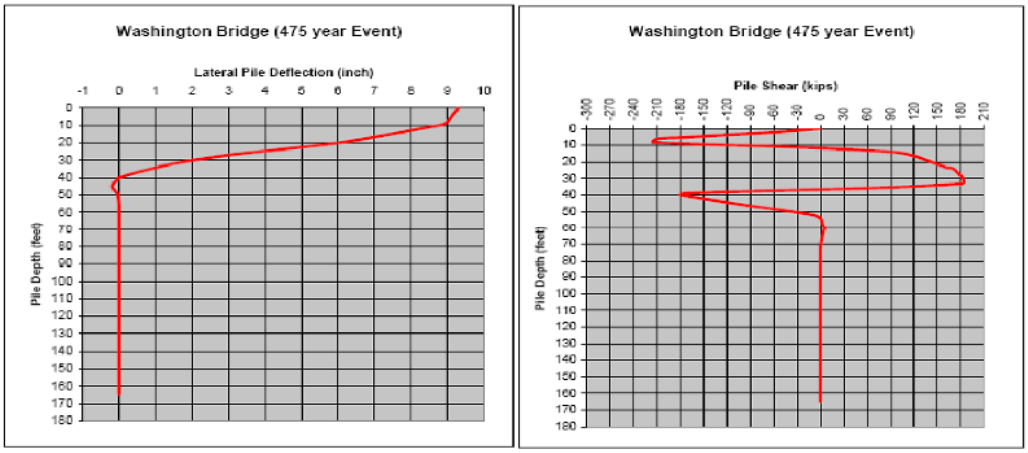

Figure 7-30: Lateral Pile Response, Washington Bridge, (475 YEAR EVENT) Pier 6

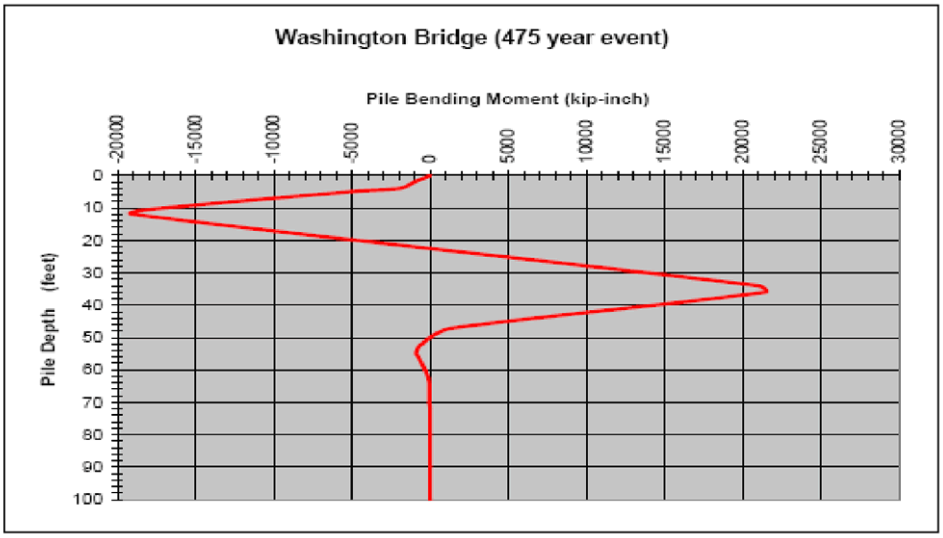

Figure 7-31: Lateral Pile Response, Washington Bridge, (475 YEAR EVENT) Pier 6

7.3.3.8. Lateral Capacity for the Pile Foundation

The moment capacity for the pile foundation for abutment 6 is based on the value stated in the NCHRP report and is computed to be 1360 kip-foot. The shear capacity for the pile is calculated to be 91 kips and was based on the assumption that the plastic hinges develop on piles supporting abutment 6, at elevations 0 and –30 and using the following equation:

pile shear capacity = (2 x Plastic moment capacity of pile) / (distance between plastic hinges)

$\Rightarrow$ Pile shear capacity = (2 x 1360 kip-foot) / 30 = 91 kips

7.3.3.9. Plastic Hinge Location

The following (Figure 7-32) depicts the location of the plastic hinges as shown in the referenced NCHRP report for the upper liquefiable layer case corresponding to pier 6, due to lateral spreading.

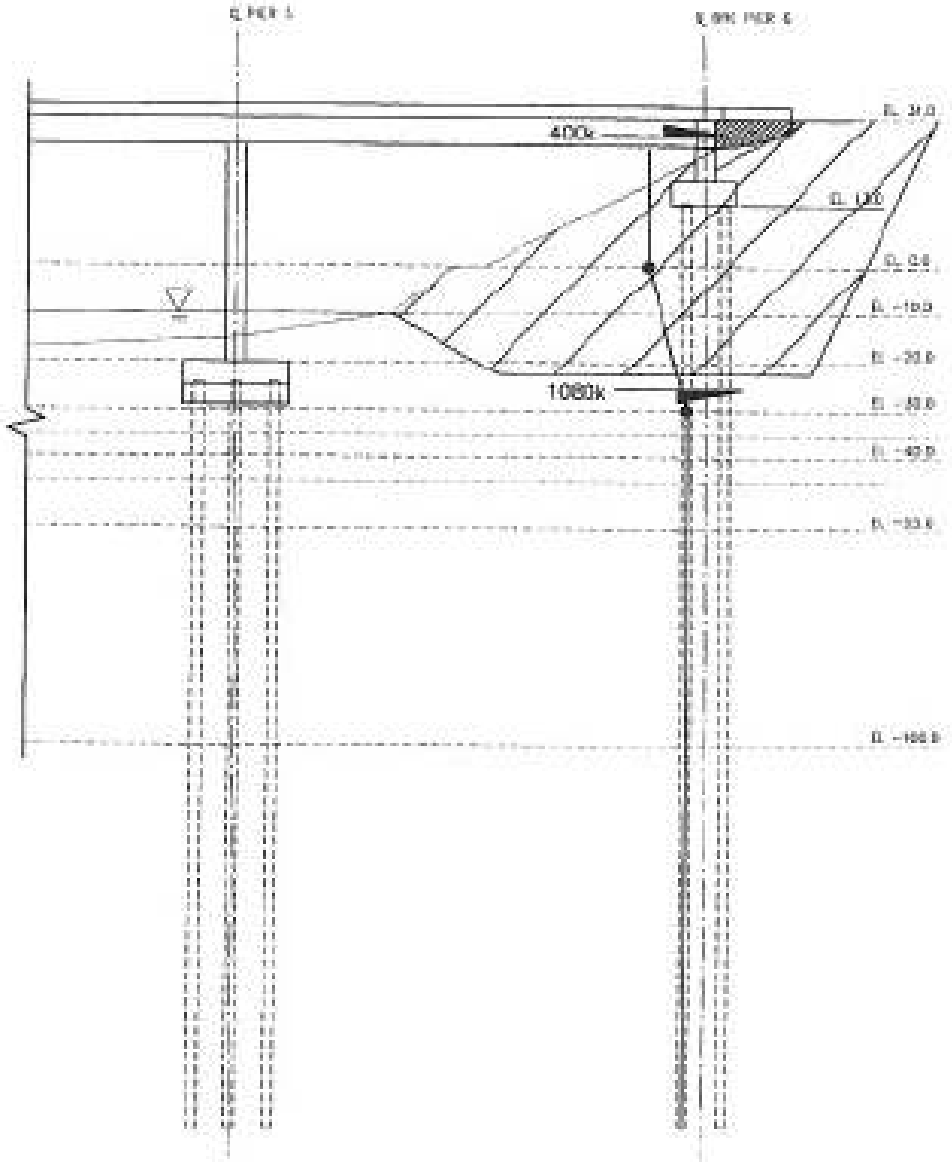

Figure 7-32: Plastic Hinge Location along the Pile, Washington Bridge, Pier 6

The following (Figure 7-33) depicts the location of the maximum bending moments with respect to the liquefiable layers, as assessed by the author. As shown the maximum bending moments occur at depths of 136 inch and 430 inch below the top of the pile, hence the plastic hinge distance is 294 inch (24.5 ft).

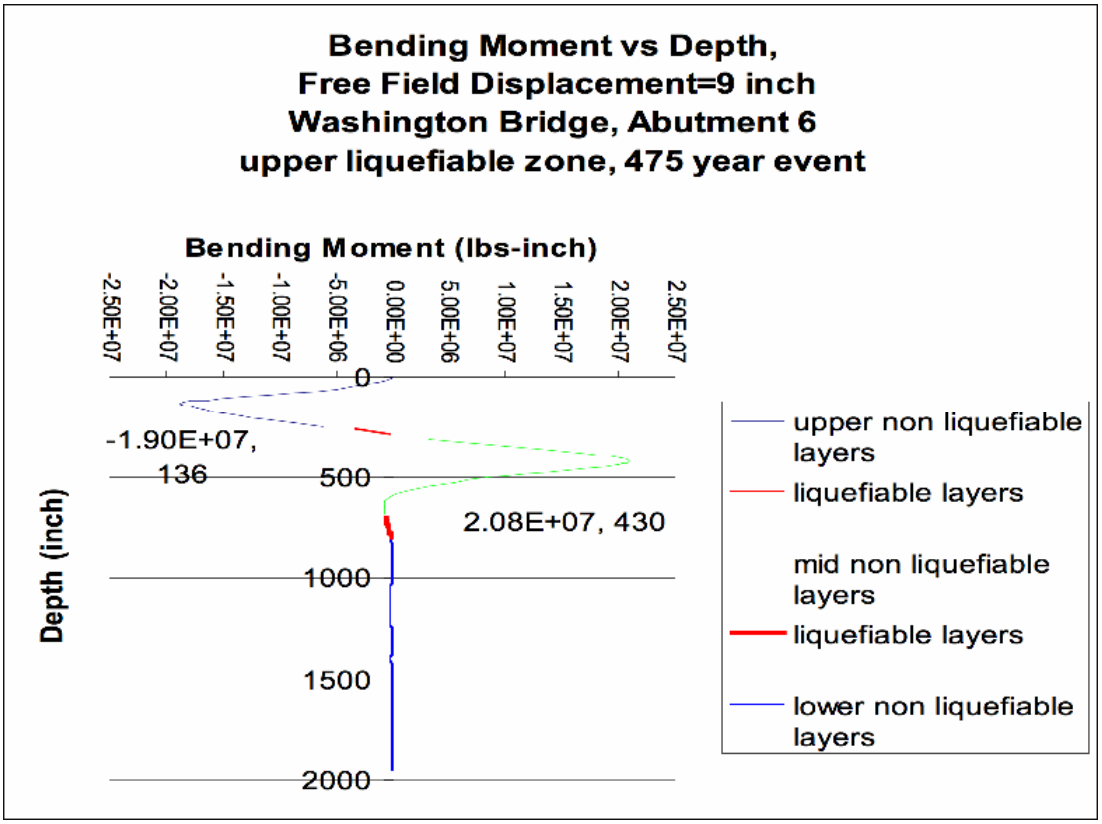

Figure 7-33: Location of the Maximum Bending Moment and Estimated Plastic Hinge Distance for Piles, pier 6, (475 YEAR EVENT) Washington Bridge

7.3.3.10. Summary

The 24 inch pipe pile foundation for pier 6was evaluated under lateral spread loading. The analysis showed that the effect of “pile pinning” in reducing the soil movement due to lateral spread is significant. Reducing the flow movement to a maximum of 9 inch of soil displacement.

Since the pile response is dependent on the relative soil displacement with respect to the pile horizontal movement, the pile pinning effect contributed significantly in reducing the lateral spread loading on the piles. Despite this contribution, the shear force demand due to lateral spread loading exceeded the shear capacity of 91 kips (by an amount of 90 kips) and the bending moment demand exceeded the bending moment capacity of 1360 kip-foot (by an amount of 300 kip-foot).

It is important to note that the author based the evaluation of the shear capacity on the equation as stated in the referenced NCHRP report. Unlike the 30 feet distance evaluated by the NCHRP report, the plastic hinge distance of 24.5 feet was evaluated based on the study performed by the author. (assuming no strain softening in soil above and below liquefaction layer)

In addition, the author evaluated the pinning force due to the piles to be equal to 225 kips for abutment 6 for the upper liquefiable case, which exceeds the value of 91 kips evaluated by the NCHRP report. No attempt in considering the free field soil

movement and the impact of the pile pinning on this movement and thus the pile pinning force was made in the NCHRP report.

For pier 5, a comparative study is needed, however this study can not be done in the fashion above since it is not clear how much of pinning effect can only be contributed to pier 5, in case of the lower liquefiable layers, as discussed before in this report.

7.3.4. Washington Bridge (2,475 Year Event)

The following is a critical review of the lateral spread loading on the existing foundation for the Washington bridge. An independent analysis is performed for the 2,475 year event on evaluating the amount of loading caused by lateral spread/flow on pile foundation for pier 6 and pier 5 of the Washington Bridge. The result of this analysis is then compared with the analysis performed and documented in the subject report (NCHRP, 2002). The pinning effect of piles and the pile response forming plastic hinges are re-evaluated and a comparative study with the result in the subject report is performed.

7.3.4.1. Seismicity

Peak Ground Acceleration (PGA) of 0.42g were used for the 2,475 year event with the mean earthquake magnitude of 6.5

7.3.4.2. Liquefaction and Lateral Spread @ Abutment 6 and Pier 5

At abutment 6, the underlying soil is subject to liquefaction from elevation –10 to –20 (upper liquefiable layer) and –45 to –55 (lower liquefiable layer). The sloping ground underlain by liquefiable soil layers at Abutment 6, may cause lateral spreading of the embankment during the design earthquake.

At pier 5, the underlying soil is subject to liquefaction from elevation –45 to –55 (lower liquefiable layer). Pier 5 is subject to lateral spreading during the design earthquake.

7.3.4.3. Embankment Stability

The slope stability performed for the embankment for abutment 6 and pier 5, reveals that the slope is not stable during the design earthquake. The design shear strength parameters used in the slope stability were based on the data made available to the author by the NCHRP report. For liquefiable layers, the value of shear strength was based on the latter report and was evaluated to be 300 psf.

The stability of the slope embankment during the design earthquake event where pier 6 and pier 5 are located, was analyzed, using XTSABL5 software program. The failure surface was designated as a block failure, with the base of the failure block passing through the upper liquefiable layer, at elevation –10 through –20. A separate

analysis was performed , where the lower liquefiable layer, at elevation -45 through –55 was designated as the layer where the base of the block failure passes through.

The slope stability calculation for the embankment for Abutment 6 led to factors of safety (FOS) of 0.631, 0.712 and 0.692 for static condition corresponding to the wedge failure through the upper liquefiable layer, through the lower liquefiable layer and deep liquefaction respectively, considering post liquefaction case. The FOS is less than 1.0 which leads to a flow condition.

7.3.4.4. Yield Acceleration & Newmark Analysis

Normally the anticipated slope displacement due to the design earthquake is evaluated using the Newmark Method. However, this is difficult when flow failures such as the failure described above occur. The Newmark Chart can not be used to compute displacements for flow conditions.

7.3.4.5. Lateral Demand/Capacity of the Pile Foundation

The lateral demand on the pile foundation was evaluated using the LPILE4M software program (ENSOFT, version 4).

For both the upper liquefiable layer and the lower liquefiable layer, the strength of the liquefiable soil was increased incrementally (Table 7-13) and the corresponding yield acceleration and the slope displacement during the design earthquake was

evaluated. The displacement of the embankment during the earthquake was calculated using the Martin and Qiu and WES graphs. Result show that the flow condition would cease to exist once the strength of the liquefiable soil is increased incrementally to a value of 700 psf. for the upper liquefiable soil layer.

7.3.4.6. Expected Displacement of the Embankment Considering Pile Pinning Effect

When the embankment soil is moving against the piles at pier 6 and pier 5 (lower liquefiable zone) and against the piles at pier 6 (upper liquefiable zone), under the design seismic event, the piles will resist the movement of the soil by producing shearing forces. These forces would provide some form of resistance against lateral spreading.

A two-front approach is used to assess the lateral spread loading on the piles and is as follows:

7.3.4.7. Upper Liquefiable Layer

In this case, only pier 6 is subject to lateral spread loading.Various soil movements were prescribed to the embankment to determine the pile shear forces found due to these prescribed soil movements. The software program LPILE4M was used to prescribe various soil movements and to evaluate the corresponding shear forces for the pier 6 piles, due to these soil movements. Shear forces are found for soil

movements of 0.5 through a maximum of 40 inches (Table 7-14 and curve designated as LPILE4M in Figures 7-34 and 7-35)

Evaluate the pile pinning effect that is the resistance to the soil movement and can be considered as the added shear strength of the soil. The initial shear strength of the liquefiable soil for upper and lower liquefiable layers is 300 psf. An increase of 296 psf in shear strength along the failure surface which was estimated to be 105 ft and 129 ft for upper and lower liquefiable layers respectively (slope stability analysis) and the spacing of 8 ft for the pipe piles, would be equal to 91 kips of pile shear force. A Newmark analysis using the value of 596 psf (the initial value being 300 psf and the increase of 296 psf would make the new shear strength to be 596 psf) would result in a Yield acceleration of 0.0 and a displacement of 100inches. Various Yield accelerations are found for various additional shear strength, resulting in various displacements. (Curve designated as Newmark curve in Figures 7-34 and 7-35)

Where the two curves converge, is the value for the actual displacement of the embankment soil due to lateral spread and the corresponding shear force that is the pinning effect of the pipe pile for pier 6.

The pinning force of the pile was evaluated based on the intersection of the curves corresponding to the LPILE4M shear values and the Newmark analysis (Table 7-13. The graphs for these curves are shown in Figures 7-34 and 7-35.

The convergence of two curves are required when we are evaluating the pinning force of the piles and their contribution to the reduction to the soil displacement. The pinning force was evaluated to be 300kips corresponding to soil displacement of 13 inch, using Newmark graph. The pinning force was evaluated to be 260 kips corresponding to soil displacement of 11 inch using Martin and Qiu data.

Newmark Analysis (upper liquefiable layer)

Initial Cohesion[1] (psf)	Increase in Cohesion (psf)	Cohesion[2] (psf)	Length of Failure Surface (ft)	Pile Spacing (ft)	Width of Footing (ft)	# of Piles	Abutment Force (kips)	Shear Force[3] (kips)	Yield acceleration	Max. Acceleration	Ay/Amax	Displacement (in)[4]	Displacement (in)[5]
300	296	596	105	8	48	12	400	91	0	0.42	0.00	very large	very large
300	400	700	105	8	48	12	400	135	0.025	0.42	0.06	very large	62
300	500	800	105	8	48	12	400	177	0.055	0.42	0.13	60	30
300	600	900	105	8	48	12	400	219	0.078	0.42	0.19	30	17
300	700	1000	105	8	48	12	400	261	0.103	0.42	0.25	20	10
300	800	1100	105	8	48	12	400	303	0.124	0.42	0.30	12	6
300	900	1200	105	8	48	12	400	345	0.142	0.42	0.34	10	4
300	1000	1300	105	8	48	12	400	387	0.160	0.42	0.38	7	3
300	1100	1400	105	8	48	12	400	429	0.178	0.42	0.42	5	2
300	1200	1500	105	8	48	12	400	471	0.194	0.42	0.46	4	1.5

1: Initial cohesion corresponds to the shear strength of liquefiable soil, where the failure surface is located
2: Cohesion corresponds to the shear strength of the liquefiable soil after the increase in cohesion is introduced. It is used for the embankment stability and Newmark analysis
3: Shear Force = (Increase In Cohesion x Length of Failure Surface x Pile Spacing) minus the abutment force
4: Displacement based on the Newmark, 1977
5: Displacement based on Martin and Qiu (1994)

Table 7-13: Newmark Analysis Results For Washington Bridge, (2,475 YEAR EVENT) Pier 6

LPILE4M (Upper Liquefiable layer)						
PILE TYPE[1]	PILE DIAMETER (in)	PILE LENGTH (ft)	MOMENT OF INERTIA (in^4)	MODULUS OF ELASTICITY (psi)	SOIL DISPLACEMENT[2] (in)	PILE SHEAR[3] (Kips)
PIPE PILE (FILLED WITH CONCRETE)	24	163	23197	3,830,000	0.5	20.5
PIPE PILE (FILLED WITH CONCRETE)	24	163	23197	3,830,000	1	33.2
PIPE PILE (FILLED WITH CONCRETE)	24	163	23197	3,830,000	2	55.2
PIPE PILE (FILLED WITH CONCRETE)	24	163	23197	3,830,000	3	75.6
PIPE PILE (FILLED WITH CONCRETE)	24	163	23197	3,830,000	4	95.2
PIPE PILE (FILLED WITH CONCRETE)	24	163	23197	3,830,000	5	116.6
PIPE PILE (FILLED WITH CONCRETE)	24	163	23197	3,830,000	6	141.9
PIPE PILE (FILLED WITH CONCRETE)	24	163	23197	3,830,000	7	165.8
PIPE PILE (FILLED WITH CONCRETE)	24	163	23197	3,830,000	8	189.7
PIPE PILE (FILLED WITH CONCRETE)	24	163	23197	3,830,000	9	212.8
PIPE PILE (FILLED WITH CONCRETE)	24	163	23197	3,830,000	10	232.6
PIPE PILE (FILLED WITH CONCRETE)	24	163	23197	3,830,000	11	252.2
PIPE PILE (FILLED WITH CONCRETE)	24	163	23197	3,830,000	12	272.7
PIPE PILE (FILLED WITH CONCRETE)	24	163	23197	3,830,000	13	293.2
PIPE PILE (FILLED WITH CONCRETE)	24	163	23197	3,830,000	14	313.5
PIPE PILE (FILLED WITH CONCRETE)	24	163	23197	3,830,000	15	332.6
PIPE PILE (FILLED WITH CONCRETE)	24	163	23197	3,830,000	16	351.4
PIPE PILE (FILLED WITH CONCRETE)	24	163	23197	3,830,000	17	370.2
PIPE PILE (FILLED WITH CONCRETE)	24	163	23197	3,830,000	18	387.5
PIPE PILE (FILLED WITH CONCRETE)	24	163	23197	3,830,000	19	404.9
PIPE PILE (FILLED WITH CONCRETE)	24	163	23197	3,830,000	20	422
PIPE PILE (FILLED WITH CONCRETE)	24	163	23197	3,830,000	25	480.7
PIPE PILE (FILLED WITH CONCRETE)	24	163	23197	3,830,000	30	519
PIPE PILE (FILLED WITH CONCRETE)	24	163	23197	3,830,000	35	524.6
PIPE PILE (FILLED WITH CONCRETE)	24	163	23197	3,830,000	40	518.6
1: Pipe pile thickness is 0.5 inch.						
2: Soil displacement prescribed, to represent the lateral spread movement from the ground surface to the bottom of the liquefiable soil layer						
3: Maximum shear force developed by the pile resisting to the prescribed soil movement						

Table 7-14: Pile Shear Force For Washington Bridge, (2,475 YEAR EVENT) Pier 6

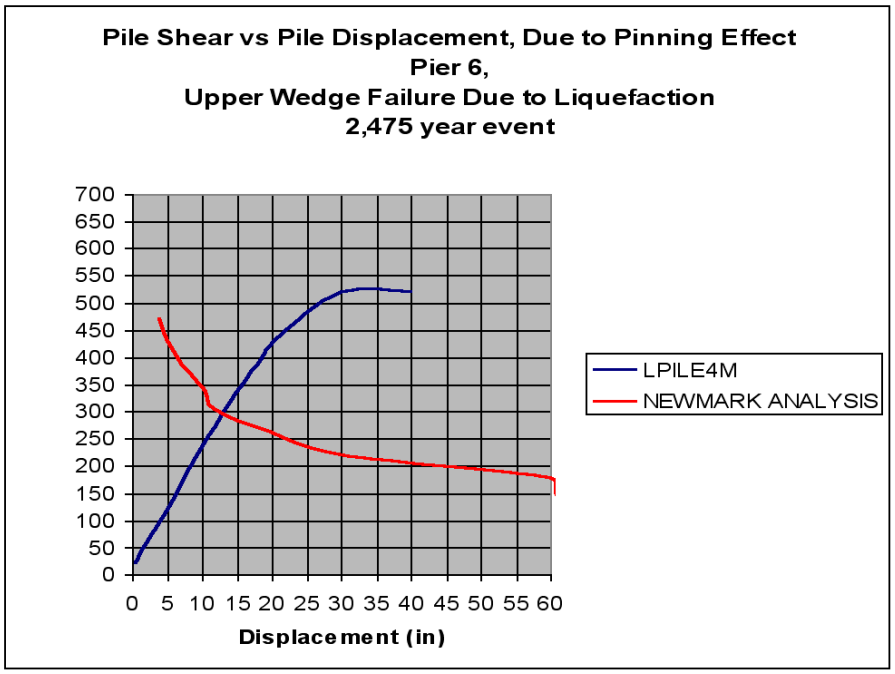

Figure 7-34: Pinning Effect on Piles, Pier 6, (2,475 YEAR EVENT) Washington Bridge

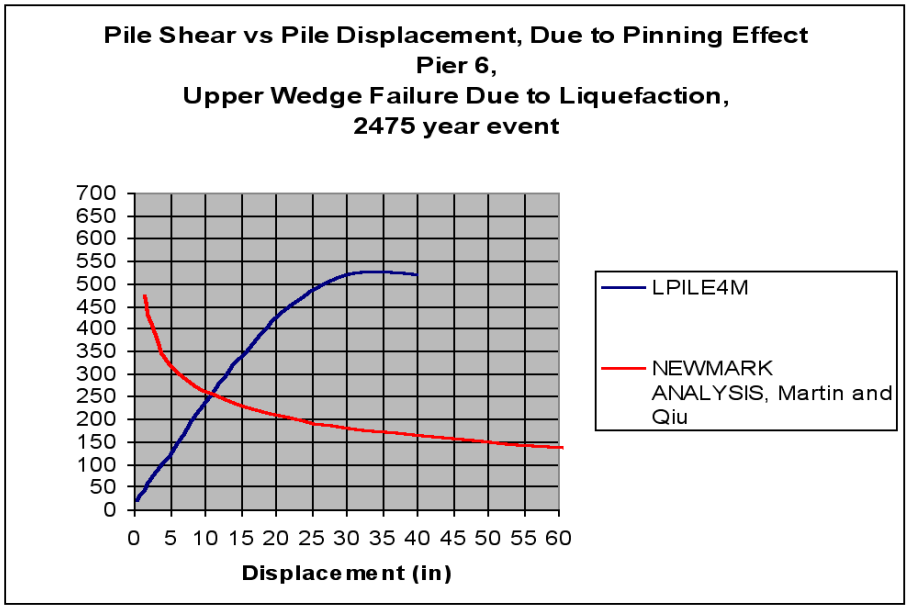

Figure 7-35: Pinning Effect on Piles, Pier 6, (2,475 YEAR EVENT), (Martin and Qiu) Washington Bridge

7.3.4.8. Lower Liquefiable Layer

In this case, both pier 5 and pier 6 piles are subject to lateral spread loading. Same approach was performed, except in this case , the length of failure plane through the lower liquefiable zone was 129 ft, the added resistance due to the columns was included (420 kips). In increase of 545 psf in shear strength along the failure surface would correspond to 91 kips of pile shear force. A Newmark analysis using the value of 845 psf the initial value being 300 psf and the increase of 545 would make the new shear strength to be 845 psf) would result in a yield acceleration of 0.01 and a displacement of 100 inches. Various yield accelerations are found for various additional shear strengths, resulting in various displacements. (Table 7-17)

The pinning force of the pile can not be evaluated using the convergence of the two curves, since the plane of failure passing through then lower liquefiable layer, passes through the pier 6 and pier 5 pile foundations.

Unlike the upper liquefiable layer case, where the plane of failure passes through only the pier 6 pile foundation, in this case the pinning force must also consider the contribution due to the pier 5 pile foundation. In order to evaluate the pinning force due to the pier 6 and pier 5, both curves corresponding to LPILE4M for these piers are converging the Newmark curve. The software program LPILE4M was used to prescribe various soil movements and to evaluate the corresponding shear forces for the piers 5 and pier 6 piles, due to these soil movements. Shear forces are found for

soil movements of 0.5 to a maximum of 40 inches (Tables 7-15 and 7-16) and Curves designated as LPILE4M in figures 7-36 and 7-37.

LPILE4M (Lower Liquefiable layer), PIER 6						
PILE TYPE [1]	PILE DIAMETER (in)	PILE LENGTH (ft)	MOMENT OF INERTIA (in^4)	MODULUS OF ELASTICITY (psi)	SOIL DISPLACEMENT [2] (in)	PILE SHEAR [3] (Kips)
PIPE PILE (FILLED WITH CONCRETE)	24	193	23197	3,830,000	0.5	23.6
PIPE PILE (FILLED WITH CONCRETE)	24	193	23197	3,830,000	1	41.7
PIPE PILE (FILLED WITH CONCRETE)	24	193	23197	3,830,000	2	76
PIPE PILE (FILLED WITH CONCRETE)	24	193	23197	3,830,000	3	109
PIPE PILE (FILLED WITH CONCRETE)	24	193	23197	3,830,000	4	140
PIPE PILE (FILLED WITH CONCRETE)	24	193	23197	3,830,000	5	170
PIPE PILE (FILLED WITH CONCRETE)	24	193	23197	3,830,000	6	200
PIPE PILE (FILLED WITH CONCRETE)	24	193	23197	3,830,000	7	230
PIPE PILE (FILLED WITH CONCRETE)	24	193	23197	3,830,000	8	256
PIPE PILE (FILLED WITH CONCRETE)	24	193	23197	3,830,000	9	278
PIPE PILE (FILLED WITH CONCRETE)	24	193	23197	3,830,000	10	300
PIPE PILE (FILLED WITH CONCRETE)	24	193	23197	3,830,000	11	321
PIPE PILE (FILLED WITH CONCRETE)	24	193	23197	3,830,000	12	340
PIPE PILE (FILLED WITH CONCRETE)	24	193	23197	3,830,000	13	357
PIPE PILE (FILLED WITH CONCRETE)	24	193	23197	3,830,000	14	373
PIPE PILE (FILLED WITH CONCRETE)	24	193	23197	3,830,000	15	388
PIPE PILE (FILLED WITH CONCRETE)	24	193	23197	3,830,000	16	403
PIPE PILE (FILLED WITH CONCRETE)	24	193	23197	3,830,000	17	417
PIPE PILE (FILLED WITH CONCRETE)	24	193	23197	3,830,000	18	431
PIPE PILE (FILLED WITH CONCRETE)	24	193	23197	3,830,000	19	443
PIPE PILE (FILLED WITH CONCRETE)	24	193	23197	3,830,000	20	455
PIPE PILE (FILLED WITH CONCRETE)	24	193	23197	3,830,000	25	506
PIPE PILE (FILLED WITH CONCRETE)	24	193	23197	3,830,000	30	550
PIPE PILE (FILLED WITH CONCRETE)	24	193	23197	3,830,000	35	587
PIPE PILE (FILLED WITH CONCRETE)	24	193	23197	3,830,000	40	622
1: Pipe pile thickness is 0.5 inch.						
2: Soil displacement prescribed, to represent the lateral spread movement from the ground surface to the bottom of the liquefiable soil layer.						
3: Maximum shear force developed by the pile resisting to the prescribed soil movement						

Table 7-15: Pile Shear Force, Pier 5, (2,475 YEAR EVENT) Washington Bridge

LPILE4M (Lower Liquefiable layer), PIER 6						
PILE TYPE[1]	PILE DIAMETER (in)	PILE LENGTH (ft)	MOMENT OF INERTIA (in^4)	MODULUS OF ELASTICITY (psi)	SOIL DISPLACEMENT [2] (in)	PILE SHEAR [3] (Kips)
PIPE PILE (FILLED WITH CONCRETE)	24	193	23197	3,830,000	0.5	23.6
PIPE PILE (FILLED WITH CONCRETE)	24	193	23197	3,830,000	1	41.7
PIPE PILE (FILLED WITH CONCRETE)	24	193	23197	3,830,000	2	76
PIPE PILE (FILLED WITH CONCRETE)	24	193	23197	3,830,000	3	109
PIPE PILE (FILLED WITH CONCRETE)	24	193	23197	3,830,000	4	140
PIPE PILE (FILLED WITH CONCRETE)	24	193	23197	3,830,000	5	170
PIPE PILE (FILLED WITH CONCRETE)	24	193	23197	3,830,000	6	200
PIPE PILE (FILLED WITH CONCRETE)	24	193	23197	3,830,000	7	230
PIPE PILE (FILLED WITH CONCRETE)	24	193	23197	3,830,000	8	256
PIPE PILE (FILLED WITH CONCRETE)	24	193	23197	3,830,000	9	278
PIPE PILE (FILLED WITH CONCRETE)	24	193	23197	3,830,000	10	300
PIPE PILE (FILLED WITH CONCRETE)	24	193	23197	3,830,000	11	321
PIPE PILE (FILLED WITH CONCRETE)	24	193	23197	3,830,000	12	340
PIPE PILE (FILLED WITH CONCRETE)	24	193	23197	3,830,000	13	357
PIPE PILE (FILLED WITH CONCRETE)	24	193	23197	3,830,000	14	373
PIPE PILE (FILLED WITH CONCRETE)	24	193	23197	3,830,000	15	388
PIPE PILE (FILLED WITH CONCRETE)	24	193	23197	3,830,000	16	403
PIPE PILE (FILLED WITH CONCRETE)	24	193	23197	3,830,000	17	417
PIPE PILE (FILLED WITH CONCRETE)	24	193	23197	3,830,000	18	431
PIPE PILE (FILLED WITH CONCRETE)	24	193	23197	3,830,000	19	443
PIPE PILE (FILLED WITH CONCRETE)	24	193	23197	3,830,000	20	455
PIPE PILE (FILLED WITH CONCRETE)	24	193	23197	3,830,000	25	506
PIPE PILE (FILLED WITH CONCRETE)	24	193	23197	3,830,000	30	550
PIPE PILE (FILLED WITH CONCRETE)	24	193	23197	3,830,000	35	587
PIPE PILE (FILLED WITH CONCRETE)	24	193	23197	3,830,000	40	622
1: Pipe pile thickness is 0.5 inch.						
2: Soil displacement prescribed, to represent the lateral spread movement from the ground surface to the bottom of the liquefiable soil layer.						
3: Maximum shear force developed by the pile resisting to the prescribed soil movement						

Table 7-16: Pile Shear Force, Pier 6, (2,475 YEAR EVENT) Washington Bridge

Newmark Analysis (lower liquefiable layer)

Initial Cohesion [1] (psf)	Increase in Cohesion (psf)	Cohesion [2] (psf)	Length of Failure Surface (ft)	Pile Spacing (ft)	Width of Footing (ft)	# of Piles	Abutment Force (kips)	Column Force (kips)	Shear Force [3] (kips)	Yield acceleration	Max. Acceleration	Ay/Amax	Displacement (in) [4]
300	545	845	129	8	48	28	400	420	91	0.01	0.42	0.02	very large
300	600	900	129	8	48	28	400	420	103	0.015	0.42	0.04	very large
300	700	1000	129	8	48	28	400	420	126	0.032	0.42	0.08	110
300	800	1100	129	8	48	28	400	420	148	0.047	0.42	0.11	70
300	900	1200	129	8	48	28	400	420	170	0.062	0.42	0.15	50
300	1000	1300	129	8	48	28	400	420	192	0.077	0.42	0.18	35
300	1100	1400	129	8	48	28	400	420	214	0.090	0.42	0.21	25
300	1200	1500	129	8	48	28	400	420	236	0.105	0.42	0.25	20
300	1300	1600	129	8	48	28	400	420	258	0.120	0.42	0.29	14
300	1400	1700	129	8	48	28	400	420	280	0.135	0.42	0.32	11
300	1500	1800	129	8	48	28	400	420	302	0.148	0.42	0.35	9
300	1700	2000	129	8	48	28	400	420	347	0.178	0.42	0.42	48
300	2000	2300	129	8	48	28	400	420	413	0.223	0.42	0.53	17

1: Initial cohesion corresponds to the shear strength of liquefiable soil, where the failure surface is located

2: Cohesion corresponds to the shear strength of the liquefiable soil after the increase in cohesion is introduced.
It is used for the embankment stability and Newmark analysis

3: Shear Force = [(Increase In Cohesion x Length of Failure Surface x Width of Footing)/ (Pile Spacing)] minus the abutment force-minus the column force

4: Displacement based on the Newmark, 1977

5: Displacement based on Martin and Qiu (1994)

Table 7-17: Newmark Analysis Results For Washington Bridge, (2,475 YEAR EVENT) Piers 5 and 6

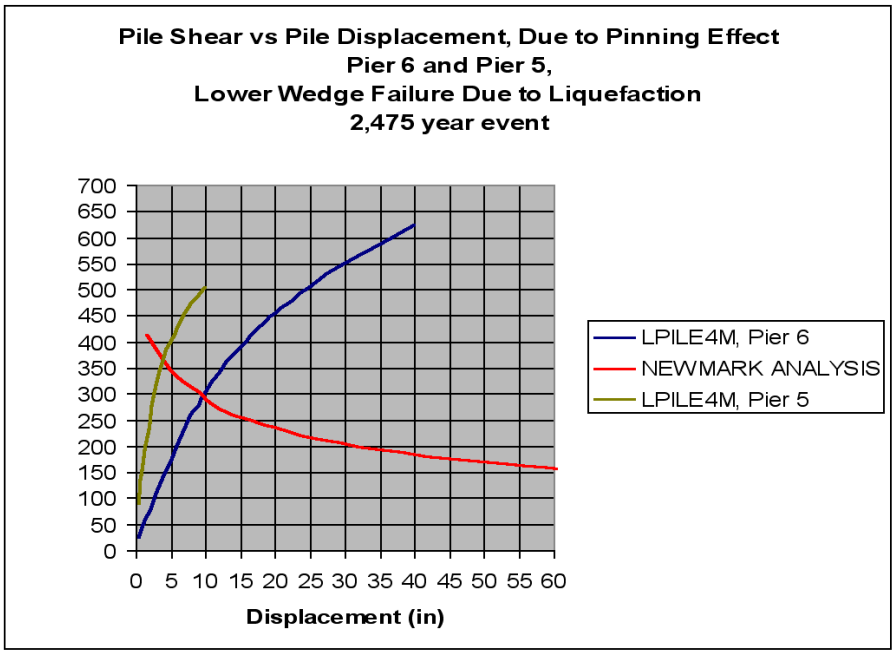

Figure 7-36: Pinning Effect on Piles, Piers 5 and 6, (2,475 YEAR EVENT) Washington Bridge

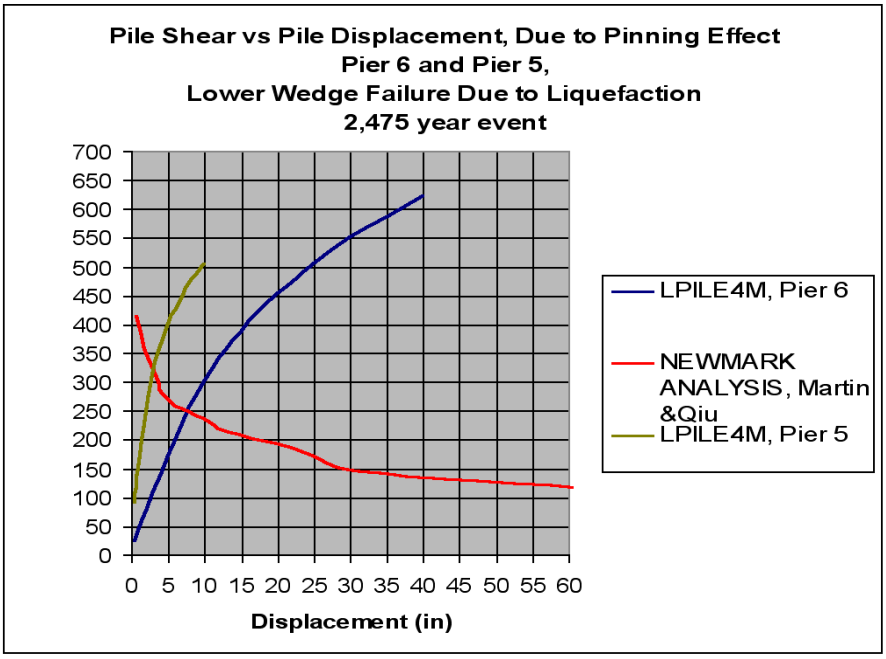

Figure 7-37: Pinning Effect on Piles, Piers 5 and 6, (2,475 YEAR EVENT), (Martin and Qiu) Washington Bridge

7.3.4.9. Lateral Demand for the Pile Foundation (pier 6 only)

The lateral demand (Figures 7-38 and 7-39) using 13 inch of displacement (The actual displacement found from step 3 described above, is used as the free field soil movement to assess the lateral demand on the pile foundation at pier 6.

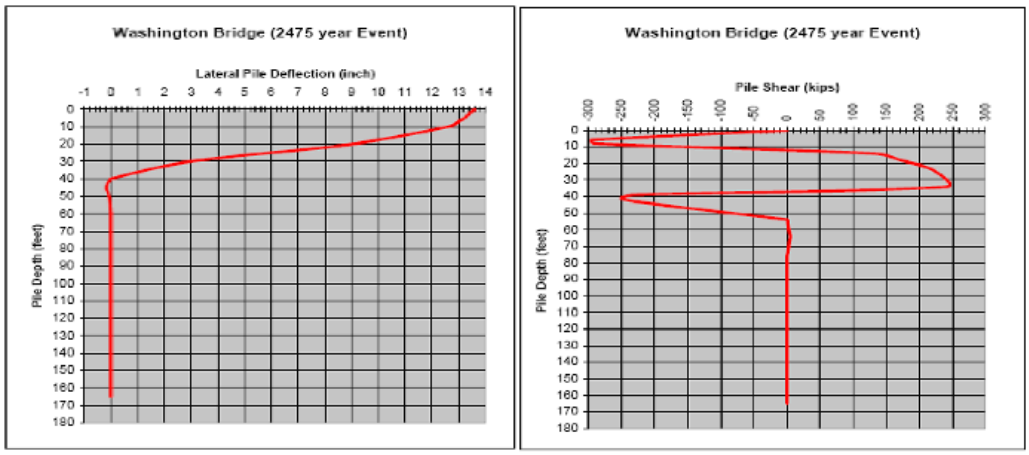

Figure 7-38: Lateral Pile Response, Washington Bridge, (2,475 YEAR EVENT) Pier 6

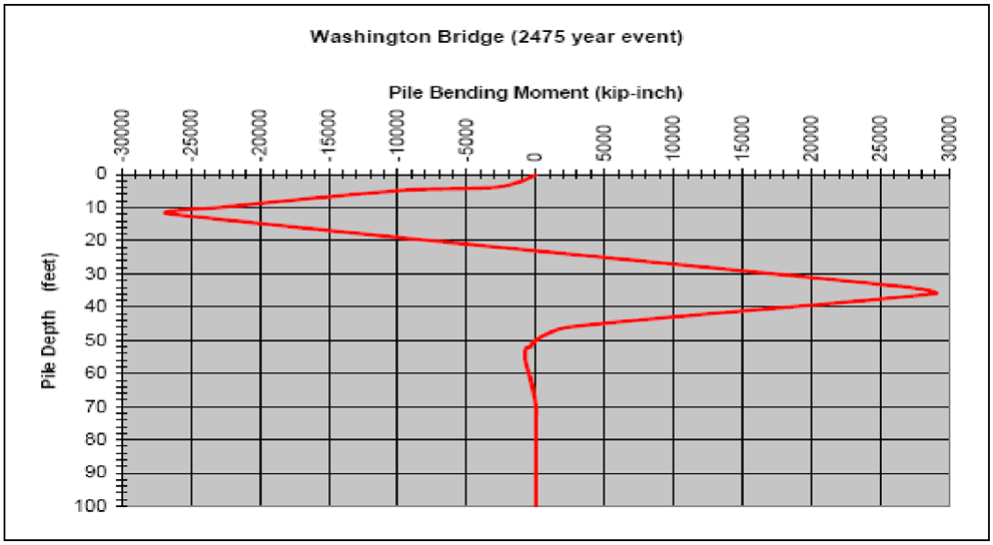

Figure 7-39: Lateral Pile Response, Washington Bridge, (2,475 YEAR EVENT) Pier 6

7.3.4.10. Lateral Capacity for the Pile Foundation

The moment capacity for the pile foundation for abutment 6 is based on the value stated in the NCHRP report and is computed to be 1360 kip-foot. The shear capacity for the pile is calculated to be 91 kips and was based on the assumption that the plastic hinges develop on piles supporting abutment 6, at elevations 0 and –30 and using the following equation:

pile shear capacity = (2 x Plastic moment capacity of pile) / (distance between plastic hinges)

$\Rightarrow$ Pile shear capacity = (2 x 1360 kip-foot) / 30 = 91 kips

7.3.4.11. Plastic Hinge Location

The following (Figure 7-40) depicts the location of the plastic hinges as shown in the referenced NCHRP report for the upper liquefiable layer case corresponding to pier 6, due to lateral spreading.

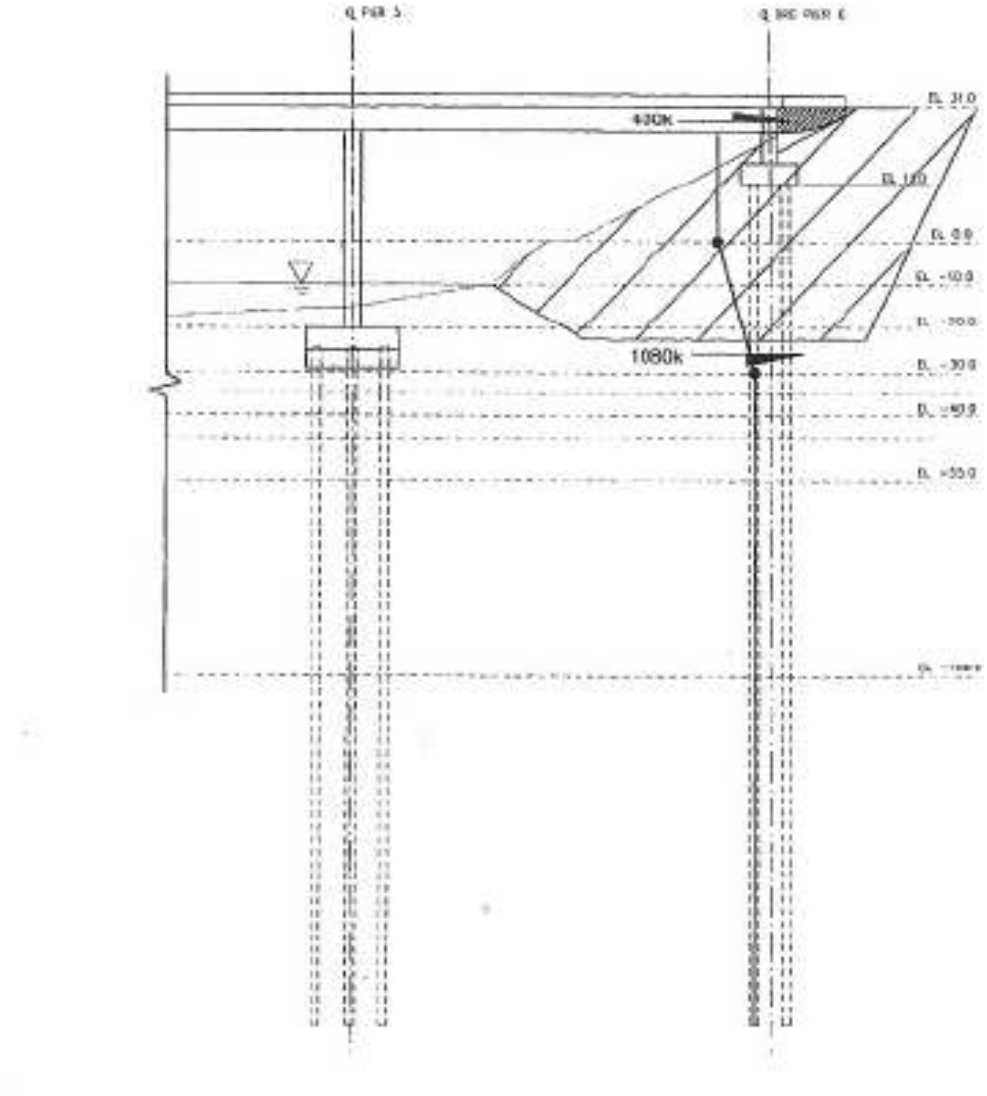

Figure 7-40: Plastic Hinge Location Along the Pile, Washington Bridge, Pier 6

The following (Figure 7-41) depicts the location of the maximum bending moments with respect to the liquefiable layers, as assessed by the author. As shown the maximum bending moments occur at depths of 137 inch and 430 inch below the top of the pile, hence the plastic hinge distance is 293 inch (24.5 ft).

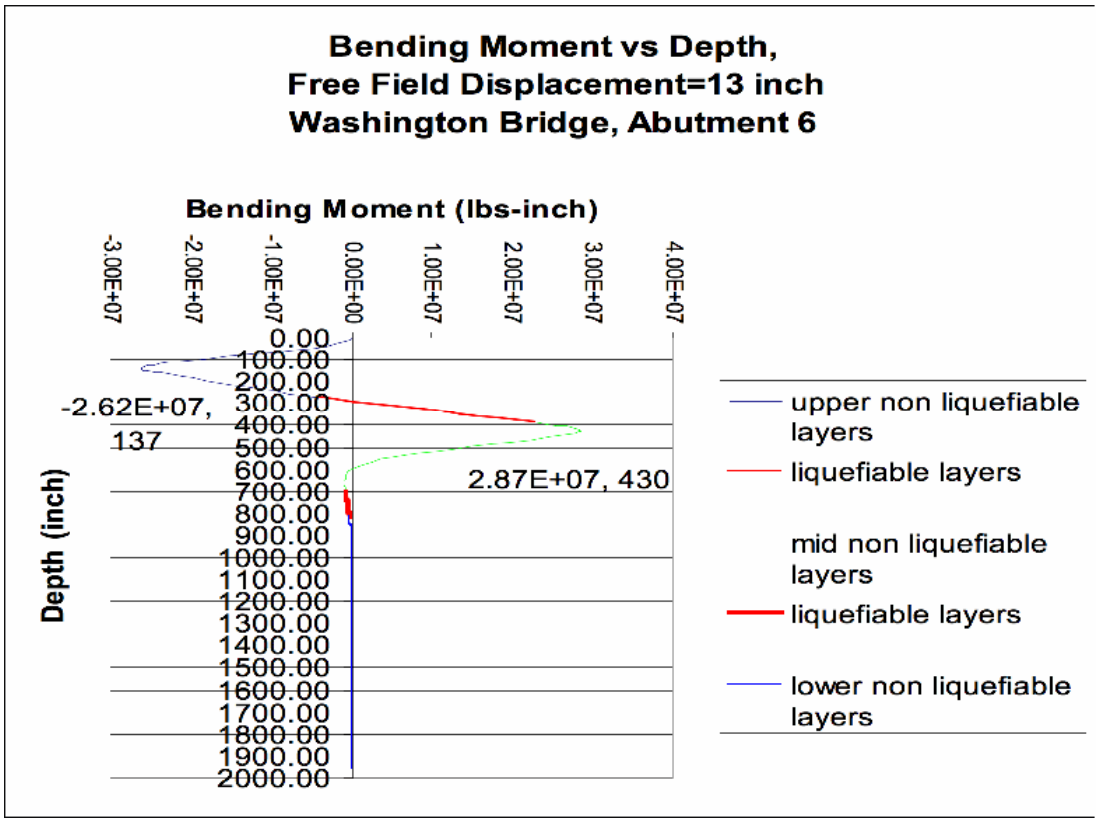

Figure 7-41: Location of the Maximum Bending Moment and Estimated Plastic Hinge Distance For Piles, pier 6, (2,475 YEAR EVENT) Washington Bridge

7.3.4.12. Summary

The 24 inch pipe pile foundation for pier 6was evaluated under lateral spread loading. The analysis showed that the effect of "pile pinning" in reducing the soil movement due to lateral spread is significant. Reducing the flow movement to a maximum of 13 inch of soil displacement for a 2,475 year earthquake event.

Since the pile response is dependent on the relative soil displacement with respect to the pile horizontal movement, the pile pinning effect contributed significantly in

reducing the lateral spread loading on the piles. Despite this contribution, the bending moment demand exceeded the bending moment capacity of 1360 kip-foot (by an amount of 970 kip-foot).

Unlike the 30 feet distance evaluated by the NCHRP report, the plastic hinge distance of 24.5 feet was evaluated based on the study performed by the author.

In addition, the author evaluated the pinning force due to the piles to be equal to 300 kips for abutment 6 for the upper liquefiable case, which exceeds the value of 91 kips evaluated by the NCHRP report. No attempt in considering the free field soil movement and the impact of the pile pinning on this movement and thus the pile pinning force was made in the NCHRP report.

For pier 5, a comparative study is needed, however this study can not be done in this report since it is not clear how much of pinning effect can only be contributed to pier 5, in case of the lower liquefiable layers, as discussed before in this report.

Figure 7-42 shows the tabulated values of the NCHRP and the results drawn from the improved methodology.

Washington Bridge		
NCHRP		
	475 year event	**2475 year event**
	Upper Liquefiable Layer	
Pinning Force (Kips)	90	90
Displacement Demand (no pinning considered) (inch)	flow	flow
Displacement Demand (pinning considered) (inch)	28	42
Plastic Hinge Location (from the top of the pile)	156 in, 516 in	156 in, 516 in
Plastic Hinge Distance (ft)	30	30
	Lower Liquefiable Layer	
Pinning Force (Kips)	90	90
Displacement Demand (no pinning considered) (inch)	flow	flow
Displacement Demand (pinning considered) (inch)	28	42
Plastic Hinge Location (from the top of the pile)	516 in, 936 in	516 in, 936 in
Plastic Hinge Distance (ft)	35	35
Improved Methodology		
	475 year event	**2475 year event**
	Upper Liquefiable Layer	
Pinning Force (Kips)	225.160	260
Displacement Demand (no pinning considered) (inch)	flow	flow
Displacement Demand (pinning considered) (inch)	9[1], 7[2]	13[1], 11[2]
Plastic Hinge Location (from the top of the pile)	136 in, 430 in	136 in, 430 in
Plastic Hinge Distance (ft)	24.5	24.5
	Lower Liquefiable Layer	
Pinning Force (Kips)	xxxx	xxxx
Displacement Demand (no pinning considered) (inch)		
Displacement Demand (pinning considered) (inch)		
Plastic Hinge Location (from the top of the pile)		
Plastic Hinge Distance (ft)		
Missouri Bridge		
NCHRP		
	475 year event	**2475 year event**
Pinning Force (Kips)	11.7	11.7
Displacement Demand (no pinning considered) (inch)	5	32
Displacement Demand (pinning considered) (inch)	< 1	3
Plastic Hinge Location (from the top of the pile)	441 in, 882 in	441 in, 882 in
Plastic Hinge Distance (ft)	40	40
Improved Methodology		
	475 year event	**2475 year event**
Pinning Force (Kips)	10	100.73
Displacement Demand (no pinning considered) (inch)	3[1]	55
Displacement Demand (pinning considered) (inch)	0.3	20[1], 12[2]
Plastic Hinge Location (from the top of the pile)	595 in, 774 in	41 ft, 64 ft
Plastic Hinge Distance (ft)	14.9	23

1. Newmark Chart (WES). 2. Martin and Qui Chart

Figure 7-42: NCHRP and Results from Improved Methodology

7.4. Revisiting Case Histories Using Improved Design Methodology

The following gives the results of the pile response re-evaluation due to lateral spread using improved design methodology, for two important case histories for bridge structures that were subject to lateral spread. The first one is the Landing Road Bridge (Keenan, 1996) damaged during the 1987 Edgecumbe earthquake, New Zealand and the second one is the Uozakihama Bridge (Ishihara, 2003) damaged during the 1995 Kobe earthquake, Japan. The analyses for the pile response due to the free field movement caused by lateral spread are performed using the LPILE program.

7.4.1. Landing Road Bridge Structure

The Landing Road Bridge is located over the Whakatane River west of the town centre. It is the main transport link for Whakatane with State Highway 2 crossing the river. Figure 7-43 shows the bridge taken from the true left bank looking south.

Figure 7-43: Landing Road Bridge, Whakatane, New Zealand (Keenan, 1996)

The north-west abutment and Piers B though F (at the right hand end of the bridge as seen in Figure 7-44, which looks upstream), are situated in relatively young sediments due to the active movement of the river channel towards the east in the last few hundred years.

Figure 7-44: Landing Road Bridge Looking South West (Keenan, 1996)

Bridge construction commenced in 1962 using standard design common through New Zealand. The superstructure is made up of 13 simply supported spans of 18.3 m length carrying a two lane concrete deck and two footpaths. The deck is supported by five post tensioned concrete I beams and diaphragms. At the beam ends the diaphragms are joined by linkage bolts over the piers and they rest on 16 mm rubber

pads. The substructure consists of tapered concrete slab piers connected to a pile cap with 8 precast pretensioned 406 mm square raked piles (raked at 1:6) approximately 10 m long beneath the cap. The piles were driven into the dense sands underlying the layer that liquefied in 1987.the abutments are supported by 5 piles on the river side and 3 on the approach side without any approach slabs. The abutment backwall is tight-packed and bolted to the beam diaphragm. The precast prestressed concrete piles contained 16 seven wire heletically wound prestressing strand with square heletical transverse reinforcement. The average axial load on each of the piles was determined to be 310 kN.

7.4.1.1. Liquefaction/Lateral Spread

The bridge was subject to lateral spreading during the Edgecumbe Earthquake of 1987 and cracks were developed in the ground and sand bowls were observed. See Figure 7-45 below. Preliminary field investigation concluded that the bridge had not been displaced significantly with the laterally spreading ground and had played a restraining role.

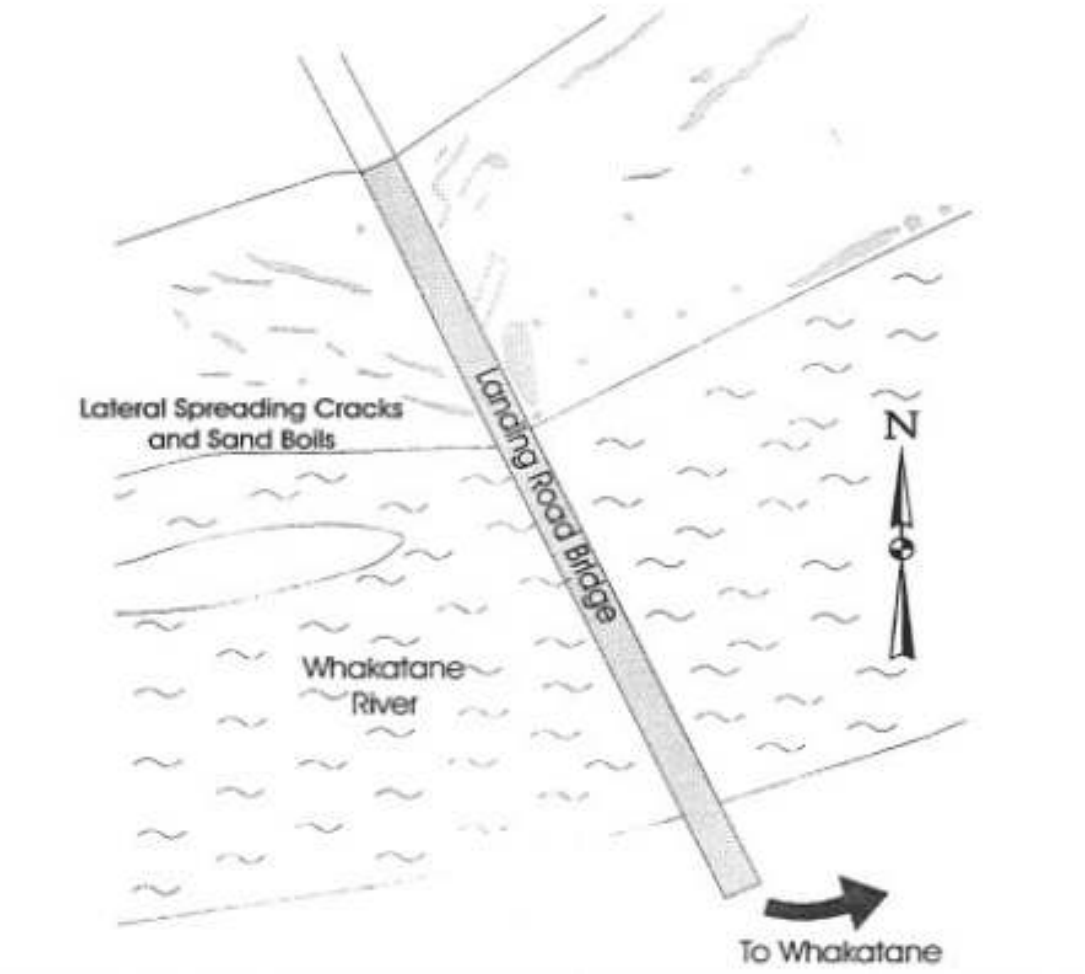

Figure 7-45: Laterally Spreading Cracks and Sand Boils on the True Left Bank (Keenan, 1996)

7.4.1.2. Pile Collapse Mechanism

The potential pile collapse mechanism is shown in Figure 7-46 below:

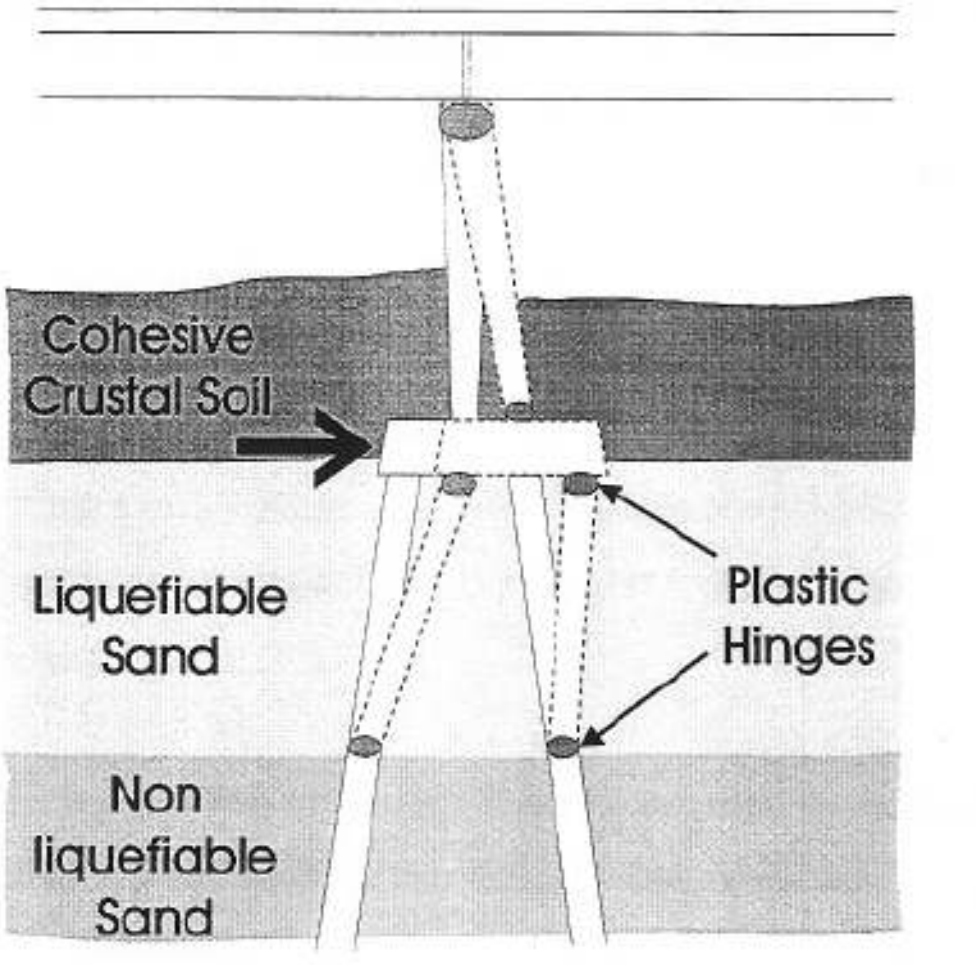

Figure 7-46: Pile Collapse Mechanism, Landing Road Bridge (Keenan, 1996)

7.4.1.3. Subsurface Soil Condition

From the ground surface the crustal cohesive soil is approximately 1.5m deep to the level of the top of the pile cap. Immediately below that there is loose, cohesionless, liquefiable sand approximately 4m thick. At this depth the SPT values increase to values greater than 30 and the sand is unlikely to liquefy.

7.4.1.4. Lateral Demand/Capacity of the Pile Foundation

The lateral demand on the pile foundation due to the free field movement caused by the lateral spread is evaluated using the LPILE software program (ENSOFT, version 5).

7.4.1.5. Lateral Capacity for The CIDH Pile

The moment capacity for the proposed pile foundation is evaluated using XTRACT software program (Imbsen). Figure 7-47 below shows the Pile Moment Curvature Diagram, which indicates the capacity of the pile.

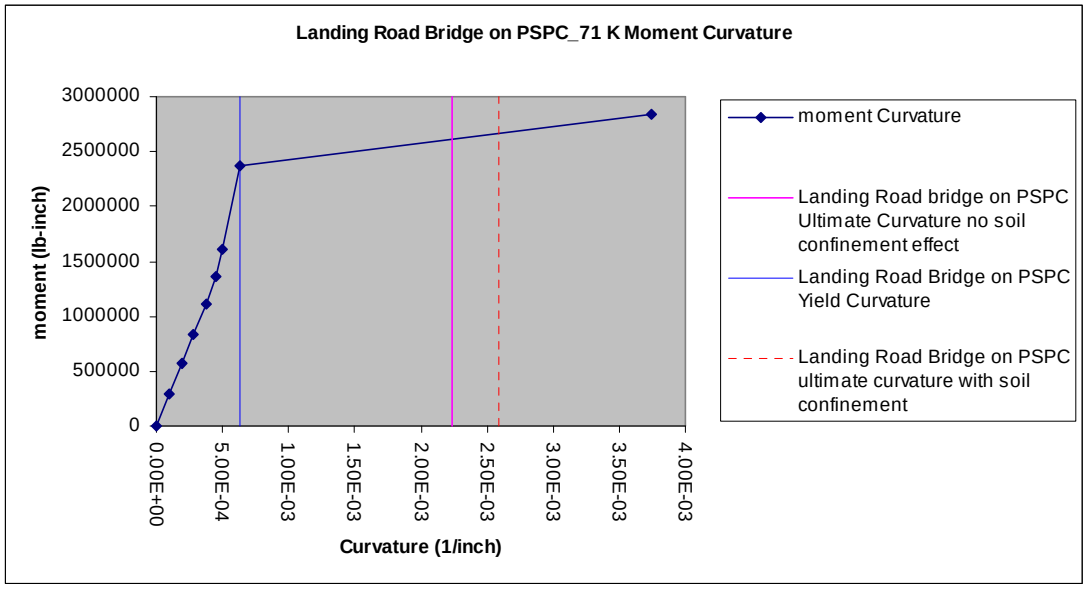

Figure 7-47: Moment Curvature Diagram for Landing Road Bridge Piles

7.4.1.6. Pile Response due to Lateral Demand

The lateral demand using 6 and 12 inch displacements is used as the free field soil movement to assess the pile response for the PSPC pile. LPILE program is used to evaluate the pile curvature demand and the bending moment developed along the PSPC pile (See Figures 7-48, 7-49,7-50 and 7-51). The subsurface soil was modeled as a 3 layer soil consisting of a non-liquefiable cohesive crust, underlying a liquefiable soil followed by a non-liquefiable non cohesive soil.

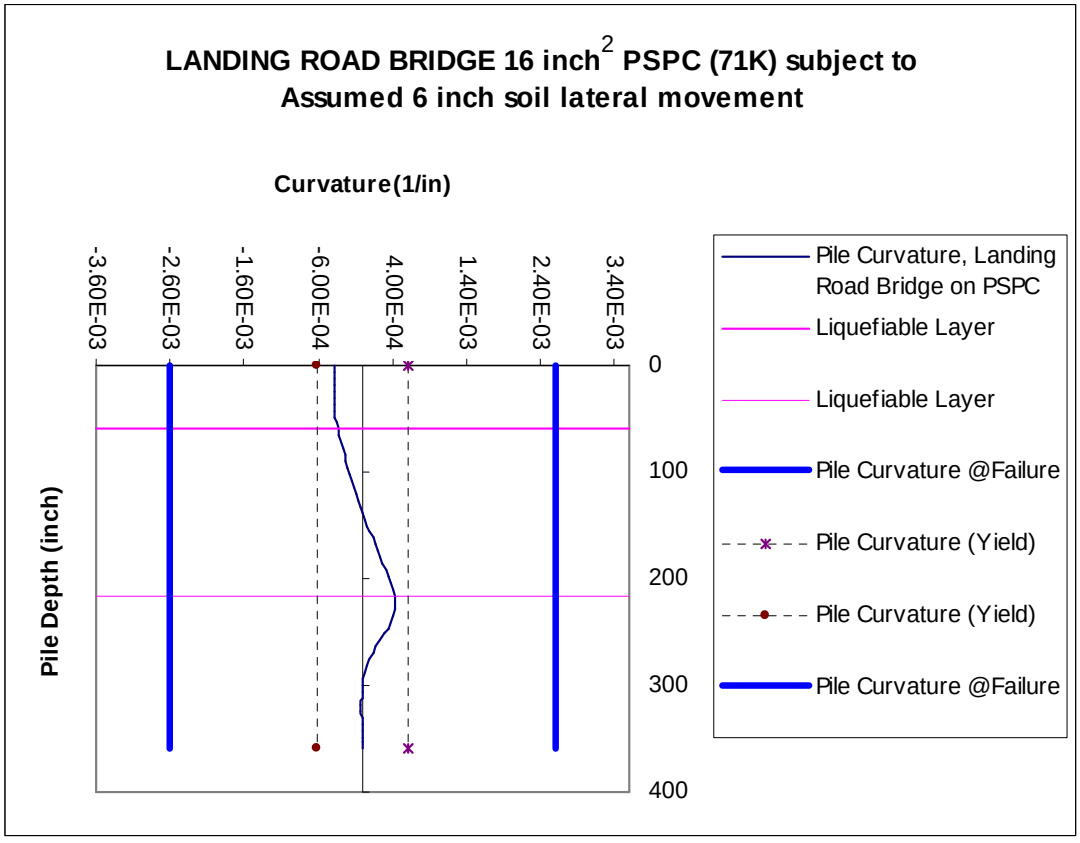

Figure 7-48: Curvature Demand for Landing Road Bridge Piles

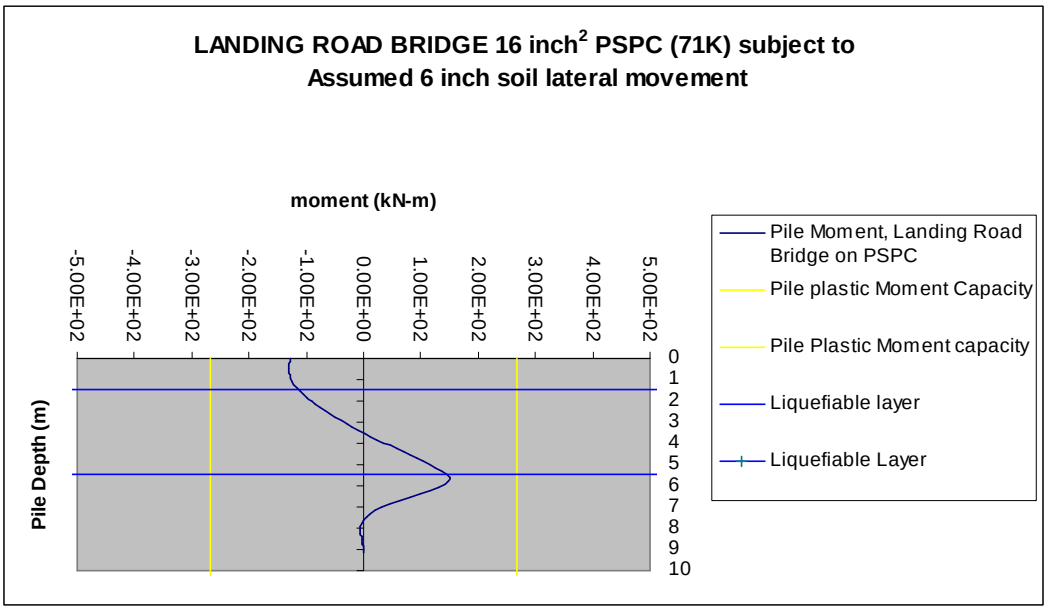

Figure 7-49: Bending Moment along the Piles for Landing Road Bridge

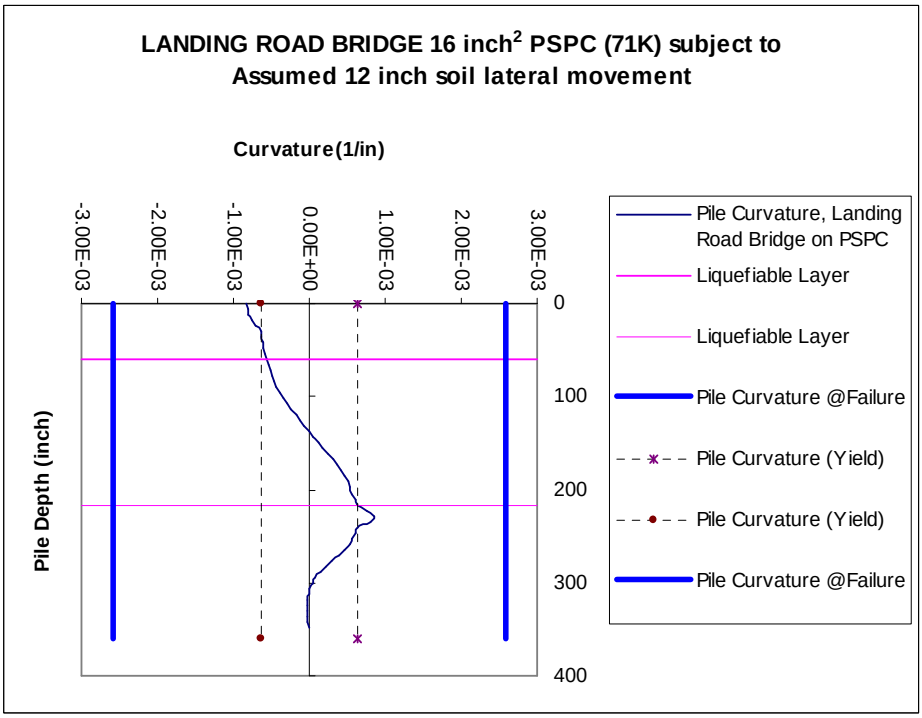

Figure 7-50: Curvature Demand for Landing Road Bridge Piles

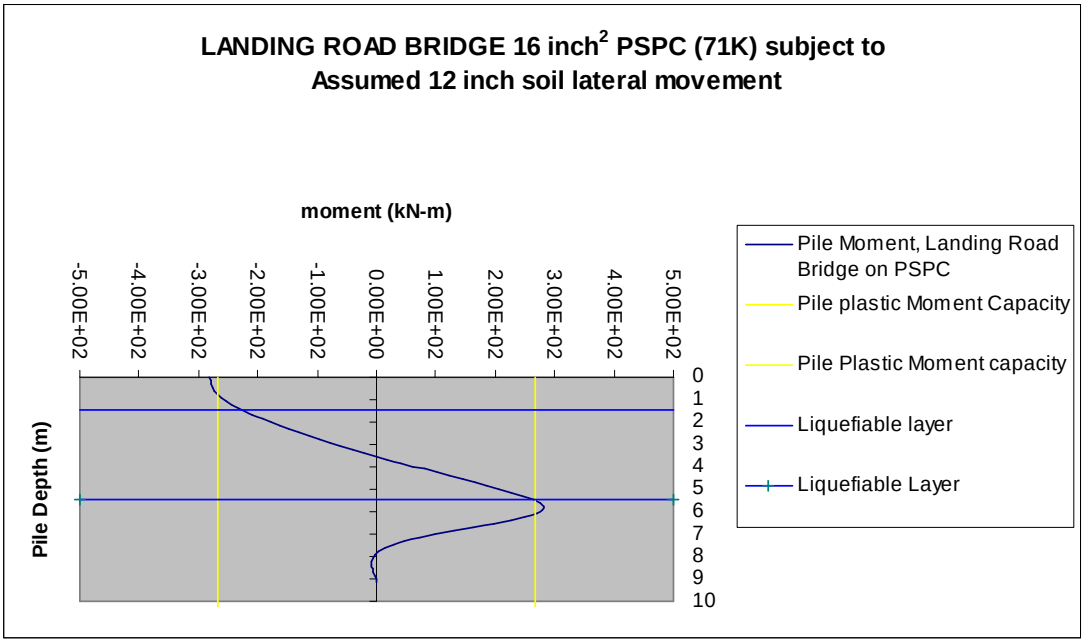

Figure 7-51: Bending Moment along the Piles for Landing Road Bridge

It is noted that the pile would undergo cracking when the net soil movement is about 6 inch and would undergo plastic hinging when the soil net movement is about 12 inch. A comparison of the results of this study with the free field soil movement (not considering the effect of pile pinning) reported in Keenan's work yields good agreement. Keenan reports that the free face free field soil movement is about 0.14m (5.5 inch) at a distance of 90m , which is approximately the distance from the river channel to the landing river Bridge abutment A. 6 inch of net soil movement yields 130 kN-m and 148 kN-m of moments at top and bottom of the pile respectively. The first cracking moment for mid-height of one riverward pile is reported as approximately 150 kN-m by Keenan. This suggests that the piles would undergo near

and/or cracking. The plastic hinges form at top and bottom of the piles at net soil crust movement of about 12 inches.

7.4.1.7. Field Observation

Field observation showed clearly that plastic hinges had not formed in piles 3 and 4 of Pier C (see Figure 7-52). Piles 1 and 2 on the river side had a greater likelihood to undergo cracking, but were not examined due to difficulty and safety issues.

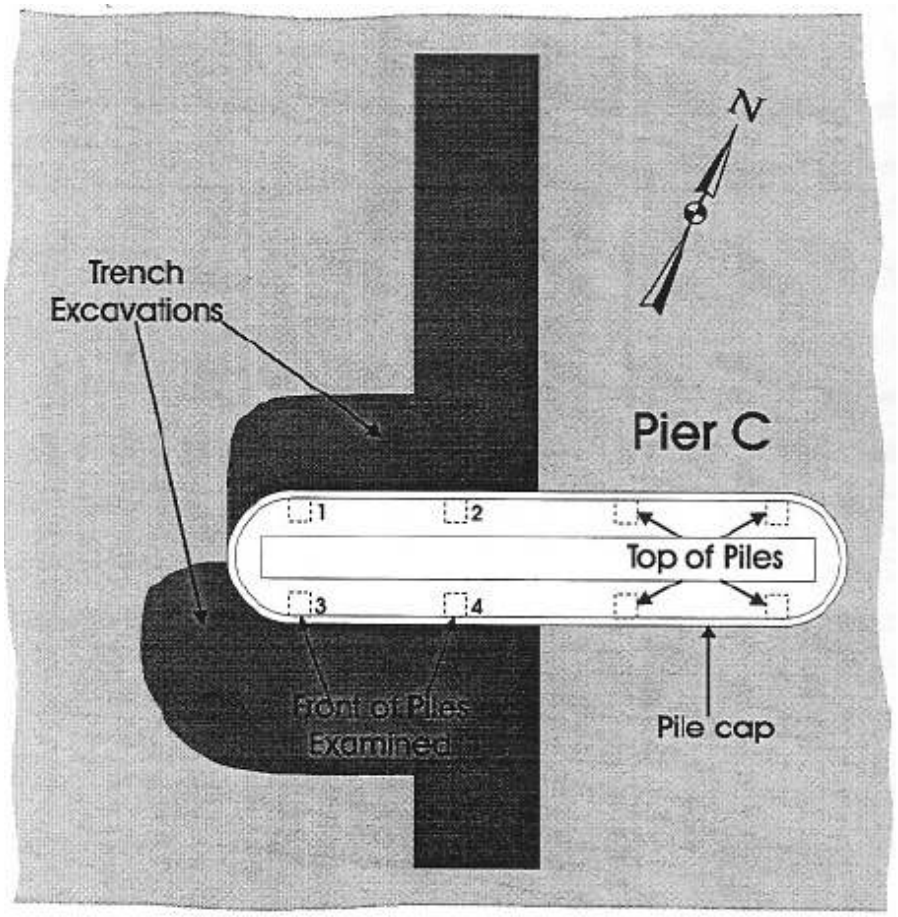

Figure 7-52: Excavation of Pier C (Keenan, 1996)

7.4.1.8. Conclusion

A case study for the lateral spread loading on piles and the earthquake response of these piles due to liquefaction was conducted. The study showed that the piles underwent movements and some cracking due to the soil crust lateral movement and plastic hinges would have potentially formed had the crust movement been slightly higher. However, the collapse of the substructure at Pier C (i.e. pile group) would have been unlikely even if the soil crust movement would have been higher resulting in forming plastic hinges, due to two important factors: 1) pile ductility and 2) the unlikelihood of the pile group undergoing plastic hinges.

7.4.2. Uozakihama Bridge Structure

Pier 211 of the elevated Hanshin Expressway No.5 Bay Route is located in the southernmost part of the Uozakihama Island. (Figure 7-53)

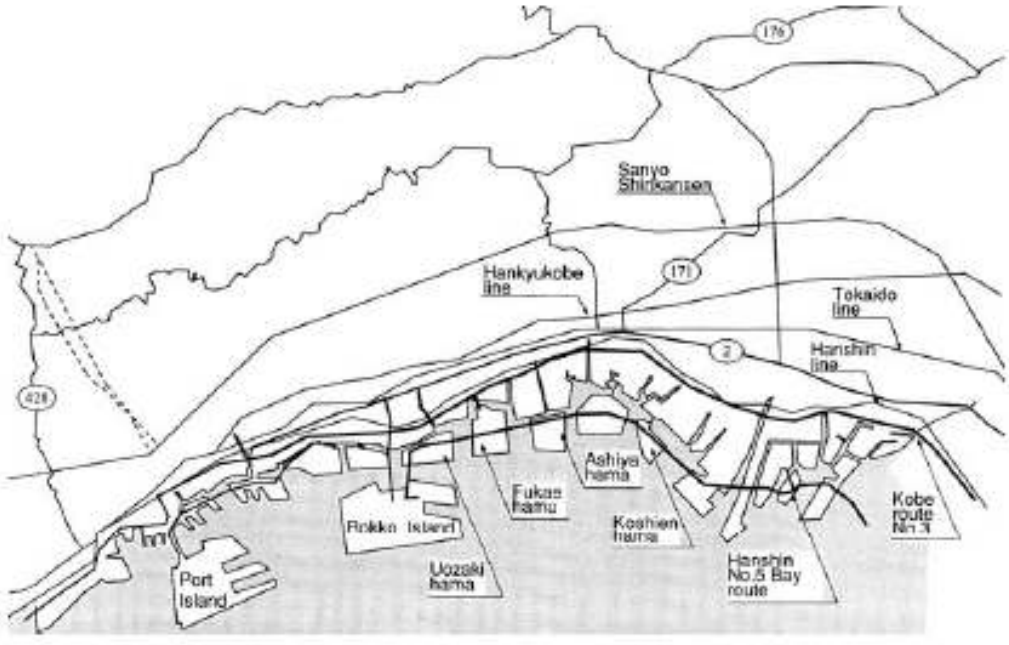

Figure 7-53: Area Map of the Uozakihama Island (Ishihara, 2003)

The structure (figure 7-54) is a steel box girder with concrete monolithic two-column bents supported that sits on a 22.5 m long and 14.5 m wide footing which is supported by 22 piles 1.5m in diameter. The piles were constructed of cast-in-place reinforced concrete.

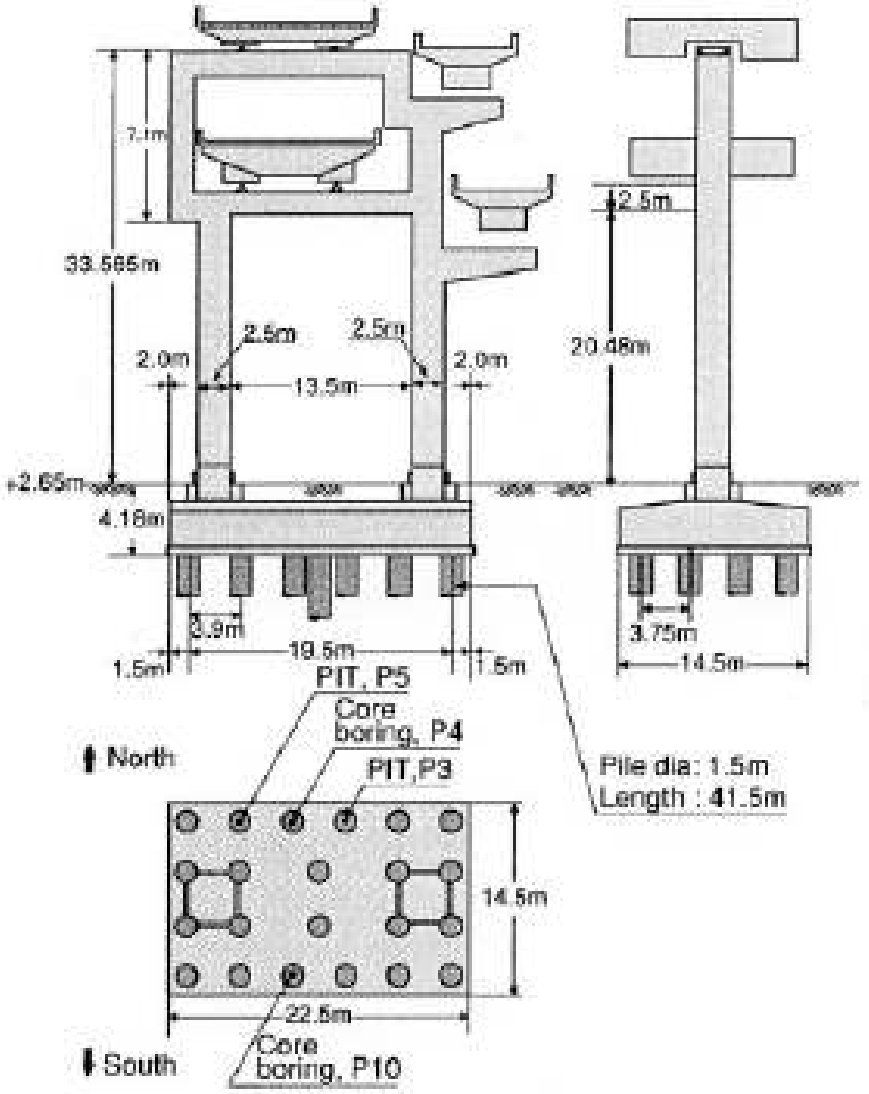

Figure 7-54: Uozakihama Bridge Structure and Foundation Configuration (Ishihara, 2003)

The pile consists of 32 (1.25 inch diameter) bars down to the pile length of 768 inch and 16 (1 inch diameter) from there to the total length of 1618 inch (Nishioka, 2008). The spacing of the transverse reinforcement (Circular hoop reinforcing) also varied at those intervals. To capture the discontinuity in the analysis of the pile response, the author did model the pile by incorporating the lower number of the bars and maximum transversal reinforcing spacing.

7.4.2.1. Liquefaction/Lateral Spread

It is highly likely that liquefaction developed in the reclaimed fills in the back land leading to widespread occurrence of lateral spreading as shown in Figure 7-55.

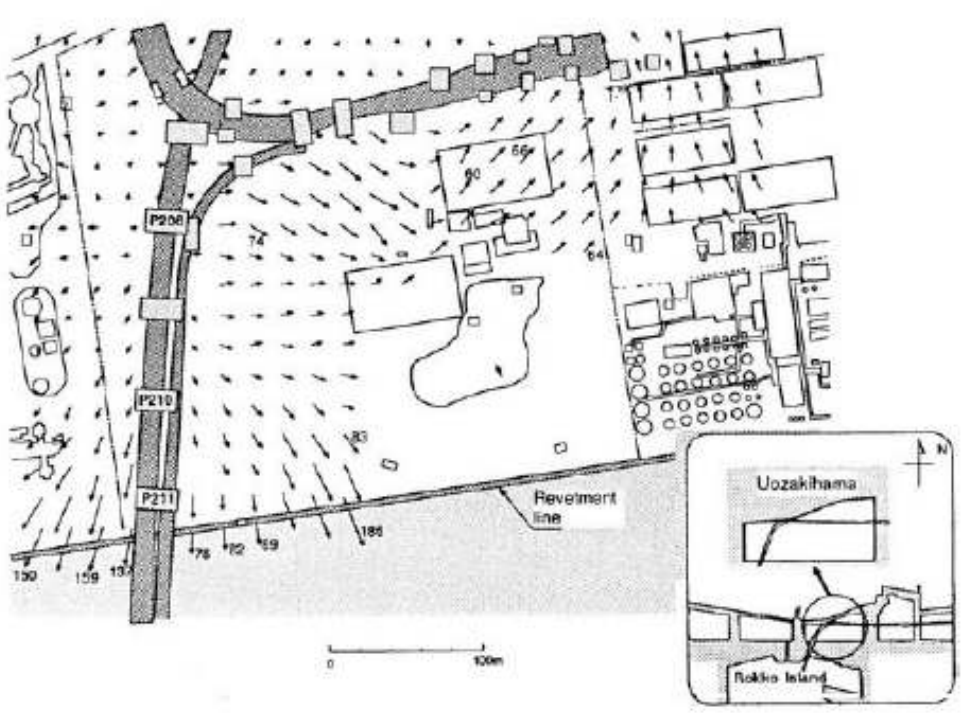

Figure 7-55: Lateral Spreading at/or around Uozakihama Bridge (Ishihara, 2003)

The lateral displacement of the ground in close proximity to the Pier 211, but free from its influence may be in the order of 40 inch. (100 cm)

7.4.2.2. Subsurface Soil Condition

The soil underlying the footing (figure 7-56) consists of very dense reclaimed fill (Masado Sand) with SPT values up to 40 above the water table down to the depth of 2 m, underlayed by the same soil type but loose to medium in consistency down to the depth of 20 m (SPT values of less than 20), overlaying by medium stiff silt and sandy silt and very dense sandy gravel.

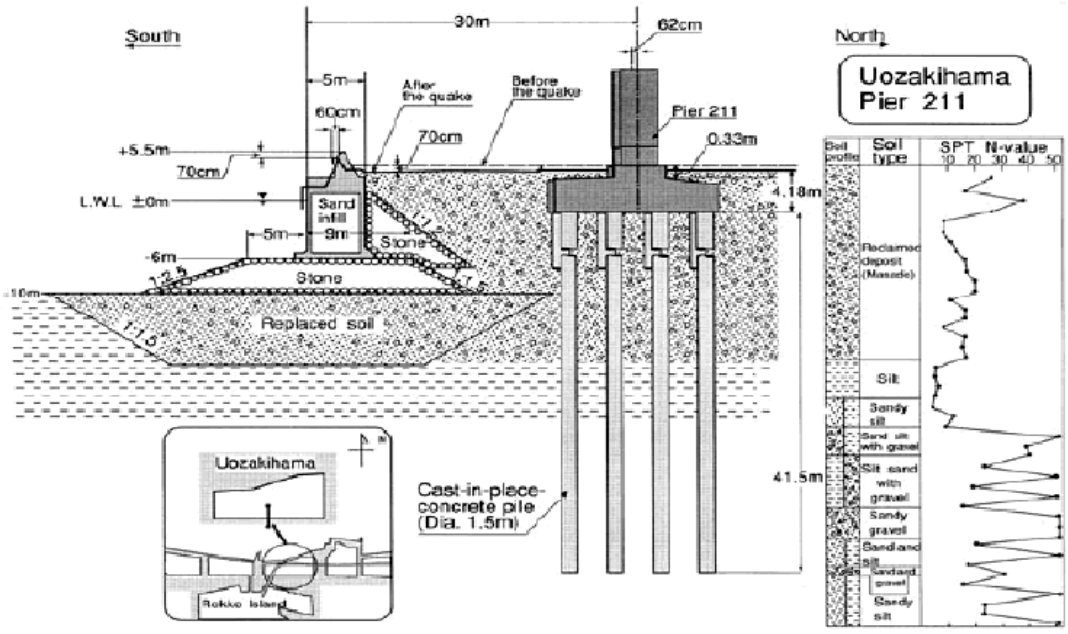

Figure 7-56: Soil Underlying the Footing at Uozakihama Bridge (Ishihara, 2003)

7.4.2.3. Lateral Demand/Capacity of the Pile Foundation

The lateral demand on the pile foundation due to the free field movement caused by the lateral spread is evaluated using the LPILE software program (ENSOFT, version 5).

7.4.2.4. Lateral Capacity for the CIDH Pile

The moment capacity for the proposed pile foundation is evaluated using XTRACT software program (Imbsen). Figure 7-57 shows the Pile Moment Curvature Diagram, which indicates the capacity of the pile.

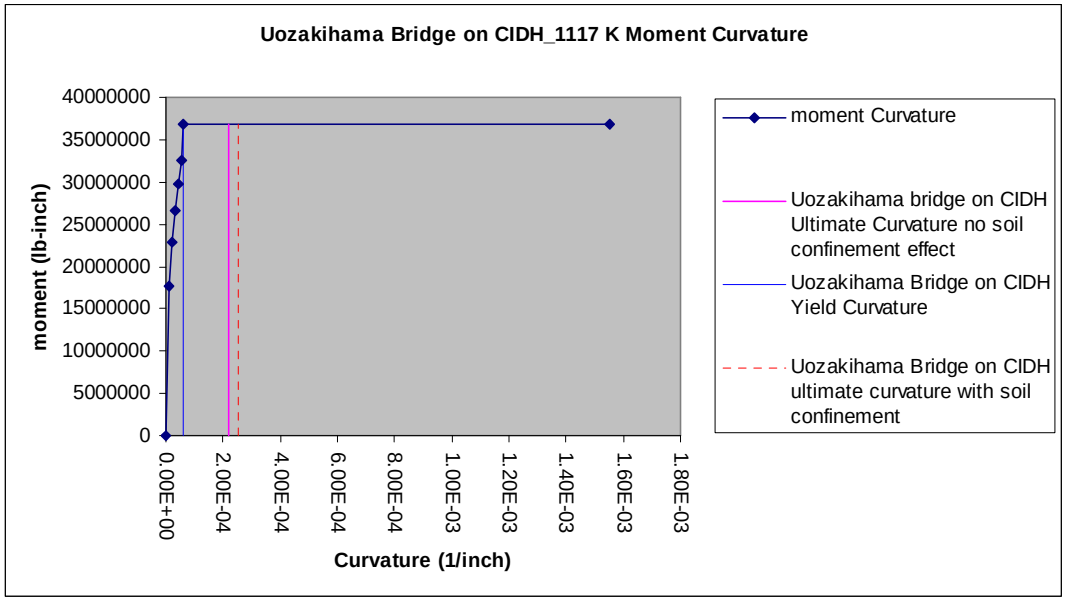

Figure 7-57: Moment Curvature Diagram for Uozakihama Bridge Piles

7.4.2.5. Pile Response due to Lateral Demand

The lateral demand using 6,12 and 15 inch displacements is used as the free field soil movement to assess the pile response for the CIDH pile. LPILE program is used to evaluate the pile curvature demand (Figures 7-58, 7-59 and 7-60) along the CIDH pile. The subsurface soil was modeled as a 3 layer soil consisting of a non-liquefiable crust, on top of a liquefiable layer overlying a liquefiable soil layer.

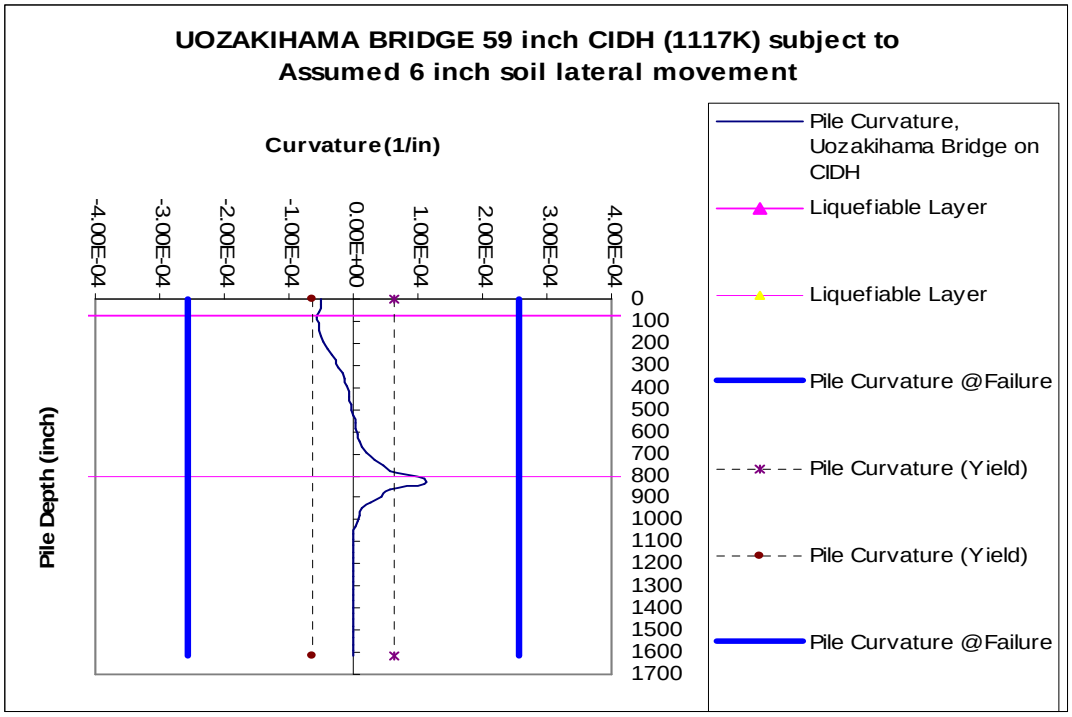

Figure 7-58: Curvature Demand for Uozakihama Bridge Piles

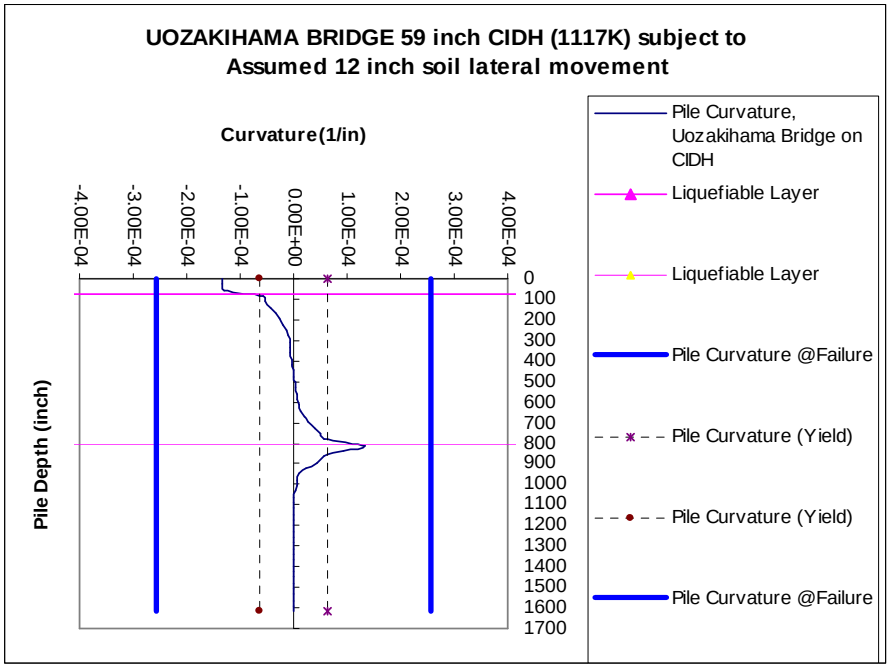

Figure 7-59: Curvature Demand for Uozakihama Bridge Piles

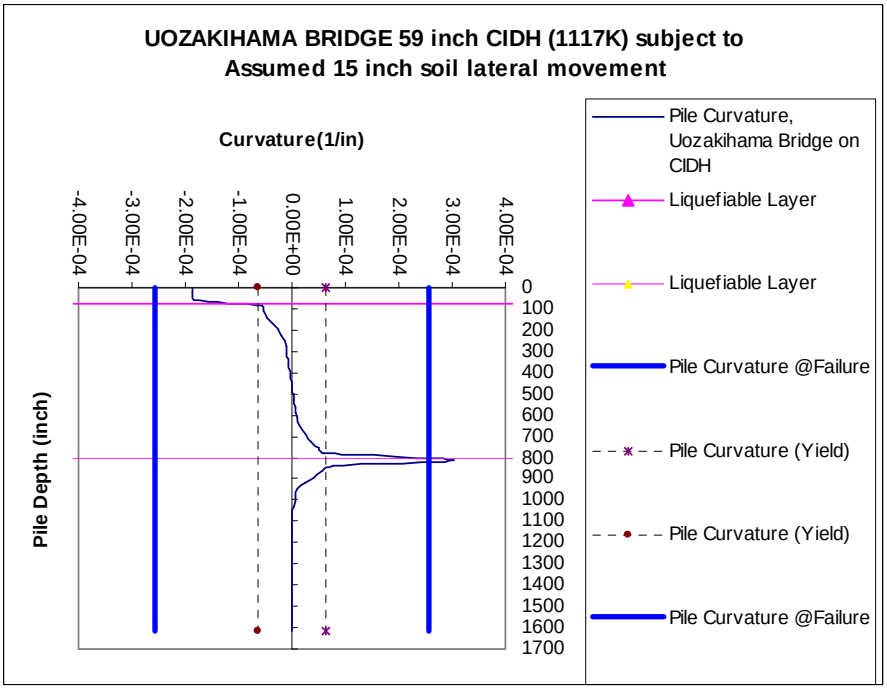

Figure 7-60: Curvature Demand for Uozakihama Bridge Piles

It is noted that the pile would undergo plastic hinging (pile yielding) on top and bottom where the non liquefiable crust moves 12 inch laterally. It is also noted that the author has chosen a pile curvature ductility of 4. The pile ductility is near 25 at the point of “failure’. So it can be concluded that the failure curvature chosen by the author is quite conservative. It is also important to note that no inertia was included in the analysis of the response of the piles.

7.4.2.6. Field Observation

The field observation (Figures 7-61 and 7-62) for the damage to the CIDH piles revealed that the piles were damaged and cracks were observed at the top and bottom at the interface of the liquefiable and non liquefiable layers and at the point of the pile discontinuity.

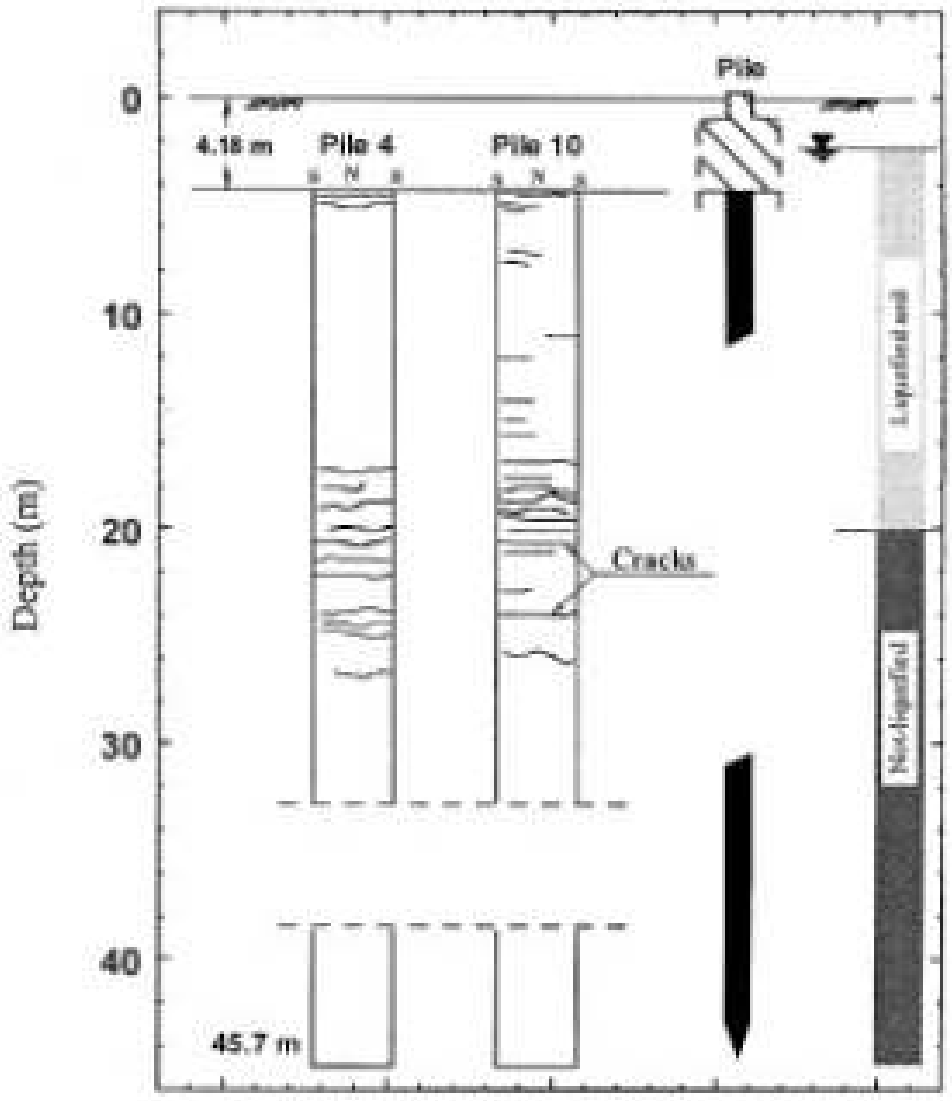

Figure 7-61: Pile Damage Observed During Field Observation (Uozakihama Bridge), (Ishihara, 2003)

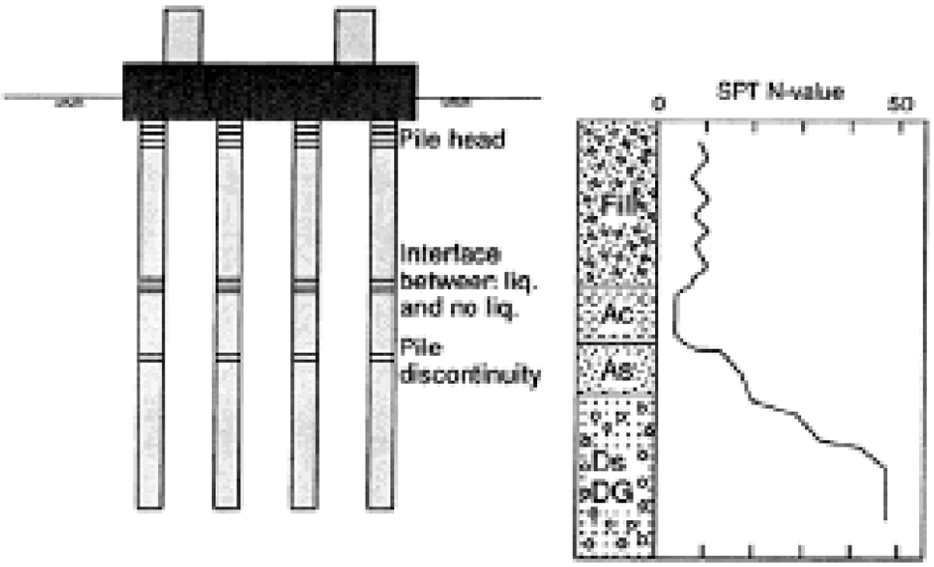

Figure 7-62: Damage Observed At the Pile Discontinuities (Uozakihama Bridge), (Ishihara, 2003)

The method of the damage survey of the piles in the field was by direct observation and by pile integrity test. (figures 7-63 and 7-64).

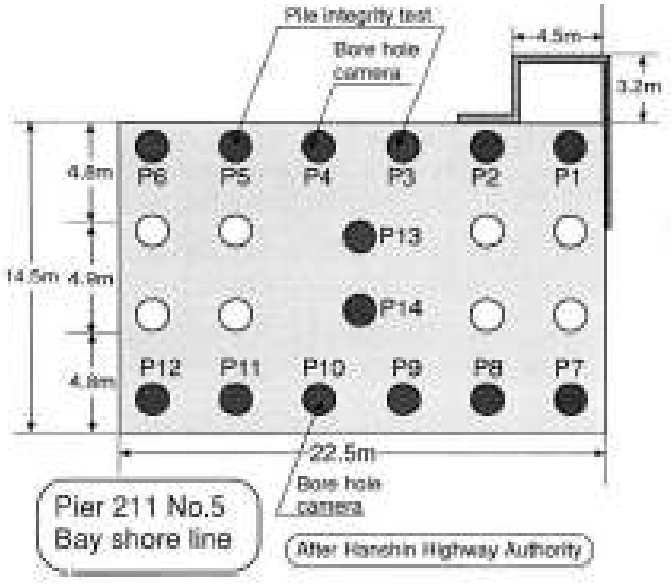

Figure 7-63: Damage Survey of Piles, Uozakihama Bridge. (Ishihara, 2003)

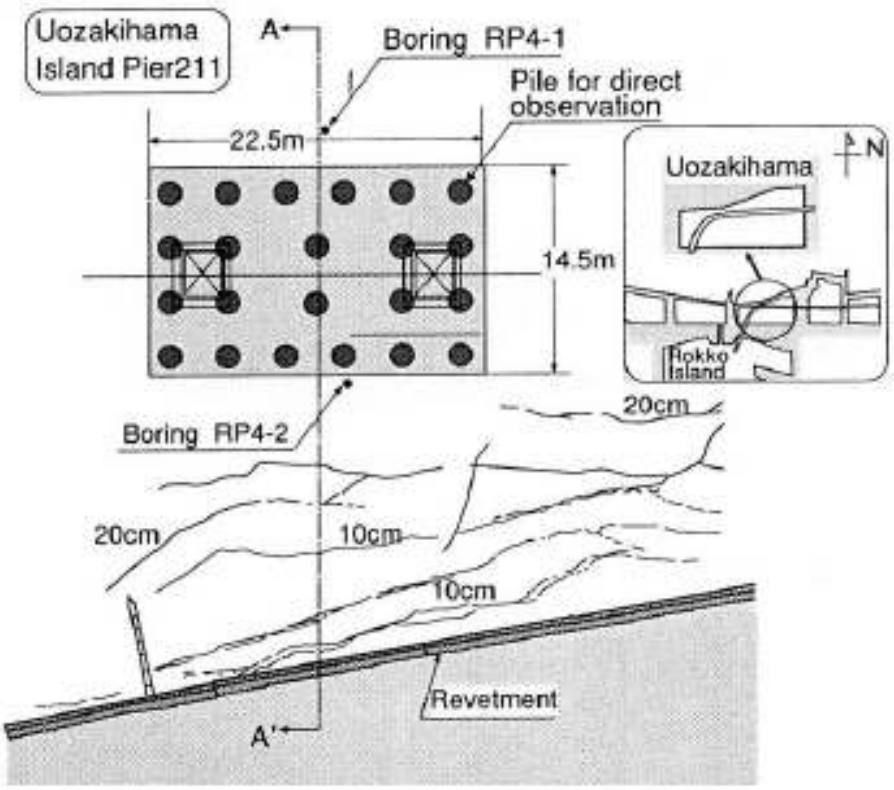

Figure 7-64: Damage Survey of Piles, Uozakihama Bridge (Ishihara, 2003)

7.4.2.7. Conclusion

The case study for the pile response to liquefaction induced lateral spread and its damage to the crust lateral displacement was evaluated. The study shows that the massive pile is subject to pile plastic hinging at non-liquefiable crustal displacement as low as 6 inch. The results of the analysis vis a vis the location along the pile where it occurred, compared very well with the actual field pile damage observation.

7.5. Proposed Methodology for Earthquake Response of Bridge Pile Foundation to Liquefaction Induced Lateral Spread: Summary

The following flow chart summarizes the steps involved in the proposed improved methodology for design for lateral spread impact assessment for bridge foundation piles, as previously discussed.

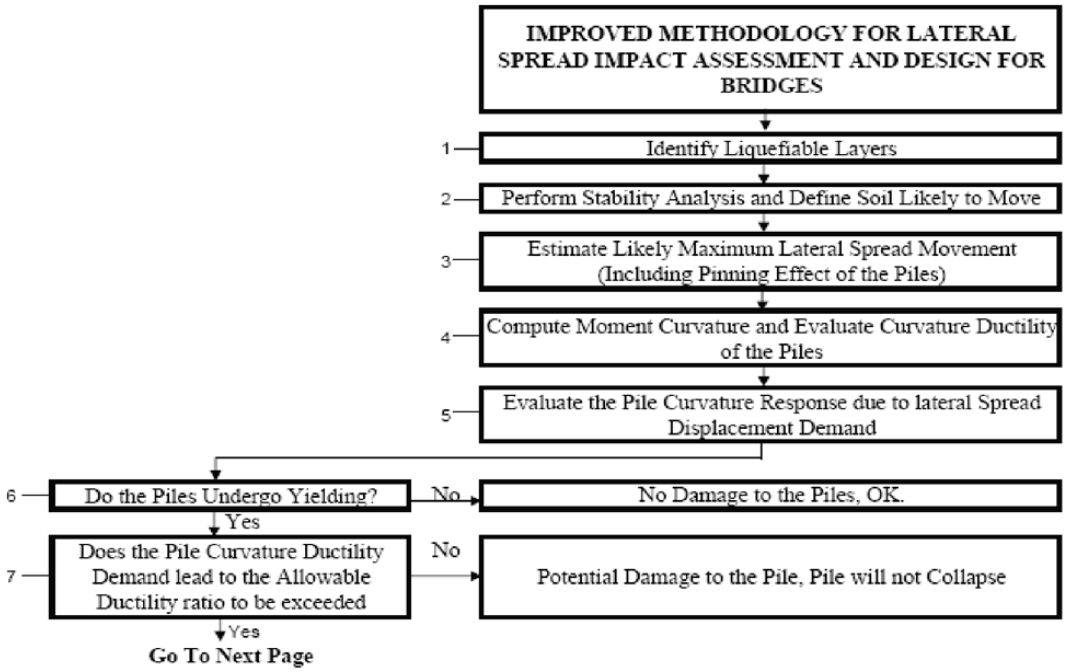

Figure 7-65 (a): Chart for Improved Methodology for Lateral Spread Impact Assessment and Design for Bridges

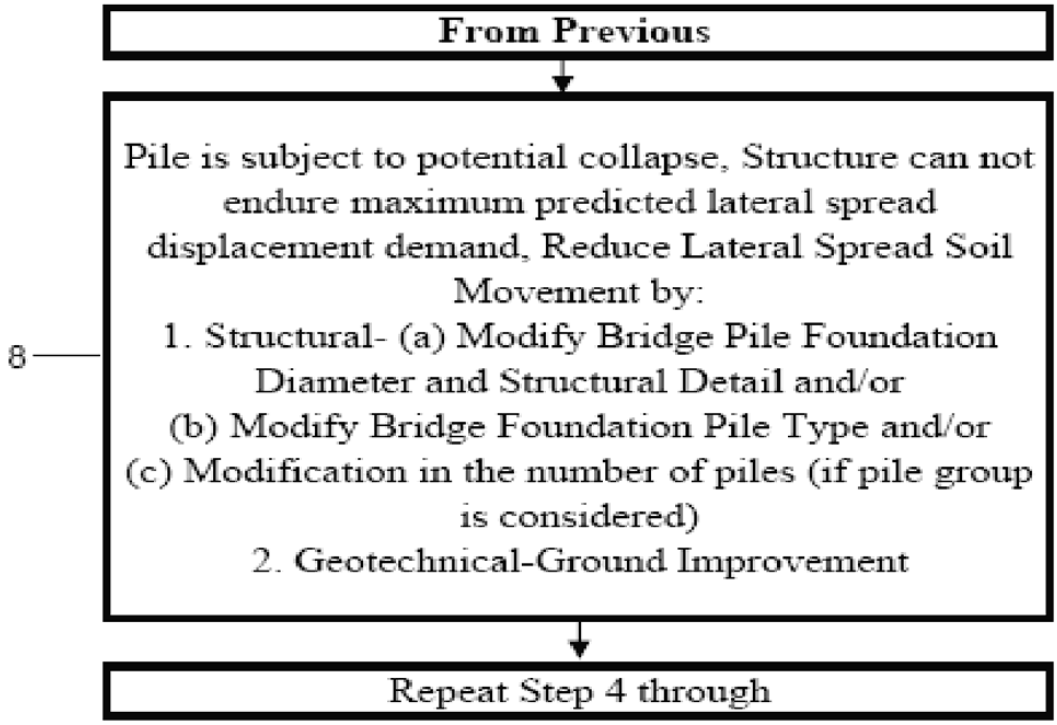

Figure 7-65 (b): Chart for Improved Methodology for Lateral Spread Impact Assessment and Design for Bridges

CHAPTER 8: DESIGN EXAMPLES, PILE TYPES AND SENSITIVITY STUDIES

8.1. Design Considerations for Lateral Spread Loading on Piles

The following design examples depict structures that are supported by typical Caltrans piles. All these piles are subject to liquefaction induced lateral spread during a design earthquake. The piles consist of both abutment and bent piles. The piles are categorized as standard CIDH (Cast In Drilled Hole) , non-standard CIDH, Type-I Pile Shaft, CISS (Cast in Steel Shell Concrete) and Pre-stressed Pre-cast Concrete.

Pile pinning and pile ductility using the improved design methodology are considered and sensitivity analyses were performed to assess the impact of the liquefiable layer thickness on the response of the pile.

The objective of the analysis using Caltrans design examples is to assess the earthquake response of the typical Caltrans pile foundations to liquefaction induced lateral spread displacement demand. In some cases a specific pile foundation type is analyzed as a possible scenario in a type selection process, for research purposes only. This does not mean that this specific pile or other piles are actually incorporated into the actual design of these specific Caltrans bridges, in practice. It is important to note that the pile types selected are used extensively in practice and the goal is to illustrate their vulnerability and/or their potential superior performance

during a design earthquake and in response to liquefaction induced lateral spread, utilizing the improved design methodology in this research.

The role of pile pinning and pile ductility and their impacts on the response of the bridge piles are investigated. It is shown through idealized design examples how each pile type respond to the liquefaction induced lateral spread, during a design earthquake . A constant ratio of 4 is used between the ultimate curvature and the yield curvature for all pile types. This ratio is the threshold value for ductility at "failure", in this research. The intent to select the latter number is to insure that the pile retains some reserved ductile capacity, by introducing conservatism in design, without introducing collapse. In theory, one may argue that the ratio in reality can be even higher, meaning the pile curvature at failure may be potentially higher in reality than the value considered in these design examples.

It should be noted that the XTRACT software used to evaluate section analysis and to compute the moment curvature capacity of the piles computes the curvature of the piles without considering the external confinement from soils in zones adjacent to plastic hinge location. To compensate the latter impact on the bridge pile response in general and its capacity in particular, a constant increment is added to the pile curvature capacity at failure, as discussed below.

The role of soil confinement in improving the earthquake response of the bridge pile to liquefaction induced lateral spread is considered by increasing the pile curvature as shown in the pile moment curvature graphs of the piles analyzed in this research. An approximate 17% increase is considered in this research, consistent in principle with the research by Blandon (2007) and Budek (2004). The effect of external confinement on flexural hinging in drilled pile shafts was examined by Budek et.al (2004) in a series of CIDH pile shafts testing to simulate the subgrade moment pattern in an in situ pile shaft. The effect of added external confinement was also seen in the ratio of experimental versus predicted plastic hinge lengths, where the minimum ratio was found to be 1.17 (Budek et al, 2004).

The subsurface conditions for the following bridge structures were generalized as a three layer system, consisting of non-liquefiable (crust) layer, followed by a second layer that is liquefiable and the third and last layer of non-liquefiable (very dense sand). The p-y relationship was generated by LPILE5 software for each of those layers. The liquefiable layer was modeled as soft clay (Matlock, 1970), the crust layer as stiff clay without free water and the bottom or third layer as very dense sand. Groundwater table was assumed as a design ground water elevation at the ground surface, which is the highest groundwater elevation during the design earthquake. No strut action from the bridge deck was considered in the examples.

8.2. Bridge Structure (Design Example I)

The bridge consists of a six span overhead structure, cast in place reinforced concrete box girder bridge structure supported by CIDH piles. The abutment is supported on 24 inch diameter CIDH piles, 550 inch long, subject to 200 kips of axial load.

8.2.1. Liquefaction/Lateral Spread and Bridge Abutment Stability

The soil layer underlying the abutment fill (crust layer) is assumed to liquefy during the design earthquake (Magnitude of 7.0 and Peak Horizontal Ground Acceleration of 0.6 g). The design soil parameters for both liquefiable and non-liquefiable layers are estimated by correlating the Standard Penetration Tests and using the Seed-Harder graph. The slope stability (SLIDE program) performed for the embankment for the abutment, indicates that during the design earthquake the abutment embankment is not stable and is subject to 10 inches of permanent displacement, using the Newmark method, corresponding to a value of $k_y/k_{max} = 0.15$ (Martin and Qiu Chart)

Figure 8-1 shows the failure surface found under pseudo-static slope stability during the design earthquake. The generalized subsurface soil conditions where the abutment piles are embedded consist of a three layer system of top non-liquefiable crust layer (20 feet thick), the middle liquefiable layer (20 feet thick) and the bottom non liquefiable layer (exceeding 50 feet).

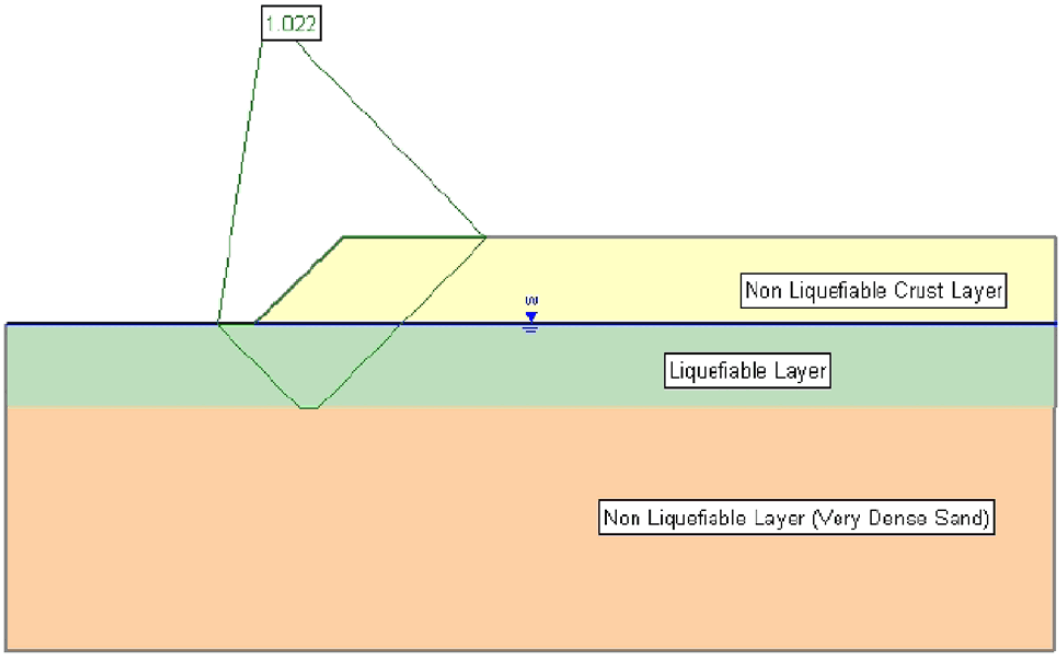

Figure 8-1: Bridge Abutment Gross Stability during Earthquake (Design Example I)

It is concluded that the embankment is subject to lateral spread during the design earthquake and the pile foundations notably at the abutment will be subject to lateral spread loading.

8.2.2. Lateral Demand/Capacity of the Proposed Pile Foundation

The lateral demand on the pile foundation due to the free field movement caused by the lateral spread is evaluated using the LPILE5 software program (ENSOFT). The p-y curves for the subsurface soils were assessed by the program modeling the liquefiable soil as soft clay. The expected free field soil displacement profile due to the lateral spread is included in the process as input into the program.

8.2.3. Pile Pinning Effect

During the lateral spread, the embankment soil is moving toward the piles at the abutment. The piles will resist the movement of the soil by applying shear forces which will counteract the shear forces due to the soil movement along the plane of the failure surface. Therefore these pile applied shear forces resist the free field movement of the soil. The lateral spread loading is evaluated considering this pile pinning effect. A two-front approach is used to assess this pinning effect and its contribution to the lateral spread loading evaluation as follows:

1. Various soil movements are prescribed to the embankment to determine the pile shear forces found due to these prescribed soils movements. LPILE5 was used to incorporate the free field soil movement and to evaluate the corresponding shear forces (pile pinning force) for the abutment piles. For each prescribed soil movement a corresponding shear force is found. The soil movements range from 1 to 10 inches and the corresponding pile shear forces range from 25 to 111 kips (maximum shear forces developed by the pile along the plane of failure). The soil displacement prescribed to represent the lateral spread movement is from the ground surface to the bottom of the liquefiable soil layer. The pile shear due to pinning effect corresponds to the maximum pile shear as evaluated by LPILE5 on the plane of failure. Table 8-1 shows the pile characteristics and the results of the analysis.

LPILE5ANALYSIS (curve I)

Pile Type	Pile Diameter (in)	Pile Length (ft)	Moment of Inertia (in^4)	Modulus of Elasticity(psi)	Soil Displacement (in)[1]	Maximum Pile Shear (kips)[2]
CIDH	24	46	16286	3250000	1	25
CIDH	24	46	16286	3250000	2	45
CIDH	24	46	16286	3250000	4	72
CIDH	24	46	16286	3250000	6	93
CIDH	24	46	16286	3250000	8	111
CIDH	24	46	16286	3250000	10	109

1: Soil displacement prescribed to represent the lateral spread movement from the ground surface to the bottom of the liquefiable soil layer
2: Maximum shear force developed by the pile resisting to the prescribed soil movement

Table 8-1: Pile Shear Forces (Design Example I)

2. To evaluate the corresponding shear forces (pile pinning force) a different approach from the previous one is used. The initial shear strength of 300 psf, which is the residual shear strength of the liquefiable layer along the failure plane, is increased by an arbitrary amount of 150 psf. This increase is designed to incorporate the pile pinning effect and its impact on the embankment movement. The shear force per pile is the product of this increase in cohesion, the length of the failure plane and the pile spacing. The Newmark analysis is performed to evaluate the new embankment displacement using this new shear strength (the residual strength + the increase in shear strength), which results in a higher yield acceleration and a lower displacement. The soil movements range from 10 inch to 0.02 inch. The shear forces range from 0 kips to 304 kips. Various yield accelerations are found, resulting in various displacements. Table 8-2 shows the results of the Newmark Analysis approach.

NEWMARK ANALYSIS (Curve II)

Initial Cohesion (psf)[3]	Increase in Cohesion (psf)	Cohesion (psf)[4]	Length of Failure Surface (ft)	Pile Spacing (ft)	Shear Force (kips)[5]	Yield Acceleration (g)	Maximum Peak Ground Acceleration (g)	Displacement (inch)
300	0	300	92	6	0	0.09	0.6	10
300	150	450	92	6	83	0.2	0.6	2
300	350	650	92	6	193	0.33	0.6	0.1
300	550	850	92	6	304	0.4	0.6	0.02

3: Initial cohesion corresponds to the shear strength of liquefiable soil, where the failure surface is located
4: Cohesion corresponds to the shear strength of the liquefiable soil after the increase in cohesion is introduced it is used for the embankment stability and Newmark analysis
5: Shear Force = Increase in cohesion x Length of Failure Surface x Pile Spacing

Table 8-2: Newmark Analysis (Design Example I)

3. The objective is to assess the pile pinning effect and its role in the lateral spread loading phenomenon. In order to meet the compatibility law in displacement, the soil displacement must be equal in both approaches described above. Where the two curves I and II converge, the values for both the actual displacement for the embankment and the pile pinning force (shear force) for the 24 inch CIDH pile for abutment 7 are found. The actual free field displacement considering the pile pinning effect is estimated to be roughly 4 inch. Figure 8-2 shows the pile pinning effect.

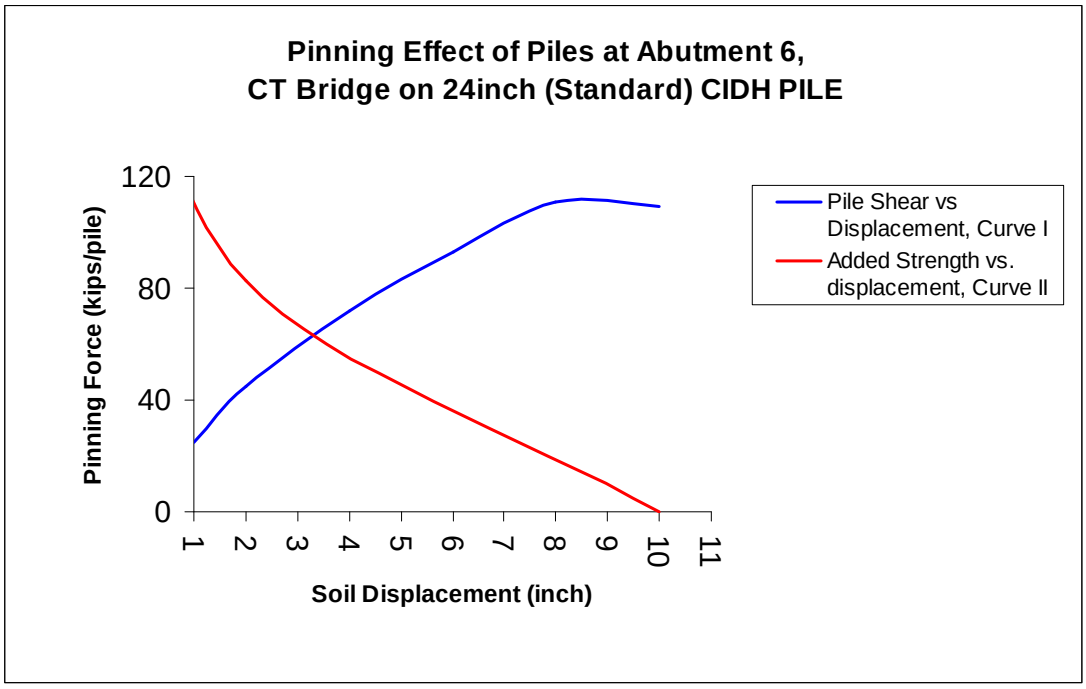

Figure 8-2: Pile Pinning Effect (Design Example I)

8.2.4. Pile Ductility for the Proposed CIDH Pile

The yield, ultimate curvatures and curvature ductility for the proposed pile foundation at abutment 7 is evaluated using XTRACT software program. Figure 8-3 shows the Pile Moment Curvature Diagram, which indicates the capacity of the pile.

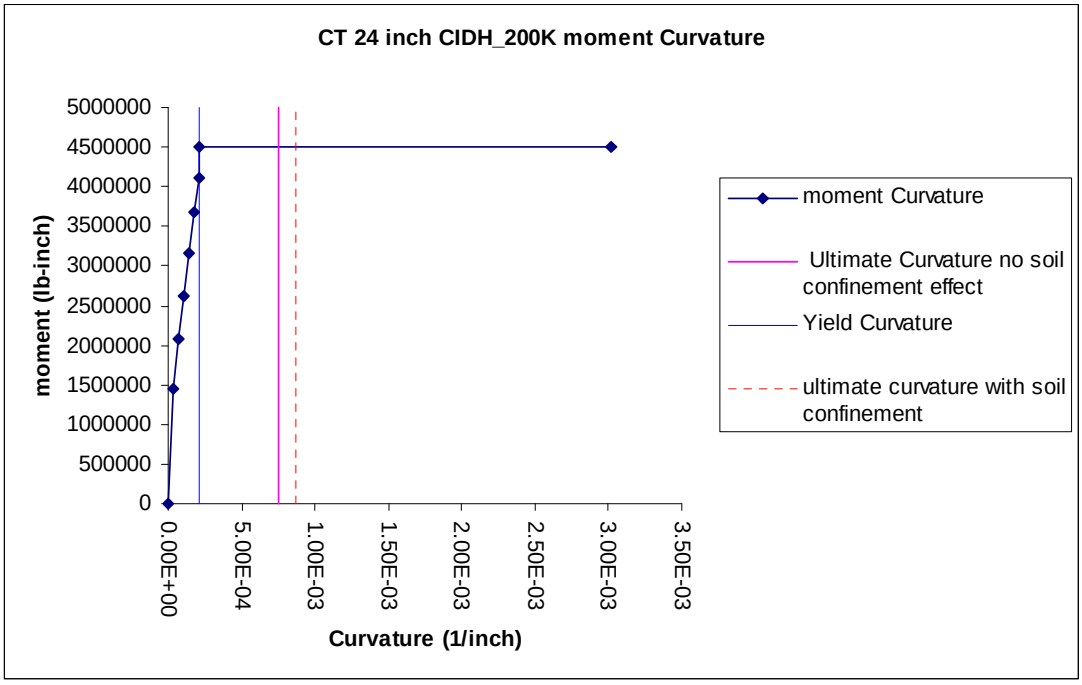

Figure 8-3: Pile Moment-Curvature Diagram (Design Example I)

8.2.5. Pile Response due to Lateral Spread

The lateral demand using 4 inch displacement is used as the soil movement and kinematic displacement demand to assess the pile response for abutment 7 and is incorporated into LPILE5 software, where the latter is used to evaluate the pile response of the 24 inch diameter CIDH pile. Figure 8-4 and Figure 8-5 show the pile response in terms of curvature and bending moment, *without* considering pinning effect.

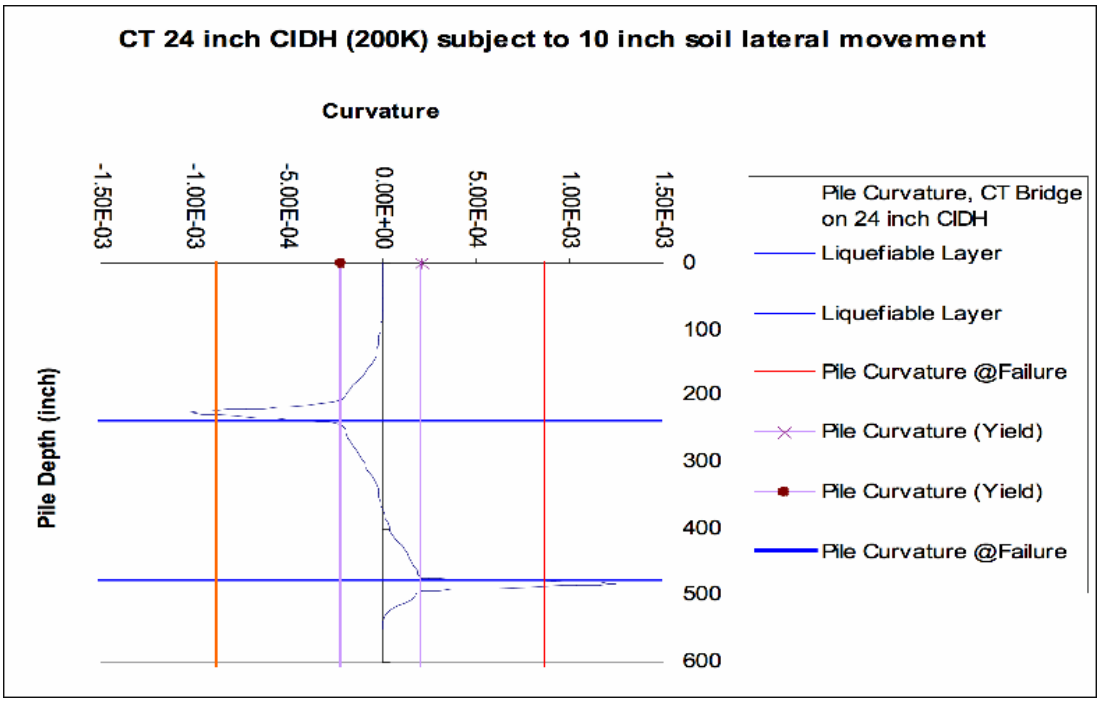

Figure 8-4: Pile Curvature Response (Design Example I)

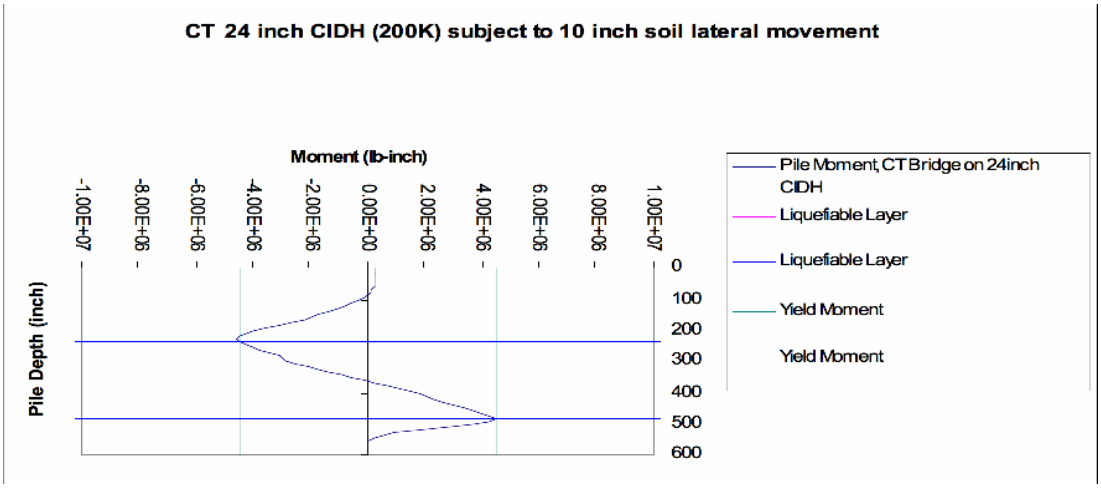

Figure 8-5: Pile Moment Response (Design Example I)

Figure 8-6 and Figure 8-7 show the pile response in terms of curvature and bending moment, *with* considering pinning effect.

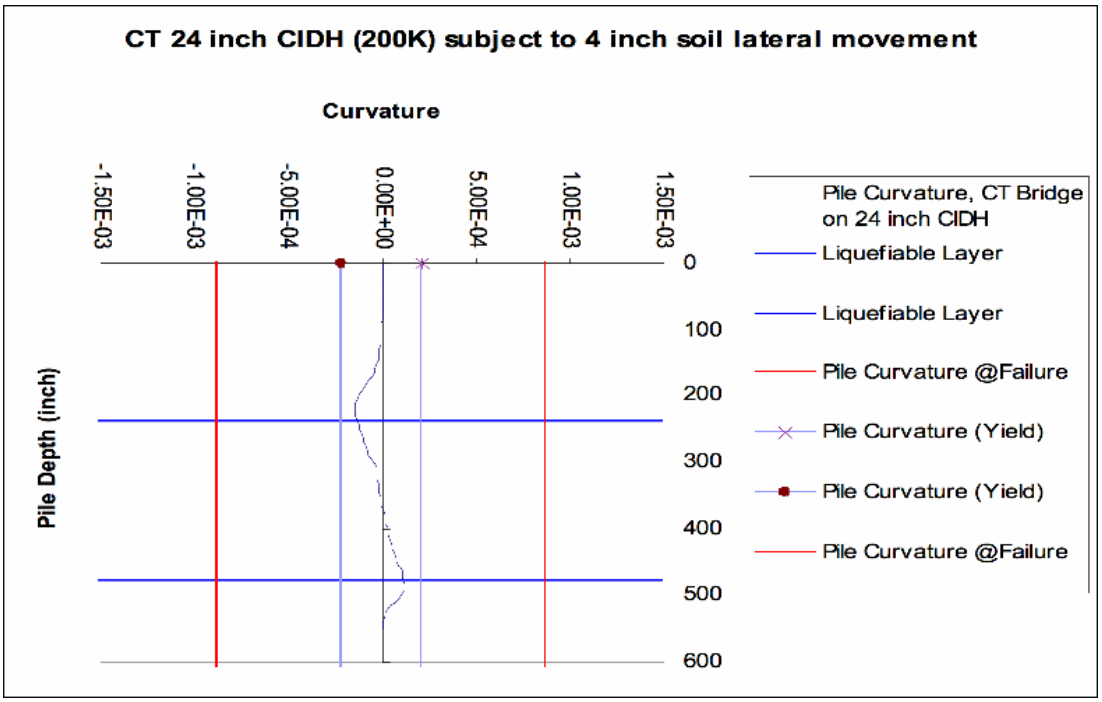

Figure 8-6: Pile Curvature Response (Design Example I)

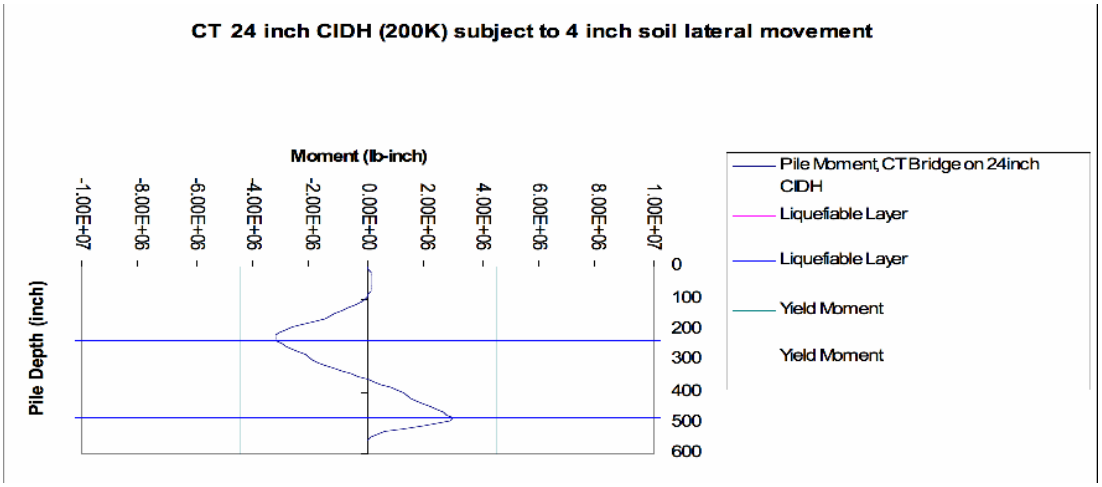

Figure 8-7: Pile Moment Response (Design Example I)

On the demand side, the following (figure 8-8) shows the pile curvature response of the 46 feet long, 24 inch diameter CIDH pile due to 4 inch of lateral spread displacement of the 20 feet thick upper crust over the 20 feet thick liquefiable soil.

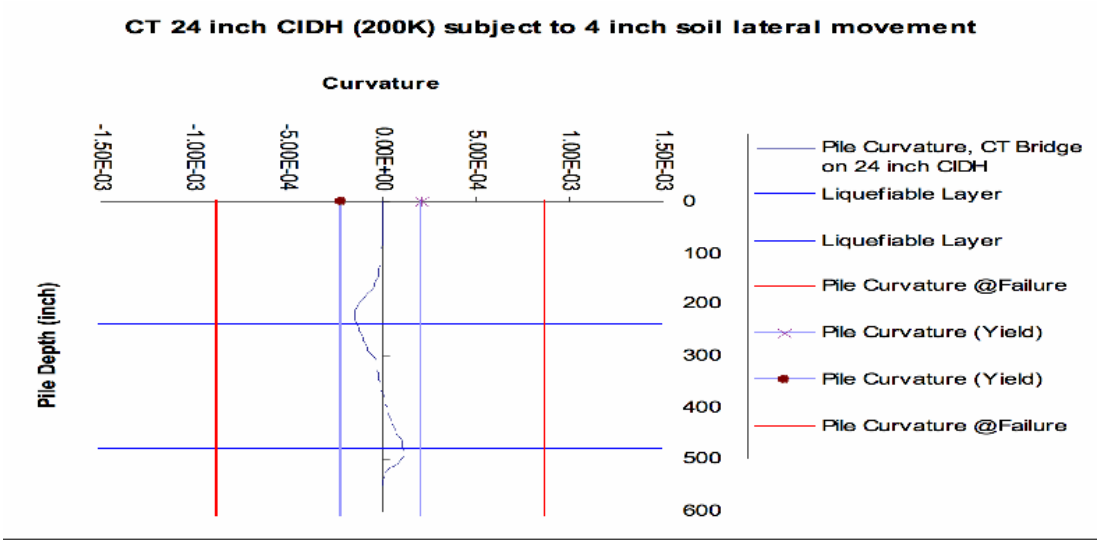

Figure 8-8: Pile Curvature Response (Design Example I)

As shown above, the 24 inch CIDH pile would not undergo plastic hinging, due to pinning effect.

8.2.6. Sensitivity Analysis

Sensitivity analysis is performed in terms of liquefaction layer thickness and its impact on the pile response.

8.2.6.1. Liquefaction Layer Thickness

The response of pile due to lateral spread was analyzed by assessing how the liquefaction layer thickness impacts the response. (Figures 8-9, 8-10, 8-11 and 8-12) The original liquefiable layer thickness of 20 feet was reduced to 15 feet, 10 feet, 5 feet, and 3 feet. The elevation at the top of the lateral spread remained unchanged. No inertia loading was considered. Only the kinematic loading on the pile fixed at the top was considered.

LIQUEFIABLE LAYER THICKNESS: 15 feet, Depth of Liquefaction (20 to 35 feet)

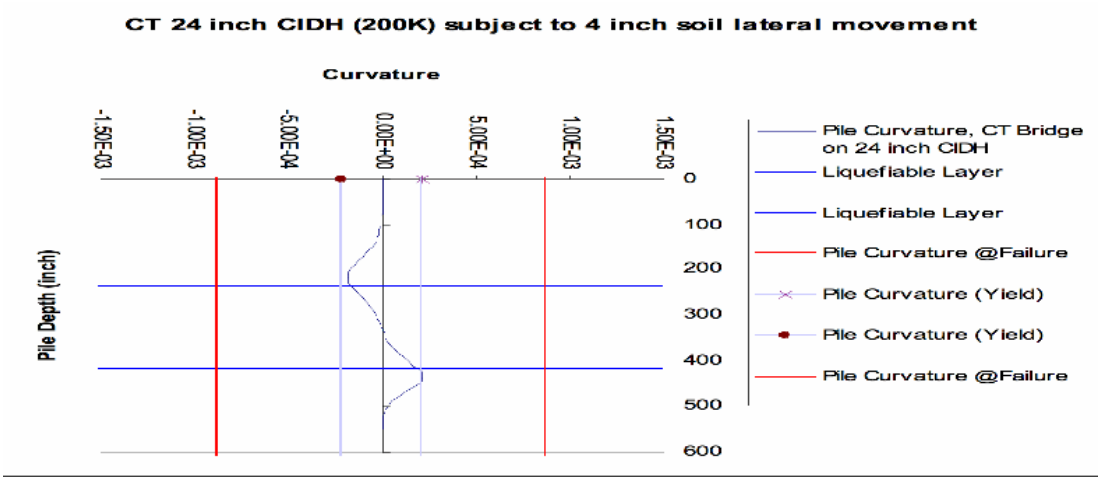

Figure 8-9: Pile Curvature Response (Design Example I)

LIQUEFIABLE LAYER THICKNESS: 10 feet, Depth of Liquefaction (20 to 30 feet)

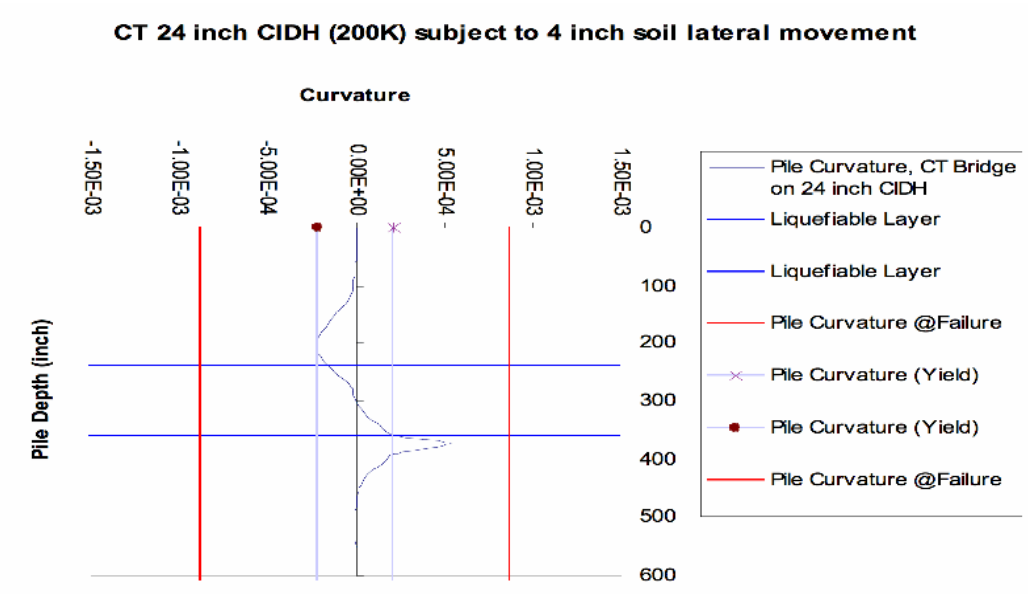

Figure 8-10: Pile Curvature Response (Design Example I)

LIQUEFIABLE LAYER THICKNESS: 5 feet, Depth of Liquefaction (20 to 25 feet)

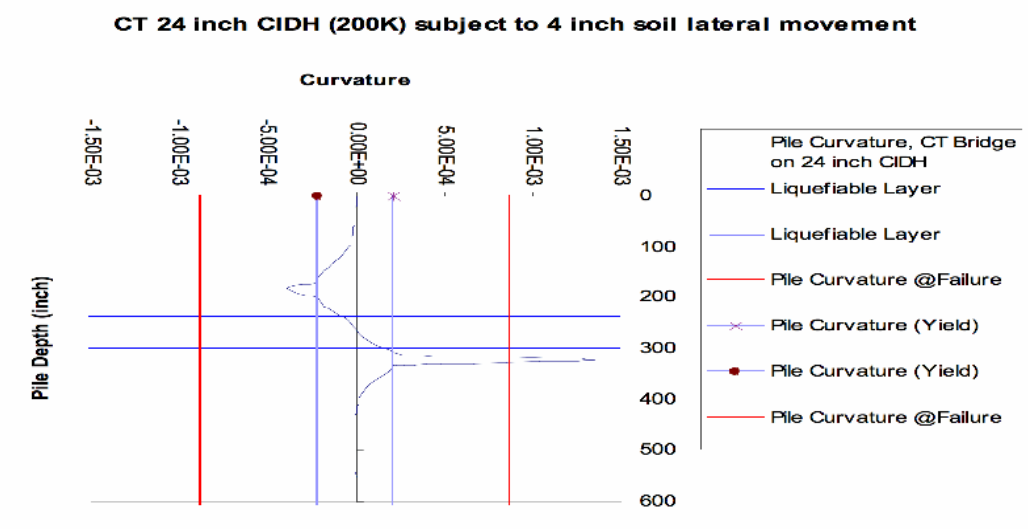

Figure 8-11: Pile Curvature Response (Design Example I)

LIQUEFIABLE LAYER THICKNESS: 3 feet, Depth of Liquefaction (20 to 23 feet)

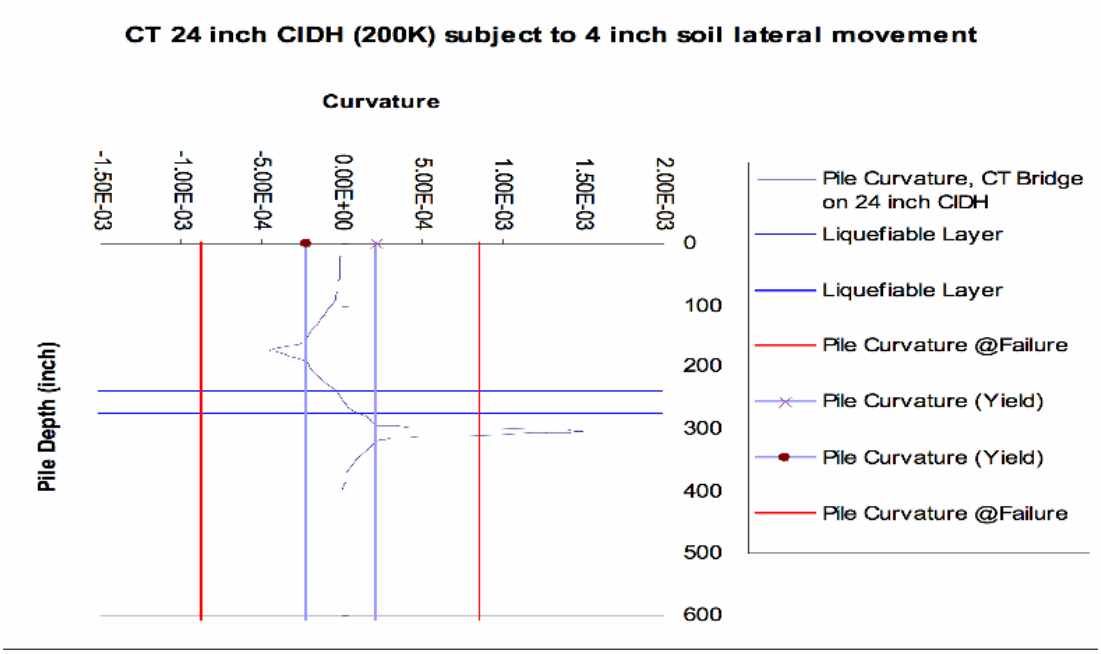

Figure 8-12: Pile Curvature Response (Design Example I)

The following (Figures 8-13 and 8-14) show the results of the pile response in terms of curvature demand, based on the thickness of the liquefiable layer.

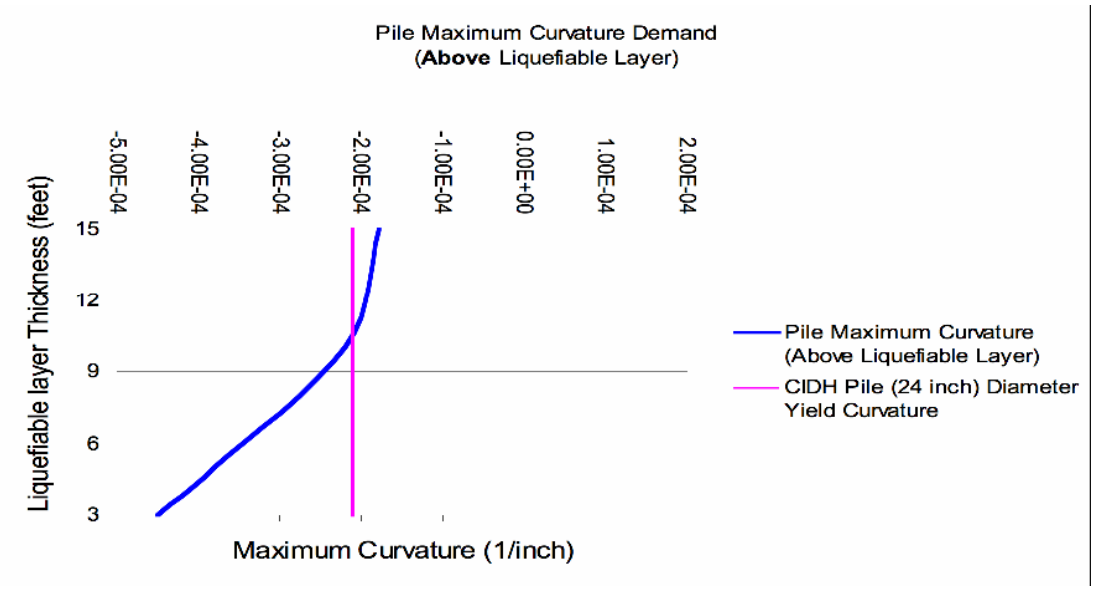

Figure 8-13: Pile Curvature Demand Based on Liquefiable Layer Thickness (Design Example I)

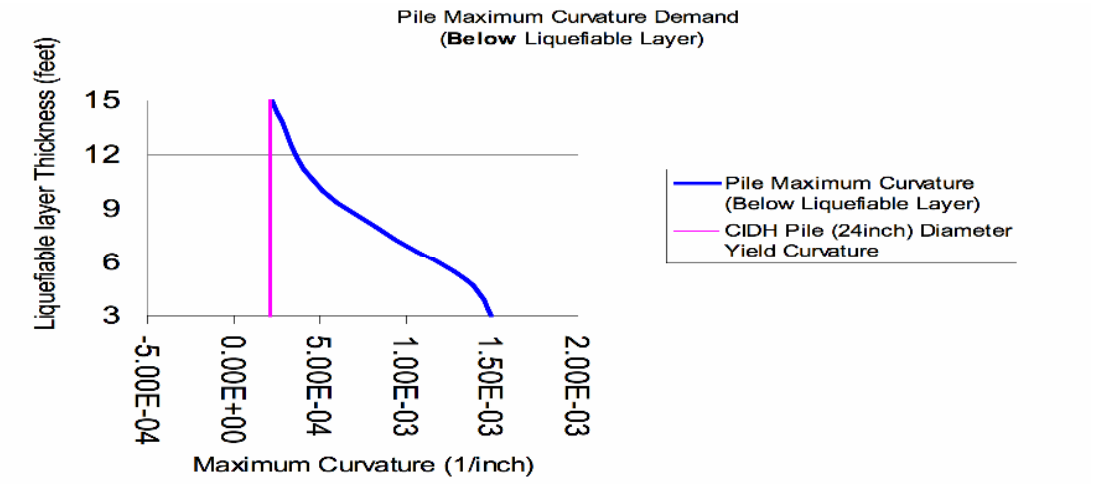

Figure 8-14: Pile Curvature Demand Based on Liquefiable Layer Thickness (Design Example I)

8.2.7. Conclusion

The proposed foundation for a multi-span bridge structure consisting of Caltrans 24inch diameter CIDH pile was evaluated subject to lateral spread loading. The embankment displacement during the design earthquake was evaluated. Pile pinning effect considering the pile resistance to the embankment displacement was assessed and the corresponding pile response (demand) was found. The lateral demand using the newly reduced free field (reduction due to the pining effect) displacement is compared to the lateral capacity of the pile: The latter being a structure characteristic of the pile. It is important to note that effect of "pile pinning" in reducing the impact of the soil movement due to lateral spread is significant. Due to this reduction, the piles at the bent will not yield. The reduction in liquefiable layer thickness, (with the top of the liquefiable layer elevation remaining unchanged) does increase the pile curvature demand, detrimental to the pile integrity. However, since the liquefiable layer thickness is reduced, the plastic shear is decreased accordingly leading to a reduced displacement demand.

8.3. Bridge Structure (Design Example II)

The bridge consists of a twelve span overcrossing structure, cast in place reinforced concrete box girder bridge structure .The existing bridge is supported by driven reinforced concrete and pipe piles of various diameter and design loading at multi columns bents and abutments. The author considered 66 inch diameter Type 1 pile

shaft, 1080 inch long, subject to 846 kips of axial load as one of several foundation alternatives for the replacement bridge consisting of multi column bents.

8.3.1. Liquefaction/Lateral Spread and Bridge Bent Stability

At bent 12 of the proposed bridge structure, the soil layer underlying the bent embankment fill will liquefy during the design earthquake. (Magnitude of 7.0 and Peak Horizontal Ground Acceleration of 0.6 g). The design soil parameters for both liquefiable and non-liquefiable layers are estimated by correlating the Standard Penetration Tests and using the Seed-Harder graph. The slope stability (SLIDE program) performed for the embankment for the bent, indicates that during the design earthquake the embankment is not stable and is subject to 22 inches of permanent displacement, using the Newmark method, corresponding to a value of $k_y/k_{max} = 0.08$ (Martin and Qiu Chart)

Figure 8-15 shows the failure surface found under pseudo-static slope stability during the design earthquake. The generalized subsurface soil conditions where the bent piles are embedded consist of a three layer system of top non-liquefiable crust layer (20 feet thick), the middle liquefiable layer (20 feet thick) and the bottom non liquefiable layer (exceeding 50 feet).

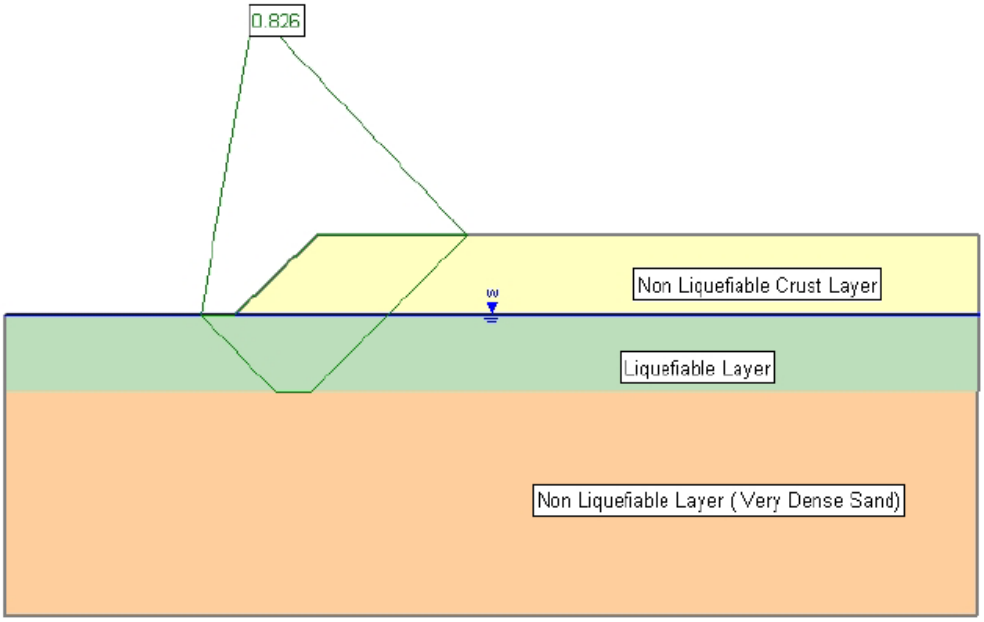

Figure 8-15: Bridge Bent Gross Stability During Earthquake (Design Example II)

It is concluded that the embankment is subject to lateral spread during the design earthquake and the pile shaft foundation notably at the bent will be subject to lateral spread loading.

8.3.2. Lateral Demand/Capacity of the Proposed Pile Foundation

The lateral demand on the pile foundation due to the free field movement caused by the lateral spread is evaluated using the LPILE5 software program (ENSOFT). The p-y curves for the subsurface soils were assessed by the program modeling the liquefiable soil as soft clay. The expected free field soil displacement profile due to the lateral spread is included in the process as input into the program.

8.3.3. Pile Pinning Effect

During the lateral spread, the embankment soil is moving toward the piles at bent 12. The piles will resist the movement of the soil by applying shear forces which will counteract the shear forces due to the soil movement along the plane of the failure surface. Therefore these pile applied shear forces resist the free field movement of the soil. The lateral spread loading is evaluated considering this pile pinning effect. A two-front approach is used to assess this pinning effect and its contribution to the lateral spread loading evaluation as follows:

1. Various soil movements are prescribed to the embankment to determine the pile shear forces found due to these prescribed soils movements. LPILE5 was used to incorporate the free field soil movement and to evaluate the corresponding shear forces (pile pinning force) for the bent 12 piles. For each prescribed soil movement a corresponding shear force is found. The soil movements range from 1 to 22 inches and the corresponding pile shear forces range from 159 to 721 kips. The soil displacement prescribed to represent the lateral spread movement is from the ground surface to the bottom of the liquefiable soil layer. The pile shear due to pinning effect corresponds to the maximum pile shear as evaluated by LPILE5. Table 8-3 shows the pile characteristics and the results of the analysis.

LPILE5ANALYSIS (curve I)

Pile Type	Pile Diameter (in)	Pile Length (ft)	Moment of Inertia (in^4)	Modulus of Elasticity(psi)	Soil Displacement (in)[1]	Maximum Pile Shear (kips)[2]
Type I Pile Shaft	66	90	931422	3250000	1	159
Type I Pile Shaft	66	90	931422	3250000	2	245
Type I Pile Shaft	66	90	931422	3250000	4	364
Type I Pile Shaft	66	90	931422	3250000	6	461
Type I Pile Shaft	66	90	931422	3250000	12	721
Type I Pile Shaft	66	90	931422	3250000	22	715

1: Soil displacement prescribed to represent the lateral spread movement from the ground surface to the bottom of the liquefiable soil layer
2: Maximum shear force developed by the pile resisting to the prescribed soil movement

Table 8-3: Pile Shear Forces (Design Example II)

2. To evaluate the corresponding shear forces (pile pinning force) a different approach from the previous one is used. The initial shear strength of 350 psf, which is the residual shear strength of the liquefiable layer along the failure plane, is increased by an arbitrary amount of 50 psf. This increase is designed to incorporate the pile pinning effect and its impact on the embankment movement. The shear force per pile is the product of this increase in cohesion, the length of the failure plane and the pile spacing. The Newmark analysis is performed to evaluate the new embankment displacement using this new shear strength (the residual strength + the increase in shear strength), which results in a higher yield acceleration and a lower displacement. The soil movements range from 22 inch to 1 inch. The shear forces range from 0 kips to 900 kips. Various yield accelerations are found, resulting in various displacements. Table 8-4 shows the results of the Newmark Analysis approach.

NEWMARK ANALYSIS (Curve II)

Initial Cohesion (psf)[3]	Increase in Cohesion (psf)	Cohesion (psf)[4]	Length of Failure Surface (ft)	Pile Spacing (ft)	Shear Force (kips)[5]	Yield Acceleration (g)	Maximum Peak Ground Acceleration (g)	Displacement (inch)
350	0	350	90	50	0	0.047	0.6	22
350	50	400	90	50	225	0.083	0.6	12
350	100	450	90	50	450	0.118	0.6	6
350	150	500	90	50	675	0.152	0.6	2.5
350	200	550	90	50	900	0.186	0.6	1

3: Initial cohesion corresponds to the shear strength of liquefiable soil, where the failure surface is located
4: Cohesion corresponds to the shear strength of the liquefiable soil after the increase in cohesion is introduced it is used for the embankment stability and Newmark analysis
5: Shear Force = Increase in cohesion x Length of Failure Surface x Pile Spacing

Table 8-4: Newmark Analysis (Design Example II)

3. The objective is to assess the pile pinning effect and its role in the lateral spread loading phenomenon. It can be concluded that in order to not violate the compatibility law in displacement, the soil displacement must be equal in both approaches described above. Where the two curves I and II converge, the values for both the actual displacement for the embankment and the pile pinning force (shear force) for the 66 inch Type I pile Shaft for bent 12 are found. The actual free field displacement considering the pile pinning effect is estimated to be roughly 6 inch. Figure 8-16 shows the pile pinning effect.

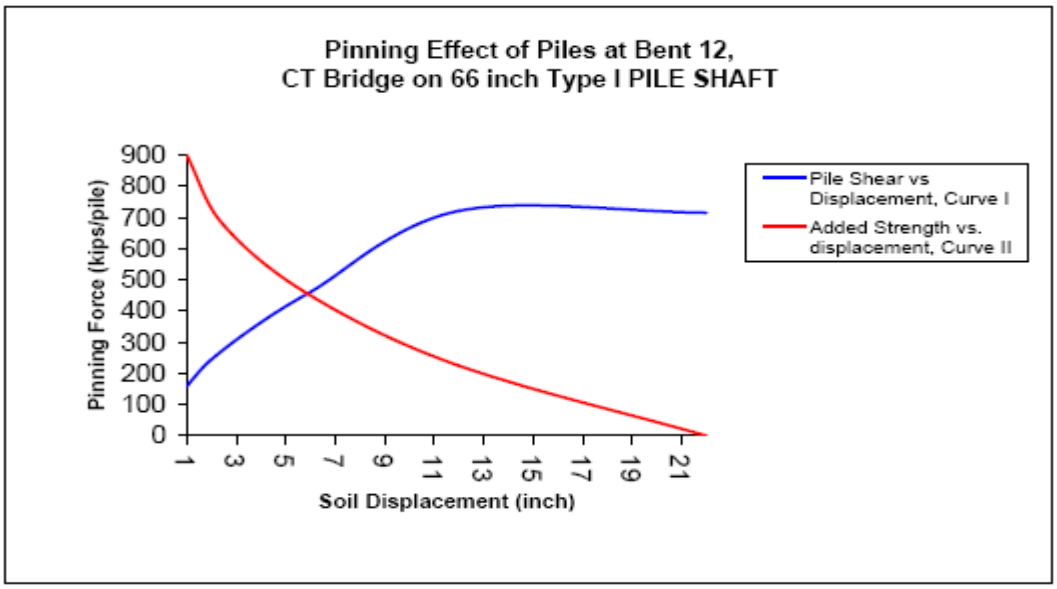

Figure 8-16: Pile Pinning Effect (Design Example II)

8.3.4. Pile Ductility for the Proposed Type I Pile Shaft

The yield, ultimate curvatures and curvature ductility for the proposed pile foundation at abutment 6 is evaluated using XTRACT software program. Figure 8-17 shows the Pile Moment Curvature Diagram, which indicates the capacity of the pile.

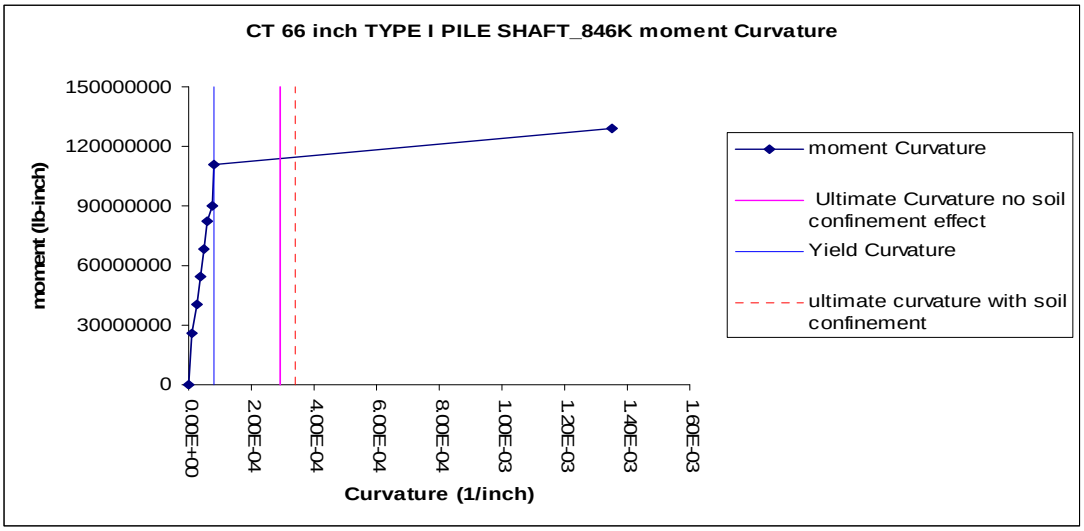

Figure 8-17: Pile Moment-Curvature Diagram (Design Example II)

8.3.5. Pile Response due to Lateral Demand

The lateral demand using 6 inch displacement is used as the soil movement and kinematic displacement demand to assess the pile response for abutment 6. LPILE5 program is used to evaluate the pile response of the 66 inch diameter Type I pile Shaft. Figures 8-18 and 8-19 show the pile response in terms of curvature and bending moment, *without* considering pinning effect.

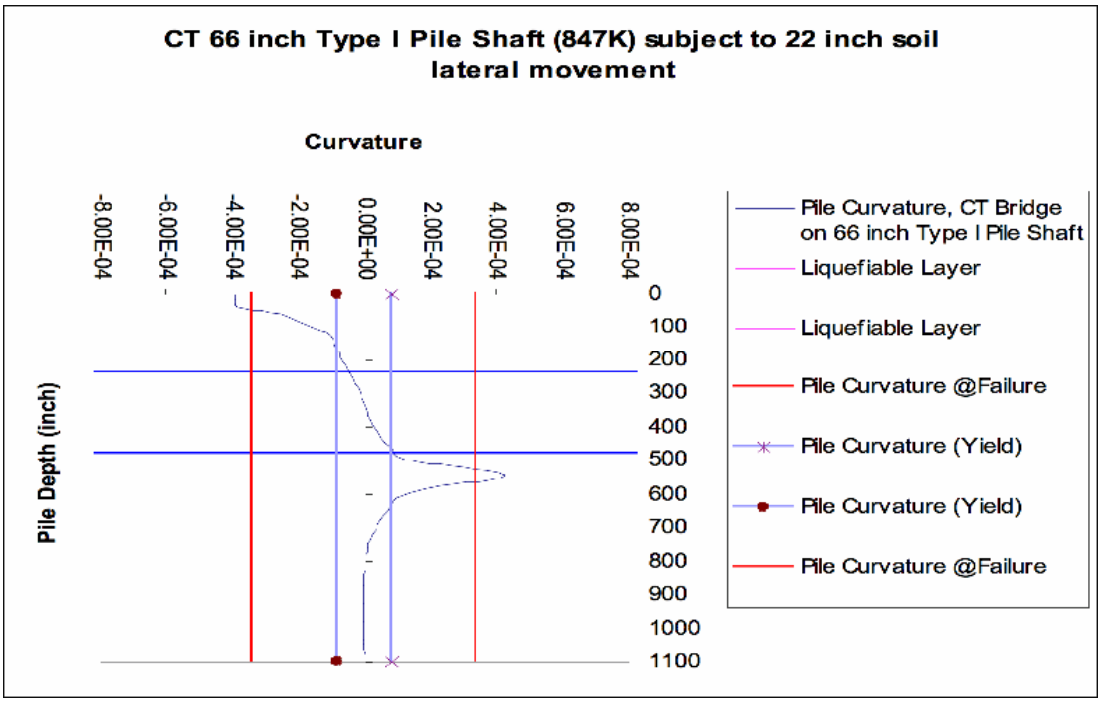

Figure 8-18: Pile Curvature Response (Design Example II)

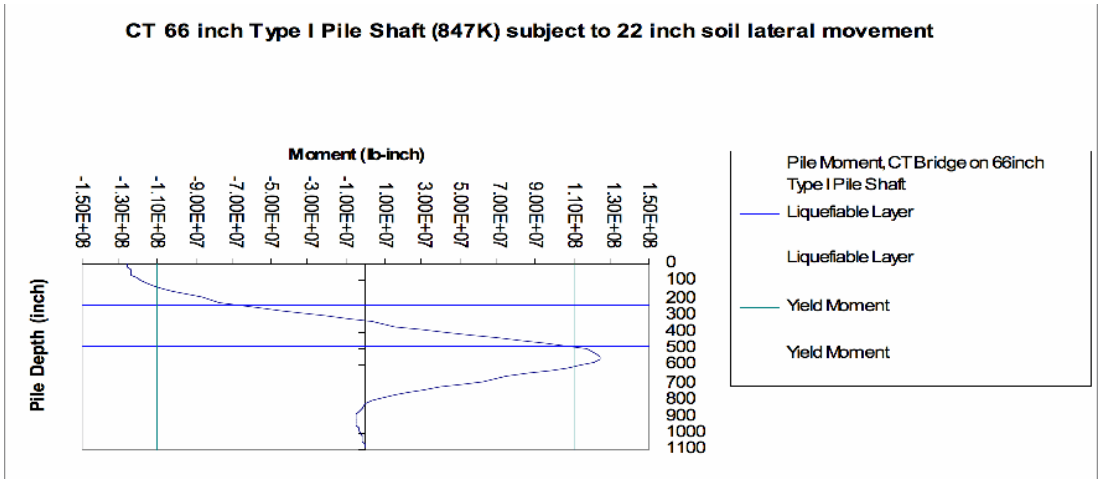

Figure 8-19: Pile Moment Response (Design Example II)

Figures 8-20 and 8-21 show the pile response in terms of curvature and bending moment, *with* considering pinning effect.

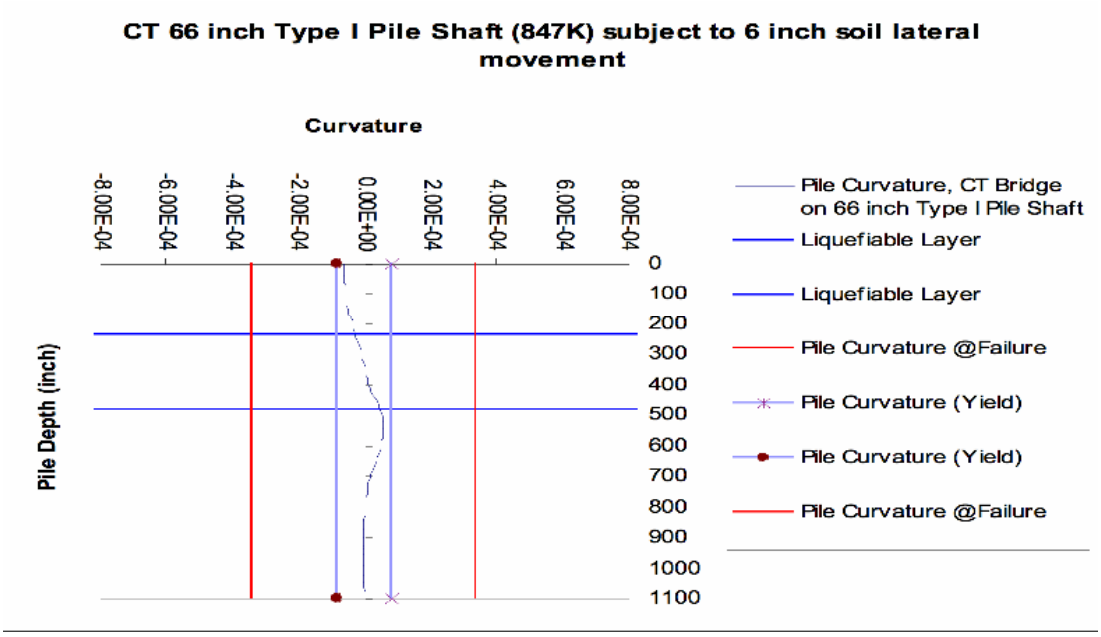

Figure 8-20: Pile Curvature Response (Design Example II)

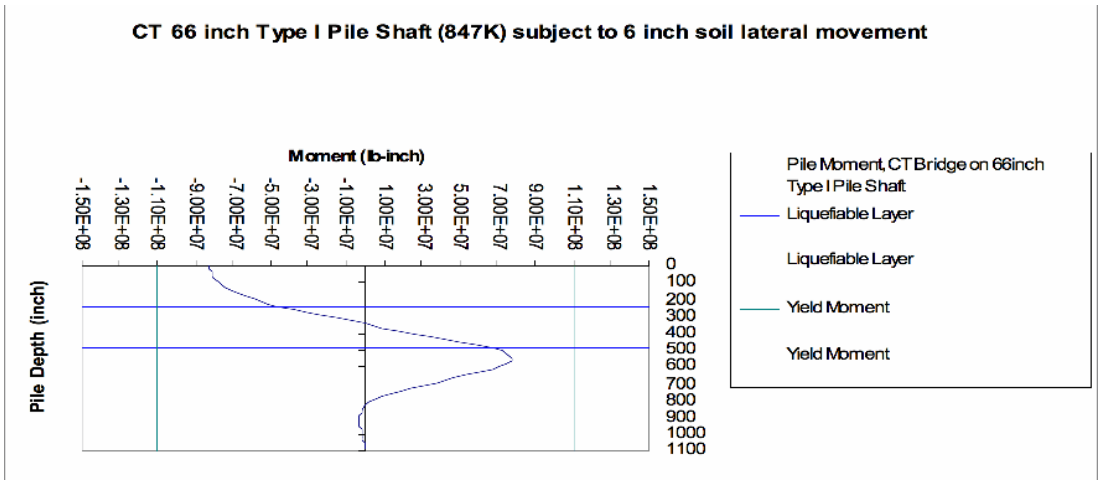

Figure 8-21: Pile Moment Response (Design Example II)

On the demand side, the following (figure 8-22) shows the pile curvature response of the 90 feet long, 66 inch diameter Type I Pile Shaft due to 6 inch of lateral spread displacement of the 20 feet thick upper crust over the 20 feet thick liquefiable soil.

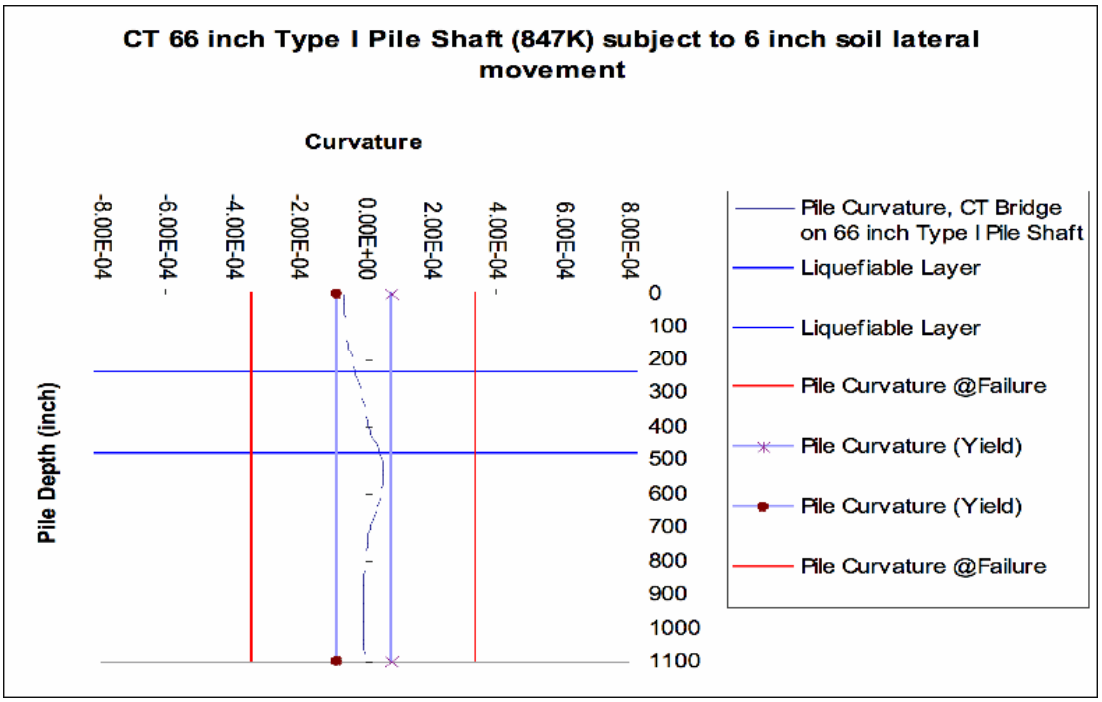

Figure 8-22: Pile Curvature Response (Design Example II)

As shown above, the 66 inch Type I pile Shaft would not undergo plastic hinging, due to pinning effect.

8.3.6. Sensitivity Analysis

Sensitivity analysis is performed in terms of liquefaction layer thickness and its impact on the pile response.

8.3.6.1. Liquefaction Layer Thickness

The response of pile due to lateral spread was analyzed by assessing how the liquefaction layer thickness impacts the response. (Figures 8-23, 8-24, 8-25 and 8-26) The original liquefiable layer thickness of 20 feet was reduced to 15 feet, 10 feet, 5 feet, and 3 feet. The elevation at the top of the lateral spread remained unchanged. No inertia loading was considered. Only the kinematic loading on the pile fixed at the top was considered.

LIQUEFIABLE LAYER THICKNESS: 15 feet, Depth of Liquefaction (20 to 35 feet)

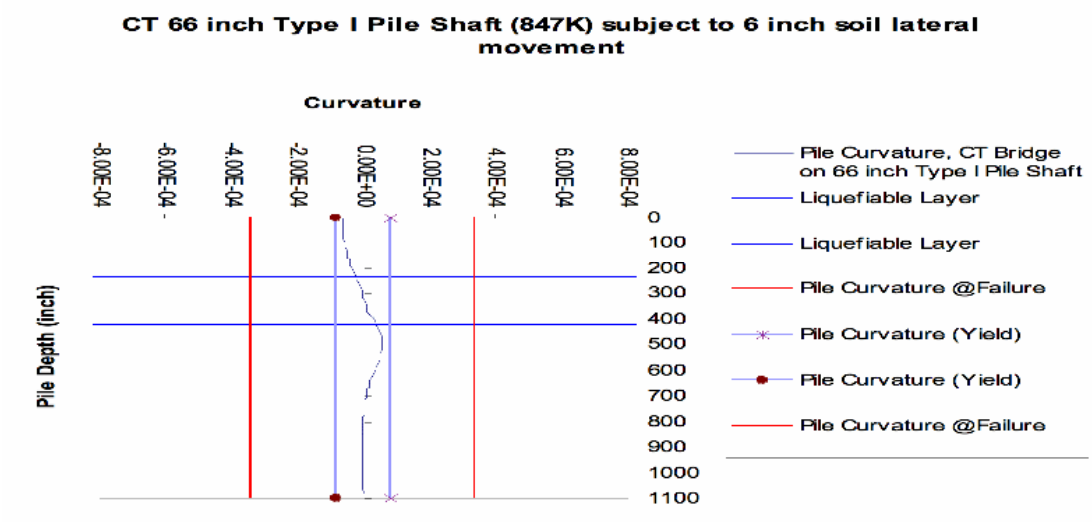

Figure 8-23: Pile Curvature Response (Design Example II)

LIQUEFIABLE LAYER THICKNESS: 10 feet, Depth of Liquefaction (20 to 30 feet)

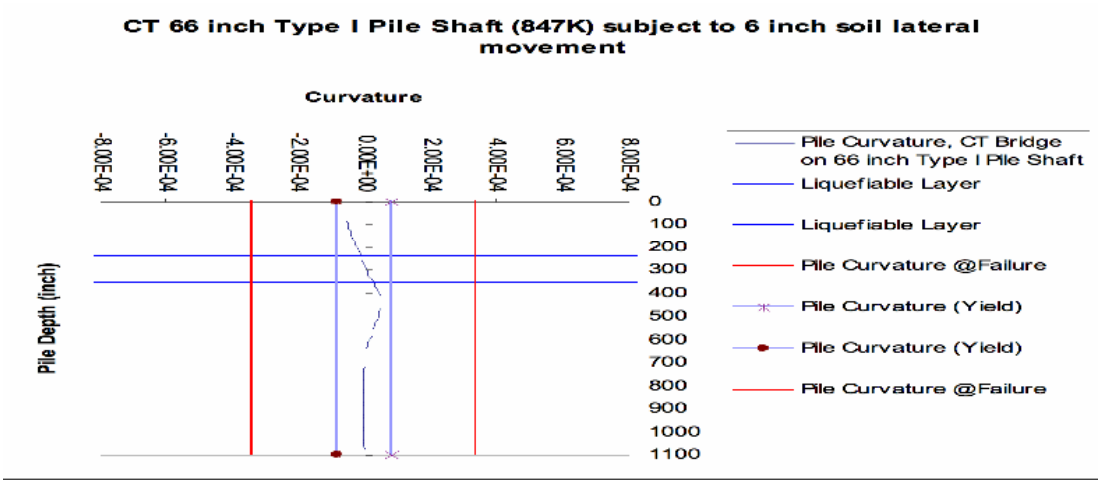

Figure 8-24: Pile Curvature Response (Design Example II)

LIQUEFIABLE LAYER THICKNESS: 5 feet, Depth of Liquefaction (20 to 25 feet)

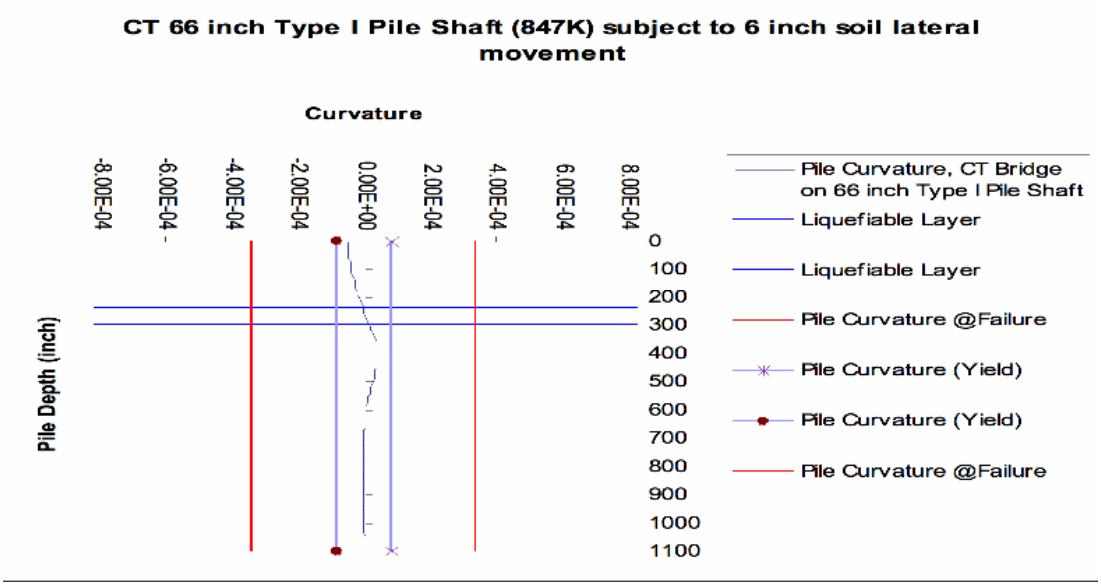

Figure 8-25: Pile Curvature Response (Design Example II)

LIQUEFIABLE LAYER THICKNESS: 3 feet, Depth of Liquefaction (20 to 23 feet)

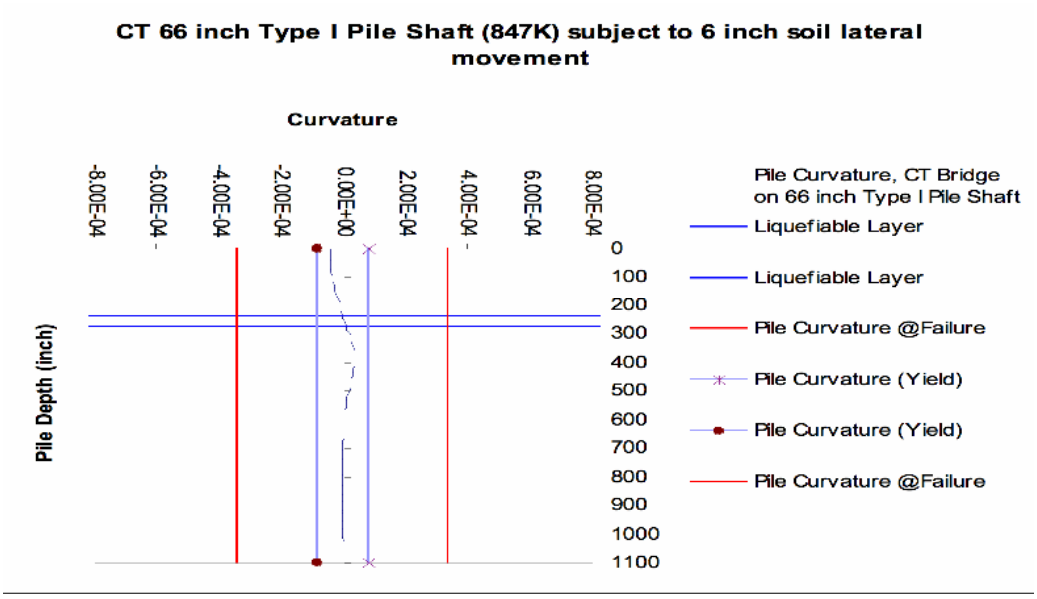

Figure 8-26: Pile Curvature Response (Design Example II)

The following (figures 8-27 and 8-28) show the results of the pile response in terms of curvature demand, based on the thickness of the liquefiable layer.

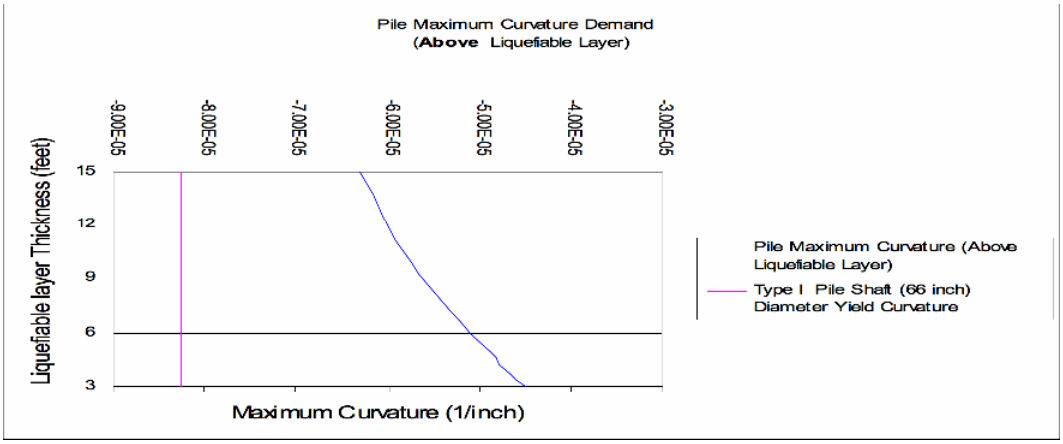

Figure 8-27: Pile Curvature Demand Based on Liquefiable Layer Thickness (Design Example II)

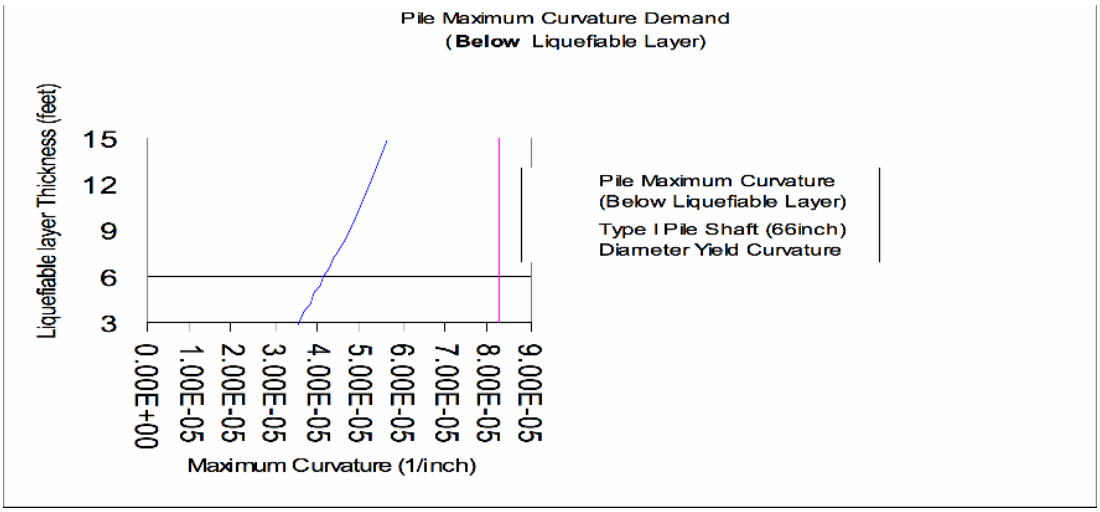

Figure 8-28: Pile Curvature Demand Based on Liquefiable Layer Thickness (Design Example II)

8.3.7. Conclusion

The proposed foundation for a multi-span bridge structure consisting of 66 inch Type I Shaft pile was evaluated subject to lateral spread loading. The embankment displacement during the design earthquake was evaluated. Pile pinning effect considering the pile resistance to the embankment displacement was assessed and the corresponding pile response (demand) was found. The lateral demand using the newly reduced free field (reduction due to the pining effect) displacement is compared to the lateral capacity of the pile: The latter being a structure characteristic of the pile. It is important to note that effect of "pile pinning" in reducing the impact of the soil movement due to lateral spread is significant. Due to this reduction, the piles at the bent will not yield. The reduction in liquefiable layer thickness, (with the top of the liquefiable layer elevation remaining unchanged) does lead to an increase

in the maximum pile curvature demand which could potentially be detrimental to the pile integrity. However, since the liquefiable layer thickness is reduced, the plastic shear is decreased accordingly leading to a reduced displacement demand.

8.4. Bridge Structure (Design Example III)

The bridge consists of a five span box/bulb-tee girder bridge structure supported by 48 inch diameter CIDH (Cast in Drilled Piles) at the bents and abutments. Abutment 6 is supported on 48 inch diameter CIDH piles, 1404 inch long, subject to 285 kips of axial load.

8.4.1. Liquefaction/Lateral Spread and Bridge Abutment Stability

At abutment 6 of the proposed bridge structure, the soil layer underlying the abutment fill (crust layer) will liquefy during the design earthquake. (Magnitude of 7.0 and Peak Horizontal Ground Acceleration of 0.5 g). The design soil parameters for both liquefiable and non-liquefiable layers are estimated by correlating the Standard Penetration Tests and using the Seed-Harder graph. The slope stability performed for the embankment for abutment 6, indicates that during the design earthquake the embankment is not stable and is subject to 30 inches of permanent displacement , using the Newmark method, corresponding to a value of $k_y/k_{max} = 0.2$.

The generalized subsurface soil conditions where the abutment piles are embedded consist of a three layer system of top non-liquefiable crust layer (47 feet thick), the

middle liquefiable layer (20 feet thick) and the bottom non liquefiable layer (exceeding 75 feet).

It is concluded that the embankment is subject to lateral spread during the design earthquake and the pile foundations notably at abutment 6 will be subject to lateral spread loading.

8.4.2. Lateral Demand/Capacity of the Proposed Pile Foundation

The lateral demand on the pile foundation due to the free field movement caused by the lateral spread is evaluated using the LPILE5 software program (ENSOFT). The p-y curves for the subsurface soils were assessed by the program modeling the liquefiable soil as soft clay. The expected free field soil displacement profile due to the lateral spread is included in the process as input into the program.

8.4.3. Pile Pinning Effect

During the lateral spread, the embankment soil is moving toward the piles at abutment 6. The piles will resist the movement of the soil by applying shear forces which will counteract the shear forces due to the soil movement along the plane of the failure surface. Therefore these pile applied shear forces resist the free field movement of the soil. The lateral spread loading is evaluated considering this pile pinning effect. A two-front approach is used to assess this pinning effect and its contribution to the lateral spread loading evaluation as follows:

1. Various soil movements are prescribed to the embankment to determine the pile shear forces found due to these prescribed soils movements. LPILE4M was used to incorporate the free field soil movement and to evaluate the corresponding shear forces (pile pinning force) for the abutment 6 piles. For each prescribed soil movement a corresponding shear force is found. The soil movements range from 0.5 to 15 inches and the corresponding pile shear forces range from 111 to 1033 kips. The soil displacement prescribed to represent the lateral spread movement is from the ground surface to the bottom of the liquefiable soil layer. The pile shear due to pinning effect corresponds to the maximum pile shear as evaluated by LPILE4M. Table 8-5 shows the pile characteristics and the results of the analysis.

LPILE4M ANALYSIS (curve I)

Pile Type	Pile Diameter (in)	Pile Length (ft)	Moment of Inertia (in^4)	Modulus of Elasticity(psi)	Soil Displacement (in)[1]	Maximum Pile Shear (kips)[2]
CIDH	48	117	115292	3250000	0.5	111
CIDH	48	117	115292	3250000	1	190
CIDH	48	117	115292	3250000	1.5	260
CIDH	48	117	115292	3250000	2	327
CIDH	48	117	115292	3250000	4	485
CIDH	48	117	115292	3250000	6	572
CIDH	48	117	115292	3250000	9	737
CIDH	48	117	115292	3250000	12	896
CIDH	48	117	115292	3250000	15	1033

1: Soil displacement prescribed to represent the lateral spread movement from the ground surface to the bottom of the liquefiable soil layer
2: Maximum shear force developed by the pile resisting to the prescribed soil movement

Table 8-5: Pile Shear Forces (Design Example III)

2. To evaluate the corresponding shear forces (pile pinning force) a different approach from the previous one is used. The initial shear strength of 150 psf, which is the residual shear strength of the liquefiable layer along the failure plane, is increased by an arbitrary amount of 150 psf. This increase is designed to incorporate the pile pinning effect and its impact on the embankment movement. The shear force per pile is the product of this increase in cohesion, the length of the failure plane and the pile spacing. The Newmark analysis is performed to evaluate the new embankment displacement using this new shear strength (the residual strength + the increase in shear strength), which results in a higher yield acceleration and a lower displacement. The soil movements range from 25 inch to 0.035 inch. The shear forces range from 270 kips to 6120 kips. Various yield accelerations are found, resulting in various displacements. Table 8-6 shows the results of the Newmark Analysis approach.

NEWMARK ANALYSIS (Curve II)

Initial Cohesion (psf)[3]	Increase in Cohesion (psf)	Cohesion (psf)[4]	Length of Failure Surface (ft)	Pile Spacing (ft)	Shear Force (kips)[5]	Yield Acceleration (g)	Maximum Peak Ground Acceleration (g)	Displacement (inch)
150	150	300	120	15	270	0.125	0.5	25
150	350	500	120	15	630	0.155	0.5	15
150	550	700	120	15	990	0.178	0.5	10
150	850	1000	120	15	1530	0.209	0.5	6
150	1350	1500	120	15	2430	0.26	0.5	2.5
150	1700	1850	120	15	3060	0.295	0.5	1
150	1850	2000	120	15	3330	0.315	0.5	0.8
150	1975	2125	120	15	3355	0.325	0.5	0.65
150	2550	2700	120	15	4590	0.375	0.5	0.15
150	3400	3550	120	15	6120	0.45	0.5	0.035

3: Initial cohesion corresponds to the shear strength of liquefiable soil, where the failure surface is located
4: Cohesion corresponds to the shear strength of the liquefiable soil after the increase in cohesion is introduced it is used for the embankment stability and Newmark analysis
5: Shear Force = Increase in cohesion x Length of Failure Surface x Pile Spacing

Table 8-6: Newmark Analysis (Design Example III)

3. The objective is to assess the pile pinning effect and its role in the lateral spread loading phenomenon. It can be concluded that in order to not violate the compatibility law in displacement, the soil displacement must be equal in both approaches described above. Where the two curves I and II converge, the values for both the actual displacement for the embankment and the pile pinning force (shear force) for the CIDH pile for abutment 6 are found. The actual free field displacement considering the pile pinning effect is estimated to be 12 inch. Figure 8-29 shows the pile pinning effect.

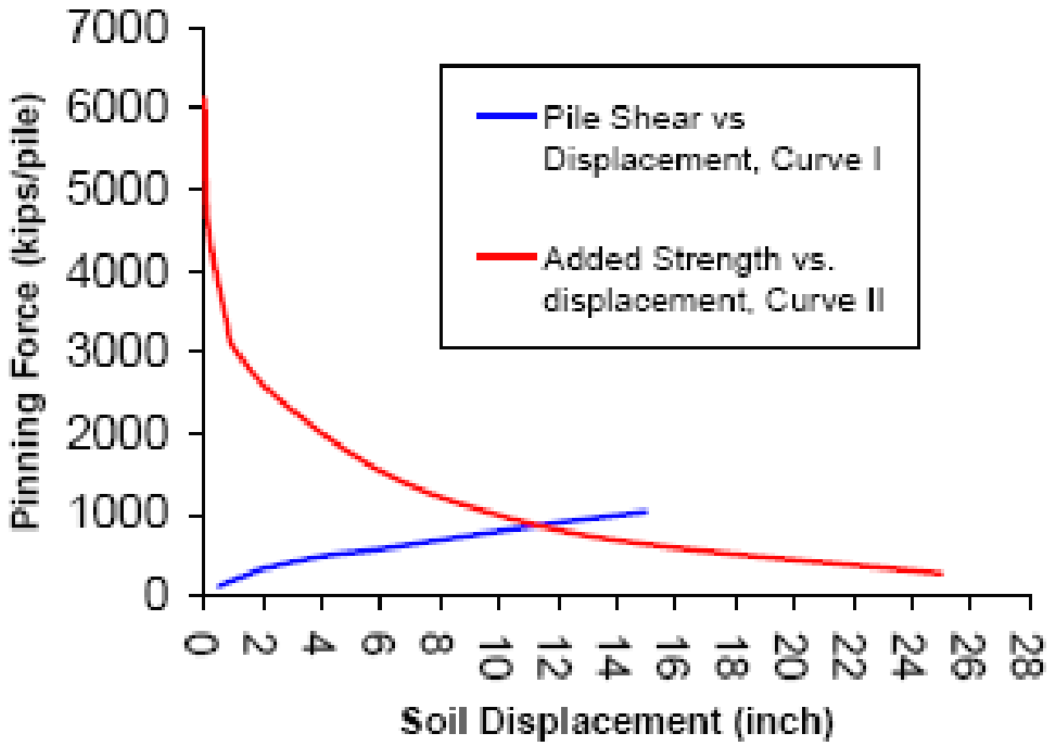

Figure 8-29: Pile Pinning Effect (Design Example III)

8.4.4. Pile Ductility for the Proposed CIDH

The yield, ultimate curvatures and curvature ductility for the proposed pile foundation at abutment 6 is evaluated using XTRACT software program. Figure 8-30 shows the Pile Moment Curvature Diagram, which indicates the capacity of the pile.

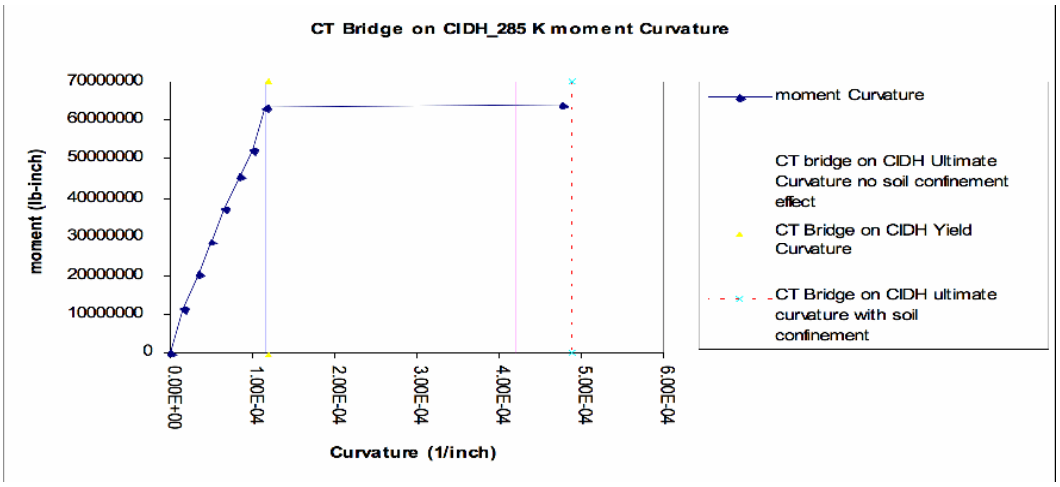

Figure 8-30: Pile Moment-Curvature Diagram (Design Example III)

8.4.5. Pile Response due to Lateral Demand

The lateral demand using 12 inch displacement (the value found from step 3 above) is used as the soil movement and kinematic displacement demand to assess the pile response for abutment 6. LPILE5 program is used to evaluate and bending moment along the CIDH pile. Figures 8-31 and 8-32 show the pile response.

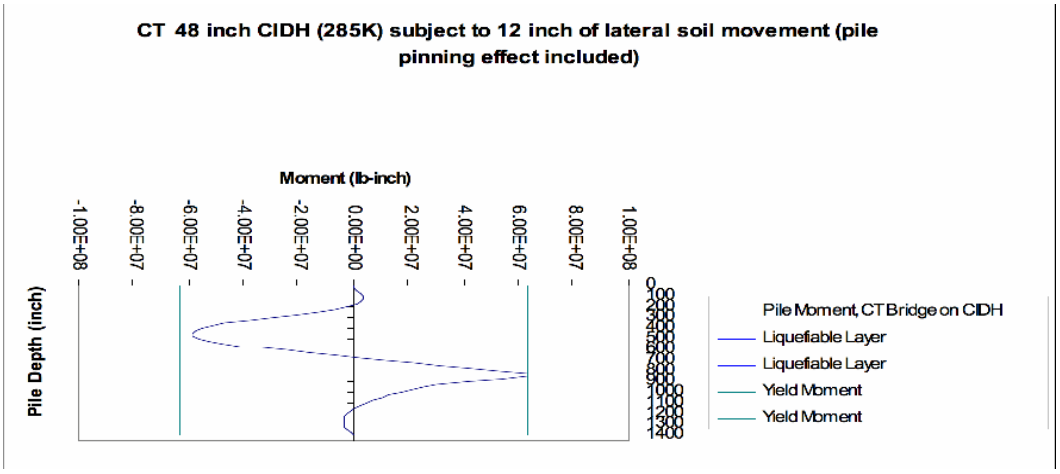

Figure 8-31: Pile Moment Response (Design Example III)

On the demand side, the following (Figure 8-32) shows the pile curvature response of the 117 feet long, 48 inch diameter CIDH pile due to 12 inch of lateral spread displacement of the upper crust over the 20 feet thick liquefiable soil.

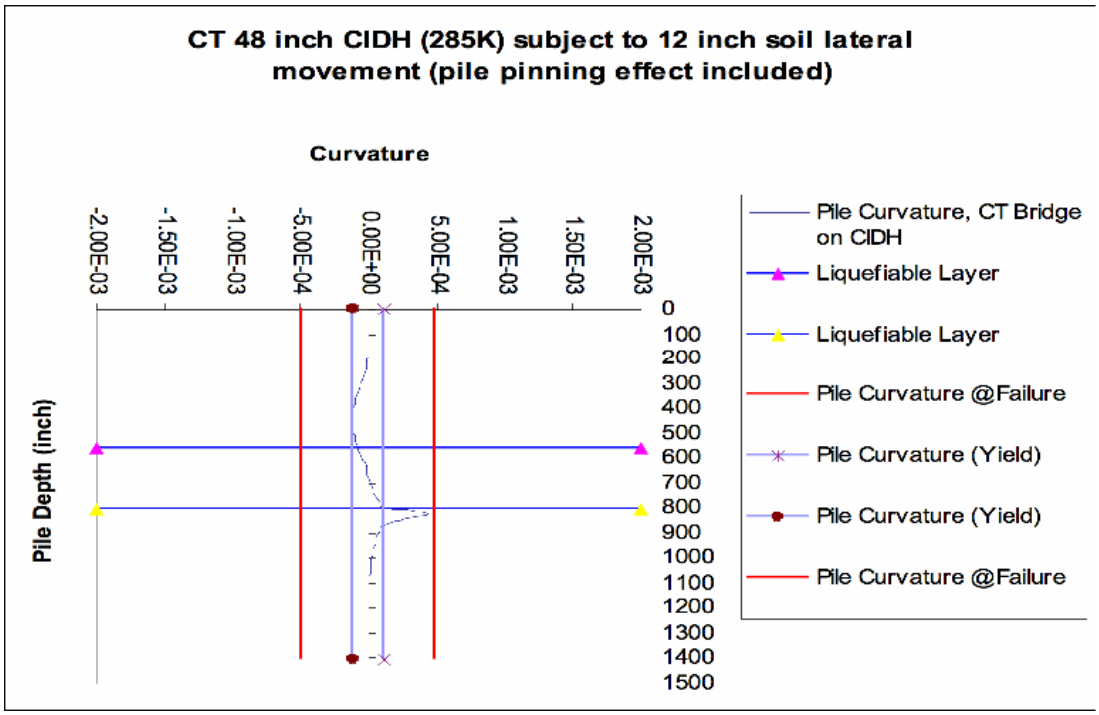

Figure 8-32: Pile Curvature Response (Design Example III)

As shown above, the CIDH pile would undergo plastic hinging at a point immediately below the liquefiable layer. However, the pile curvature demand would not exceed its ultimate curvature capacity value.

8.4.6. Sensitivity Analysis

Sensitivity analysis is performed in terms of liquefaction layer thickness and its impact on the pile response.

8.4.6.1. Liquefaction Layer Thickness, Deep Liquefaction

The response of pile due to lateral spread was analyzed by assessing how the liquefaction layer thickness impacts the response. The original liquefiable layer thickness of 20 feet was reduced to 15 feet, 10 feet, 5 feet, 4 feet, 3 feet and 2 feet. The elevation at the top of the lateral spread remained unchanged. No inertia loading was considered. Only the kinematic loading on the pile fixed at the top was considered.

LIQUEFIABLE LAYER THICKNESS: 20 feet, Depth of Liquefaction (47 to 67 feet)

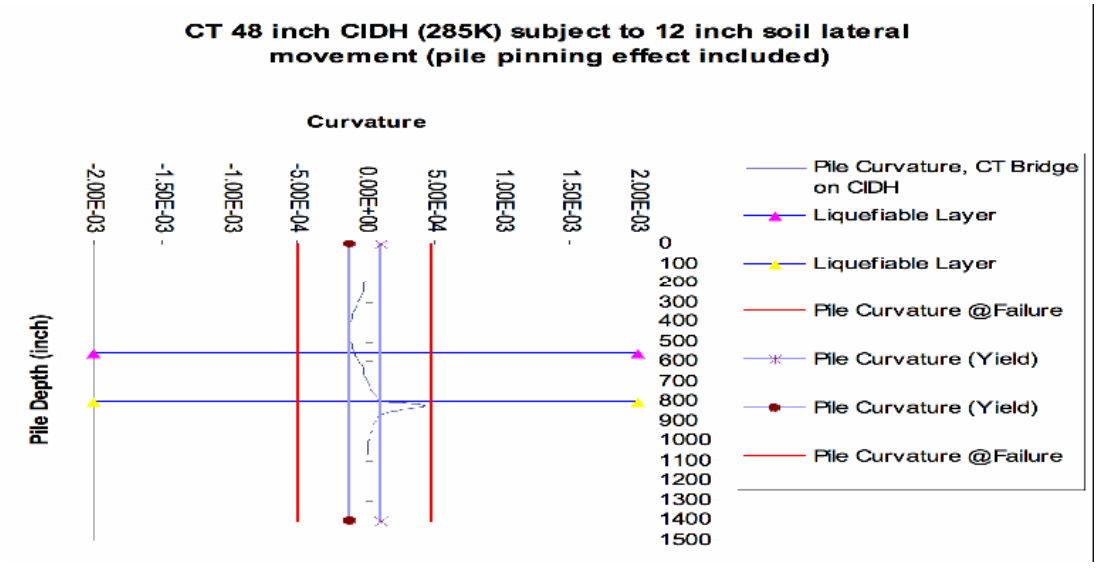

Figure 8-33: Pile Curvature Response (Design Example III)

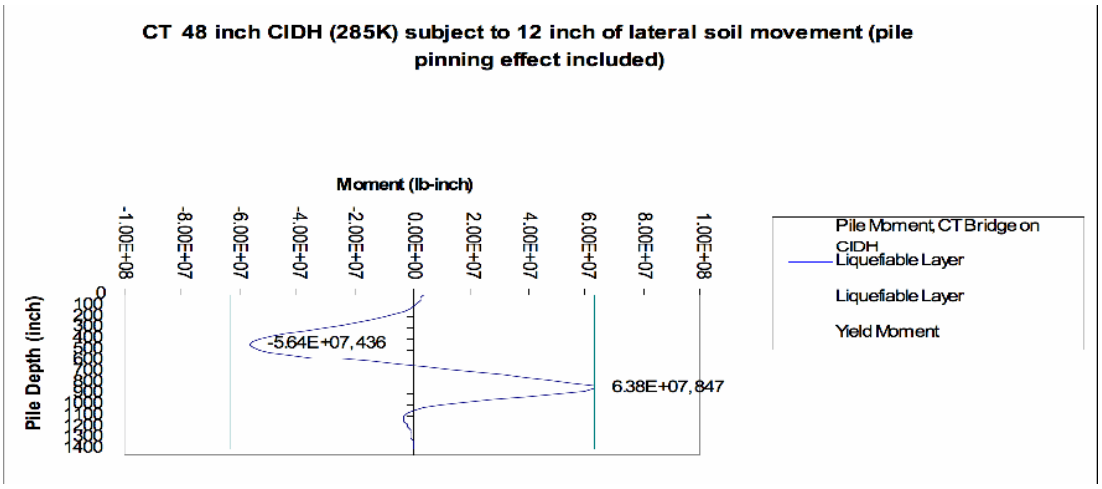

Figure 8-34: Pile Moment Response (Design Example III)

LIQUEFIABLE LAYER THICKNESS: 15 feet, Depth of Liquefaction (47 to 62 feet)

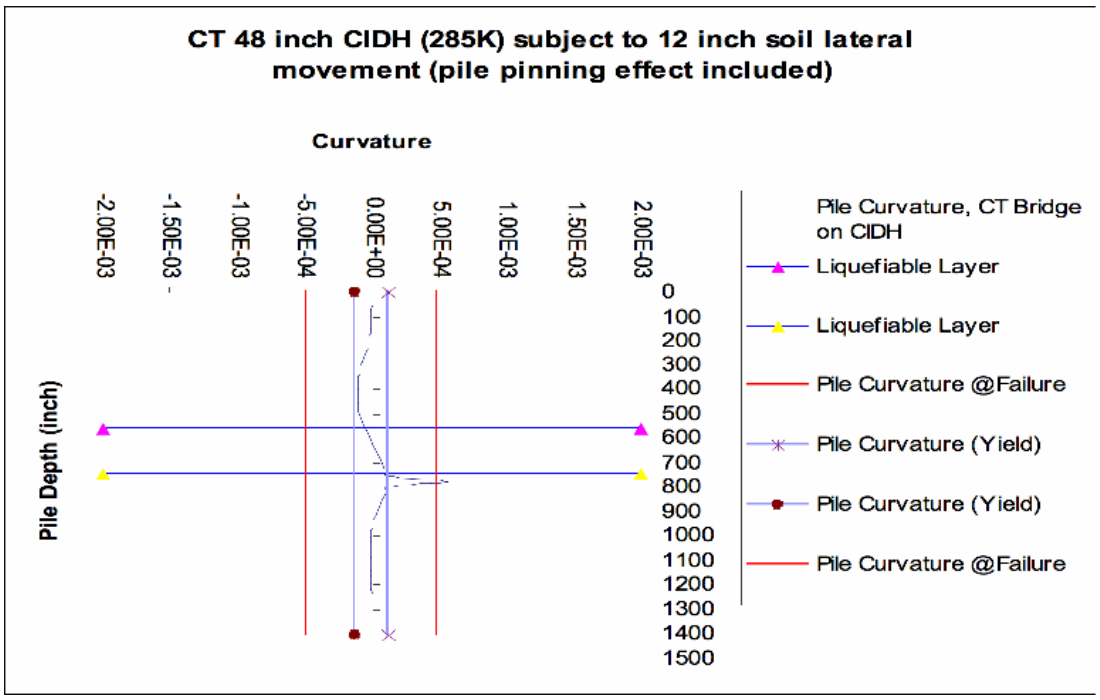

Figure 8-35: Pile Curvature Response (Design Example III)

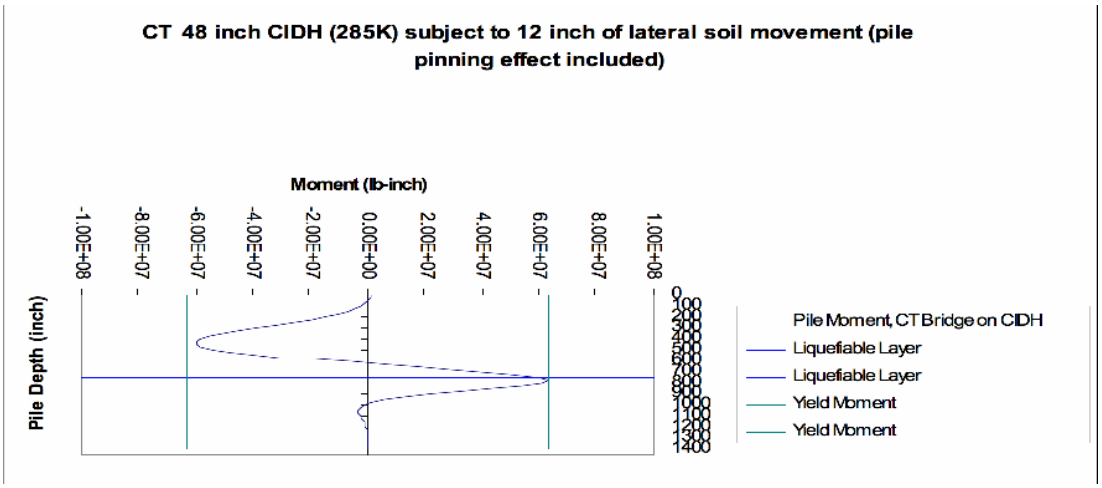

Figure 8-36: Pile Moment Response (Design Example III)

LIQUEFIABLE LAYER THICKNESS: 10 feet, Depth of Liquefaction (47 to 57 feet)

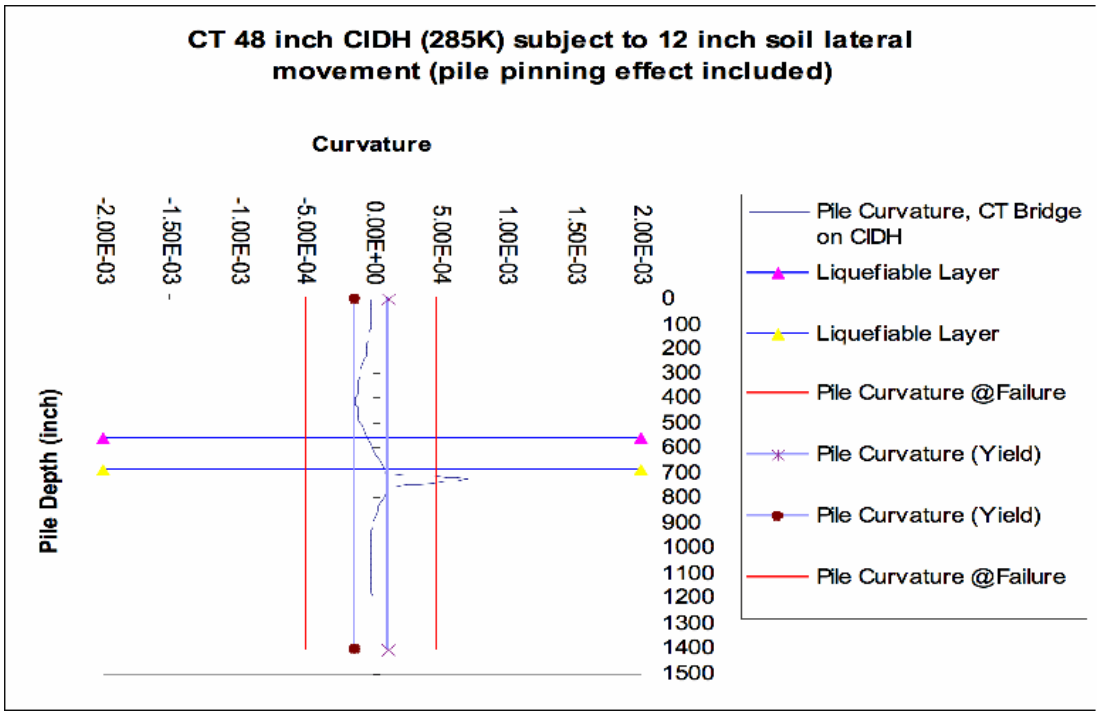

Figure 8-37: Pile Curvature Response (Design Example III)

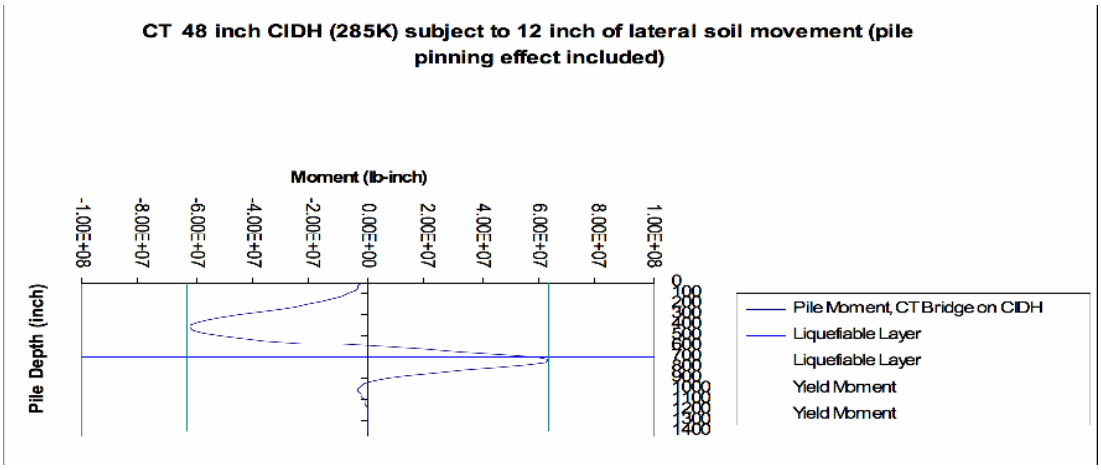

Figure 8-38: Pile Moment Response (Design Example III)

LIQUEFIABLE LAYER THICKNESS: 5 feet, Depth of Liquefaction (47 to 52 feet)

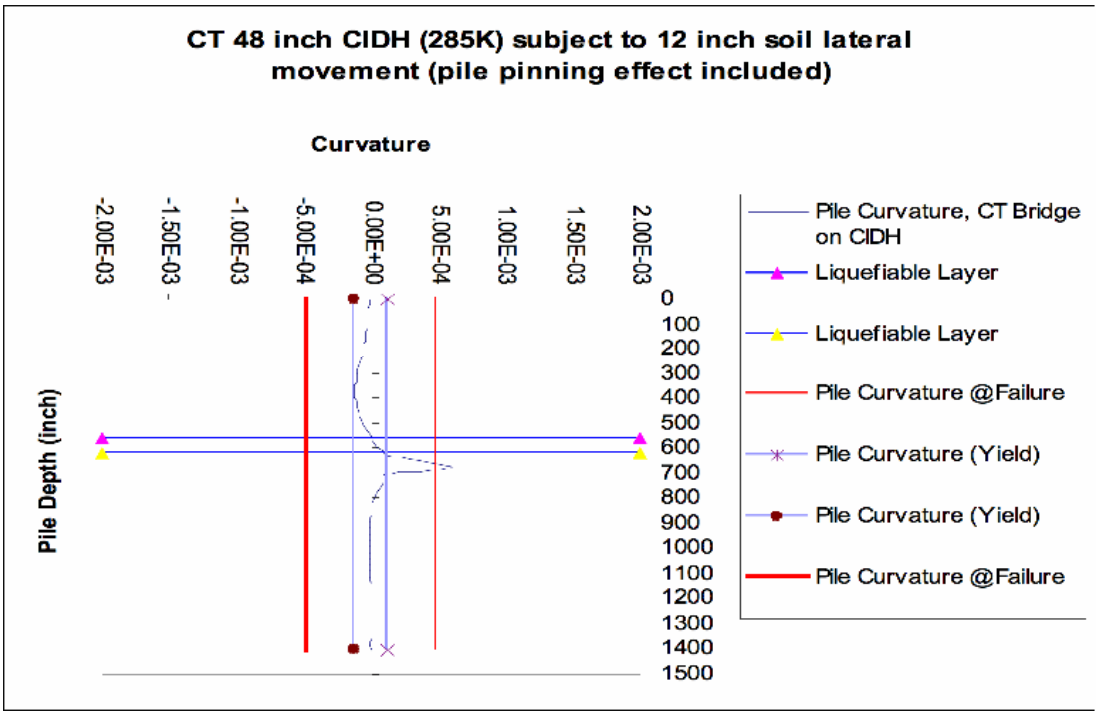

Figure 8-39: Pile Curvature Response (Design Example III)

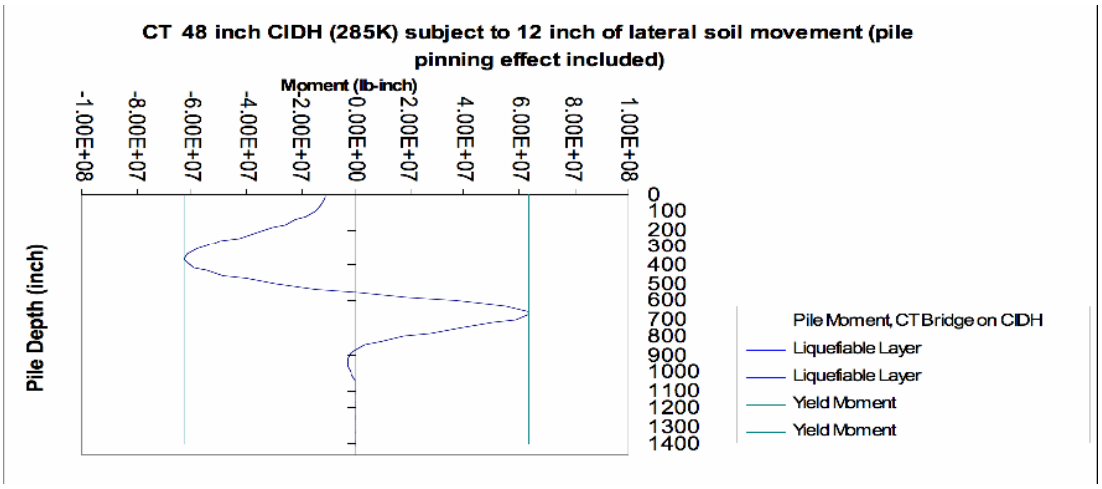

Figure 8-40: Pile Moment Response (Design Example III)

LIQUEFIABLE LAYER THICKNESS: 4 feet, Depth of Liquefaction (47 to 51 feet)

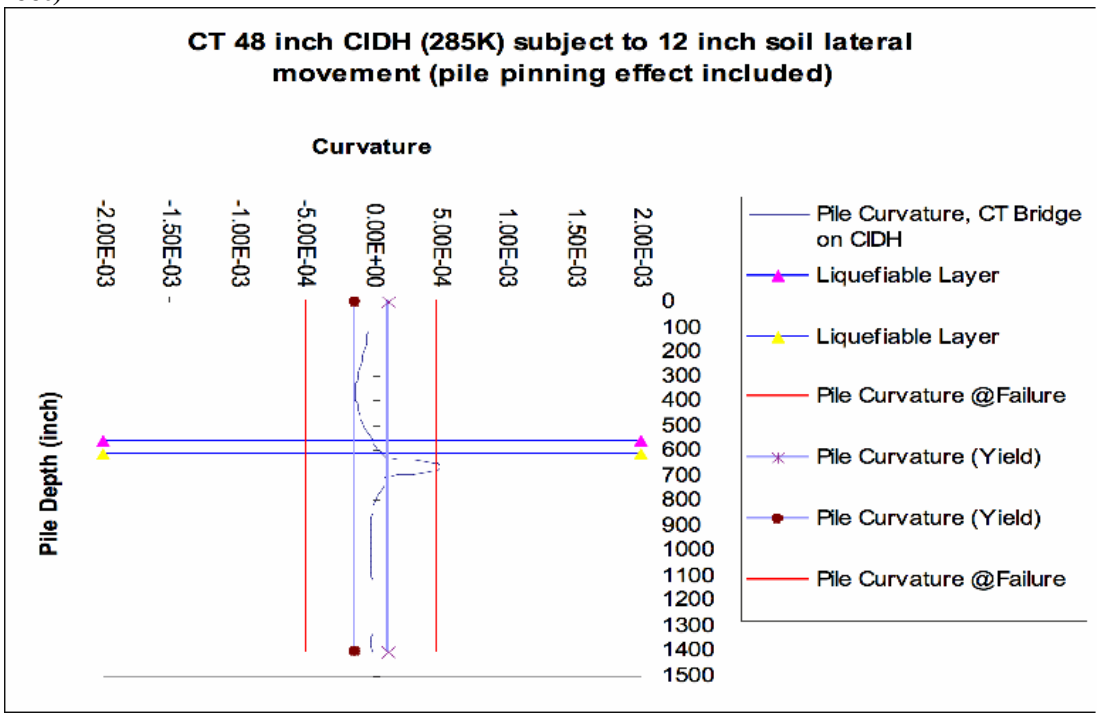

Figure 8-41: Pile Curvature Response (Design Example III)

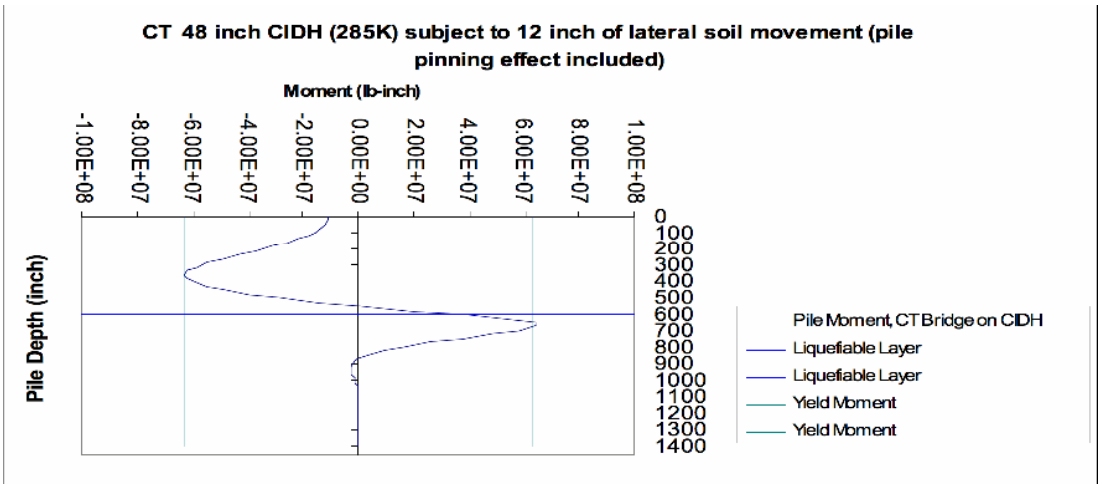

Figure 8-42: Pile Moment Response (Design Example III)

LIQUEFIABLE LAYER THICKNESS: 3 feet, Depth of Liquefaction (47 to 50 feet)

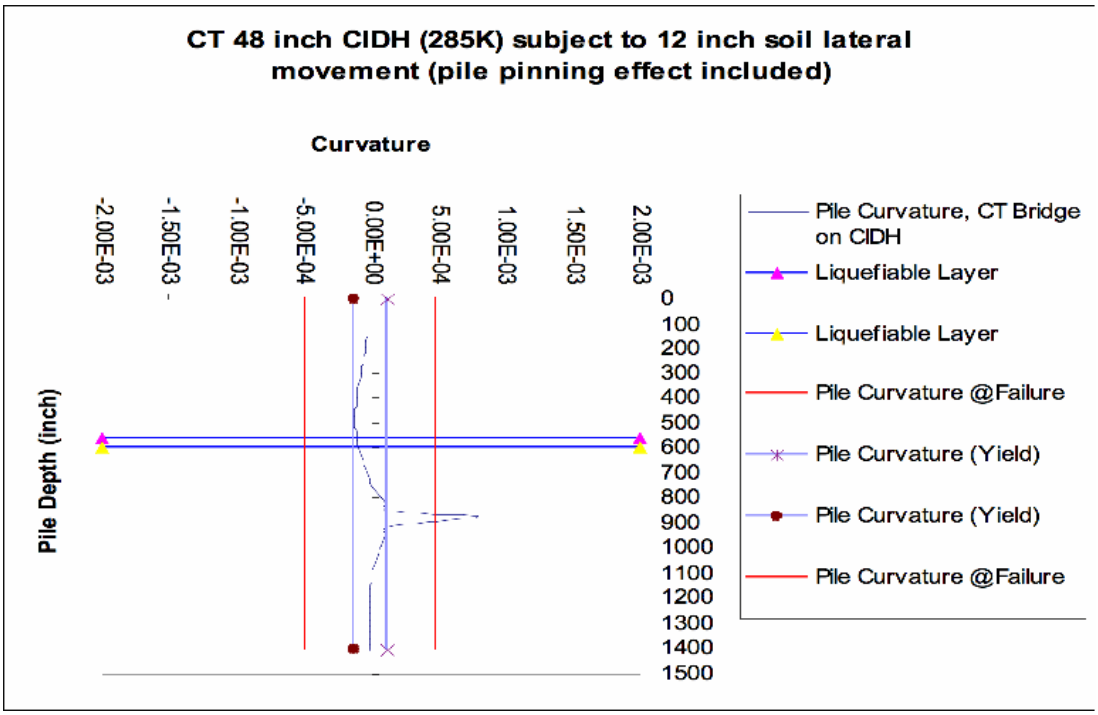

Figure 8-43: Pile Curvature Response (Design Example III)

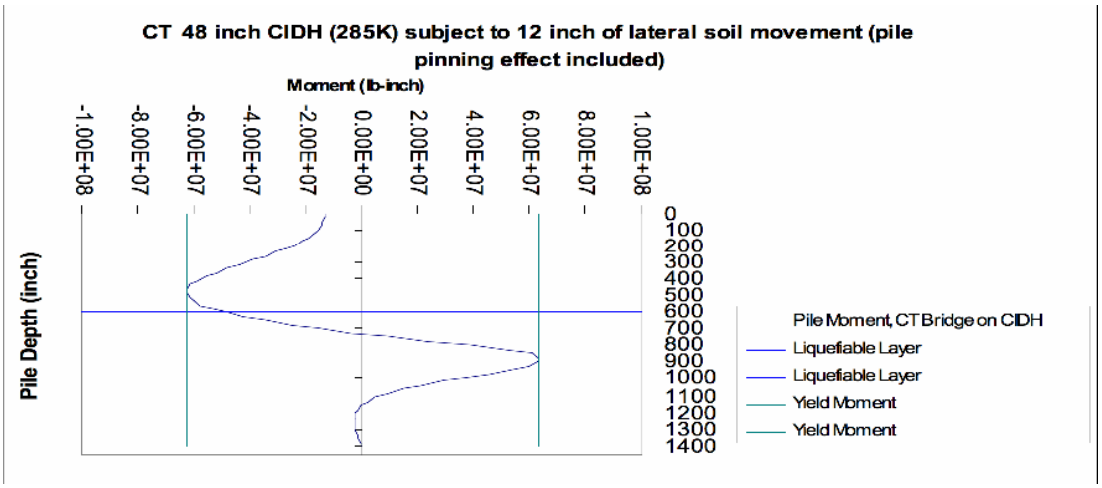

Figure 8-44: Pile Moment Response (Design Example III)

LIQUEFIABLE LAYER THICKNESS: 2 feet, Depth of Liquefaction (47 to 49 feet)

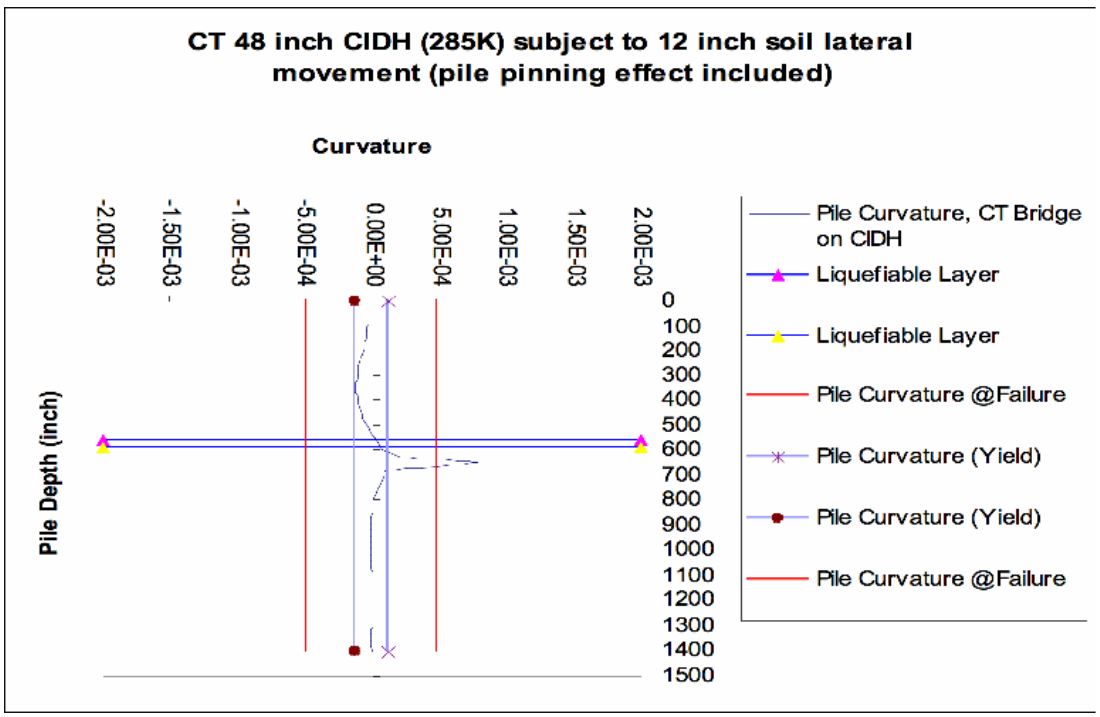

Figure 8-45: Pile Curvature Response (Design Example III)

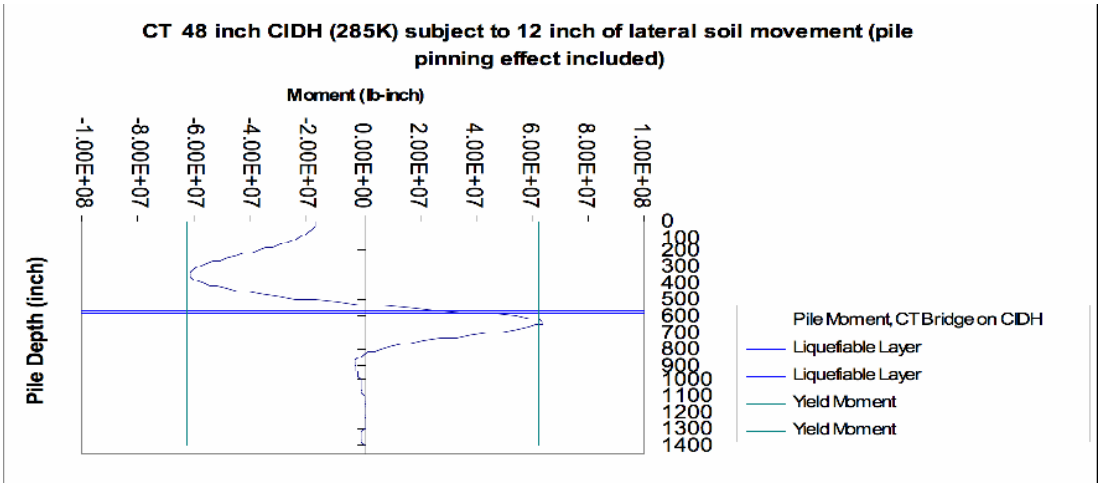

Figure 8-46: Pile Moment Response (Design Example III)

The following (figure 8-47) show the results of the pile response in terms of curvature demand, based on the thickness of the liquefiable layer.

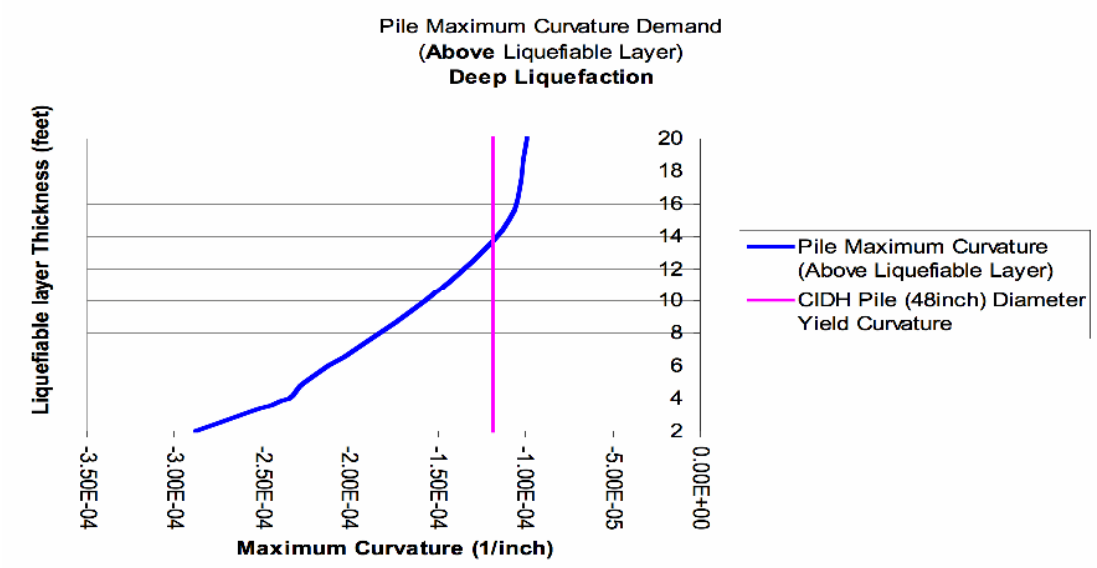

Figure 8-47: Pile Curvature Demand Based on Liquefiable Layer Thickness (Design Example III)

8.4.7. Conclusion

The proposed foundation for a multi-span bridge structure consisting of a 48 inch diameter CIDH pile was evaluated subject to lateral spread loading. The embankment displacement during the design earthquake was evaluated. Pile pinning effect considering the pile resistance to the embankment displacement was assessed and the corresponding pile response (demand) was found. The lateral demand using the newly reduced free field (reduction due to the pining effect) displacement is compared to the lateral capacity of the pile: The latter being a structure characteristic of the pile. It is important to note that effect of "pile pinning" in reducing the impact of the soil movement due to lateral spread is significant. However, despite this reduction, the piles at the abutment will yield and form plastic hinge at the upper (for liquefaction layer thickness of 14 feet and less) and lower sections (at all liquefaction thicknesses) of the pile. The pile will form plastic hinges but will not collapse since the curvature demand does not exceed the ultimate curvature capacity. The variance in liquefiable layer thickness, (with the base of the liquefiable layer remaining unchanged) does impact the pile curvature response. The maximum curvature value increases as the liquefiable layer thickness decreases.

8.5. Bridge Structure (Design Example IV)

The bridge consists of a sixteen span, prestressed and reinforced concrete box girder bridge structure. During the retrofit, the author considers the bent 15 to be

seismically retrofitted with 30 feet long, 24 inch diameter CISS piles as an alternative, subject to 500 kips of axial load.

8.5.1. Liquefaction/Lateral Spread and Bridge Bent Stability

At bent 15 of the bridge structure, the soil layer underlying the bent embankment will liquefy during the design earthquake. (Magnitude of 7.0 and Peak Horizontal Ground Acceleration of 0.5 g). The design soil parameters for both liquefiable and non-liquefiable layers are estimated by correlating the Standard Penetration Tests and using the Seed-Harder graph. The slope stability (SLIDE program) performed for the embankment for the bent, indicates that during the design earthquake the embankment is not stable and is subject to 50 inches of permanent displacement, using the Newmark method, corresponding to a value of $k_y/k_{max} = 0.023$ (Martin and Qiu Chart). Figure 8-48 shows the failure surface found under pseudo-static slope stability during the design earthquake. The generalized subsurface soil conditions where the bent piles are embedded consist of a three layer system of top non-liquefiable crust layer (192 inch thick), the middle liquefiable layer (108 inch thick) and the bottom non liquefiable layer (exceeding 50 feet).

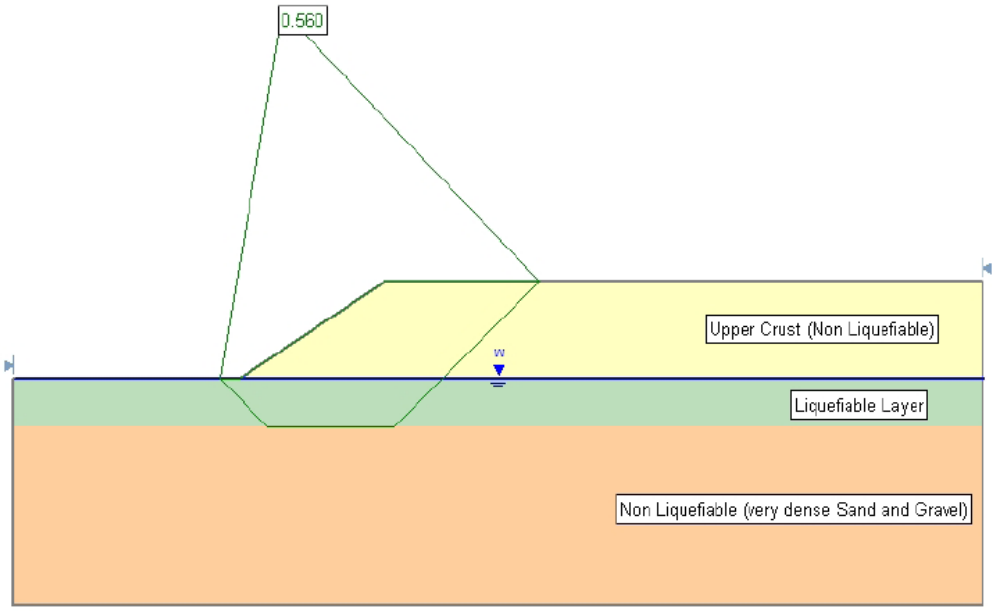

Figure 8-48: Bridge Bent Gross Stability During Earthquake (Design Example IV)

It is concluded that the embankment is subject to lateral spread during the design earthquake and the pile foundations notably at the bent will be subject to lateral spread loading.

8.5.2. Lateral Demand/Capacity of the Proposed Pile Foundation

The lateral demand on the pile foundation due to the free field movement caused by the lateral spread is evaluated using the LPILE5 software program (ENSOFT). The p-y curves for the subsurface soils were assessed by the program modeling the liquefiable soil as soft clay. The expected free field soil displacement profile due to the lateral spread is included in the process as input into the program.

8.5.3. Pile Pinning Effect

During the lateral spread, the embankment soil is moving toward the piles at bent 15. The piles will resist the movement of the soil by applying shear forces which will counteract the shear forces due to the soil movement along the plane of the failure surface. Therefore these pile applied shear forces resist the free field movement of the soil. The lateral spread loading is evaluated considering this pile pinning effect. A two-front approach is used to assess this pinning effect and its contribution to the lateral spread loading evaluation as follows:

1. Various soil movements are prescribed to the embankment to determine the pile shear forces found due to these prescribed soils movements. LPILE5 was used to incorporate the free field soil movement and to evaluate the corresponding shear forces (pile pinning force) for the bent 15 piles. For each prescribed soil movement a corresponding shear force is found. The soil movements range from 1 to 50 inches and the corresponding pile shear forces range from 28 to 261 kips. The soil displacement prescribed to represent the lateral spread movement is from the ground surface to the bottom of the liquefiable soil layer. The pile shear due to pinning effect corresponds to the maximum pile shear as evaluated by LPILE5. Table 8-7 shows the pile characteristics and the results of the analysis.

LPILE5ANALYSIS (curve I)

Pile Type	Pile Diameter (in)	Pile Length (ft)	Moment of Inertia (in^4)	Modulus of Elasticity(psi)	Soil Displacement (in)[1]	Maximum Pile Shear (kips)[2]
CIIS	24	30	16286	3250000	1	28
CIIS	24	30	16286	3250000	2	44
CIIS	24	30	16286	3250000	4	70
CIIS	24	30	16286	3250000	10	129
CIIS	24	30	16286	3250000	20	173
CIIS	24	30	16286	3250000	40	228
CIIS	24	30	16286	3250000	50	261

1: Soil displacement prescribed to represent the lateral spread movement from the ground surface to the bottom of the liquefiable soil layer
2: Maximum shear force developed by the pile resisting to the prescribed soil movement

Table 8-7: Pile Shear Forces (Design Example IV)

2. To evaluate the corresponding shear forces (pile pinning force) a different approach from the previous one is used. The initial shear strength of 400 psf, which is the residual shear strength of the liquefiable layer along the failure plane, is increased by an arbitrary amount of 150 psf. This increase is designed to incorporate the pile pinning effect and its impact on the embankment movement. The shear force per pile is the product of this increase in cohesion, the length of the failure plane and the pile spacing. The Newmark analysis is performed to evaluate the new embankment displacement using this new shear strength (the residual strength + the increase in shear strength), which results in a higher yield acceleration and a lower displacement. The soil movements range from 50 inch to 0.001 inch. The shear forces range from 111 kips to 1976 kips. Various yield

accelerations are found, resulting in various displacements. Table 8-8 shows the results of the Newmark Analysis approach.

NEWMARK ANALYSIS (Curve II)

Initial Cohesion (psf)[3]	Increase in Cohesion (psf)	Cohesion (psf)[4]	Length of Failure Surface (ft)	Pile Spacing (ft)	Shear Force (kips)[5]	Yield Acceleration (g)	Maximum Peak Ground Acceleration (g)	Displacement (inch)
400	150	550	123	6	111	0.01	0.5	50
400	350	750	123	6	258	0.085	0.5	8
400	550	950	123	6	406	0.168	0.5	2
400	850	1250	244	6	1244	0.275	0.5	0.2
400	1350	1750	244	6	1976	0.409	0.5	0.001

3: Initial cohesion corresponds to the shear strength of liquefiable soil, where the failure surface is located
4: Cohesion corresponds to the shear strength of the liquefiable soil after the increase in cohesion is introduced it is used for the embankment stability and Newmark analysis
5: Shear Force = Increase in cohesion x Length of Failure Surface x Pile Spacing

Table 8-8: Newmark Analysis (Design Example IV)

3. The objective is to assess the pile pinning effect and its role in the lateral spread loading phenomenon. It can be concluded that in order to not violate the compatibility law in displacement, the soil displacement must be equal in both approaches described above. Where the two curves I and II converge, the values for both the actual displacement for the embankment and the pile pinning force (shear force) for the CISS pile for bent 15 are found. The actual free field displacement considering the pile pinning effect is estimated to be 25 inch. Figure 8-49 shows the pile pinning effect.

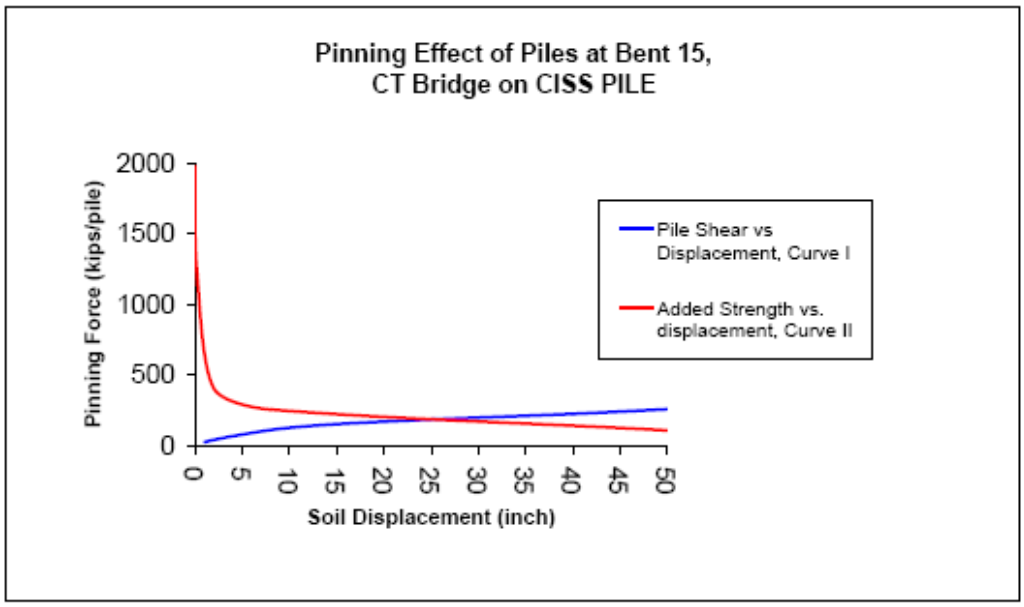

Figure 8-49: Pile Pinning Effect (Design Example IV)

8.5.4. Pile Ductility for the Proposed CIIS Pile

The yield, ultimate curvatures and curvature ductility for the proposed pile foundation at bent 15 is evaluated using XTRACT software program. Figure 8-50 shows the Pile Moment Curvature Diagram, which indicates the capacity of the pile.

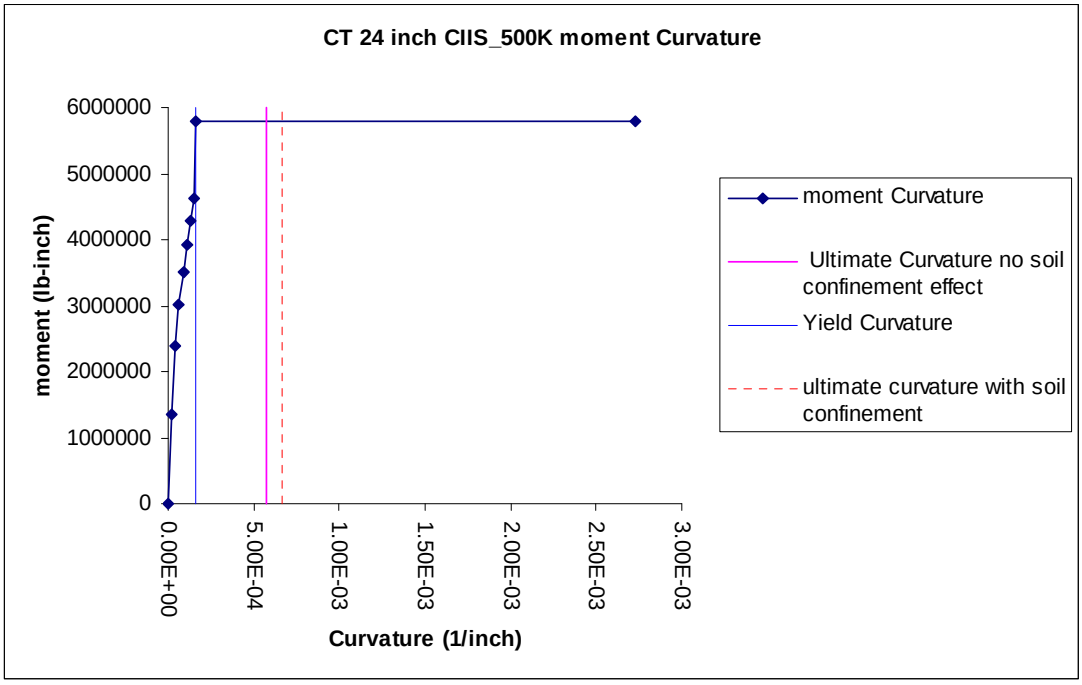

Figure 8-50: Pile Moment-Curvature Diagram (Design Example IV)

8.5.5. Pile Response due to Lateral Demand

The lateral demand using 25 inch displacement is used as the soil movement and kinematic displacement demand to assess the pile response for bent 15. LPILE5 program is used to evaluate the pile response of the 24 inch diameter CISS pile. Figures 8-51 and 8-52 show the pile response in terms of curvature and bending moment.

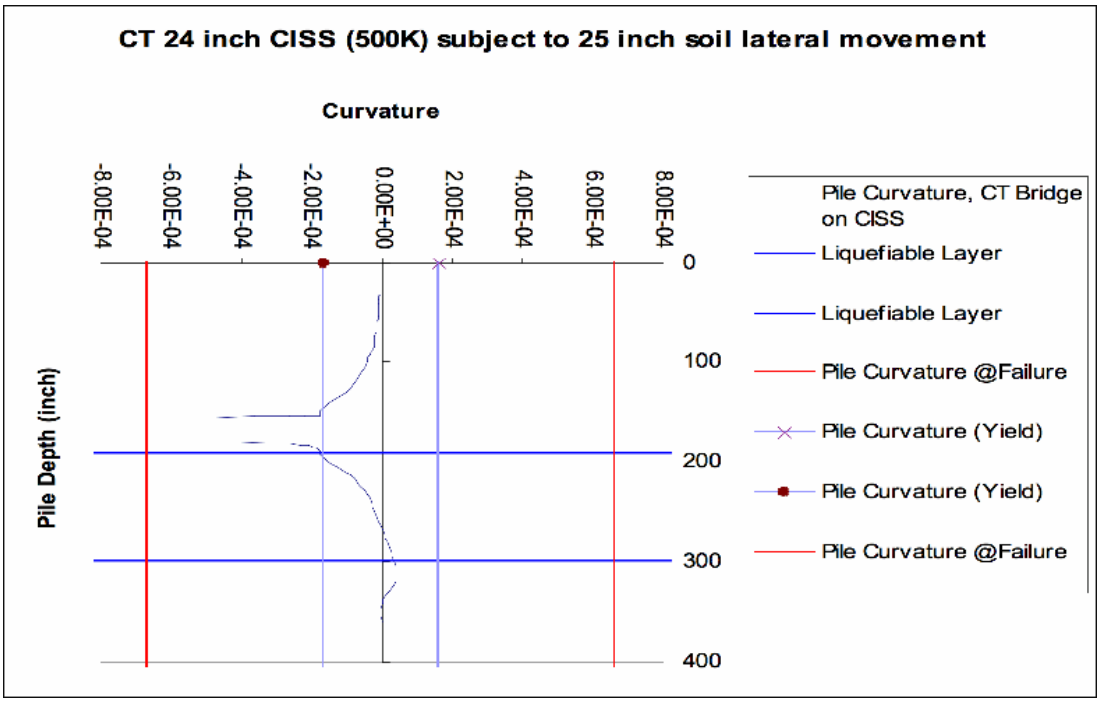

Figure 8-51: Pile Curvature Response (Design Example IV)

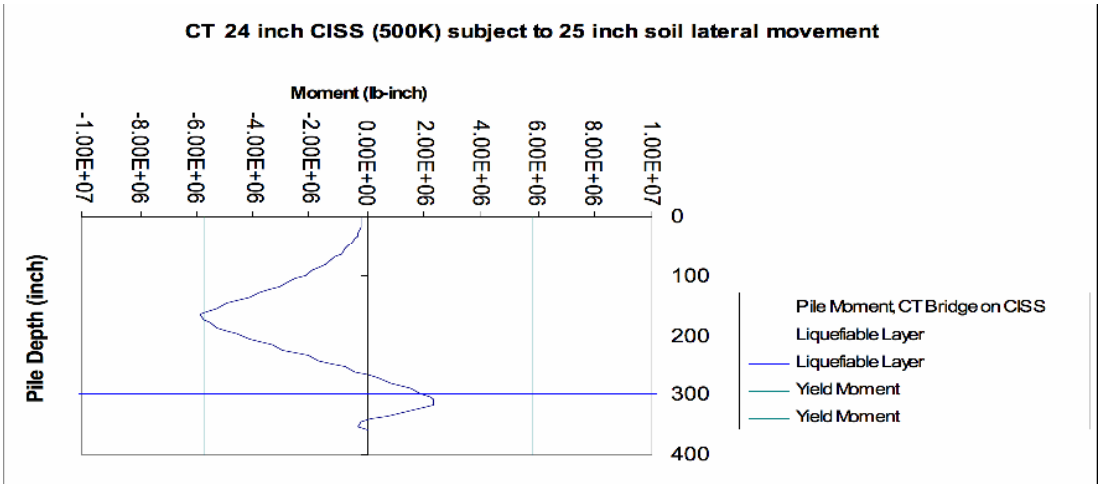

Figure 8-52: Pile Moment Response (Design Example IV)

The following (figures 8-53, 8-54 and 8-55) show the response of the Cast In Steel Shell (CISS) pile due to soil movement for values considerably less than 25 inch:

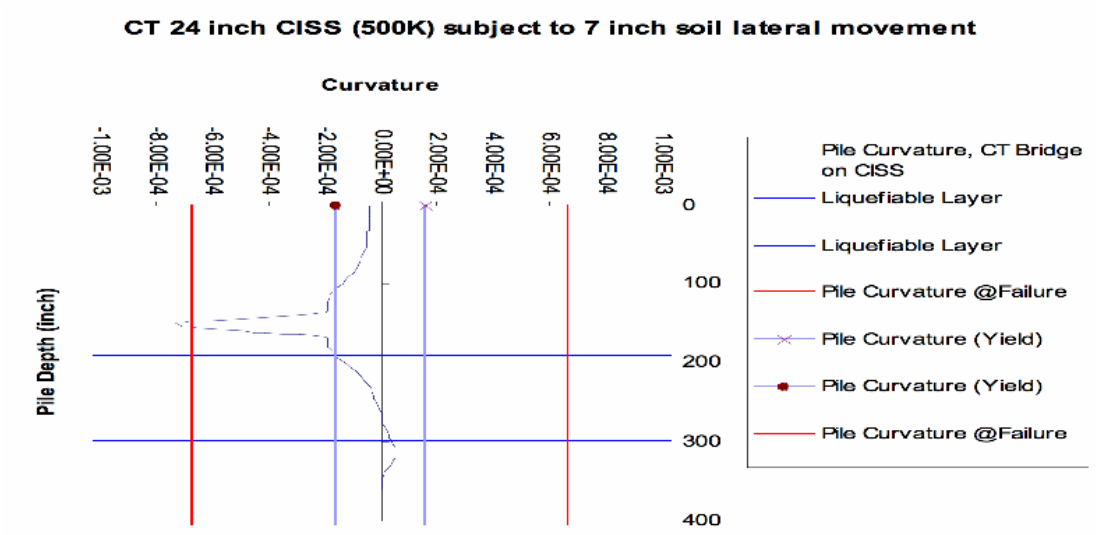

Figure 8-53: Pile Curvature Response (Design Example IV)

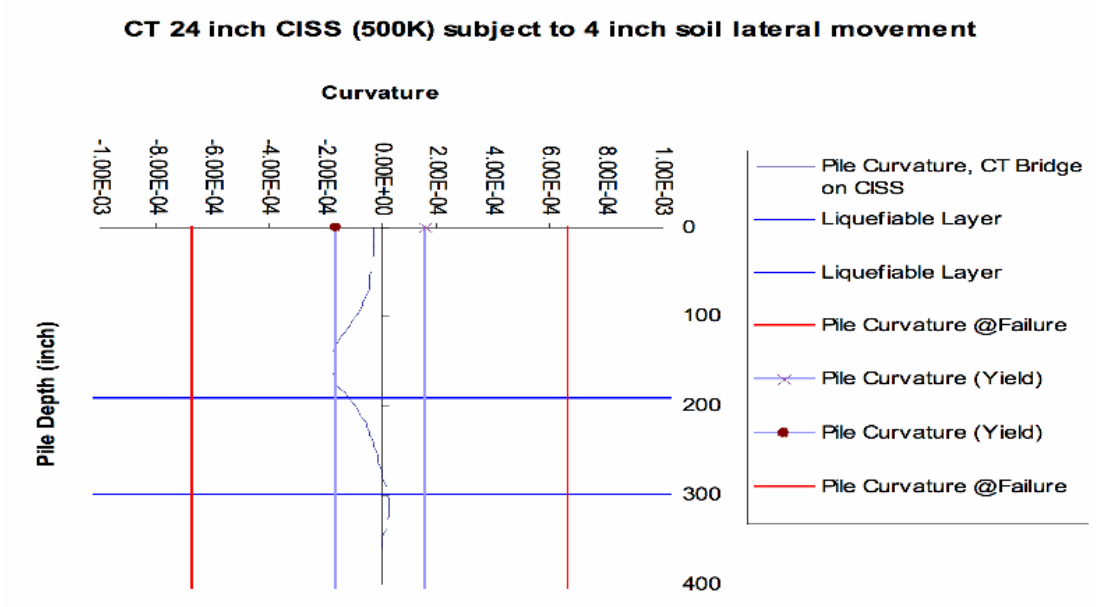

Figure 8-54: Pile Curvature Response (Design Example IV)

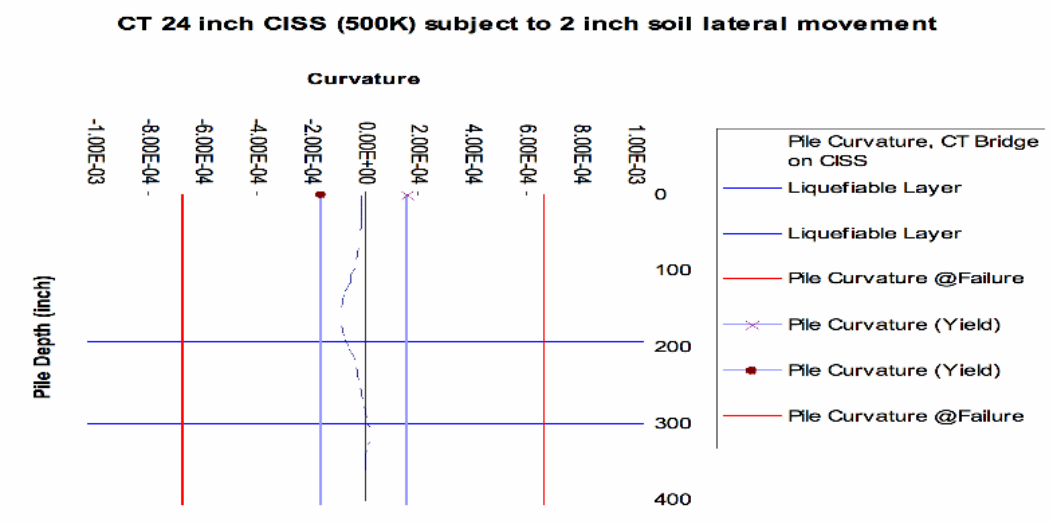

Figure 8-55: Pile Curvature Response (Design Example IV)

On the demand side, the following shows the pile curvature response of the 30 feet long, 24 inch diameter CISS pile due to 25 inch of lateral spread displacement of the upper crust over the 9 feet thick liquefiable soil.

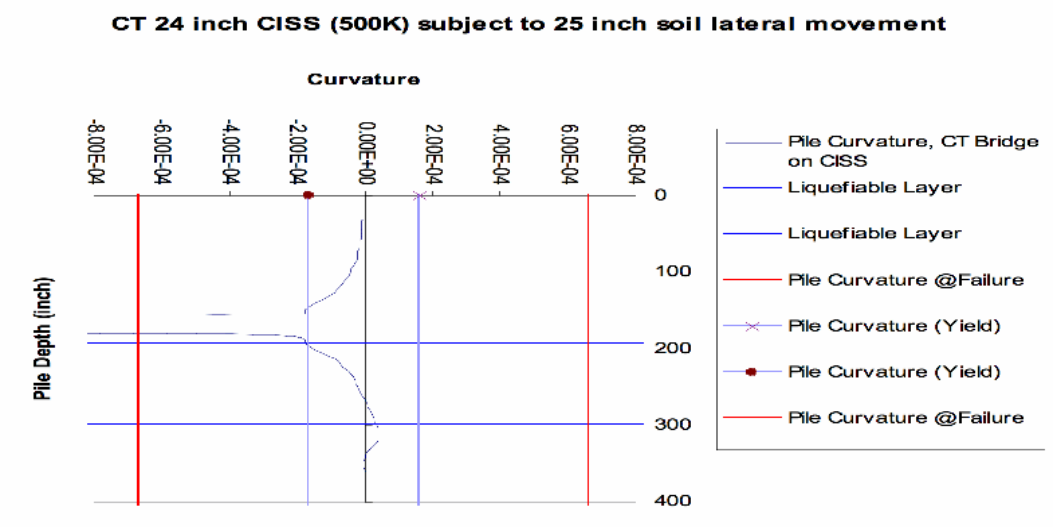

Figure 8-56: Pile Curvature Response (Design Example IV)

As shown above, the CISS pile would undergo plastic hinging and would "fail" at a point above the liquefiable layer. The pile curvature demand exceeds its ultimate curvature capacity value. No plastic hinging and/or failure is observed below the liquefiable layer.

8.5.6. Sensitivity Analysis

Sensitivity analysis is performed in terms of liquefaction layer thickness and its impact on the pile response.

8.5.6.1. Liquefaction Layer Thickness

The response of pile due to lateral spread was analyzed by assessing how the liquefaction layer thickness impacts the response. The original liquefiable layer thickness of 9 feet was reduced to 8 feet,5 feet, 4 feet, and 3 feet. The elevation at the top of the lateral spread remained unchanged. No inertia loading was considered. Only the kinematic loading on the pile fixed at the top was considered.

LIQUEFIABLE LAYER THICKNESS: 9 feet, Depth of Liquefaction (16 to 25 feet)

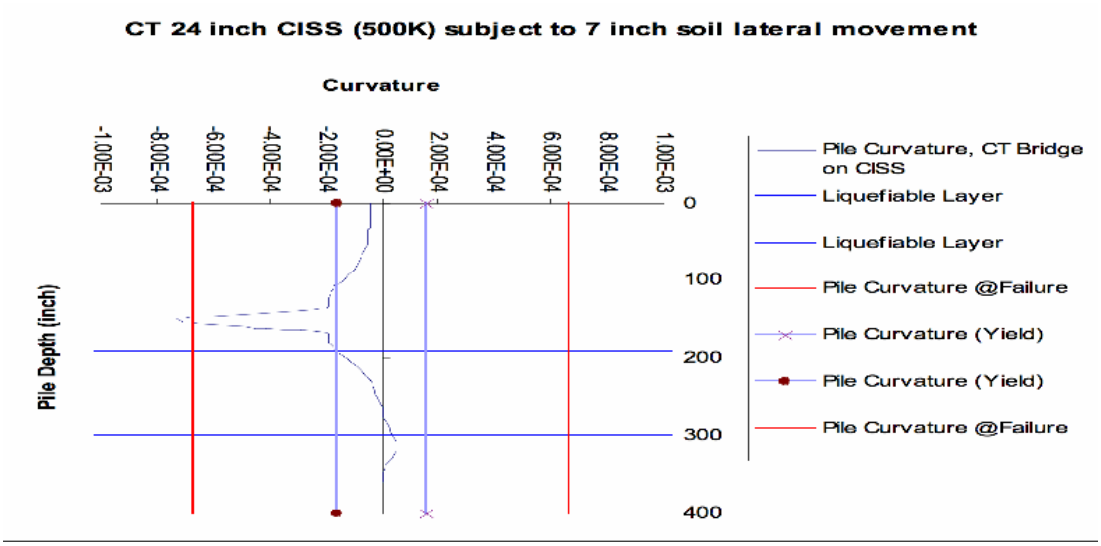

Figure 8-57: Pile Curvature Response (Design Example IV)

LIQUEFIABLE LAYER THICKNESS: 8 feet, Depth of Liquefaction (16 to 24 feet)

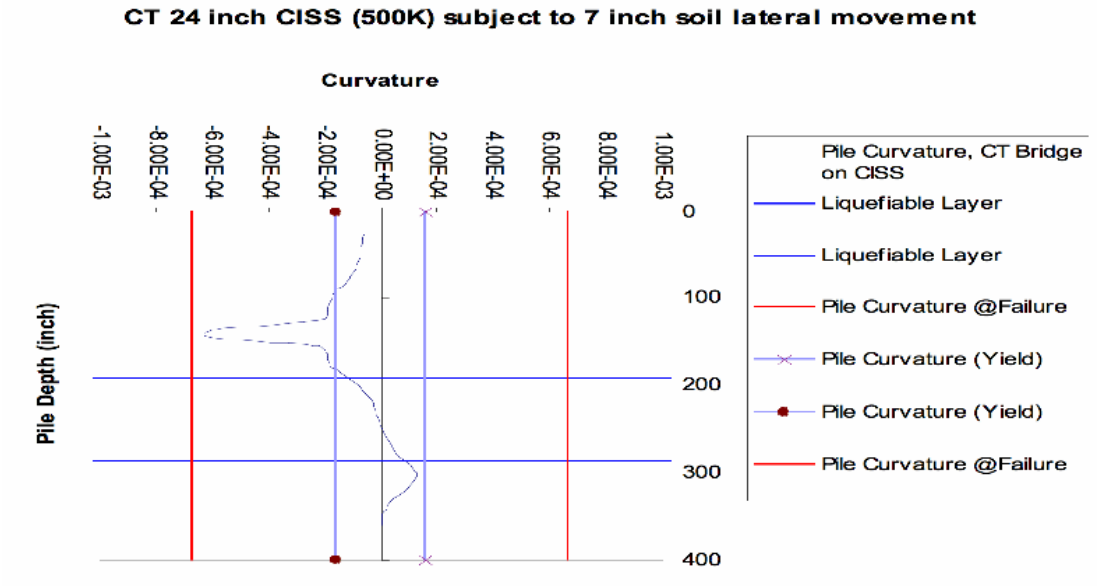

Figure 8-58: Pile Curvature Response (Design Example IV)

LIQUEFIABLE LAYER THICKNESS: 5 feet, Depth of Liquefaction (16 to 21 feet)

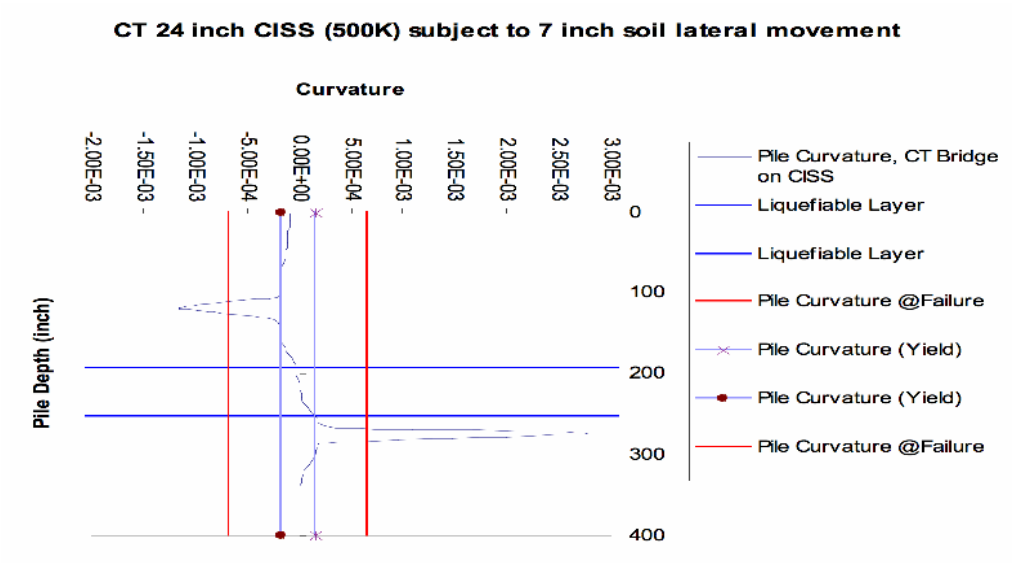

Figure 8-59: Pile Curvature Response (Design Example IV)

LIQUEFIABLE LAYER THICKNESS: 4 feet, Depth of Liquefaction (16 to 20 feet)

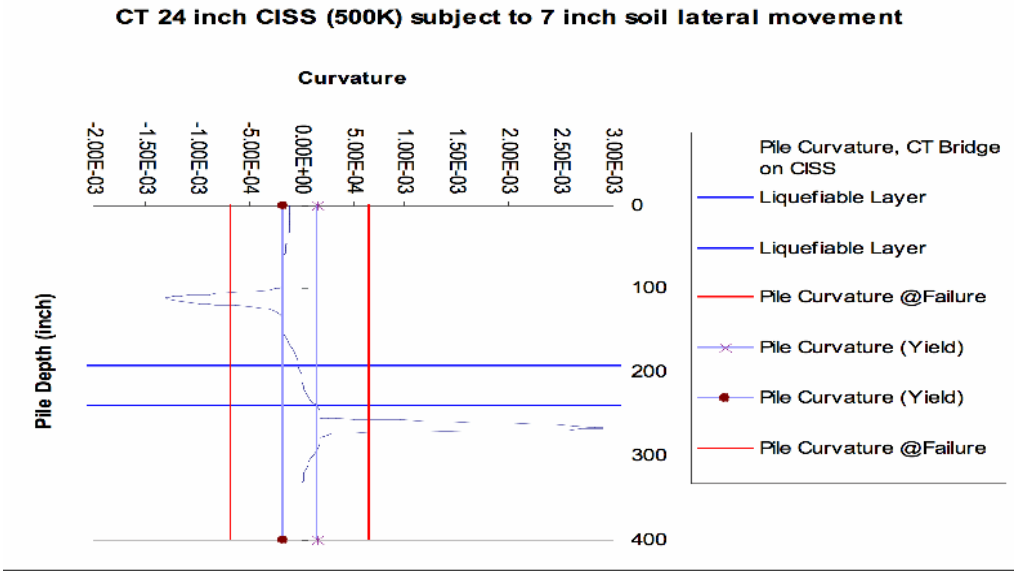

Figure 8-60: Pile Curvature Response (Design Example IV)

LIQUEFIABLE LAYER THICKNESS: 3 feet, Depth of Liquefaction (16 to 19 feet)

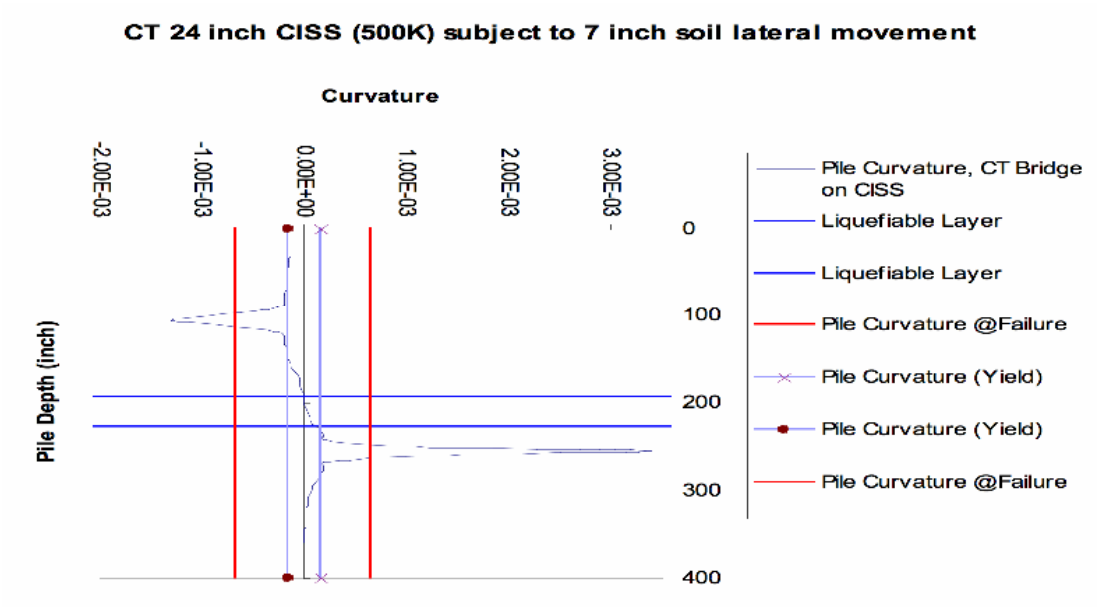

Figure 8-61: Pile Curvature Response (Design Example IV)

The following (Figures 8-62 and 8-63) show the results of the pile response in terms of curvature demand, based on the thickness of the liquefiable layer.

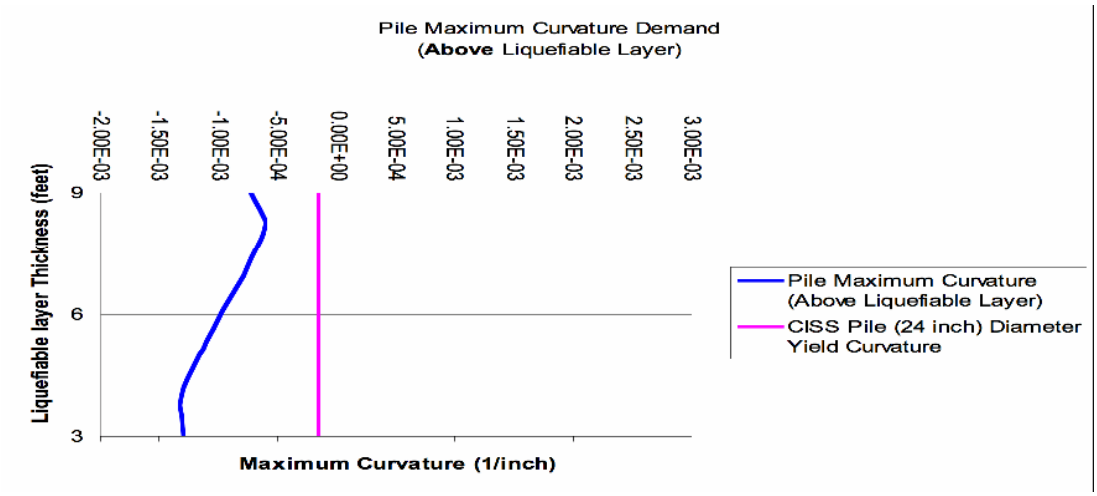

Figure 8-62: Pile Curvature Demand Based on Liquefiable Layer Thickness (Design Example IV)

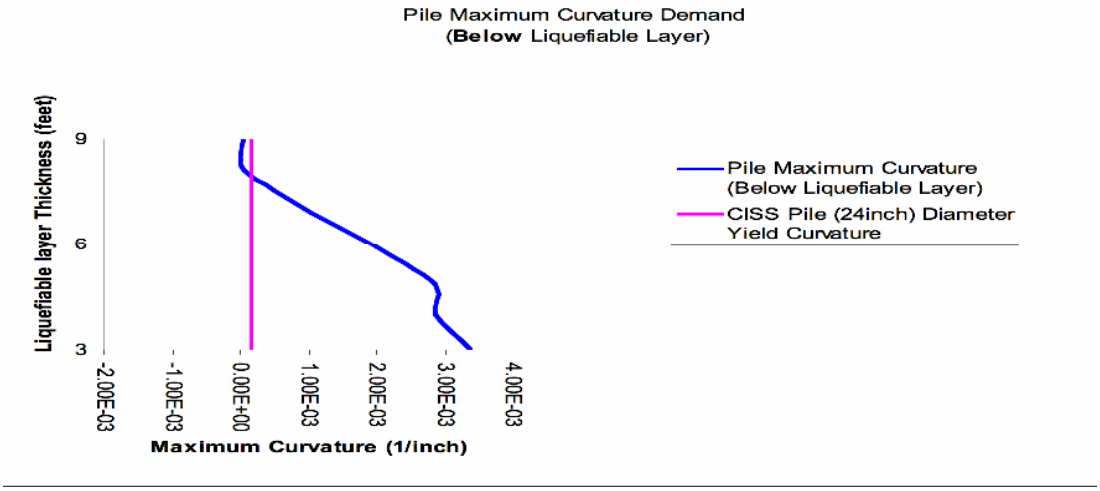

Figure 8-63: Pile Curvature Demand Based on Liquefiable Layer Thickness (Design Example IV)

8.5.7. Conclusion

The proposed foundation for a multi-span bridge structure consisting of 24inch CISS pile was evaluated subject to lateral spread loading. The embankment displacement during the design earthquake was evaluated. Pile pinning effect considering the pile resistance to the embankment displacement was assessed and the corresponding pile response (demand) was found. The lateral demand using the newly reduced free field (reduction due to the pining effect) displacement is compared to the lateral capacity of the pile: The latter being a structure characteristic of the pile. It is important to note that effect of "pile pinning" in reducing the impact of the soil movement due to lateral spread is significant. However, despite this reduction, the piles at the bent will "fail" at the upper sections of the pile, above the 9 feet thick liquefiable layer, since the curvature demand does exceed the ultimate curvature capacity. The reduction in liquefiable layer thickness, (with the top of the liquefiable layer elevation remaining unchanged) does increase the pile curvature demand, detrimental to the pile integrity.

It is also worth noting that the CISS pile would begin undergoing plastic hinging at least at one location along its length, due to soil crust lateral movement of as low as 4 inches.

8.6. Bridge Structure (Design Example V)

The bridge consists of a three span box/bulb-tee girder bridge structure supported by driven 45 ton concrete piles at bents and abutments. Abutment fill placed on the

original ground is 30 feet high. The author considered Caltrans 90 ton pile prestressed precast pile, 15 inch in diameter driven to the design tip elevation resulting in 793 inch long piles, subject to 180 kips of axial load as one of several foundation alternatives for the replacement bridge.

8.6.1. Liquefaction/Lateral Spread and Bridge Abutment Embankment Stability

At abutments 1 and 4 of the bridge structure, some of the underlying soil layers with varying thickness will liquefy during the design earthquake. (Magnitude of 7.0 and Peak Horizontal Ground Acceleration of 0.5 g). The design soil parameters for both liquefiable and non-liquefiable layers are estimated by correlating the Standard Penetration Tests and using the Seed-Harder graph. The slope stability performed for the embankment for both abutments, reveals that during the design earthquake the embankment is not stable and is subject to lateral flow.

Figure 8-64 shows the failure surface found under pseudo-static slope stability during the design earthquake. The generalized subsurface soil conditions where the abutment piles are embedded consist of a three layer system of top non-liquefiable crust layer (468 inch thick), the middle liquefiable layer (20 feet thick) and the bottom non liquefiable layer (exceeding 50 feet).

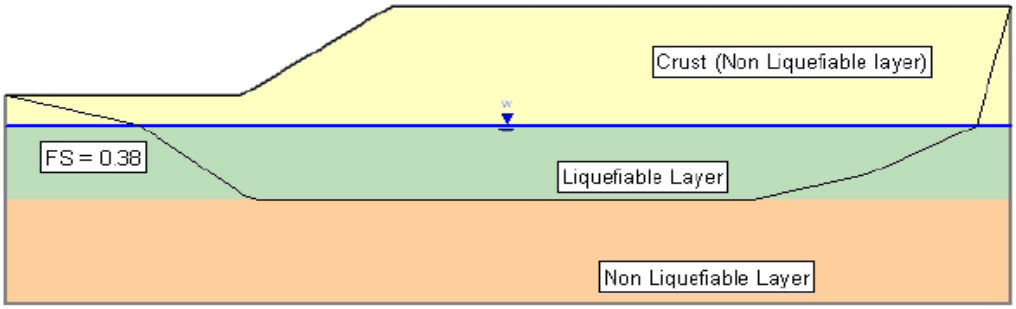

Figure 8-64: Bridge Abutment Gross Stability during Earthquake (Design Example V)

It is concluded that the embankment is subject to lateral spread during the design earthquake and the pile foundations notably at abutment will be subject to lateral spread loading.

8.6.2. Lateral Demand/Capacity of the Proposed Pile Foundation

The lateral demand on the pile foundation due to the free field movement caused by the lateral spread is evaluated using the LPILE5 software program (ENSOFT). The p-y curves for the subsurface soils were assessed by the program modeling the liquefiable soil as soft clay. The expected free field soil displacement profile due to the lateral spread is included in the process as input into the program.

8.6.3. Pile Pinning Effect

The condition at the subject site is a flow liquefaction, hence Newmark method can not be used. However, pinning effect would still have a reducing impact on the soil

crust displacement. It is assumed that the soil would displace a minimum of 12 inches, due to liquefaction during the design earthquake.

8.6.4. Pile Ductility for the Proposed PSPC Pile

The yield, ultimate curvatures and curvature ductility for the proposed pile foundation at abutment 6 is evaluated using XTRACT software program. Figure 8-65 shows the Pile Moment Curvature Diagram, which indicates the capacity of the pile.

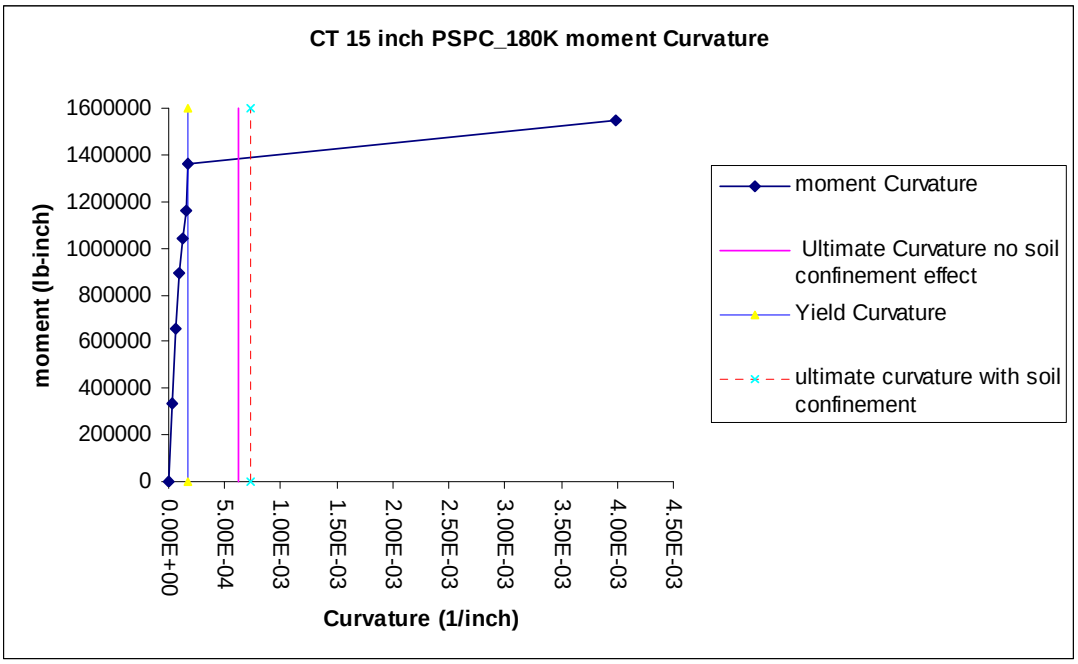

Figure 8-65: Pile Moment-Curvature Diagram (Design Example V)

8.6.5. Pile Response due to Lateral Demand

The lateral demand using 12 inch displacement is used as the soil movement and kinematic displacement demand to assess the pile response for abutment 4. LPILE5 program is used to evaluate the pile response of the 15 inch diameter PSPC pile. Figures 8-66 and 8-67 show the pile response in terms of curvature and bending moment.

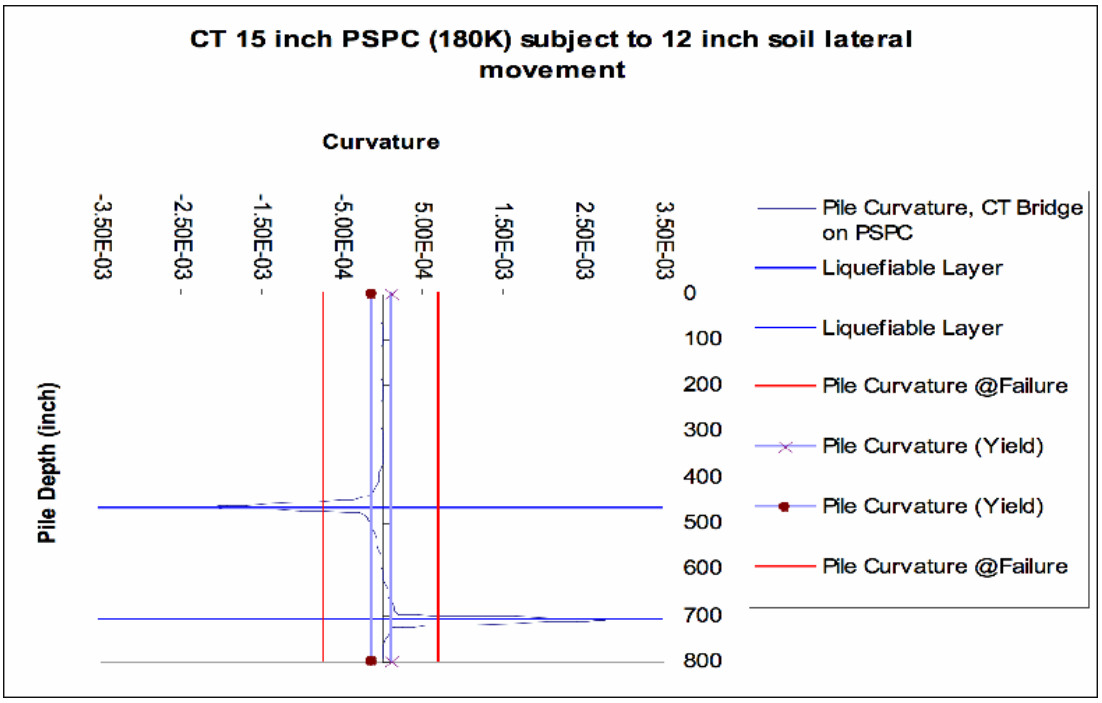

Figure 8-66: Pile Curvature Response (Design Example V)

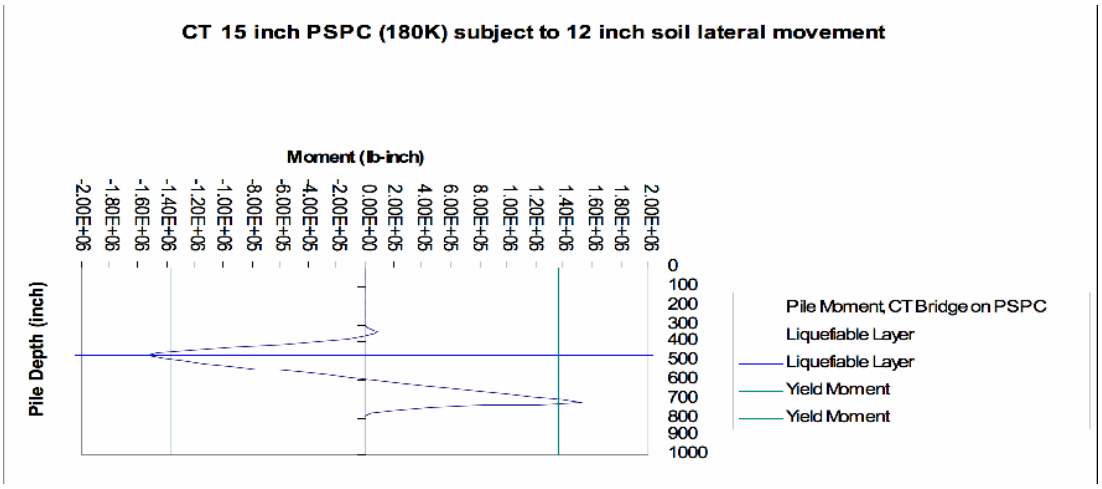

Figure 8-67: Pile Moment Response (Design Example V)

The following (figure 8-68 through Figure 8-71) show the response of the prestressed precast driven concrete pile due to soil movement for values considerably less than 12 inch:

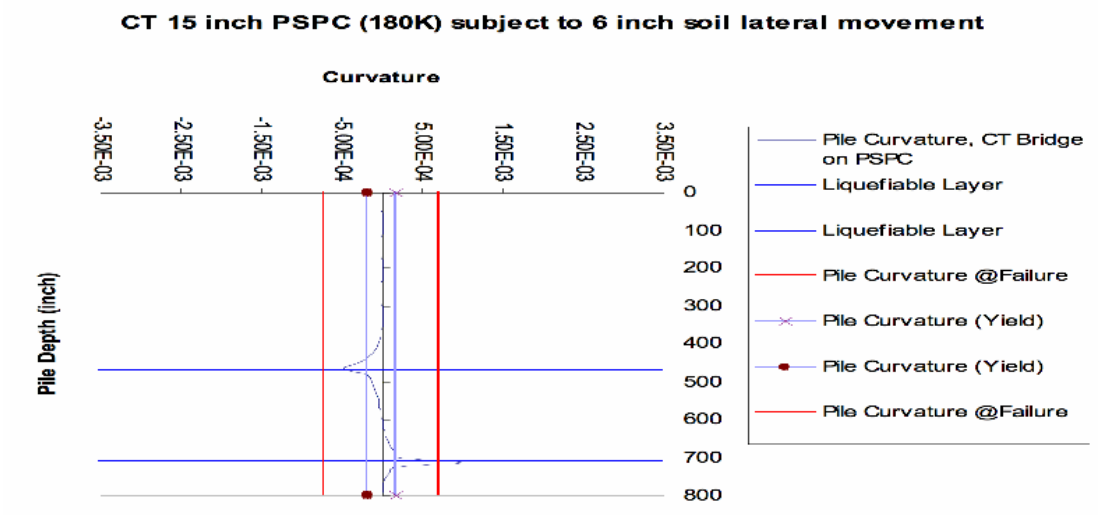

Figure 8-68: Pile Curvature Response (Design Example V)

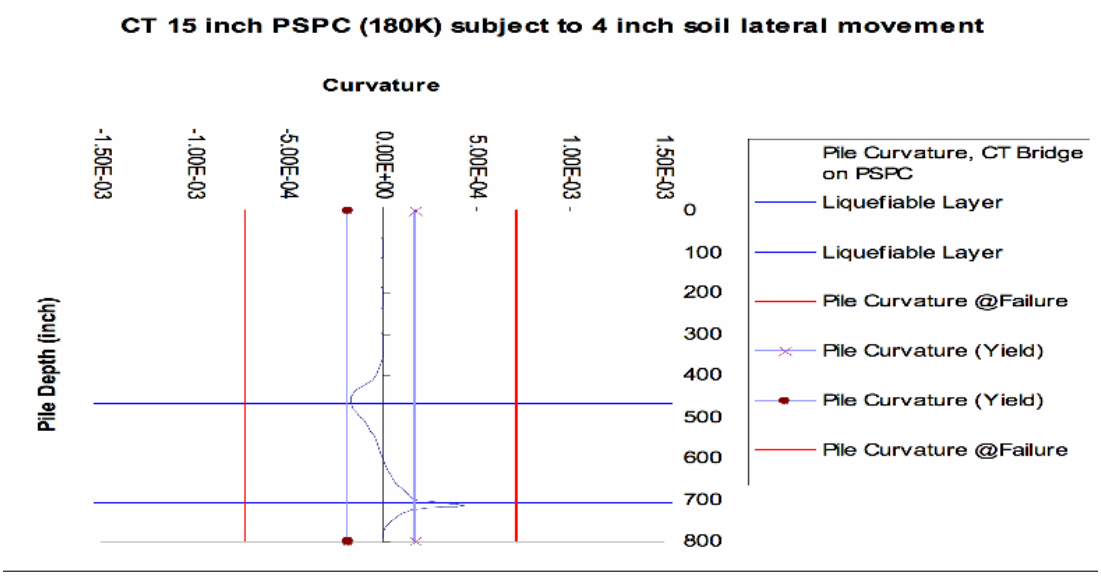

Figure 8-69: Pile Curvature Response (Design Example V)

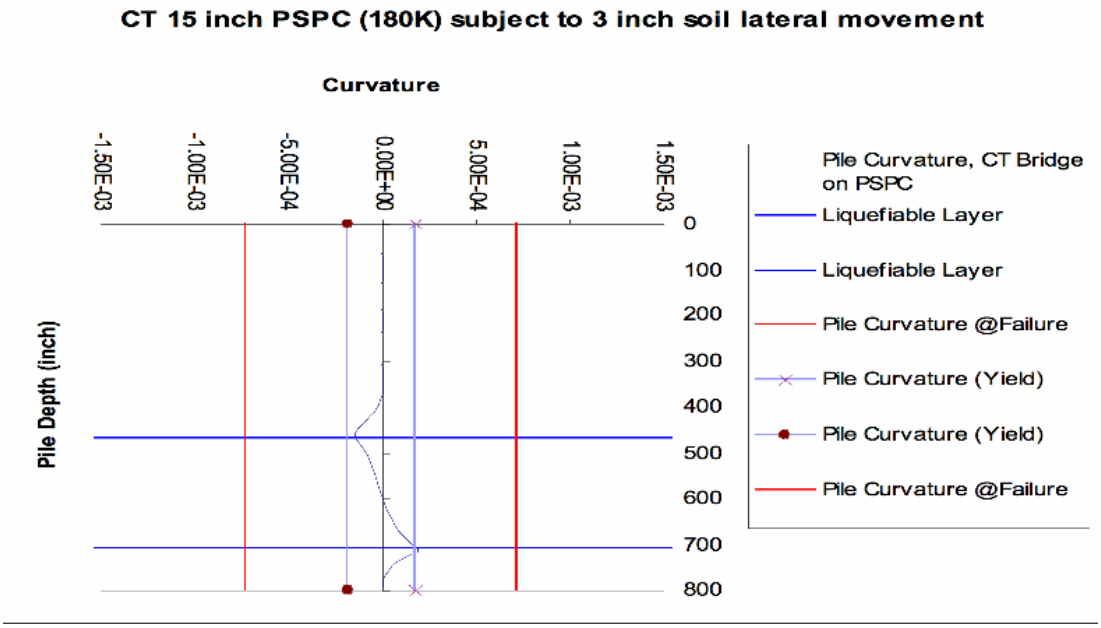

Figure 8-70: Pile Curvature Response (Design Example V)

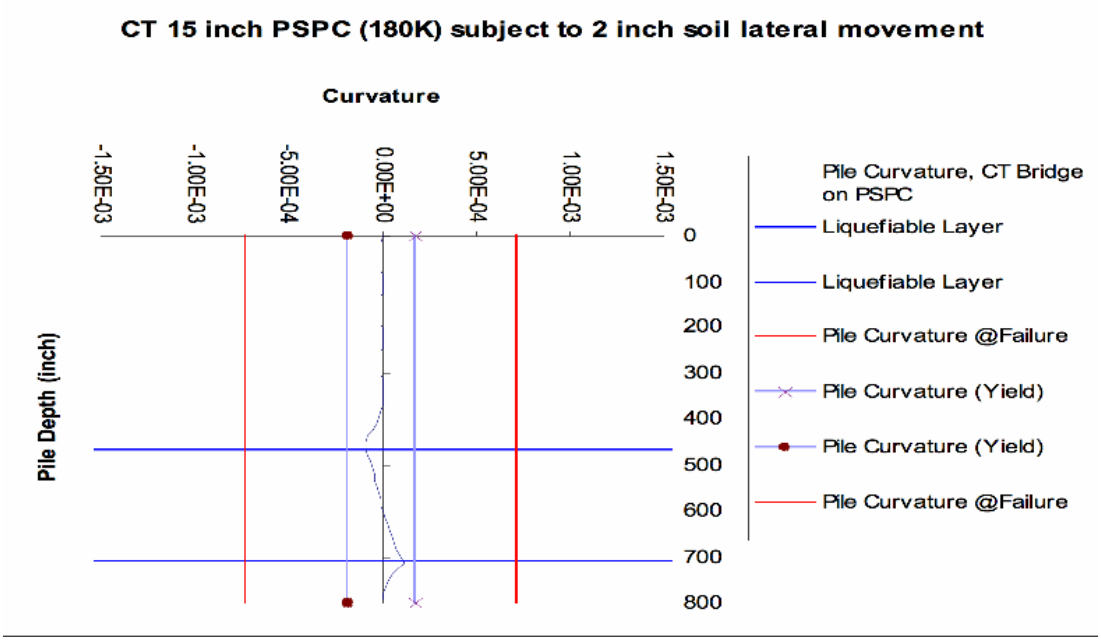

Figure 8-71: Pile Curvature Response (Design Example V)

On the demand side, the following (Figure 8-72) shows the pile curvature response of the 66 feet long , 15 inch diameter PSPC pile due to 12 inch of lateral spread displacement of the upper crust over the 20 feet thick liquefiable soil.

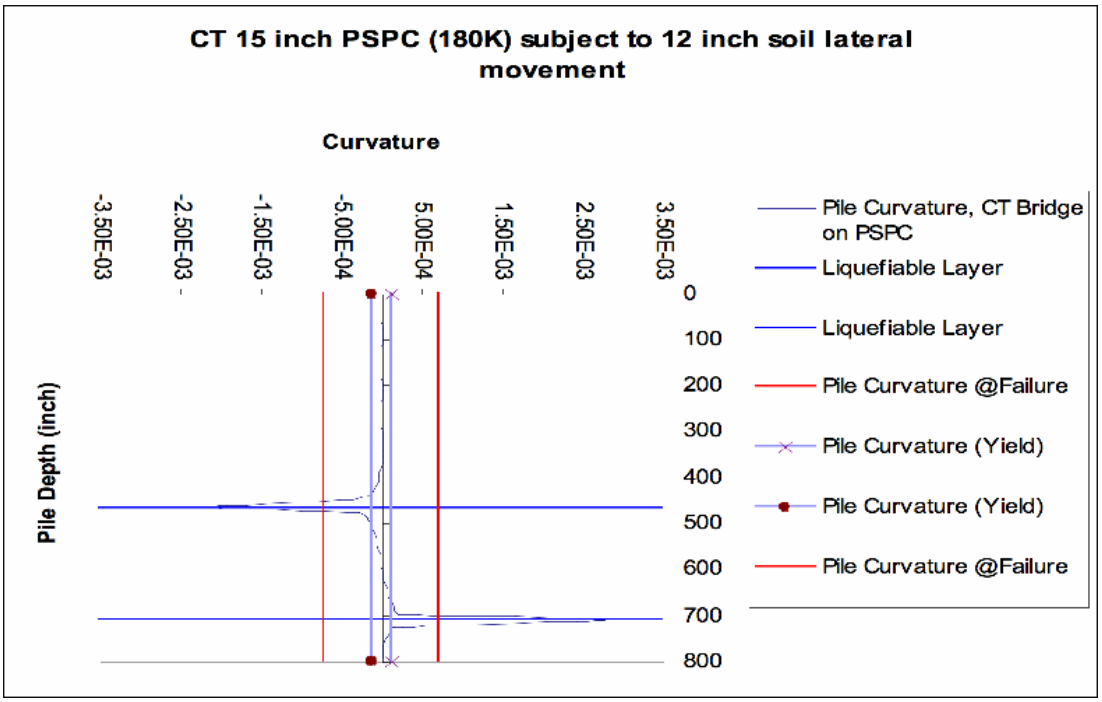

Figure 8-72: Pile Curvature Response (Design Example V)

As shown above, the PSPC pile would undergo plastic hinging and would "fail"at points immediately below and above the liquefiable layer. The pile curvature demand exceeds its ultimate curvature capacity value.

8.6.6. Sensitivity Analysis

Sensitivity analysis is performed in terms of liquefaction layer thickness and its impact on the pile response.

8.6.6.1. Liquefaction Layer Thickness, Deep Liquefaction

The response of pile due to lateral spread was analyzed by assessing how the liquefaction layer thickness impacts the response. The original liquefiable layer thickness of 20 feet was reduced to 15 feet, 10 feet, 5 feet, 4 feet, 3 feet and 2 feet. The elevation at the top of the lateral spread remained unchanged. No inertia loading was considered. Only the kinematic loading on the pile fixed at the top was considered.

LIQUEFIABLE LAYER THICKNESS: 20 feet, Depth of Liquefaction (39 to 59 feet)

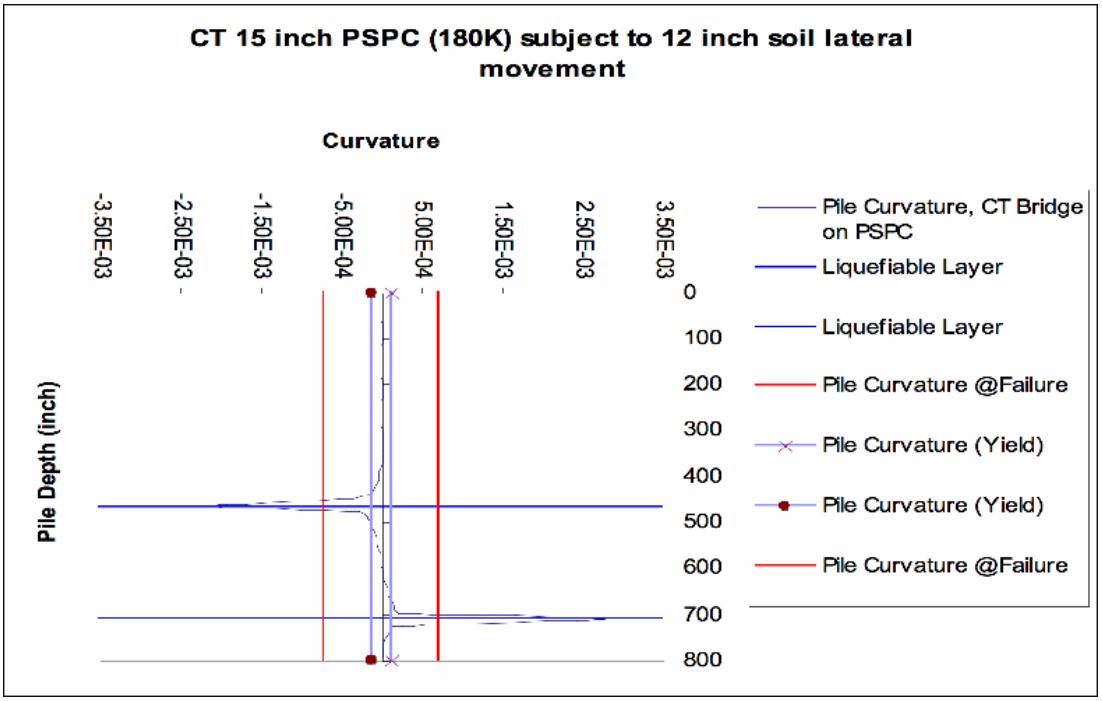

Figure 8-73: Pile Curvature Response (Design Example V)

LIQUEFIABLE LAYER THICKNESS: 15 feet, Depth of Liquefaction (39 to 54 feet)

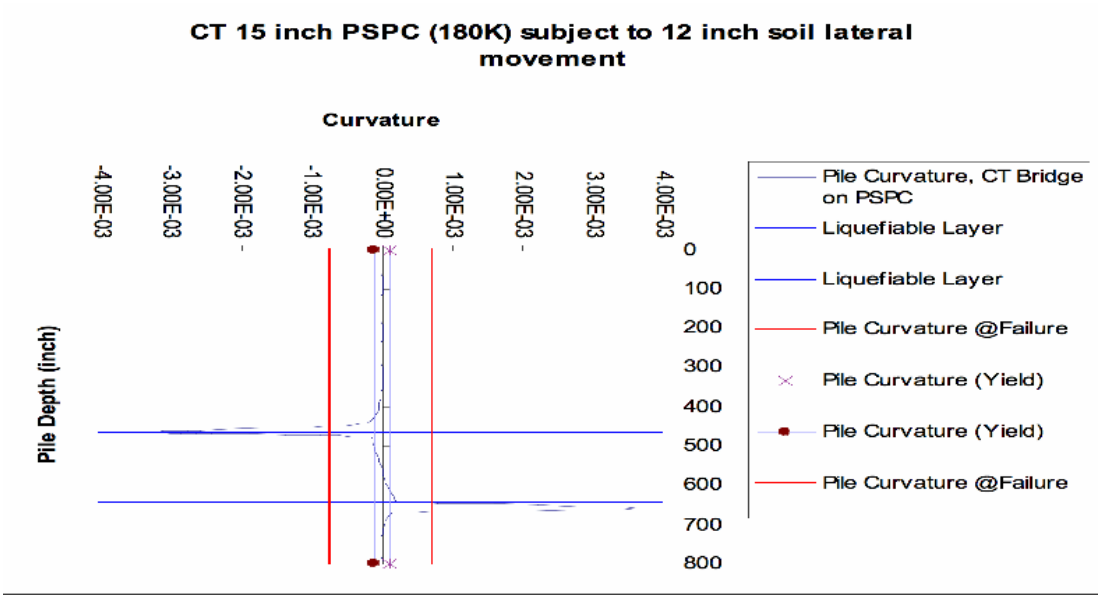

Figure 8-74: Pile Curvature Response (Design Example V)

LIQUEFIABLE LAYER THICKNESS: 10 feet, Depth of Liquefaction (39 to 49 feet)

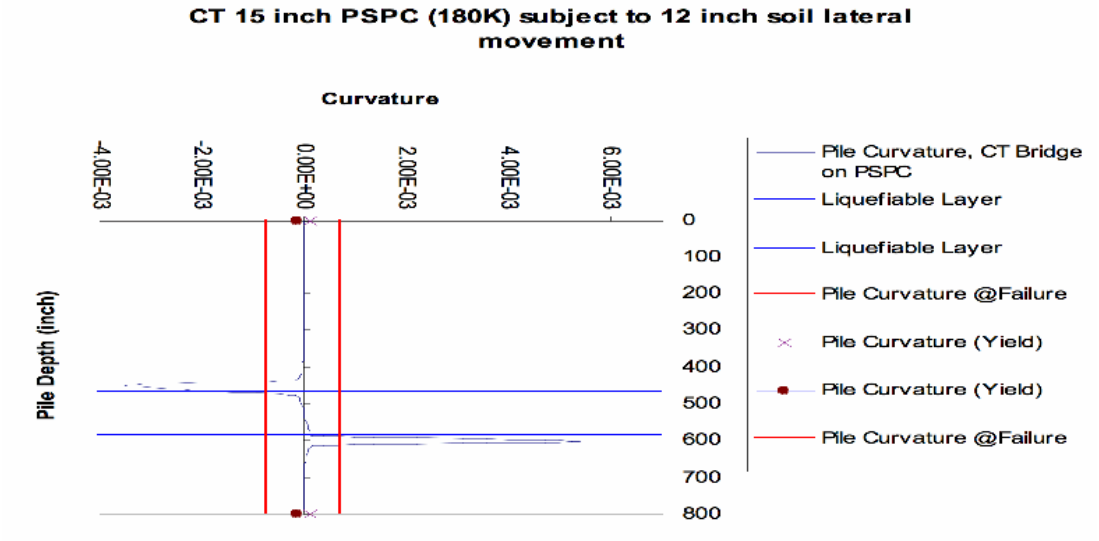

Figure 8-75: Pile Curvature Response (Design Example V)

LIQUEFIABLE LAYER THICKNESS: 5 feet, Depth of Liquefaction (39 to 44 feet)

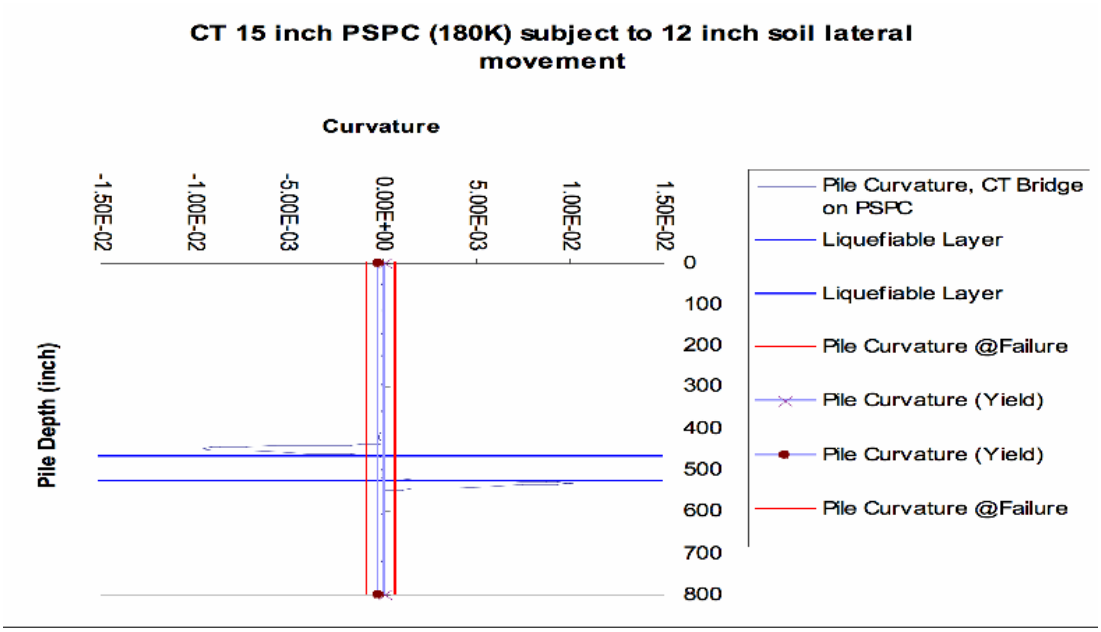

Figure 8-76: Pile Curvature Response (Design Example V)

The following (figures 8-77 and 8-78) show the results of the pile response in terms of curvature demand, based on the thickness of the liquefiable layer.

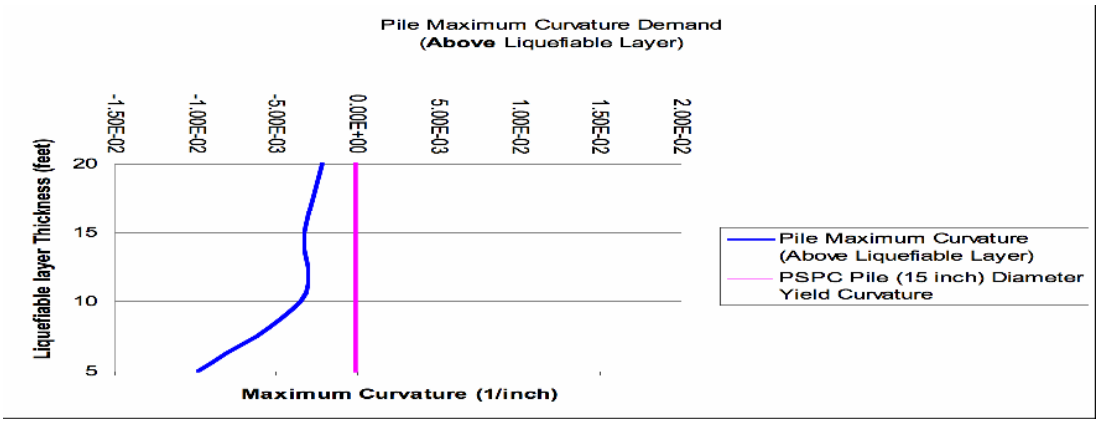

Figure 8-77: Pile Curvature Demand Based on Liquefiable Layer Thickness (Design Example V)

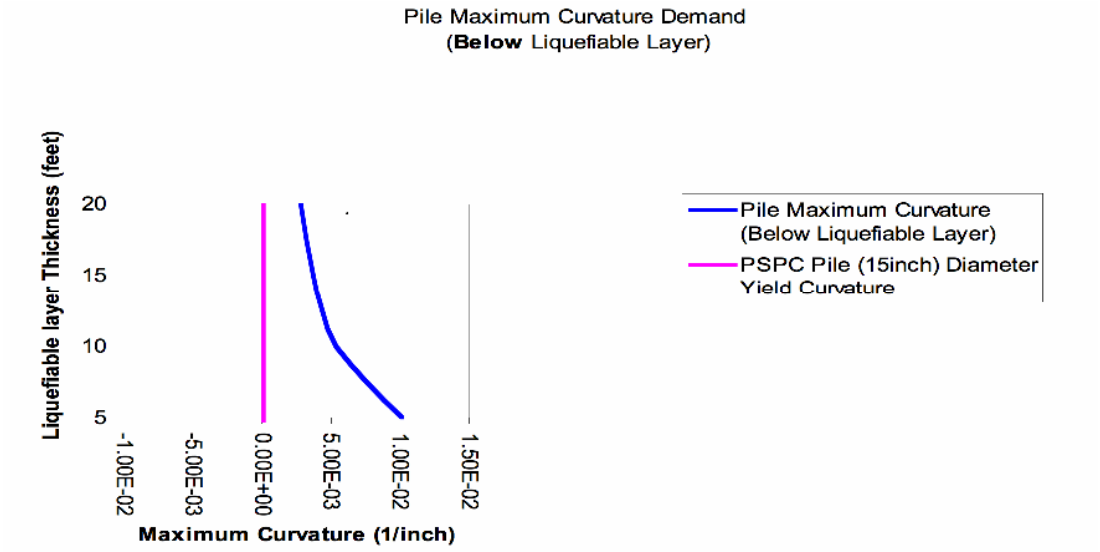

Figure 8-78: Pile Curvature Demand Based on Liquefiable Layer Thickness (Design Example V)

8.6.7. Conclusion

The proposed foundation for a multi-span bridge structure consisting of a 15 inch octagonal Caltrans Prestressed Precast Concrete pile was evaluated subject to lateral spread loading. The embankment displacement during the design earthquake was evaluated. Pile pinning effect considering the pile resistance to the embankment displacement was assessed and the corresponding pile response (demand) was found. The lateral demand using the newly reduced free field (reduction due to the pining effect) displacement is compared to the lateral capacity of the pile: The latter being a structure characteristic of the pile. It is important to note that effect of "pile pinning" in reducing the impact of the soil movement due to lateral spread is significant. However, despite this reduction, the piles at the abutment will yield and form plastic hinge at the upper and lower sections of the pile. The pile will form plastic hinges and will collapse since the curvature demand does exceed the ultimate curvature capacity. The reduction in liquefiable layer thickness, (with the base of the liquefiable layer remaining unchanged) does increase the pile curvature demand, detrimental to the pile integrity.

It is also worth noting that the PSPC pile would begin undergoing plastic hinging at least at one location along its length, due to soil crust lateral movement of as low as 3 inches.

8.7. Summary

To assess the earthquake bridge pile response to liquefaction induced lateral spread, five bridge pile types were considered in this chapter. Some of these pile types such as 24 inch cast in place drilled hole piles (CIDH) and 15 inch prestressed precast reinforced concrete driven piles are used extensively in California and the use of the pile shafts, Cast in steel shell (CISS) piles and larger diameter CIDH such as 48 inch are increasing for variety of reasons, both geotechnical and structural in nature. All these piles have progressively replaced the "traditional" piles such as the 14 inch CIDH, smaller capacity driven reinforced concrete piles and the steel H section piles, given the importance of the seismicity, the required constructability and design performance of the bridge piles in liquefiable sites located in high seismic zones.

All the design example bridge piles were subject to liquefaction induced lateral spread displacement demands of various magnitudes. In all these cases the abutment piles in all cases and the bent piles on occasion were embedded in a soil profile where the crust was comprised of non liquefiable engineering fill , a term used to describe the nature of the soil based on borrow soil and compacted to a required relative compaction.

The results demonstrated that pile pinning based on displacement compatibility introduced in this research as an improved design methodology played a significant role in reducing these kinematic demands on the bridge piles. The latter was used as

a soil movement profile applied to the pile and incorporated into the soil pile interaction model.

All the five pile types structural configuration, such as the type of reinforcing (hoop, etc…) transverse and longitudinal reinforcing, stress strain characteristics for unconfined concrete for cover, confined concrete used for core and the steel were incorporated and considered in evaluation of the response of all these bridge pile types.

The axial load applied from the superstructure has impact though minor on the structural ductile capacity of the piles. Nevertheless, axial load for each of these bridge pile types was included in evaluation of the ductile capacity of the design example bridge piles and hence overall earthquake response of these piles to liquefaction induced lateral spread. The introduction of the axial load into the lateral response of the pile, in particular the inelastic response of the pile offers a unique and new approach in the design methodology.

The curvature ductility of these piles was highest for the 15 inch PSPC pile (a value of 23) and lowest for the 48 inch CIDH (a value of 4) . This is the ratio of the ultimate curvature to the plastic curvature. As noted earlier a value of 4 was used in this research to characterize the curvature at failure for all these design example

bridge piles, and assess the earthquake response, leading to a conservative approach in design and response analysis.

It is important to note that the results above are only based on the outcome of the varying displacement demands, in other words the piles that did not fail were subject to half to a third of the displacement demand corresponding to the piles that did fail.

Finally, three of the five pile types (48 inch CIDH, 24 inch CISS and 15 inch PSPC) of the design example piles failed (meaning the curvature demand equal or larger than the curvature capacity at failure) due to kinematic displacement demand initiated by liquefaction lateral spread . The remaining two (24 inch CIDH and Pile Shaft Type 1) did not fail. The following table summarizes the results.

Pile Type	Liquefiable Layer Thickness (feet)	Displacement (no pinning) inch	Displacement (with pinning) inch	Pile Maximum Curvature Demand(1/inch)	Pile Curvature Capacity at Failure (1/inch)
CIDH (24 inch)	20	10	4	0.000142	0.00087
Caltrans Pile Shaft Type I (66 inch)	20	22	6	0.0000573	0.000341
CIDH (48 inch)	20	30	12	0.000443	0.000486
CIIS (24 inch)	9	50	25	0.0131	0.000665
Caltrans PSPC (15 inch)	20	NA	12	0.00278	0.000722

Table 8-9: Summary of the Design Examples Bridge Piles Performance

CHAPTER 9: SUMMARY & CONCLUSIONS

9.1. Summary

The research conducted comprised the following parts:

I) A review of liquefaction induced lateral spread case histories related to bridge pile foundations.

II) A review of liquefaction evaluation and lateral spread/pile modeling concepts.

III) A review of the NCHRP 12-49(2003) design method for bridge pile earthquake response to liquefaction induced lateral spread.

IV) A review of CALTRANS design approach for bridge pile earthquake response to liquefaction induced lateral spread

V) Recommendations for improved design methodologies for earthquake response of bridge piles to lateral spread based on the NCHRP 12-49 approach and re-evaluation of representative bridges discussed in the NCHRP report.

VI) Case Study Analysis and re-evaluation of the bridge pile response to lateral spread for 1987 Edgecumbe and 1995 Kobe earthquake events based on the recommended approach.

VII) Independent comparative analysis to Finite Element Modeling of Port of Los Angeles wharf pile response to lateral spread loading using LPILE5.

VIII) Pile response analysis of representative Caltrans bridge piles through Design Examples

Based on a review of the recommended NCHRP guidelines and current Caltrans practice, it was clear that improvement in design approaches were needed. Research considerations in this thesis resulted in recommendations which included:

1) Pile pinning should be recognized as an important element in analyzing earthquake response of bridge piles to liquefaction induced lateral spread. And can be evaluated by using a displacement compatibility approach, as discussed and illustrated in Chapter 7.
2) Pile ductile design is recommended and displacement based method of analysis for modeling pile response should replace the force based design approach.
3) Pile curvature ductility should be studied and evaluated for bridge piles to help the bridge designer with the type selection process.
4) Inelastic behavior of piles can accommodate large ground displacement without bridge collapse.

9.2. Conclusions

The mechanisms of pile pinning and pile ductility fundamentally alter design methodologies for the earthquake response of bridge pile foundations to liquefaction induced lateral spread. The role of pile pinning in potentially reducing the displacement demands on the bridge foundation is significant and pile ductility

allows the bridge pile foundation to potentially resist greater displacement demands without allowing structure collapse during a design earthquake event.

The displacement compatibility concept discussed in this research captures the fundamentals of pile pinning based on relative pile and lateral spread soil movement and allows the bridge designer to assess the displacement demand based on site specific conditions unique to the bridge structure foundation and site geotechnical subsurface conditions.

The pile ductility concept allows the pile to undergo greater displacement without potential collapse. Pile plastic curvature capacity specific to a pile type can be evaluated using accepted modeling procedures. By allowing the piles to form a plastic hinge and to mobilize ductility, less earthquake displacement demand is transferred up to the bridge columns and superstructure.

The recommended design approach would be enhanced by establishing a platform where the bridge and geotechnical designers can interact freely and actively engage in the type selection of a foundation system designed for lateral spread displacement demands.. The role of geotechnical designers and bridge foundation designers can potentially be altered to have one “foundation designer” who is well informed about both the geotechnical and structural aspects of the bridge foundation.

9.3. Future Research

The research conducted in this thesis has focused on refinements to the NCHRP 12-49 design approach to improve evaluations of pile ductility capacity and pile pinning effects based on pile hinge locations. To demonstrate these refinements simple examples of lateral spreading of representative bridge abutment piles on simple three layer crust, liquefied layer, dense sand configurations have been used, coupled with LPILE5 pushover analyses. Recognizing the many simplifying assumptions in the above studies, it is recommended that future research should consider:

1. An evaluation of the errors associated with using conventional p-y springs for displacement based pushover analyses, as discussed by Lam (2008)
2. Improved evaluation of pile pinning effects to reflect the progressive mobilization of pile shear with displacement, and hence time dependent changes in yield accelerations versus the displacement equilibrium approach examples used for simplicity in this study.
3. The adoption of an improved Newmark sliding block approach to determine embankment displacement profiles, reflecting a non rigid sliding mass, particularly for higher embankment slide zones.
4. Development of appropriate methods to consider potential restraining forces from the bridge superstructure and pier foundations in a global displacement model.
5. Studies to define when it is appropriate to decouple intertial bridge loading from kinematic displacement base demands on pile foundations.

REFERENCES

Abdoun, T.H. (1997). "Modeling of Seismically Induced Lateral Spreading of Multi-Layered Soil and its Effect on Pile Foundations." PhD Dissertation, Rensselaer Polytechnic Institute.

Abdoun, T.; Dobry, R.; O'Rourke, T.D.; Goh, S.H. (2003). " Pile Response to Lateral Spreads: Centrifuge Modeling." Journal of Geotechnical and Geoenvironmental Engineering, Vo.119, p.869-879

American Petroleum Institute (2000) " Recommended Practice for Planning, Designing and Constructing Fixed Offshore Platforms-Working Stress Design" API Recommended Practice 2a-Wsd (Rp-2a-Wsd) Twenty –First Edition, December

Amini, F.and G.Z.Qi.(2000). " Liquefaction Testing of Stratified Silty Soils," Journal of Geotechnical and Geoenvironmental Engineering 126(3):208-216

Anchorage Museum of Arts and History (1964): Photo for Earthquake Damage to bridge over the twenty mile river during the 1964 Alaska earthquake

Andrews, D.C.A and G.R. Martin (2000) " Criteria for liquefaction of silty soils" Proc. 12th World Conference on Earthquake Engineering, Auckland, New Zealand, 2000.

Armstrong, R.J.; Boulanger, R.W.; Gulerce, U.; Kutter, B.L.; Wilson, D.W. (2008), " Centrifuge Modeling of Pile Pinning Effects," Geotechnical Earthquake Engineering and Soil Dynamics IV.

Auckland Regional Government (2008), 1964 Niigata earthquake from http://www.arc.govt.nz/council/civil-defence-emergency-management/natural-hazards/earthquakes.cfm, Retrieved 2008.

Baziar,M.H., and R.Dobry. (1995) " Residual Strength and Large-Deformation Potential of Loose Silty Sands," Journal of Geotechnical Engineering 121(12): 896-906

Berrill, J.B. et al (1997), "Lateral-Spreading loads on a piled bridge foundation", Seismic behavior of ground and Geotechnical Structures.

Berrill, J.B. and S. Yasuda. (2002) " Liquefaction and piled foundations: some issues , Journal of Earthquake Engineering. Special Issue.

Blandon, C.A. (2007), "" Seismic Analysis and Design of Pile Supported Wharves", A Thesis Submitted in partial fulfillment of the requirements for the Degree of Doctor of Philosophy in Earthquake Engineering, University of California San Diego

Boulanger,R.W. M.W.Meyers,L.H.Mejia and I.M.Idriss.(1998). " Behavior of a Fine-grained Soil during the Loma Prieta Earthquake," Canadian Geotechnical Journal 35;146-158

Boulanger, R. W., and Idriss, I. M. (2006). "Liquefaction susceptibility criteria for silts and clays." Journal of Geotechnical and Geoenvironmental Engineering, ASCE, 132(11), 1413-1426.

Boulanger, R.W. Chang, D., Brandenberg, S.J., Armstrong,R.J., Kutter, B.L. (2007) " Seismic Design of Pile Foundations for Liquefaction Effects," 4th International Conference on Geotechnical Earthquake Engineering, Greece, June 2007

Brandenberg, S.J. (2005). "Behavior of Pile Foundations in Liquefied and Laterally Spreading Ground." PhD Dissertation, University of California Davis.

Budek,A.M; Priestley,M.J.N; Benzoni, G.;(2004) "The Effects of External Confinement on Flexural Hinging in Drilled Pile Shafts", Earthquake Spectra, Vol.20, Issue 1, pp. 1-24, February 2004

Castro, G. (1975). " Liquefaction and Cyclic Mobility of Saturated Sands," Journal of the Geotechnical Engineering Division 101(GT6):551-569

Chaudhuri, D. (1998). "Liquefaction and Lateral Soil Movement Effects On Piles." PhD Dissertation, Cornell University.

Cubrinovski, M.; Ishihara., K. (2005), " Simplified Method for Analysis of Piles Undergoing Lateral Spreading in Liquefied Soils," Japanese Geotechnical Society.

Cubrinovski, M. (2006). "Pile Response to Lateral Spreading of Liquefied Soils," NZGS 2006 Symposium: Earthquakes and Urban Development , Nelson, 127-142

Dickenson,S.E., B.J.Wavra, and J.Sunitsakul. (2000). " Seismic Performance of the Columbia River Levee Adjacent to the Portland International Airport (PDX), Portland, Oregon," Report to the U.S.Army Corps of Engineers, Portland District,113p.,plus appendices

1987 Edgecumbe earthquake. (2008, May 24). In *Wikipedia, The Free Encyclopedia*. Retrieved 00:58, June 8, 2008, from http://en.wikipedia.org/w/index.php?title=1987_Edgecumbe_earthquake&oldid=214723852

Environment Waikato Regional Council (2008): http://www.ew.govt.nz/enviroinfo/hazards/naturalhazards/earthquake

Expediamaps.com (Microsoft, 1998): http://www.geocities.com/Colosseum/Slope/2017/mapp.html

Fear, C.E., and Robertson,P.K. (1995). " Evaluating the Undrained Strength of Sand: A Theoretical Framework." Canadian Geotechnical Journal,32: 859-870

Franklin, A.G. and Chang, F.K. (1977); "Permanent Displacements of Earth Embankments by Newmark Sliding Block Analysis, Report 5, Miscellaneous Paper S-71-17, U.S. Army Corps of Engineers Waterway Experiment Station, Vicksburg, Mississippi.

Franks, C.A.M. (1988). Engineering geological aspects of the Edgecumbe, New Zealand earthquake of 2 March 1987. *Quarterly Journal of Engineering Geology* **21**

Galgana, G. et al. (2007) Analysis of crustal deformation in Luzon, Philippines using geodetic observations and earthquake focal mechanisms. Elsevier, Tectonophysics 432 (2007) 63-87

Goh, S.H. (2001). "Soil-Pile Interaction During Liquefaction-Induced Lateral Spread." PhD Dissertation, Cornell University.

Great Hanshin earthquake. (2008, June 8). In *Wikipedia, The Free Encyclopedia*. Retrieved 19:39, June 8, 2008, from http://en.wikipedia.org/w/index.php?title=Great_Hanshin_earthquake&oldid=217938586

Hall, J.R., and Scott, R.F. (1995) "Evaluation of Bridge Damage in the 1990 Luzon and 1991 Costa Rica Earthquake," Southern California Earthquake Center, Task H-6 Report to Caltrans and the City and County of Los Angeles, on the Characteristics of Earthquake Ground Motion for Seismic Design.

Hamada, M. (1992), " Large Ground Deformations and Their Effects on Lifelines: 1964 Niigata Earthquake." Case Studies of Liquefaction and Lifeline Performance During Past Earthquakes, Vol.1, Japanese Case Studies, Technical Report, NCEER-92-0001, NCEER, Buffalo, NY.

Hamada.M.; Isoyama,R.;Wakamatsu,K., (1996) " Liquefaction-Induced ground Displacement and its Related Damage to Lifeline Facilities", Special Issue of Soils And Foundations, 81-97, January, Japanese Geotechnical Society.

Hamada, M. , Yasuda, S., Isoyama, R. and Emoto, K. (1986), "Study on liquefaction induced permanent ground displacements."Association for the Development of Earthquake Prediction in Japan. 87

Hanshin Highway Authority (1996). Investigations of seismic damage of bridge foundations in reclaimed land.

Hetenyi, M., (1946) "Beams on Elastic Foundation, The University of Michigan Press, Ann Arbor, 1946.

Housner, G.W (1994). (Chairman, Seismic Advisory Board) " The Continuing Challenge," Report to the Director, California Department of Transportation on the 1994 Northridge Earthquake, Seismic Advisory Board, Sacramento, California.

Hynes-Griffin, M.E.and Franklin, A.G. (1984); "Rationalizing the Seismic Coefficient Method," Miscellaneous Paper GI-84-13.U.S. Army Corps of Engineers Waterways Experiment Station, Vicksburg, Mississippi, 21.pp

Ishihara, K.; (2003) " Liquefaction-Induced Lateral Flow and its effects on Foundation Piles", Fifth National Conference on Earthquake Engineering, 26-30 May 2003, Istanbul, Turkey

Ishihara, K. and Cubrinovski, M. (1998). "Performance of large-diameter piles subjected to lateral spreading of liquefied soils," *Keynote Lecture, Proc. 13th Southeast Asian Geotechnical Conf.*, Taipei, pp. 1-14.

Ishihara, K., Acacio, A. and Towhata, I., (1993) "Liquefaction Induced Ground Damage in Dagupan in the July 16, 1990 LUZON EARTHQUAKE, Soils and Foundations, Vol.33,No. 1, 133-154, Mar.1993, Japanese Society of Soil Mechanics and Foundation Engineering

Ishihara, K.(1993). " Liquefaction and Flow Failure During Earthquakes," Geotechnique, The Institution of Civil Engineers 43(3); 351-415

Ishihara, K. (1996). "Soil Behavior in Earthquake Geotechnics," Clarendon Press, Oxford,350p.

Keenan, Richard P., (1996) "Foundation loads due to lateral spreading at the Landing Road Bridge, Whakatane" University of Canterbury, Christchurch, New Zealand, Master of Engineering Thesis.

Konrad, J.M., and Watts,B.D.(1995). " Undrained Shear Strength For Liquefaction Flow Failure Analysis." Canadian Geotechnical Journal,32: 783-794

Kramer, S.L Elgamal, A-W, (2001) " Modeling Soil Liquefaction Hazards For Performance-Based Earthquake Engineering," Pacific Earthquake Engineering Research Center, College of Engineering, University of California, Berkeley, February 2001.

Kramer, Steven.L (1996), "Geotechnical Earthquake Engineering", Prentice Hall

Lagos, Lenart.L.G. (2005). "Centrifuge Modeling of Permeability and Pinning Reinforcement Effects on Pile Response to Lateral Spreading." PhD Dissertation, Rensselaer Polytechnic Institute.

Lam, I.P., Arduino,P. and Mackenzie-Helnwein,P. (2007), " Openseess Soil-Pile Interaction Study under Lateral Spread Loading", November.

Ledezma, C.; Bray, J.D. (2008), " Factors that Affect the Performance of Bridge Foundations Undergoing Liquefaction-Induced Lateral Spreading," Geotechnical Earthquake Engineering and Soil Dynamics IV.

Liao, S.C and R.V. Whitman. (1985). " Overburden Correction Factors for SPT in Sand," Journal of Geotechnical Engineering 112(3):373-377

LPILE MANUAL (2004) : LPILE^{PLUS} 5.0 For Windows , Technical Manual (2004), Ensoft, Inc.

1990 Luzon earthquake. (2008, May 20). In *Wikipedia, The Free Encyclopedia*. Retrieved 22:19, June 8, 2008, from http://en.wikipedia.org/w/index.php?title=1990_Luzon_earthquake&oldid=213676179

Mander, J.B., Priestley,M.J.N.,and Park, R., (1988) " Theoretical Stress-Strain Model for Confined Concrete," Journal of Structural Engineering, ASCE, Vol. 114, No.8, August 1988, pp.1804-1826.

Mander, J.B., Priestley,M.J.N.,and Park, R., (1988) " Observed Stress-Strain Behavior of Confined Concrete," Journal of Structural Engineering, ASCE, Vol. 114, No.8, August 1988, pp.1827-1849.

Marcuson, W.F., M.E. Hynes, and A.G. Franklin. (1992). " Seismic Stability and Permanent Deformation Analyses: the Last Twenty Five Years," Proc. of Stability and Performance of Slopes and Embankments-II, ASCE Geotechnical Special Publication 31(1):552-592

Martin, G.R.(2004) " The Seismic Design of Bridges-Geotechnical and Foundation Design Issues", Geotrans 2004: Geo-Institute Conference on Geotechnical Engineering For Transportation Projects. Los Angeles, California, USA, July.p. 137-166

Martin G.R., Marsh,L.M., Anderson, D.G. , Mayes, R.L., Power, M.S. (2002) "Recommended Design Approach for Liquefaction Induced Lateral Spreads", Proceedings of the Third National Seismic Conference and Workshop on Bridges and Highways, Portland, Oregon, May

Martin, G.R., and Qiu, P.(1994). "Effects of Liquefaction on Vulnerability Assessment," NCEER Highway Project on Seismic Vulnerability of New and Existing Highway Construction. One Year Research. Technical Research Paper.

Martin, G.R. and Bray .J(2006) "Performance-Based evaluation of bridges on liquefiable soils", empirically-based approach, PEER Project

Marzouk, H., and Chen, Z., (1993)" Tension Stiffening Model for High Strength Slabs," Proceedings, 1993, CSCE/CPCA Structural Concrete Conference, Torronto, Canada, May, 1993, pp 127-140

Matlock, H. (1970)" Correlations for Design of Laterally Loaded Piles in Soft Clay," Proceedings, Offshore Technology Conference, Houston, Texas, 1970, Paper No.1204, pp. 577-594

McClelland, B., and J.A.Focht,Jr., (1958) " Soil Modulus for Laterally Loaded Piles," Transactions, American Society of Civil Engineers, Vol. 123,pp. 1049-1086

MCEER/ATC 49-1 (2003), "Comprehensive Specifications for the seismic design of highway bridges, Liquefaction Study Report", MCEER/ATC 49-1

MCEER/ATC 49-2 (2003), "Design Examples, Recommended LRFD Guidelines for the seismic design of highway bridges", MCEER/ATC 49-2

MCEER/ATC 49 (2003a), "Recommended LRFD guidelines for the seismic design of highway bridges , Part I : Specifications.

MCEER/ATC 49 (2003b), "Recommended LRFD guidelines for the seismic design of highway bridges , Part II : Commentary and Appendices.

Meyersohn, D.W. (2003). " Internal Caltrans Draft (unpublished) paper.

Meyersohn, D.W. (1994). " Pile Response to Liquefaction Induced Lateral Spread." PhD Dissertation, Cornell University.

Mier, J.G.M.van, (1987) "Examples of Non-Linear Analysis of Reinforced Concrete Structures with DIANA," HERON, Delft University of Technology, Delft, Netherlands, Vol.22, No.3 1987.

Molnia, Bruce, "http://www.earthscienceworld.org, photo ID ipar6d, photograph by Bruce Molnia".

MTD 20-1 (1999) : "Caltrans Memo to Designers 20-1, 1999.

NCHRP (2002), " NCHRP 12-49, Comprehensive Specifications For the Seismic Design of Bridges, Liquefaction Study Report," October 8th, 2002.

NEES (2004): Network for Earthquake Engineering Simulation , Preventing Earthquake Disasters: The Grand Challenge in Earthquake Engineering: A Research Agenda for the Network for Earthquake Engineering Simulation (NEES), http://www.nap.edu

Nevada Seismological Laboratory, From http://www.seismo.unr.edu/ftp/pub/updates/louie/kobe/kobe-tect.html

Newmark, N. (1965). " Effects of earthquakes on Dams and Embankments." Geotechnique 15(2):139-160.

Nishioka,T. (2008), " Pile data courtesy Dr. Tsutomu Nishioka via Personal communication, Hanshin Expressway Company Limited, Chuo-ku, Osaka, Japan, 2008".

NZDSIR, Staff (1987) :New Zealand Department of Scientific and Industrial Research. The March 2, 1987, Earthquake Near Edgecumbe, North Island, New Zealand. *Eos* **68**: 1162-1171.

Olson, S.M., Johnson, C.I.; (2008) " Analyzing Liquefaction Induced Lateral Spreads Using Strength Ratios," Journal of Geotechnical and Geoenvironmental Engineering, Vol.134, No.8.

Olsen, R.S (1997). " Cyclic Liquefaction Based on the Cone Penetrometer Test." Proceeding of the NCEER Workshop on Evaluation of Liquefaction Resistance of Soils. Technical Report NCEER-97-0022, Salt Lake City, UT.pp.225-276.

Olson, S.M.; and T. D.Stark (2002) " Liquefied Strength Ratio From Liquefaction Flow Failure Case Histories". Canadian Geotechnical Journal, 39:629-647

PGFSR (2007), "Draft Caltrans Pile Group Foundation Study Report, 2007

Poulos, S. (1981). "The Steady State of Deformation," Journal of the Geotechnical Engineering Division 107(GT5):553-561

Poulos, S.J.G.Castro, and J.W.France.(1985). "Liquefaction Evaluation Procedure,"Journal of Geotechnical Engineering 111(6):772-791

Personal communication with Dr. Takao Okada of PWRI of Japan (2008)

Priestley, N.M.(2005), " Port of Los Angeles Seismic Code: Structural Aspects" Port of Los Angeles, POLA Seismic Code Workshop, San Pedro, September 2005

Priestley, Seible and Calvi (1996) ".Seismic Design and Retrofit of Bridges"

Rajaparthy, S.R.; Zhang, Z.; Hutchinson, T.C.; and Lang,F., (2008) " Plastic Hinge Formation in Pile Foundations due to Liquefaction-Induced Loads," Geotechnical Earthquake Engineering and Soil Dynamics IV.

Ramos, R. (1999). "Centrifuge Study of Bending Response of Pile Foundation to a Lateral Spread Including Restraining Effect of Superstructure." PhD Dissertation, Rensselaer Polytechnic Institute.

Robertson, P.K., and C.E. Wride (1997b). " Evaluation of Cyclic Liquefaction Potential Based on the CPT" Seismic Behavior of Ground and Geotechnical Structures. Seco e Pinto (ed.), A.A. Balkema, Brookfield, pp. 269-277..

Robertson, P.K. and R.G. Campanella (1985). " Liquefaction Potential of Sands Using the CPT," Journal of geotechnical Engineering 111(3): 384-403

Robertson, P.K., and C.E. Wride. (1997a). " Cyclic Liquefaction and its Evaluation Based on the SPT and CPT," Proceeding of the NCEER Workshop on Evaluation of Liquefaction Resistance of Soils. Technical Report NCEER-97-0022.Salt Lake City, U.T.pp.41-87.

Rollins, K.M.., Gerber, T.M., Lane, J.D, Ashford, S.A.(2005), " Lateral Resistance of a Full-Scale Pile Group in Liquefied Sand", Journal of Geotechnical and Geoenvironmental Engineering , Vol. 131, No.1, January 1, 2005

SDC (2006): Caltrans Seismic Design Criteria, 2006

Seed, H.B., (1979), Soil Liquefaction and cyclic mobility evaluation for level ground during earthquakes, Journal of Geotechnical Engineering Division, 105, (GT2), 201-255.

Seed and Idriss (1971), " Simplified Procedure for evaluating soil liquefaction potential", Journal of Soil Mechanics and Foundations Division, ASCE Vol.97, No.SM9, P.1249-1273

Seed, H.B., and P.DeAlba. (1986). "Use of SPT and CPT Tests for Evaluating the Liquefaction Resistance of Sands," in Clemence, ASCE Geotechnical Special Publication No.6,Use of In Situ Tests in Geotechnical Engineering, New York, N.Y.pp.281-301

Seed, H.B., K. Tokimatsu, L.F.Harder, and R.M. Chung. (1985). "Influence of SPT Procedures in Soil Liquefaction Resistance Evaluations," Journal of Geotechnical Engineering 111(12):1425-1445.

Seed, H.B. and I.M. Idriss. (1982). "Ground Motion and Soil Liquefaction During Earthquakes," EERI Monograph, Earthquake Engineering Research Institute.134p.

Seed, H.B. (1987) " Design Problems in Soil Liquefaction," Journal of the Geotechnical Engineering Division 113(8):827-845

Seed, R.B., and L.F. Harder Jr. (1990). " SPT-Based Analysis of Cyclic Pore Pressure Generation and Undrained Residual Strength," Proceedings, H.Bolton Seed Memorial Symposium, Vol.2, BiTech Publishing, Vancouver,B.C.pp.351-376

Seed, H.B., Idriss, I.M., and Arrango, I., 1983, " Evaluation of Liquefaction Potential Using Field Performance Data," Journal of the Geotechnical Engineering Division, ASCE, Vol.109, No.3, March.

Seed, R.B. and H.L. Jong. (1987). " Factors Affecting Post-Liquefaction Strength Assessment." Proceedings, Fifth Canadian Conference on Earthquake Engineering, Ottawa, Canada,pp.483-492

Shibata, T.; Oka, F., Ozawa, Y. (1996); "Characteristics of Ground Deformation Due to Liquefaction", Special Issue of Soils and Foundations, 65-99, Jan.1996, Japanese Geotechnical Society.

Stark, T.D.,S.M. Olson,S.L.Kramer, and T.L.Youd,editors.(1997). " Final Proceedings of the Workshop-Shear Strength of Liquefied Soils," National Science Foundation, NSF Grant CMS-95-31678,80p.,available from the Mid-America Earthquake Center at http:mae.ce.uiuc.edu/

Stark, T.D. and G.Mesri,(1992). "Undrained Shear Strength of Liquefied Sands For Stability Analysis," Journal of Geotechnical Engineering 118(11):1727-1747

Terzaghi, K., (1955). "Evaluation of Coefficients of Subgrade Modulus," Geotechnique,Vol. V, pp.297-326.

The Encyclopedia of New Zealand: http://www.teara.govt.nz/EarthSeaAndSky/NaturalHazardsAndDisasters/Earthquakes/2/ENZ-Resources

Tokimatsu, K. (1999), " Performance of Pile Foundations in Laterally Spreading Soils," Proc. of the 2nd International Conference on Earthquake Geotechnical Engineering .

(USGS1): U.S. Geological Survey Photographic Library, Photo ID: Alaska Earthquake No. 29ct aeq00029, http://libraryphoto.cr.usgs.gov

(USGS2): U.S. Geological Survey, Professional Paper 541, Figure 24, U.S. Geological Survey Photographic Library, Photo ID: Alaska Earthquake No. 71ct aeq00071,

(USGS3): U.S. Geological Survey Photographic Library, Photo ID: Alaska Earthquake No. 74ct aeq00074,

(USGS4): U.S. Geological Survey Photographic Library, Photo ID: Alaska Earthquake No. 303 ake00303, http://libraryphoto.cr.usgs.gov, U.S. Geological Survey Professional Paper, 545-C, Figure 37, Photo by R. Kachadorian, view is northeast.

(USGS5): U.S. Geological Survey Photographic Library, Photo ID: Alaska Earthquake No. 320 ake00320, http://libraryphoto.cr.usgs.gov, Photo by A. Grantz. Figure 14-B, U.S. Geological Survey Circular 491

Wakamatsu, K., et al (1991). Liquefaction Induced Ground Failure During The 1990 Philippines Earthquake, MCEER 91-0001

Wang, W.S. (1979) “Some findings in soil liquefaction” Water Conservancy and Hydroelectric Power Scientific Research Institute, Beijing, China.

Wang, S-T., and Reese, L.C. (1998) “ Design of Pile Foundations in Liquefied Soils.” Geotechnical Earthquake Engineering and Soil Dynamics III, GSP No.75, P. Dakoulas and M. Yegian,eds. Vol.2, ASCE, Reston Va., 1331-1343

WES (1977), Waterways Experimentation Station, Chart for Newmark Displacement of Slopes

Wilson, D.W. (2000). “Soil-Pile -Superstructure Interaction In Liquefying Sand And Soft Clay.” PhD Dissertation, University of California Davis.

Wong, C.P and Whitman, R.V. (1982), “ Seismic Analysis and Improved Seismic Design Procedure For Gravity Retaining Walls,” Research Report 82-83 Department of Civil Engineering, Massachusetts Institute of Technology, Cambridge, M.A.

XTRACT (2008), Software for cross sectional and structural analysis for components, Imbsen

Yasuda, S.,and Berrill, J.B. (2000), “Observations of the earthquake response of foundations in soil profile containing saturated sands,” Proc.GeoEng. 2000 Conf, Melbourne, Australia.

Youd, T.L and I.M. Idriss,editors. (1997). “Proceedings of the NCEER Workshop on Evaluation of Liquefaction Resistance of Soils, “ National Center for Earthquake Engineering Research, Technical Report NCEER-97-0022.Salt Lake City,UT.275 p.